Conjugated Semiconducting Organic Materials for Electronic Applications

Dissertation

Zur Erlangung des Grades

"Doktor der Naturwissenschaften"

am Fachbereich Chemie, Pharmazie und Geowissenschaften der

Johannes Gutenberg-Universität in Mainz

Changduk Yang

geboren in Nonsan / Republic of Korea

Mainz, 2006

Dekan:

1. Berichterstatter :

2. Berichterstatter :

Tag der mündlichem Prüfung

Die vorliegende Arbeit wurde in der Zeit von 2003 bis 2006 im Max-Plannk-Institute für Polymerforschung in Mainz unter Anleitung von Herrn Prof. Dr. K. Müllen ausgeführt.

Ich danke Herrn Prof. Dr. K. Müllen für seine wissenschaftliche und persönliche Unterstützung sowie für seine ständige Diskussionsbereitschaft.

Table of Contents

List of Figures

List of Schemes

List of Tables

List of Charts

Glossary of Abbreviations

Alq_3	Tris(8-hydroxy-quinoline) aluminum
9-BBN	9-Borabicyclo[3.3.1]nonane
BOC	*tert*-Butoxycarbonyl
BPEA	9,10-Bis(phenylethynyl)anthracene
bpy	Bipyridine
BTA	Bisthiazol-2-yl-amine
CAN	Ceric ammonium nitrate
CHP	Cyclohexa-*meta*-phenylene
COD	1,3-Cyclooctadiene
CPDT	4H-cyclopenta[2,1-b:3,4-b']dithiophene
CV	Cyclic voltammetry/voltammogram
DCM	Dichloromethane
DMAP	4-Dimethylaminopyridine
DMF	N,N-dimethylformamide
DMSO	Dimethylsulfoxide
DPA	9,10-Diphenylanthracene
DSC	Differential scanning calorimetry
EB	Emeraldine base
EDOT	3,4-Ethylenedioxythiophene
EL	Electroluminescence
EPR	Electron paramagnetic resonance
EQE	External quantum efficiency
ET	Electron-transfer
FD-MS	Field Desorption Mass Spectrometry
FET	Field effect transistor
FTIR	Fourier transform infrared
GPC	Gel permeation chromatography
HBC	Hexa-*peri*-hexabenzocoronone

HOMO	Highest energy occupied molecular orbital
ICT	Intramolecular charge transfer
ITO	Indium-tin oxide
LDA	Lithium diisopropylamine
LEB	Leucoemeraldine base
LED	Light-emitting diode
LMC	Ladder model compound
3,6-LPAP	Linear poly-3,6-(9,10-diarylphenanthrylene)
LPPP	Ladder-type poly-*p*-phenylene
LPPPA	Ladder poly(*p*-phenylene-*alt*-anthrylene)
LUMO	Lowest energy unoccupied molecular orbital
MALDI-TOF	Matrix-assisted laser desorption/ionization time-of-flight
MCT	Macrocyclic trimer
MED	Microemissive displays
MEH-PPV	Poly(1-methoxy-4-(2-ethylhexyloxy)-*p*-phenylenevinylene)
MS	Metal-semiconductor
2,7-MT	2,7-Linked model trimer
3,6-MT	3,6-Linked model trimer
NBS	*N*-bromosuccinimide
NLO	Nonlinear optical
NMR	Nuclear magnetic resonance
NNP	*N*-methyl-2-pyrrolidone
NPD	*N,N′*-bis(1-naphthyl)-*N,N′*-diphenyl-1,1'-biphenyl-4,4'-diamine
OLED	Organic light-emitting diode
PANI	Polyaniline
2,7-PAP	Poly-2,7-(9,10-diarylphenanthrylene)
PAP	Poly-3,6-(9,10-diarylphenanthrylene)
PBD	2-(4-Biphenylyl)-5-(4-*tert*-bytylphenyl)-1,3,4-doxadiazole
PCC	Pyridinium chlorochromate
PCC	Pyridinium chlorochromate

PCz	Poly(2,7-carbazoles)
PDDBT	Poly(4,4'-didecyl-2,2'-bithiophene)
PDI	Perylene tetracarboxydiimide
PDT	Poly(3-decylthiophene)
PEDOT	Polyethylenedioxythiophene
PF	Poly(fluorene)
PFn	Polyfuran
2,8-PIF	Poly-2,8-indenofluorene
PITN	Polyisothianaphthene
2,7-PKP	Poly-2,7-(9,10-dialkylphenanthrylene)
3,6-PKP	Poly-3,6-(9,10-dialkylphenanthrylene)
PL	Photoluminescence
PLED	Polymer light-emitting diode
PNB	Pernigraniline base
PPE	Poly-*p*-phenyleneethynylene
PPh_3	Triphenylphosphine
PPP	Poly-*p*-phenylene
PPV	Poly-*p*-phenylenevinylene
PPy	Polypyrrole
PT	Polythiophene
SLMC	Step-ladder model compound
SLPPPA	Step-ladder poly(*p*-phenylene-*alt*-anthrylene)
TCNQ	Tetracyoanoquinonedimethane
TGA	Thermal gravimetric analysis
THF	Tetrahydrofuran
TMS	Trimethylsilyl
TMTSeF	Tetramethyl tetraselena fulvalene
TPD	*N,N'*-diphenyl-*N,N'*-bis(3-methylphenyl)-1,1'-biphenyl-4,4'-diamine
TTF	Tetrethiafulvalene
UV-vis	Ultraviolet-visible

VEH	Valence effective Hamiltonian
2D-WAXS	2D-wide-angle X-ray scattering

Chapter 1 Introduction: Conjugated Polymers

1.1 Conjugated Polymers; General

Polymers with spatially extended π-bonding system, abbreviated as "conjugated polymers" although known for many years, did not draw significant research attention until the mid 1970s. This was caused by the fact that the vast majority of them were intractable and, in many respects, showed inferior properties as compared to already developed polymers. Before 1977, studies dealing with polyconjugated systems were rare and the research devoted to these materials was not systematic. Neither molecular nor electronic structures of conjugated polymers in their undoped state were elucidated. In 1977 Heeger, MacDiarmid and Shirakawa showed that polyacetylene, which is the simplest polyconjugated system, can be rendered conductive by reaction with bromine or iodine vapors.[1] Spectroscopic studies that followed demonstrated without any ambiguity that this reaction is redox in nature and consists of the transformation of neutral polymer chains into polycarbocations with simultaneous insertion of the corresponding number of Br_3^- or I_3^- anions between the polymer chains in order to neutralize the positive charge generated on the polymer chain in the course of the doping reaction.[2] This important discovery initiated an extensive and systematic research into various aspects of the chemistry and physics of conjugated polymers both in their neutral (undoped) and charged (doped) states. To date, a surge of research on conjugated polymers has occurred, due to their potential use as components for electronic applications, such as superconducting polymers,[3] organic light-emitting diodes (OLEDs),[4-9] photovoltaic cells or photodiodes,[10-13] chemical sensors,[14] electrochemical cells,[15-17] photonic crystals,[18] actuators,[19] and field effect transistors (FETs).[20-25] In addition, there has been much recent interest in the demonstration that conjugated organic materials can be used in optically pumped microcavity lasers.[26-30]

In this Chapter, a general introduction into the principles behind the development of conducting polymers as well as the use of conjugated polymers as semiconducting,

emissive materials in OLEDs (their basic chemical/physical properties, mechanism, applications, etc.) are discussed. Even though conjugated polymers have been widely used for other applications as mentioned above, they are only briefly described since the main focus of this work is the synthesis and characterization of conjugated polymers for use in OLEDs. Finally, the motivation and framework of this thesis are presented.

1.2 Organic Conductors from Doped Conjugated Polymers

1.2.1 Principles of Conducting Polymers

It is convenient to start the discussion of the peculiarities of macromolecular polyconducting systems by the description of the electronic structure of polyacetylene for two reasons. First, polyacetylene is the simplest conjugated polymer and therefore can be considered as a prototype of other polyconjugated systems. Second, historically the discovery of doping in polyacetylene triggered most of the subsequent developments in electroactive polymers.

Polyacetylene can exist in two isomeric forms: cis-transoid and trans-transoid, commonly called *cis*- and *trans*-polyacetylene, respectively (see Figure 1.1). The latter form is thermodynamically more stable and cis-trans isomerization is irreversible. In polyacetylene each carbon atom is sp^2 hybridized and hence this polymer can be formally treated as a one-dimensional analogue of graphite. There exists, however, an important difference between the bonding systems in the graphene plane of graphite and in a polyacetylene chain. Unlike in graphite, the C-C bonds in polyacetylene are not equivalent, *i.e.* they are alternatively slightly longer and slightly shorter. This is due to the so-called Peierls distortion. This bond non-equivalence has an important effect on the electronic properties of polyacetylene because it opens a gap between the highest energy occupied molecular orbital (HOMO) level corresponding to a fully occupied π-band (valence band) and the lowest energy unoccupied molecular orbital (LUMO) level corresponding to an empty π^*-band (conducting band). Thus, in the simplest approach, polyacetylene can be treated as an intrinsic semiconductor with a bandgap of 1.5 eV.[31] In the years which followed several polyene-type and aromatic conjugated polymers were synthesized and characterized, the most extensively studied ones are depicted in Figure 1.1. All polymers

shown in Figure 1.1 exhibit strong absorption in the visible region of the electromagnetic spectrum usually attributed to a π-π^* optical transition (Figure 1.1). The first low bandgap semiconducting polymer was polyisothianaphthene (PITN) prepared by Wudl et al.[32] whose bandgap (1.1 eV) was about 1.0 eV lower than that of polythiophene (PT). Since then, several dozens of narrow gap polymers were synthesized which were mainly derivatives of PITN but also polymers based on 3,4-ethylenedioxythiophene (EDOT) units and vinylene units.[33,34] This research direction has drawn significant interest of the scientific community over the past years, however, a conjugated polymer with a vanishingly small bandgap has not yet been reported.

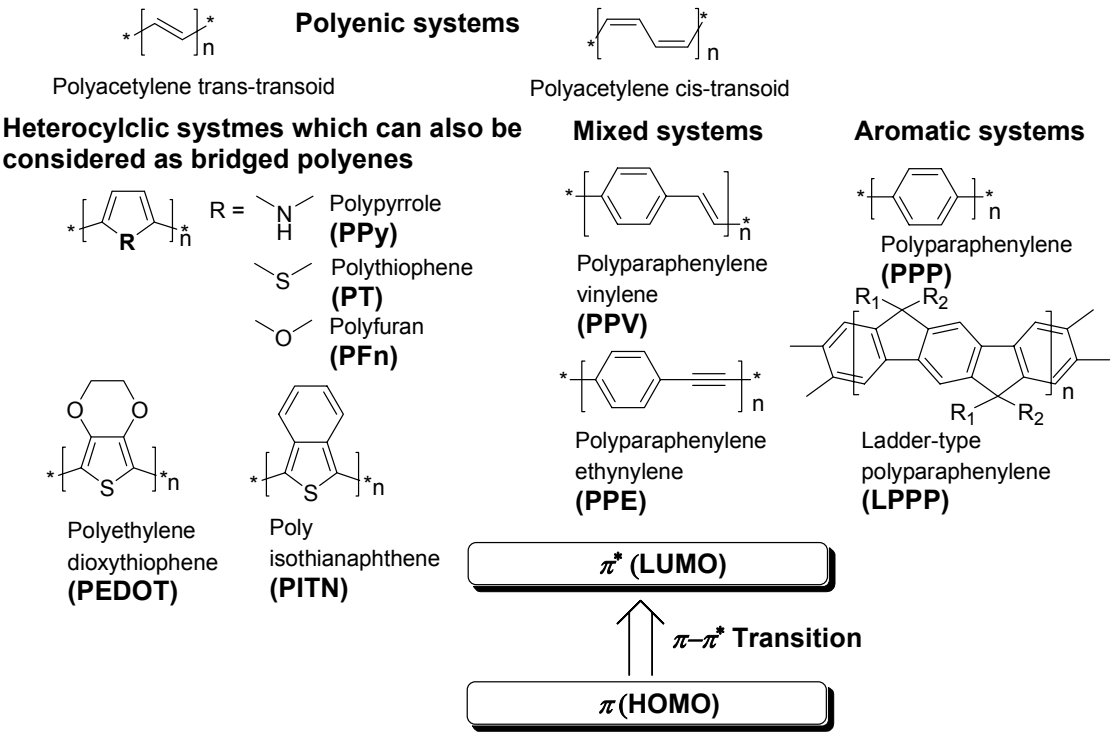

Figure 1.1. Representative conjugated polymers.

The chemical nature of the doping process as well as the structural and electronic properties of the resulting polymers have been extremely investigated. Two types of doping processes are usually encountered: the redox-type and the acid-base type.

Polyacetylene, poly-*p*-phenylene (PPP), polyheterocyclic polymers (polythiophene

(PT), polypyrrole (PPy), polyfuran (PFn), and their derivatives) and other polyconjugated systems with no strong basic centers in their backbone usually undergo the redox-type doping. The doping process is explained below using polyacetylene and PT as examples.

Oxidative (p-type) doping of polyacetylene can be carried out chemically or electrochemically and involves either chemical or anodic oxidation of the polymer chain to polycarbonium cations with simultaneous insertion of an appropriate number of anions between the polymer chains to neutralize the charge. Positive charges of polycarbonium cations are mobile and oxidized polyacetylene is a p-type (hole) conductor as shown from Hall effect and thermopower measurements.[35-37] The doping process is schematically depicted in Figure 1.2A.

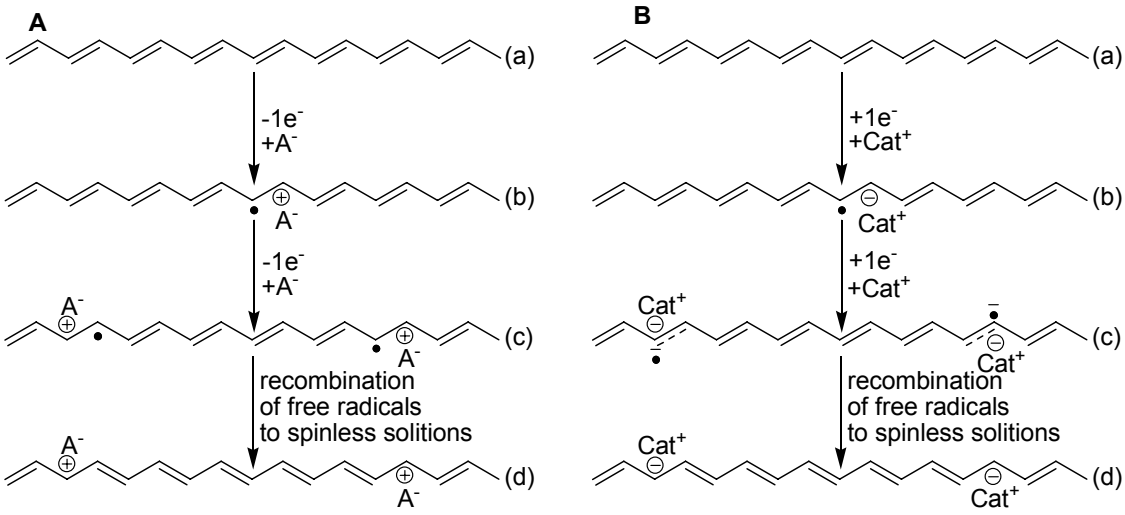

Figure 1.2. Doping of polyacetylene (A) p- type (B) n-type.

First, the abstraction of an electron from the π-system of polyacetylene chain results in the formation of a radical cation. Removal of a second electron gives rise to a second radical cation. The two radicals combine to give a spinless dication. Further oxidation occurring in the same manner leads to spinless charge carriers called positive solitons.[38] Note that each soliton constitutes a boundary which separates domains differing in the phase of their π-bonds. By hole-electron symmetry, one may postulate an analogous picture for n-type doping of polyacetylene. In this case

neutral chains are either chemically or electrochemically reduced to polycarbonium anions and simultaneously charge compensated cations are inserted into the polymer matrix. Figure 1.2B shows schematically the doping process. In this case, negatively charged, spinless solitons are the charge carriers.

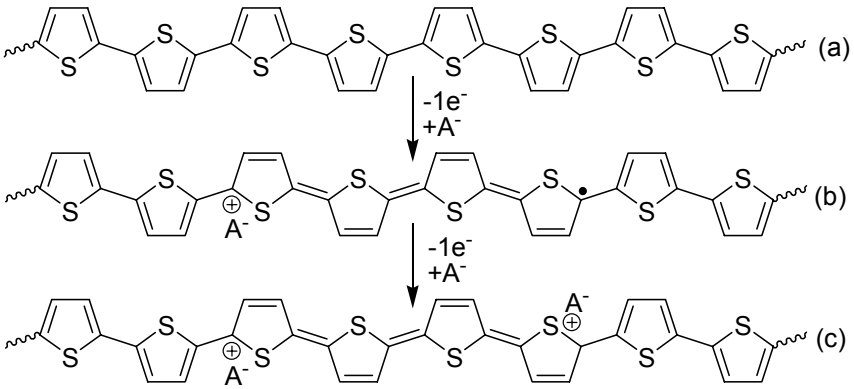

Figure 1.3. p-Type doping of poly(thiophene).

With heterocyclic conjugated polymers, different charge configurations are formed upon doping. The removal of one electron from the π-conjugated system of PT results in the formation of a radical cation (Figure. 1.3b). This radical cation, called a polaron, is of a special nature because its presence induces the creation of a quinone-type domain within the poly(2,5-thienylene) chain. The removal of the next electron then leads to the creation of another polaron or to a spinless bipolaron which is a dication separating the quinoid domain from the aromatic region of the polymer chain (Figure. 1.3c). Electrochemical doping is especially suitable for the identification of the type of charge carriers. If the charge introduced during electrochemical doping is measured by coulometry and at the same time the number of spins created is monitored by electron paramagnetic resonance (EPR), a spin-charge correlation can be established. In the case of PT such correlation unequivocally shows that during doping polarons are formed initially which then recombine to bipolarons.[39]

The π-conjugated system in all polymers is formed by the overlap of carbon p_z orbitals. There exists, however, another family of conjugated polymers in which p_z orbitals of nitrogen also contribute to the conjugation. The representatives of this type of macromolecular compounds include polyaniline (PANI),[40] its derivatives, aromatic

polyazomethines and others.[41,42] It is suitable to discuss PANI separately from other conjugated polymers because it shows distinctly different chemistry as compared to other polyconjugated systems. This is mainly associated with the presence of basic centers (amine and imine nitrogens) in its conjugated backbone. Polyaniline is the most extensively studied macromolecular compound from this category of conjugated polymers for conducting materials.

Neutral PANI can exist in a variety of forms which differ in their oxidation states. Principal neutral (base) forms of PANI are depicted in Figure 1.4A. The most reduced form, commonly called leuco-emeraldine, consists of phenylene rings joined together by amine type nitrogens. In fully oxidized PANI, termed pernigraniline, phenylene rings with benzenoid type sequence of bonds and rings of quinoid type of bonds are present in the ratio 1:1 and are separated by imine nitrogens. In the half oxidized polymer (emeraldine) imine and amine nitrogens are in equal numbers but the ratio of benzenoid type rings to the quinoid type ones is 3:1. For this reason the repeat unit of emeraldine must consist of four rings and four nitrogens.

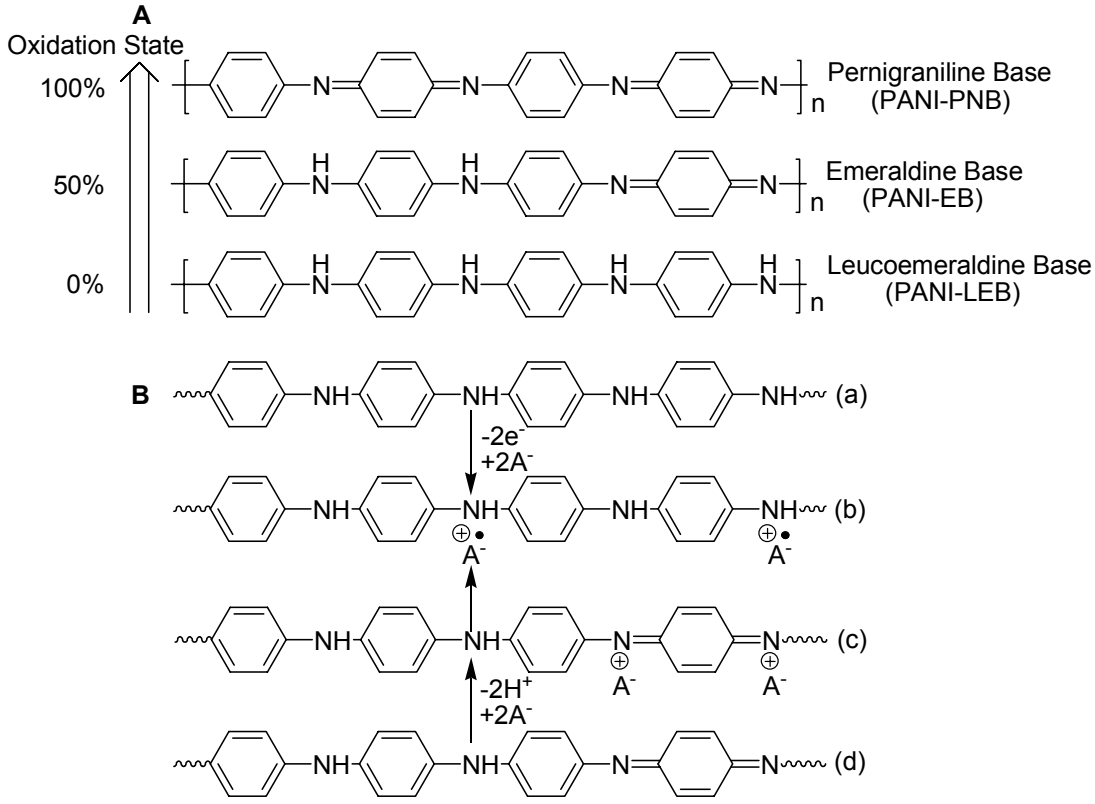

Figure 1.4. Polyaniline (A) principal forms and (B) oxidation and acid-base doping.

The most reduced form of PANI-leucoemeraldine-LB can also undergo oxidative type of doping (see Figure 1.4B (a) and (c)). In this case the oxidation of neutral LB chain leads to radical cations, *i.e.* polarons. However, PANI and other conjugated polymers possessing strong basic centers in their backbone can be doped not only in a redox process but also by an acid-base one. This type of acid-base doping can be most clearly explained using the semi-oxidized form of PANI, emeraldine base (EB) as an example. EB can be protonated with a sufficiently strong protonic acid to give the corresponding salt form (ES). It is known from spectroscopic studies that imine nitrogens are preferentially protonated. Thus protonation of EB gives initially a product in which the charge is stored in the form of bipolarons (see Figure 1.4B (c) and (d)). Then charge redistribution occurs which can be considered as an internal redox process which transforms the bipolarons into polarons (so-called polaron lattice). The polymer chain adopts the structure of polysemiquinone radical. Note that the oxidative doping of LB leads to the same product as the acid-base doping of EB. However, in the latter case the number of electrons in the polymer chain does not change upon doping and the charge is introduced by protonation. Fully doped EB is frequently depicted in the literature as PANI$(HA)_{0.5}$ where PANI corresponds to the repeat unit consisting of one ring and one nitrogen of the average formula $C_6H_{4.5}N$ and HA is the protonating acid molecule.

To summarize, since the doping process involves the transfer of the charge to or from π-bonding system of the conjugated polymer, leaving the σ-system essentially intact, the structural identity of an individual chain is preserved. However, vibrational, electronic, and other properties of the polymer are strongly altered upon doping as well as its supramolecular structure. The most important consequence of doping is the increase in polymer conductivity by several orders of magnitude. In some cases conjugated polymers reach the conductivity of metals with a negative temperature coefficient which is characteristic of metallic behavior.[43-47]

1.2.2 Mechanism and Methods of Doping

The electrical conductivity results from the existence of charge carriers (through doping) and the ability of these charge carriers to move along the π-bonded "highway."

Doped conjugated polymers are good conductors for two reasons:

(1) Doping introduces carriers into the electronic structure. Since every repeat unit is a potential redox site, conjugated polymers can be doped reductively (n-type) or oxidatively (p-type) to generate a relatively high density of charge carriers.[48]

(2) The attraction of an electron in one repeat unit to the nuclei in the neighboring units leads to carrier delocalization along the polymer chain and to charge carrier mobility, which is extended into three dimensions through interchain electron transfer.

Charge injection onto conjugated, semiconducting macromolecular chains i. e. doping, leads to a wide variety of interesting and important phenomena that define the field. As summarized in Figure 1.5, reversible charge injection by "doping" can be accomplished in a number of ways.

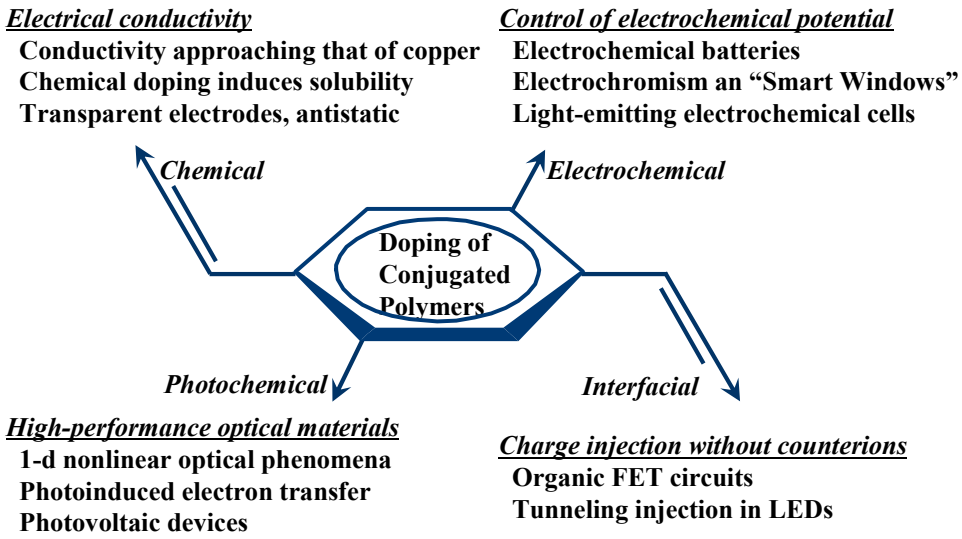

Figure 1.5. Doping mechanisms and related application.

A. Chemical Doping by Charge Transfer. The initial discovery of the ability to dope conjugated polymers involved charge-transfer redox chemistry, oxidation (p-type doping), or reduction (n-type doping),[48-50] as illustrated by the following examples:

a. p-type

$$(\pi\text{-polymer})_n + 3/2\ ny(I_2) \rightarrow [(\pi\text{-polymer})^{+y}(I_3^-)_y]_n \qquad (1)$$

b. n-type

$$(\pi\text{-polymer})_n + [Na^+(\text{naphthalide})^\bullet]_y \rightarrow [(Na^+)_y((\pi\text{-polymer})^{-y}] + (\text{naphthalene})^0 \qquad (2)$$

When the doping level is sufficiently high, the electronic structure evolves towards that of a metal.

B. Electrochemical Doping. Although chemical doping is an efficient and straightforward process, it is typically difficult to control. Complete doping to the highest concentrations yields reasonably high quality materials. However, attempts to obtain intermediate doping levels often result in inhomogeneous doping. Electrochemical doping was adopted to circumvent this problem.[51] In electrochemical doping, the electrode supplies the redox charge to the conducting polymer, while ions diffuse into (or out of) the polymer structure from the nearby electrolyte to compensate the electronic charge. The doping level is determined by the voltage between the conducting polymer and the counter electrode; at electrochemical equilibrium the doping level is precisely defined by that voltage. Thus, doping at any level can be achieved by setting the electrochemical cell at a fixed applied voltage and simply waiting as long as necessary for the system to come to electrochemical equilibrium (as indicated by the current through the cell going to zero). Electrochemical doping is illustrated by the following examples:

a. p-type

$$(\pi\text{-polymer})_n + [Li^+(BF_4^-)]_{soln} \rightarrow [(\pi\text{-polymer})^{+y}(BF_4^-)_y]_n + Li(electrode)^0 \quad (3)$$

b. n-type

$$(\pi\text{-polymer})_n + Li(electrode) \rightarrow [(Li^+)_y(\pi\text{-polymer})^{-y}]_n + Li^+(BF_4^-)_{soln} \quad (4)$$

C. Doping of Polyaniline by Acid-Base Chemistry. Polyaniline provides the prototypical example of a chemically distinct doping mechanism as described previously (Figure 1.4). Other methods (photo-and interfacial-doping) have also been of interest. However, since those studies are outside the scope of my work, they are not discussed herein. It should be pointed out that n-doped conjugated polymers are much more reactive than the p-type. Usually their conductivity drops drastically upon exposure to ambient atmosphere even for a short duration due to reaction with aerial oxygen.

As indicated in Figure 1.5, each of the methods of charge-injection doping leads to unique and important phenomena. In the case of chemical and/or electrochemical doping, the induced electrical conductivity is permanent, until the carriers are chemically compensated or until the carriers are purposely removed by "undoping."

In the case of photoexcitation, the photoconductivity is transient and lasts only until the excitations are either trapped or decay back to the ground state. In the case of charge injection at a metal-semiconductor (MS) interface, electrons reside in the π^*-band and/or holes reside in the π-band only as long as the biasing voltage is applied.

Because of the self-localization associated with the formation of solitons, polarons, and bipolarons, charge injection leads to the formation of localized structural distortions and electronic states in the energy gap.[52] In the case of "photodoping", the redistribution of oscillator strength associated with the subgap infrared absorption and the corresponding bleaching of the interband (π-π^*) transition provide a route to nonlinear optical (NLO) response. Real occupation of low-energy excited states[52,53] and virtual occupation of higher energy excited states lead to, respectively, resonant and nonresonant NLO response.

By charge-injection doping at an MS interface, the polymer semiconductor can be used as the active element in thin film diodes[54] and field effect transistors (FETs).[20,55,56] Tomozawa et al.[54] demonstrated the first example of an electronic device component fabricated by casting the active polymer directly from solution; even these early diodes exhibited excellent current-voltage characteristics. Dual carrier injection in metal/polymer/metal structures provides the basis for polymer light-emitting diodes (LEDs).[57] In polymer LEDs, electrons and holes are injected from the cathode and anode, respectively, into the undoped semiconducting polymer; light is emitted when the injected electrons and holes meet in the bulk of the polymer and recombine with the emission of radiation.[4] Thus, as summarized in Figure 1.5, doping is a common feature of conducting polymers; doping leads to a remarkably wide range of electronic phenomena.

1.2.3 Application of Doped Conjugated Polymers

Not surprisingly π-conjugated polymers have been the focus of extensive research,[58] ranging from applications of “conventional” polymers *(e.g.,* PT, PANI, PPy) in charge storage devices such as batteries and supercapacitors, to new polymers with specialized conductivity properties such as low bandgap and intrinsically conducting polymers. Indeed, many successful commercial applications of these polymers have

been available for more than fifteen years, including electrolytic capacitors, "coin" batteries, magnetic storage media, electrostatic loudspeakers, and anti-static bags. It has been estimated[59] that the annual global sales of conducting polymers in the year 2006 will surpass more than one billion US dollars.

There are two main groups of applications for these polymers. The first group utilizes their conductivity as its main property. The second group utilizes their electroactivity. The extended systems of conjugated polymers are highly susceptible to chemical or electrochemical oxidation and reduction. These alter the electrical and optical properties of the polymer, and by controlling this oxidation and reduction, it is possible to precisely tailor their properties. Since these reactions are often reversible, it is possible to systematically control the electrical and optical properties with a great deal of precision. It is even possible to switch from a conducting state to an insulating state. The two groups of applications are shown below:

Group 1	**Group 2**
Electrostatic materials	Molecular electronics
Conducting adhesives	Electrical displays
Electromagnetic shielding	Chemical, biochemical and thermal sensors
Printed circuit boards	Rechargeable batteries and solid electrolytes
Artificial nerves	Drug release systems
Antistatic clothing	Optical computers
Piezoceramics	Ion exchange membranes
Active electronics (diodes, transistors)	Electromechanical actuators
Aircraft structures	'Smart' structures
	Switches

1.2.4 Polymeric Superconductors

The first organic superconductor was discovered in the early 1980s.[60] It was prepared by electrochemical oxidation of tetramethyl tetraselena fulvalene (TMTSeF) to give a salt of the following stoichiometry $(TMTSeF)^{+}_{2}X^{-}$ (where X^{-} is a monovalent anion of ClO_4^{-}, PF_6^{-} or other type). TMTSeF is a derivative of tetrethiafulvalene (TTF) which is the electron donating component of the first organic metal, *i.e.* a charge transfer complex of

TTF-TCNQ (where TCNQ is the abbreviation for tetracyoanoquinonedimethane a well-known organic acceptor). In the years which followed several new ion-radical salts were discovered. The success in the preparation of organic superconductors, among others, was based on the fact that single crystals of sufficient quality to observe superconductivity could be grown on the electrode if sufficiently low current densities were used. The preparation of such highly ordered structures is of course much more difficult in the case of macromolecular systems. Therefore up to 2001 the only known case of a polymeric superconductor was poly(sulfur nitride) $(SN)_X$. This inorganic polymer, which becomes a superconductor at extremely low temperature, *i.e.* T_c = 0.26 K, can be prepared in the form of single crystals via solid-state polymerization of S_2N_2.[3] The preparation of ordered layers of conjugated organic polymers is of course much more difficult. First, chains with highly regular microstructure and low polydispersity must be prepared. Second, special solution processing conditions must be used which facilitate the crystallization of ordered structures. Then chemical or electrochemical doping must be carried out in order to create free charge carriers. The latter process is the least desirable in that doping induces disorder even in cases where it was carried out in solution using, counter-ion induced processability. Solution processed doped polymers are only partially ordered and their crystallinity index usually does not exceed 40 %.[61]

To date no chemically or electrochemically doped conjugated polymer has been found to be superconducting. This is probably due to the fact that doping and processing techniques developed to date do not lead to supramolecular structures sufficiently ordered to assure the formation of a continuous network of superconducting zones. Many scientists strongly believe, however, that the recent rapid progress in this area of materials research will lead to chemically doped conjugated polymer superconductors in the near future.

1.3 Organic Semiconductors from Undoped Conjugated Polymers

1.3.1 Background

Inorganic semiconductor devices have been instrumental in shaping the development of our modern society which is so dependent on rapid communication of information. Recently, electronics and photonics technologies have widened

their materials base to include organics, in particular π-conjugated oligomers and polymers as semiconductors. The goal with organic/polymeric-based devices is not necessarily to attain or exceed the level of performance of inorganic semiconductor technologies (silicon is still the best material for many of the current applications) but to benefit from a unique set of characteristics combining the electrical properties of semiconductors with the properties typical of plastics, that is, low cost, versatility of chemical synthesis, ease of processing, and flexibility.

A major breakthrough in the field of organic electronics was the 1987 report by Tang and VanSlyke at Kodak of the first electroluminescent device based on a π-conjugated molecular material, tris(8-hydroxy-quinoline) aluminum (Alq_3).[62] Shortly thereafter, Friend and his group at Cambridge discovered electroluminescence (EL) in a conjugated polymer, poly-*p*-phenylenevinylene (PPV), thereby opening the way for the fabrication of polymer light-emitting diodes (PLEDs).[4] Since then there has been a considerable amount of research time and effort devoted to developing conjugated materials for use in electronic display applications such as PLEDs, polymer lasers, photovoltaic cells, field effect transistors, etc. The rest of this chapter will focus on electroluminescence (EL) from organic materials and discuss OLEDs in detail whereas other areas (solar cell, FET, and etc.) will only briefly be touched upon.

1.3.2 Application of Undoped Conjugated Polymers

Typically, an organic light-emitting diode (OLED)[5] is comprised of the following components: a transparent electrode made of a high work function compound, usually indium-tin oxide (ITO); one or more organic layers that in the case of molecular materials are generally deposited by vacuum sublimation[63] or in the case of polymers are generally deposited by spin coating or ink-jet printing;[64] and a top metallic electrode made of a low work function metal or alloy. Four main processes occur upon application of a forward bias to an OLED device, as sketched on the top of Figure 1.6. (i) Charge injection: Electrons (holes) are injected from the Fermi level of the low (high) work function metal into the lowest unoccupied (highest occupied) electronic levels of the organic material present at the metal-

organic interface. (ii) Charge transport: Electrons and holes drift in opposite directions within the organic layer(s) (usually in a dispersive manner) under the influence of the static electric field generated by the forward bias. (iii) Charge recombination: Electrons and holes approaching one another are captured and recombine to form either singlet or triplet excitons; during their lifetimes, excitons can hop among molecules/chains via energy-transfer processes. (iv) Excitation decay: When excitons decay radiatively, the generated light can escape from the device through the transparent side.

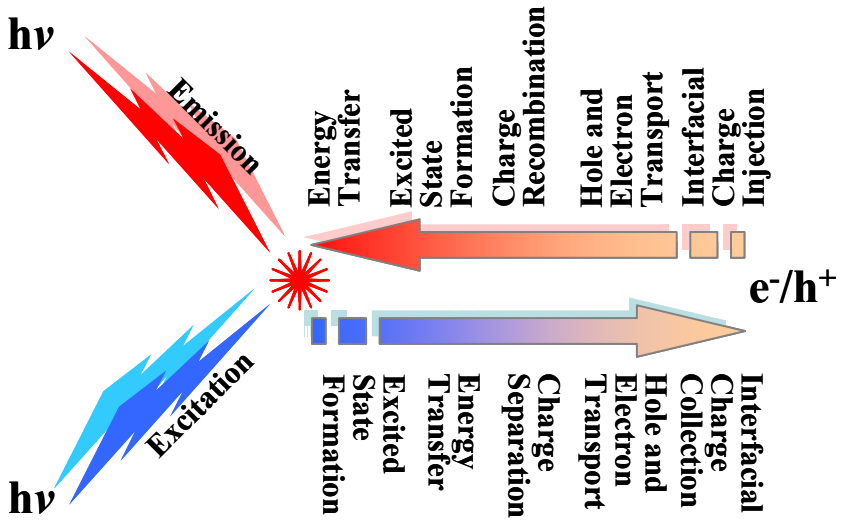

Figure 1.6. Illustration of the various processes governing the operation of (top) OLEDs and (bottom) solar cells.

In electrophosphorescent diodes, a phosphorescent dye is present as a guest in a host matrix and exciton transfer can take place from the host matrix to the guest; high efficiencies are reached since both singlet and triplet excitations generated in the host can transfer to the guest and contribute to the luminescence signal.[65] In PLEDs, in the absence of phosphorescent dyes, only singlet excitons generate light.

OLEDs have recently entered the market place as active elements in low-resolution displays such as those commercialized, for instance, by Pioneer in car stereo systems, by Kodak in digital cameras, or by Philips in electric shavers.[66] The

production of high-resolution full-color flexible displays for television screens is the next target.

Organic materials are also emerging as promising candidates for the fabrication of transistors, photo-diodes and solar cells, and (bio)chemical sensors.[11,12,67-71] Photovoltaic devices have an overall architecture similar to that of LEDs; the active organic layers are generally made of two components and sandwiched between two electrodes of a different or the same nature. However, the mode of operation is opposite to that of LEDs, as illustrated on the bottom of Figure 1.6. The main steps are as follows. (i) Light absorption: Light is absorbed in the organic layers and generates singlet excitons; for solar cells, absorption should match the solar spectrum as closely as possible, (ii) Energy-transfer and exciton dissociation: Excitons have to migrate toward the interfacial region between the organic components where charge separation occurs as a result of electron-transfer (ET) between the donor and acceptor;[11,12] the efficiency of the charge separation process very much depends on the supramolecular organization at the heterojunction. (iii) Charge transport: The charges that remain separated (and hence do not recombine after exciton dissociation) drift in the organic layers under the influence of the electric field generated by the equalization of the Fermi energy levels of the two electrodes. (iv) Charge collection: The charges ultimately have to be collected at the electrodes.

In organic field effect transistors, the key steps are as follows: (i) formation of a conducting channel within the organic semiconductor due to the application of a gate voltage; upon application of a drain voltage, (ii) charge injection from the source electrode into the organic semiconductor, or (ii) charge transport across the organic layer; and (iii) charge collection at the drain electrode. Charge injection and collection processes actually correspond to redox reactions, that is, electron-transfer reactions. Biochemical or chemical sensors based on π-conjugated polymers usually rely on optical absorption, followed by fast energy transfer and charge separation at the quenching (sensing) site.[69-71]

In principle, the same conjugated polymers can be used for the fabrication of optically pumped conjugated polymer based lasers. In the simplest description

lasers are devices emitting a spectrally narrow radiation, which is spatially coherent and strongly polarized. Lasing in conjugated polymers was first reported by Moses[72] who used poly(1-methoxy-4-(2-ethylhexyloxy)-*p*-phenylenevinylene) (MEH-PPV) in a solution of xylene or chloroform. The construction of conjugated polymer-based photopumped lasers raised the question whether electrically-driven polymer diode lasers can be made? This is a more difficult task because of the fact that losses in diode structures are much higher than in photopumped waveguides. They are mainly associated with charge induced absorption and the absorption of the metal electrode. Electrically-driven organic lasers have yet to be constructed.

1.3.3 Design and Configuration of Organic Light-Emitting Diodes (OLEDs)

In the simplest version a PLED consists of a single layer of an electroluminescent polymer and two electrodes as depicted on the right of Figure 1.7. One of the electrodes must be transparent to transmit light emitted during electroluminescence. This is usually the anode (hole injecting electrode), the typically used material being ITO a conductor which shows high transparency in thin layers. In a simpler form, the operation of the single-layer device was formerly described, which is schematically described on the left of Figure 1.7. At the electrodes there exist barriers for hole and electron injection (ΔE_h and ΔE_e). Usually the barrier for electron injection from the metal electrode is higher than that for hole injection from the ITO electrode. Injected opposite charge carriers may form either singlet or triplet excitons, of which the former decay radiatively, *i.e.* give out light. In the majority of conjugated polymer-based LEDs holes are dominant charge carriers due to the fact that $\Delta E_e > \Delta E_h$. The phenomenon of electroluminescence requires however both types of carriers, the quantum efficiency will therefore depend strongly on the electron injection barrier.

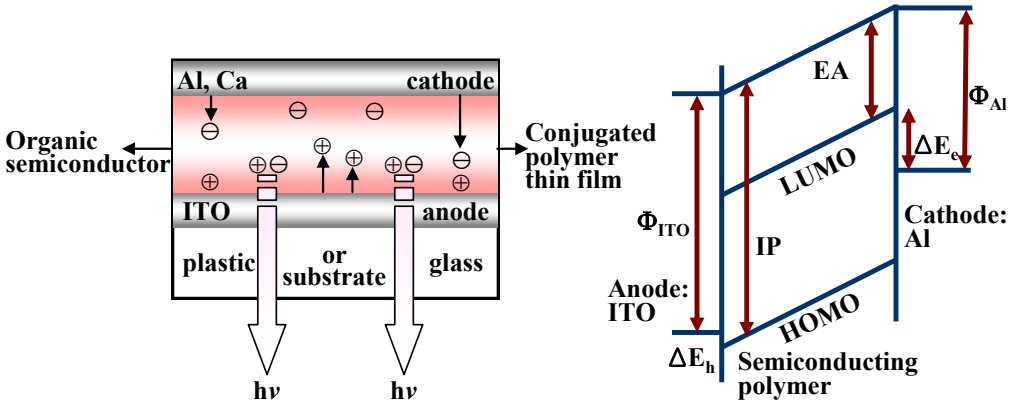

Figure 1.7. Schematic structure and band diagram of a single-layer OLED.

In single-layer PLED devices the electroluminescence mainly occurs in the vicinity of the cathode because the mobility of positive charges in conjugated polymers is usually higher. This has a negative impact on the luminance efficiency because near the electrode the probability of non-radiative recombinations is very high. Thus it is favorable to generate the excitons away from the electrodes. One of the possible solutions is to fabricate a two-layer device in which the cathode and the electroluminescent polymer are separated by an electron transporting layer (Figure 1.8).[73,74] It is instructive to give one example of such an approach. A PPV derivative with solubilizing alkoxy groups on the ring and cyano group attached to the vinylic carbon (MEH-CN-PPV) has significantly different properties as compared to unsubstituted PPV. First, it is solution processable. Second, the presence of electron withdrawing group increases the electron affinity of this polymer while maintaining the π-π^* gap similar to that measured for MEH-PPV.

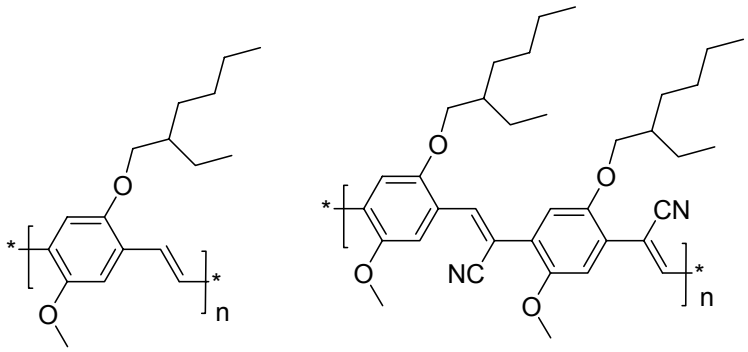

MEH-PPV **MEH-CN-PPV**

Due to higher electron affinity, MEH-CN-PPV is a much better n-type conductor and can be used for the deposition of an electron transporting layer. In a two layer device (PPV/MEH-CN-PPV), the formation of the excitons followed by their radiative decay occurs at the interface between both polymers. As a result, the electroluminescence quantum efficiency increases. Also, more facile electron injection from the metal electrode with higher work function, for example Al, is now possible. The replacement of Ca by Al greatly facilitates the fabrication of PLEDs.[6] Similarly one can separate the anode from the light-emitting polymer by introducing a hole transporting layer which facilitates hole injection and in many cases improves the stability of the PLED and decreases its operating bias voltage. Several types of materials were used for this purpose, among other thin transparent layer of doped conjugated polymers exhibiting p-type conductivity such as doped PANI [75-78] or doped PEDOT.[79] In principle one can design three- or more-layer devices in order to improve the device parameters, one must however be aware of the fact that the cost of fabrication increases significantly for multilayer heterostructures and the possible disruption of the lower layers boosts when depositing upper layers.

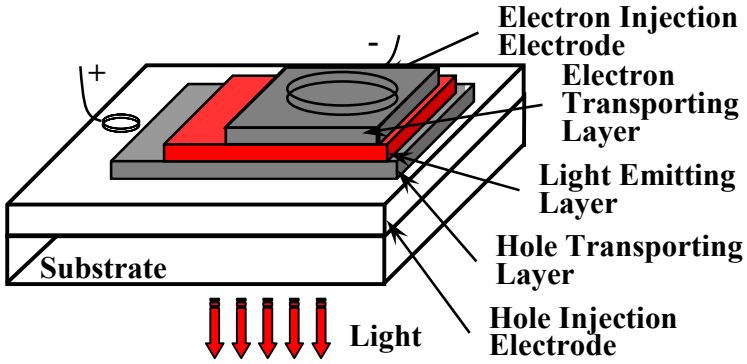

Figure 1.8. Schematic configuration of a two-layer OLED.

The design and fabrication of PLED based displays is a challenging task for chemists, materials scientists, physicists and electronic engineers. In view of the application of PLEDs in multicolor displays it is necessary to precisely tune the color with the goal to obtain red, green and blue PLEDs with a relatively narrow

emission peak. This can be done by appropriate functionalization of the polymers and varying their π-π^* optical gap. Electroluminescence of poly(alkylthiophene)s is an instructive example of such an approach.[80] Regioregular, head-to-tail coupled poly(3-decylthiophene) (PDT) is an electroluminescent polymer emitting in the red with good color purity. Its main disadvantage is a rather low quantum yield. Its isomer regioregular poly(4,4'-didecyl-2,2'-bithiophene) (PDDBT) which has a head-to-head, tail-to-tail coupling sequence shows one order of magnitude higher quantum efficiency for photo and electroluminescence and emits in the green. The observed blue shift in the electroluminescence spectra is due to significantly larger optical gap in PDDBT as compared to PDT caused by the head-to-head linkages inducing out-of-plane twisting of the polymer backbone. Similar influence of regioregularity and substituent alteration on the color of light-emitting was reported for pyridine-based analogues of PPV.[81] As it has already been mentioned ring-disubstitued PPV derivatives with CN group attached to the vinylic carbon constitute another family of electroluminescent polymers with tunable color of emitted light from near infrared to blue.[82]

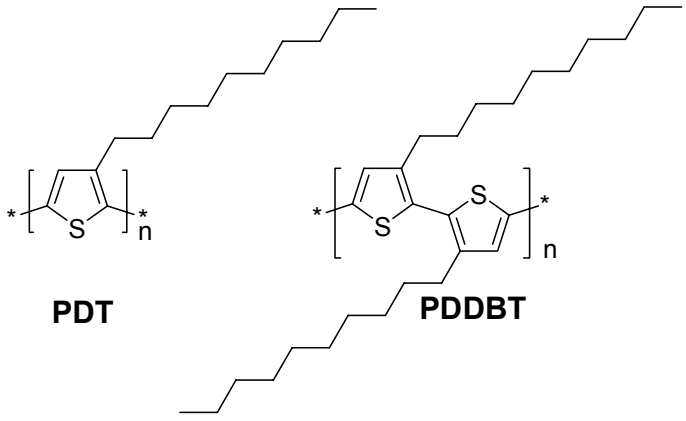

Blue emission is the most difficult to achieve not only in PLEDs but also in inorganic semiconductor-based LEDs. Polymers suitable for the fabrication of blue emitting PLEDs must show a high π-π^* (HOMO-LUMO) gap. Phenylene-based polymers can be used for this purpose, including poly(fluorene)s (PFs) (including both homo- and copolymers)[6] and ladder poly(*p*-phenylene)s (LPPPs).[83]

Due to solution processability of new generations of electroluminescent polymers, ink-jet techniques can be applied in the fabrication PLED-based multicolor displays. Commercial application of PLED-based devices requires materials with high purity, facile processability, good thermal and oxidative stability. Enormous progress has been achieved in this respect in the last few years.[6]

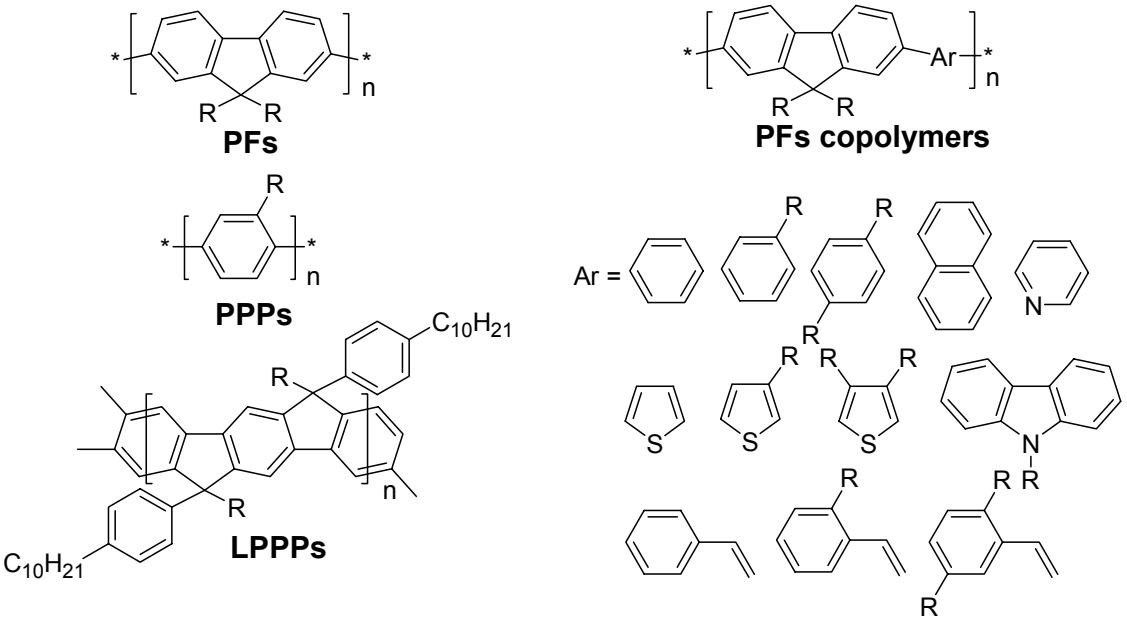

1.3.4 Why are PLEDs important?

The first high profile commercial PLED product a shaver made by Philips was advertised in 2002. In 2003, significant improvements in device lifetimes based on PLED technology, including over 20,000 hour lifetimes for blue polymer devices were achieved. These achievements marked great steps towards the successful commercialization of PLEDs. And in 2004, Philips incorporated a PLED display into a "Magic Mirror" mobile telephone. In the same year, CDT licensee Microemissive Displays (MED) produced a display for a NHJ 3-in-1 miniature camera/MP3 player incorporating a PLED microdisplay as viewfinder. Since their discovery, PLEDs have been researched intensively worldwide; resulting from their special advantages compared with other kinds of displays materials. The main

advantages of PLED can be summarized as :

Figure 1.9. Example of various colors (left) and view angle of PLEDs (right).

(1) High brightness and long lifetime can be achieved; The brightnesses of PLEDs have increased very rapidly since their discovery. Currently the Luxeon LED family of light bulbs from Philips lasts 100 times longer, and is up to 4 times brighter than standard incandescent bulbs. And a long lifetime for PLEDs has been achieved by CDT as mentioned above.

(2) Low power consumption; High brightness at low voltage and high power efficiency are obtained.

(3) All kinds of color are available from light emitting polymers, as shown in Figure 1.9 (left).

(4) No viewing angle dependence; Compared with LCD displays, one important advantage is that PLEDs do not have a view angle dependence. Their view angle can be large as 160° as displayed in Figure 1.9 (right).

(5) Permits flexible lighting and displays.

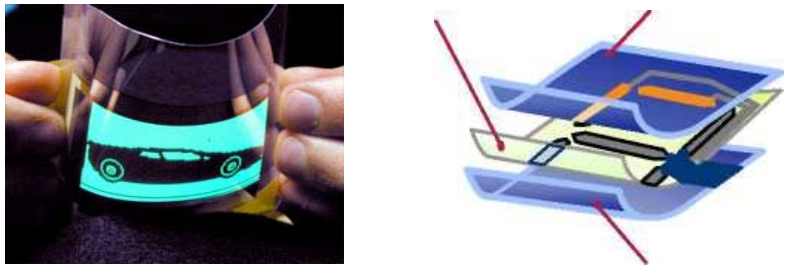

Figure 1.10. Potential application as flexible lighting and displays.

(6) Simple to use technology; PLEDs are much cheaper to make than conventional solid-state LED and lasers. Spin-coating and ink-jet printing (developed by CDT and Seiko-Epson) are two of the most important techniques.

(7) Useful for large area lighting; Ink-jet printing technique provides the possibility to make large are lighting, using PLED.

Properties of light emitting polymers determined many aspects of PLEDs, especially their emitting efficiency. Current light emitting polymers are not efficient enough for applications. And new light emitting polymers are still needed to be researched, and the way of increasing the emission efficiency by modify some structure are necessary. The most important parameter of a PLED is its efficiency, which can be expressed as an equation:

$$\eta_\Phi = \gamma\eta_F\eta_\gamma \quad (5)$$

In the above equation, γ is charge injection factor, η_F fluorescence quantum yield, and η_γ efficiency of singlet exciton formation.

Many conjugated molecules are highly luminescent when they are dilute in solution. For example, the dyes in dye lasers can achieve an efficiency *ca*. 100%, and for PPP: η_F *ca*. 30% has been achieved. The efficiency of singlet excitons formation (η_γ) is strongly material and chemical structure dependent.

To summarize, OLEDs have greatly been improved with respect to reliability, efficiency and tunability. Their performance is now comparable to, and in some cases even better than, that of commercially available light-emitting devices based on inorganic semiconductors. Moreover, they can produce polarized light and emit any color in the visible region, including white - something that is still difficult to achieve with inorganic materials. Materials scientists have designed and synthesized a great variety of appropriate materials over the last couple of years. Only a few of them have been investigated thoroughly. Possibly, the best materials are still unknown or the potential of already available materials has not been recognized. Currently, two concepts compete for prevalence in the field of organic electroluminescence. Devices of both conjugated polymers and low molecular weight materials have been reported to exhibit excellent performances. Up to now, the most promising materials are PFs, polyquinoxalines, and PPVs on one hand and

multicomponent systems comprising metal chelates (Alq_3), highly fluorescent dopant emitters (rubrene, coumarins, quinacridone), triarylamines (*N,N′*-diphenyl-*N,N′*-bis(3-methylphenyl)-1,1'-biphenyl-4,4'-diamine (TPD), *N,N′*-bis(1-naphthyl)-*N,N′*-diphenyl-1,1'-biphenyl-4,4'-diamine (NPD)) and simple oxadiazole compounds (2-(4-biphenylyl)-5-(4-*tert*-bytylphenyl)-1,3,4-doxadiazole (PBD)) on the other hand. The highest luminous efficiency reported for a poly(9,9-dialkylfluorene)-based OLED exceeded a value of 20 Lm/W and is hence already competitive with commercially available inorganic LEDs. On the contrary, the highest external quantum efficiency (>7 %) has been attained for a coumarin-doped sublimed molecular film device that used an Alq_3 derivative as electron and NPD as hole transporting material. Though the "small-molecule" approach has a tentative advantage in brightness (with values surpassing 140,000 cd/m^2) and demonstrated lifetime (exceeding 50,000 h of continuous operation), the current rate of development and improvement of diodes based on both types of materials are extremely fast. The polymer approach seems to be less sensitive to higher temperatures and holds the promise of much lower fabrication costs. Whilst the production of sublimed molecular film devices typically requires vapor deposition, conjugated polymers offer the possibility to manufacture large area displays by simple roll-to-roll coating techniques. However, the two concepts seem not to exclude one another, since combinations of both approaches have already been demonstrated. For the near term, it appears that both technologies with their specific advantages and drawbacks will coexist. Although efficiency and durability of devices based on any type of organic material still can and need to be further improved with respect to high-end applications, these obstacles will soon be overcome if the current rate of progress continues.

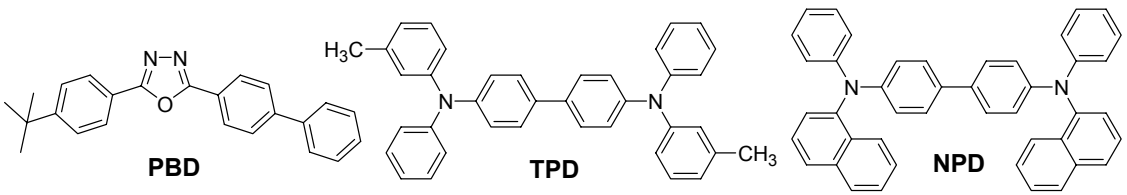

1.4 Motivation for the Present Work

1.4.1 Can metallopolymers be rendered highly conductive?

As reviewed above, the study of conducting polymers has blossomed into a mature field over the last six decades.[84] Tremendous progress has been made towards the goal of developing functional organic materials with delocalized *pi*-electrons as electronic conductors.[34] In such systems, chemical or electrochemical doping produces charged species within the polymer backbone and the mobility of these charges defines the bulk conductivity of a given material. In organic based materials, charge is efficiently shuttled due to isoenergetic states throughout the polymer backbone that can be interrupted by defects in the polymer strand (*i.e.*, non-conjugated linkages, short conjugation length, or chemically altered monomer units). The vast majority of investigations performed in this field to date have dealt with purely organic frameworks and electron/hole transport in these systems is reasonably well understood. The incorporation of transition metals has the potential to greatly expand the function and ultimate applications of conducting polymer systems. More specifically, there is a steady and growing effort to incorporate redox-active metal centers into conducting polymer structures to create highly efficient redox conductivity for sensory (*i.e.*, anions and small molecules), catalytic, photochemical, and photoelectronic applications. In conducting metallopolymers an understanding of the interactive roles that the metal centers and the organic polymer backbone play is in its early stages. Metal centers can provide not only efficient sites for redox activity but also act as thermodynamic sinks that trap/localize charges due to the introduction of low-lying energetic states. A few selected systems have demonstrated important applications, however, the potential of conducting metallopolymers is largely unrealized. In this context, the paper[85] by Swager et al which highlights the general principles that need to be met in order to generate highly conductive metallopolymers must be mentioned. This is classified into one of two categories (inner or outer sphere) depending on the mode of interaction between the transition metal centers with each other and the conducting polymer backbone.

1.4.1.1 Mechanisms of Conductivity in Metallopolymers

Two distinctly different redox conductivity mechanisms pervade the conducting metallopolymer literature. In accord with classic inorganic electron transfer theory,[86,87] Figure 1.11A details outer and inner sphere electron transfer mechanisms in mixed valence systems (top and bottom, respectively). The outer sphere mechanism is distinguished by the lack of mixing of the respective metal orbitals. In contrast, the inner sphere mechanism involves the communication of the two metal centers by orbital overlap via a mutual bridging ligand. It is important to note that the rate of electron transfer by this mechanism is highly dependent on the nature of the bridging ligand and its orbital overlap with the two metal centers.[86] In conducting polymer systems, incorporation of redox-active transition metal centers was reported under two unique environments. In the outer sphere arrangement, redox-active metals centers or complexes that decorate the periphery of the conducting polymer strand but have no direct interaction with the delocalized orbitals of the conducting organic polymer backbone are generated, Figure. 1.11B (top). Although the transition metals in this system may not be intimately involved in the conjugative pathway, they can still provide important charge transfer mechanisms. Analogous to molecular systems, in outer sphere architectures the metal centers are often tethered to the conducting polymer and have independent coordination spheres. In contrast, inner sphere architectures involve the incorporation of the transition metal centers into the polymer backbone with strong coupling between the orbitals of the transition metal and those involved in charge transport through the polymer strand, Figure 1.11B (bottom). When the energies of the orbitals are equivalent (same redox potential or redox matched) strong coupling provides for efficient additional charge transport pathways that intimately involve the transition metal centers leading to highly conductive materials.

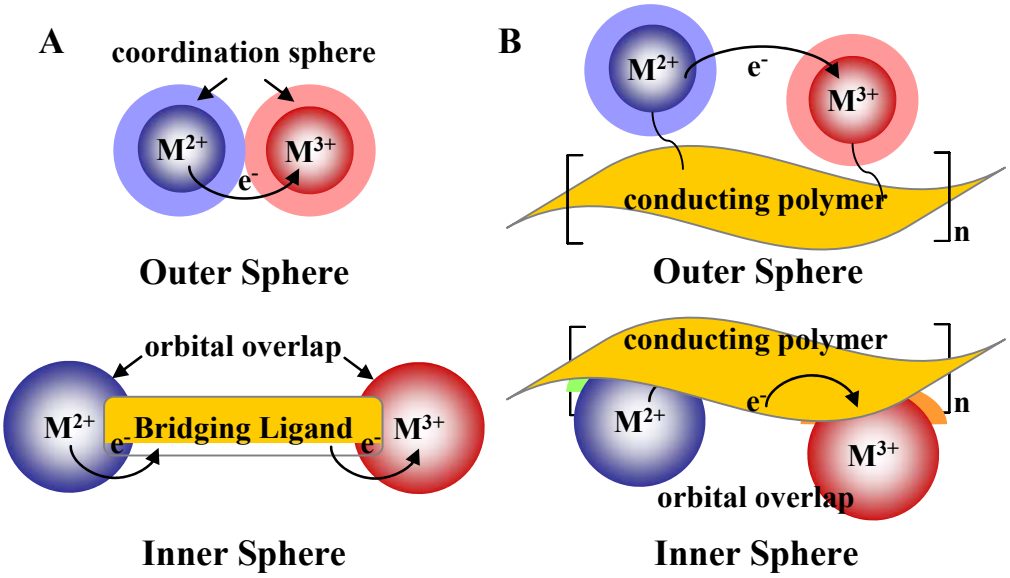

Figure 1.11. Mechanisms of electron transfer in molecular (left) and conducting (right) systems.

1.4.1.2 Materials Based on Bisthiazol-2-yl-amine Moiety

The driving force for the widespread interest in hybrid materials consisting of transition metals and conjugated polymers is that the optical and electronic properties can easily be modified in a controlled fashion by varying the transition metal component. Several features unique to metal-organic systems allow this tunability including: (1) strong electronic interaction between the transition metal and π-delocalized electron system, (2) the rich chemistry of transition metal complexes and conjugated polymers and (3) the accessibility of a variety of structurally diverse materials using modern synthetic methodology.[14,82,88-90] Due to the versatile properties of metal-organic hybrid materials, there is significant promise that these materials can find use in optical or electronic devices in the future.

There has been some interest recently in thiazole-based conjugated polymers.[91-93] Bredas and co-worker[91] have used valence effective Hamiltonian (VEH) calculations, a method known to give very good band structures for sulfur- and nitrogen-containing polymers,[94] to investigate the effect of placing nitrogen atoms in the conduction pathway of a poly(α-thiophene) structure. They conclude that doped polythiazoles should be good conductors.

An important goal of the present study is to explore the synthesis and characterization of novel conducting polymers based on thiazole moiety. Bisthiazol-2-yl-amine moiety was chosen as polymer backbone for a number of reasons:

(1) Various π-conjugated poly(arylene)s containing electrowithdrawing imine nitrogens in the arylene units have been prepared, and they have been converted into electrically conducting materials by reduction.[95-97] However, most of the studies on the poly(arylene)s with imine nitrogens have been carried out with those compounds containing six-membered rings (*e.g.* poly(pyridine-2,5-diyl) and poly(quinoxaline-2,6-diyl)), and only a few studies have been reported on π-conjugated five-membered poly(arylene)s containing the electron-withdrawing imine nitrogens. Hoffmann et al. proposed that polymers built from sulfur, carbon, and nitrogen-containing five-membered rings would theoretically display magnetic ordering.[98] The synthesis of bisthiazol-2-yl-amine moiety based materials should reveal interesting properties especially in terms of conductivity and provide comprehensive studies of thiazole-based systems.

(2) It is well known that bisthiazole can coordinate with many kinds of metal ions. Therefore, this project represents an attempt to combine the unique characteristics of conjugated conducting polymers with transition metals to form interesting new materials. Coordinated metal sites could be used to increase order in the polymer, to act as centers for electron transfer, and to promote counter-ion induced solubility.

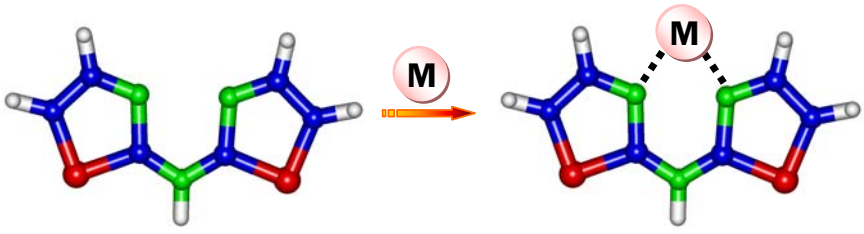

Figure 1.12. Schematic structure of bisthiazol-2-yl-amine and its metal complex (sulfur atoms are colorized in red, carbon in blue, nitrogen in green, and hydrogen in white. M is metal).

Therefore, this project undoubtedly meets a need for further experimental studies into the potential of metallopolymers as well as introducing a new class of polymers based on bisthiazol-2-yl-amine units (Figure 1.12).

1.4.2 Can anthracene- and phenanthrene-based materials be suitable for use as emitting materials?

The development of new fabrication techniques and new device structures for LEDs will continue to provide new exciting opportunities for new materials with optimal properties. In addition there still exists considerable scope for development of new and improved techniques for synthesizing, purifying, characterizing and processing conjugated polymers so as to optimize the performance of known materials, and to make accessible novel ones for study. In every sense of term, conjugated polymers have a bright future ahead of them. Efficient, highly bright, and stable blue-light-emitting materials are still under intensive research because blue light is necessary for full color EL display applications. It is an objective of the present study to synthesize and characterize new classes of luminescent polymeric materials (based on anthracene and phenanthrene moieties) useful for polymer EL devices (see below).

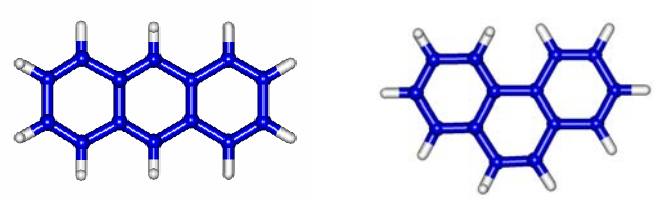

Anthracene **Phenanthrene**

Figure 1.13. Schematic structures of anthracene and phenanthrene (carbons atoms are colorized in blue and hydrogen in white).

1.4.2.1 Conjugated Polymers Containing Anthracene Moiety

The polymers based on anthracene are of interest owing to their potential application in electrophotography and electroluminescent devices and anthracene derivatives have been studied for OLED[99] and PLED[100,101] devices. Among the fluorescent materials, 9,10-diphenylanthracene (DPA) and 9,10-bis(phenylethynyl)anthracene (BPEA) have not only

near unity fluorescence quantum efficiency in dilute solution[102,103] but they are also highly fluorescent in the solid state. Therefore, polymers containing anthrylene units could be materials with promising optical properties for use in PLEDs.

For most conjugated polymers, the barrier for electron injection is much higher than that for hole injection. To improve efficiency of PLEDs, it is necessary to balance the rate of injection of electrons and holes from the opposite electrodes into the device as depicted previously. Anthracene itself is known as a hole- and electron-transporting light emitter.[104] As a result, incorporation of anthracene which has an electron-rich structure into polymer main chains might solve this problem and so produce materials which are good candidates for PLEDs and other polymer-based optical and electrooptical applications.

These considerations led us to explore a series of conjugated polymers containing anthrylene units.

1.4.2.2 Conjugated Polymers Containing Phenanthrene Moiety

As discussed above, one of the most important aims for use as emissive polymers in PLEDs is the obtaining of pure blue-emitting materials, since the high-energy visible emission can be transformed into red and green light via internal[105] or external color conversion.[106] Phenylene-based polymers are one of the most attractive classes of conjugated materials for electronic application.

Unsubstituted PPP is insoluble, so that films have to be prepared by precursor routes. In the case of introduction of alkyl or alkoxy substituents on the PPP backbone,[107,108] the steric interactions between the solubilizing sidechains cause a marked increase in the phenylene-phenylene torsion angle, from 23° to over 60°, with a concurrent loss of π-overlap and a marked blue-shift in the emission wavelength. To overcome this, a totally planarized ladder-type PPP (LPPP),[109] was prepared, which shows a PL emission maximum at 450 nm, with a remarkably small Stokes shift. This material, however, tends to produce an extra emission band in the yellow region of the spectrum which has variously been attributed to aggregates[110] or defects.[111] As a result, considerable attention has been paid to "step-ladder" polymers in which the PPP backbone is partially planarized by short

alkanediyl bridges, to investigate whether interruption of the planarity would reduce aggregation. From this logical concept, a series of semiladder polyphenylenes with a structure intermediate between PF and ladder-type polyphenylene have recently been developed in our group. These semiladder polyphenylenes with repeat units from indenofluorene to bridged pentaphenylene tune the emission color from 430 to 460 nm, which red-shifts with increasing the rigidity of the polymer chains.[112] However, under certain circumstances, methylene-bridged ladder type PPP based polymers show a tailed emission band at longer wavelengths in solid-state or light-emitting devices, leading to both color instability and reduced efficency.[6,113] The source of this long wavelength emission was initially attributed to the formation of an excimer, owing to interchain interactions and π-π stacking interactions between the planar-conjugated main chains.[113-115] but more recently, it has been confirmed that the long-wavelength emission arises from ketone defects formed by oxidative electro- and photodegradation at the methine bridge when nonsubstituted or monosubstituted fluorene units are present in the polymer main chain.[116-118]

A step-ladder polymer containing the phenanthrylene moiety is anticipated to provide the following advantages: (1) emission in the pure blue region of PL spectra, comparable to that from the parent PPP, (2) ability to introduce solubilizing groups at the 9,10-positions without disturbing the conjugation along the chain, and (3) provide unique optical properties and photostability, compared to the methine bridged semiladder and ladder type polymers due to the cis-stilbene bridges.

It is thus resolved to prepare and study a novel class of soluble step-ladder type polymers containing phenanthrylene moieties which could be applied as active layers in PLEDs.

1.5 References

(1) Shirakawa, H.; Louis, E. J.; MacDiarmid, A. D.; Chiang, C. K.; Heeger, A. J. *J. Chem. Soc., Chem. Commun.* **1977**, *16*, 578-579.
(2) Lefrant, S.; Lichtman, L. S.; Temkin, M.; Fichten, D. C.; Miller, D. C.; Whitwell, G. E.; Burlich, J. M. *Solid State Commun.* **1979**, *29*, 191-196.
(3) Greene, R. L.; Street, B. R.; Suter, L. J. *Phys. Rev. Lett.* **1975**, *34*, 577-579.
(4) Burroughes, J. H.; Bradley, D. D. C.; Brown, A. R.; Marks, R. N.; Mackay, K.;

Friend, R. H.; Burns, P. L.; Holmes, A. B. *Nature* **1990**, *347*, 539-541.
(5) Friend, R. H.; Gymer, R. W.; Holmes, A. B.; Burroughes, J. H.; Marks, R. N.; Taliani, C.; Bradley, D. D. C.; Dos Santos, D. A.; Bredas, J. L.; Logdlund, M.; Salaneck, W. R. *Nature* **1999**, *397*, 121-128.
(6) Bernius, M. T.; Inbasekaran, M.; O'Brien, J.; Wu, W. S. *Adv. Mater.* **2000**, *12*, 1737-1750.
(7) Dai, L. M.; Winkler, B.; Dong, L. M.; Tong, L.; Mau, A. W. H. *Adv. Mater.* **2001**, *13*, 915-925.
(8) Fukuda, Y.; Watanabe, T.; Wakimoto, T.; Miyaguchi, S.; Tsuchida, M. *Synth. Met.* **2000**, *111*, 1-6.
(9) Kobayashi, H.; Kanbe, S.; Seki, S.; Kigchi, H.; Kimura, M.; Yudasaka, I.; Miyashita, S.; Shimoda, T.; Towns, C. R.; Burroughes, J. H.; Friend, R. H. *Synth. Met.* **2000**, *111*, 125-128.
(10) Sariciftci, N. S.; Smilowitz, L.; Heeger, A. J.; Wudl, F. *Science* **1992**, *258*, 1474-1475.
(11) Halls, J. J. M.; Walsh, C. A.; Greenham, N. C.; Marseglia, E. A.; Friend, R. H.; Moratti, S. C.; Holmes, A. B. *Nature* **1995**, *376*, 498-500.
(12) Brabec, C. J.; Sariciftci, N. S.; Hummelen, J. C. *Adv. Funct. Mater.* **2001**, *11*, 15-26.
(13) Shaheen, S. E.; Brabec, C. J.; Sariciftci, N. S. *Appl. Phys. Lett.* **2001**, *78*, 841-843.
(14) Segura, J. L.; Martin, N. *J. Mater. Chem.* **2000**, *10*, 2403-2435.
(15) Johansson, T.; Mammo, W.; Andersson, M. R.; Inganas, O. *Chem. Mater.* **1999**, *11*, 3133-3139.
(16) Yu, G.; Cao, Y.; Andersson, M.; Gao, J.; Heeger, A. J. *Adv. Mater.* **1998**, *10*, 385-388.
(17) Pei, Q. B.; Yu, G.; Zhang, C.; Yang, Y.; Heeger, A. J. *Science* **1995**, *269*, 1086-1088.
(18) Edrington, A. C.; Urbas, A. M.; DeRege, P.; Chen, C. X.; Swager, T. M.; Hadjichristidis, N.; Xenidou, M.; Fetters, L. J.; Joannopoulos, J. D.; Fink, Y.; Thomas, E. L. *Adv. Mater.* **2001**, *13*, 421-425.
(19) Jager, E. W. H.; Smela, E.; Inganas, O. *Science* **2000**, *290*, 1540-1545.
(20) Garnier, F.; Hajlaoui, R.; Yassar, A.; Srivastava, P. *Science* **1994**, *265*, 1684-1685.
(21) Katz, H. E.; Bao, Z. N.; Gilat, S. L. *Acc. Chem. Res.* **2001**, *34*, 359-369.
(22) Facchetti, A.; Deng, Y.; Wang, A. C.; Koide, Y.; Sirringhaus, H.; Marks, T. J.; Friend, R. H. *Angew. Chem., Int. Ed. Engl.* **2000**, *39*, 4547-4551.
(23) Horowitz, G.; Hajlaoui, M. E. *Adv. Mater.* **2000**, *12*, 1046-1050.
(24) Katz, H. E.; Bao, Z. *J. Phys. Chem., B* **2000**, *104*, 671-678.
(25) Katz, H. E. *J. Mater. Chem.* **1997**, *7*, 369-376.
(26) Tessler, N.; Pinner, D. J.; Cleave, V.; Ho, P. K. H.; Friend, R. H.; Yahioglu, G.; Barny, P. L.; Gray, J.; de Souza, M.; Rumbles, G. *Synth. Met.* **2000**, *115*, 57-62.
(27) Hide, F.; DiazGarcia, M. A.; Schwartz, B. J.; Andersson, M. R.; Pei, Q. B.; Heeger, A. J. *Science* **1996**, *273*, 1833-1836.
(28) Tessler, N.; Denton, G. J.; Friend, R. H. *Nature* **1996**, *382*, 695-697.
(29) Tessler, N. *Adv. Mater.* **1999**, *11*, 363-370.
(30) McGehee, M. D.; Heeger, A. J. *Adv. Mater.* **2000**, *12*, 1655-1668.
(31) Heeger, A. J. In *Handbook of conducting polymers*; Skotheim, T. A. ed.; New York: Marcel Dekker: 1986; Vol. 2, p 729-756.
(32) Wudl, F.; Kobayashi, M.; Heeger, A. J. *J. Org. Chem.* **1984**, *49*, 3382-3384.

(33) Roncali, J. *Chem. Rev.* **1997**, *97*, 173-205.
(34) Pomerantz, M. In *Handbook of conducting polymers, 2nd*; Skotheim T. A.; Elsenbaumer, R. L.; Reynoldes, J. R. ed.; Marcel Dekker: New York, 1998, p 277-309.
(35) Kaiser, A. B. *Phys. Rev. B* **1989**, *40*, 2806-2813.
(36) Park, Y. W.; Han, W. K.; Choi, C. H.; Shirakawa, H. *Phys. Rev. B* **1984**, *30*, 5847-5851.
(37) Feldblum, A.; Park, Y. W.; Heeger, A. J.; Macdiarmid, A. G.; Wnek, G.; Karasz, F.; Chien, J. C. W. *J. Polym. Sci., Part B: Polym. Phys.* **1981**, *19*, 173-179.
(38) Su, W. P.; Schrieffer, J. R.; Heeger, A. J. *Phys. Rev. Lett.* **1979**, *42*, 1698-1701.
(39) Devreux, F.; Genound, F.; Nechtschein, M.; Villeret, B. *Springer Ser Solid-State Sci.* **1987**, *76*, 270-276.
(40) Michaelson, J. C. *Endeavour* **1993**, *17*, 121-126.
(41) Yang, C. J.; Jenekhe, S. A. *Macromolecules* **1995**, *28*, 1180-1196.
(42) Yang, C. J.; Jenekhe, S. A. *Chem. Mater.* **1991**, *3*, 878-887.
(43) Rannou, P.; Gawlicka, A.; Berner, D.; Pron, A.; Nechtschein, M.; Djurado, D. *Macromolecules* **1998**, *31*, 3007-3015.
(44) Yoon, C. O.; Reghu, M.; Moses, D.; Heeger, A. J. *Phys. Rev. B* **1994**, *49*, 10851-10863.
(45) Reghu, M.; Cao, Y.; Moses, D.; Heeger, A. J. *Phys. Rev. B* **1993**, *47*, 1758-1764.
(46) Hagiwara, T.; Hirasaka, M.; Sato, K.; Yamaura, M. *Synth. Met.* **1990**, *36*, 241-252.
(47) Naarmann, H.; Theophilou, N. *Synth. Met.* **1987**, *22*, 1-8.
(48) Chiang, C. K.; Gau, S. C.; Fincher, C. R.; Park, Y. W.; Macdiarmid, A. G.; Heeger, A. J. *Appl. Phys. Lett.* **1978**, *33*, 18-20.
(49) Chiang, C. K.; Fincher, C. R.; Park, Y. W.; Heeger, A. J.; Shirakawa, H.; Louis, E. J.; Gau, S. C.; Macdiarmid, A. G. *Phys. Rev. Lett.* **1977**, *39*, 1098-1101.
(50) Shirakawa, H.; Louis, E. J.; Macdiarmid, A. G.; Chiang, C. K.; Heeger, A. J. *J. Chem. Soc., Chem. Commun.* **1977**, 578-580.
(51) Nigrey, P. J.; Macdiarmid, A. G.; Heeger, A. J. *J. Chem. Soc., Chem. Commun.* **1979**, 594-595.
(52) Heeger, A. J.; Kivelson, S.; Schrieffer, J. R.; Su, W. P. *Rev. Mod. Phys.* **1988**, *60*, 781-850.
(53) Maniloff, E. S.; Vacar, D.; McBranch, D. W.; Wang, H.; Mattes, B. R.; Gao, J.; Heeger, A. J. *Opt. Commun.* **1997**, *141*, 243-246.
(54) Tomozawa, H.; Braun, D.; Philips, S.; Heeger, A. J.; Kroemer, H. *Synth. Met.* **1987**, *22*, 63.
(55) Burroughes, J. H.; Jones, C. A.; Friend, R. H. *Nature* **1988**, *335*, 137-141.
(56) Drury, C. J.; Mutsaers, C. M. J.; Hart, C. M.; Matters, M.; de Leeuw, D. M. *Appl. Phys. Lett.* **1998**, *73*, 108-110.
(57) Parker, I. D. *J. Appl. Phys.* **1994**, *75*, 1656-1666.
(58) Frommer, J. E.; Chance, R. R. In *Encyclopedia of Polymer Science and Engineering* New York, 1986; Vol. 5.
(59) Miller, J. S. *Adv. Mater.* **1993**, *5*, 671-676.
(60) Jerome, D.; Mazaud, A.; Ribault, M.; Bechgaard, K. *Journal De Physique Lettres* **1980**, *41*, L95-L98.
(61) Luzny, W.; Trznadel, M.; Pron, A. *Synth. Met.* **1996**, *81*, 71-74.

(62) Tang, C. W.; Vanslyke, S. A. *Appl. Phys. Lett.* **1987**, *51*, 913-915.
(63) Sheats, J. R.; Antoniadis, H.; Hueschen, M.; Leonard, W.; Miller, J.; Moon, R.; Roitman, D.; Stocking, A. *Science* **1996**, *273*, 884-888.
(64) Sirringhaus, H.; Kawase, T.; Friend, R. H.; Shimoda, T.; Inbasekaran, M.; Wu, W.; Woo, E. P. *Science* **2000**, *290*, 2123-2126.
(65) Baldo, M. A.; Thompson, M. E.; Forrest, S. R. *Nature* **2000**, *403*, 750-753.
(66) Grant, E.; Nolan, P.; Pinner, D. *McKinsey Q.* **2002**, *1*, 18.
(67) Horowitz, G. *Adv. Mater.* **1998**, *10*, 365-377.
(68) Huitema, H. E. A.; Gelinck, G. H.; van der Putten, J.; Kuijk, K. E.; Hart, K. M.; Cantatore, E.; de Leeuw, D. M. *Adv. Mater.* **2002**, *14*, 1201-1204.
(69) McQuade, D. T.; Hegedus, A. H.; Swager, T. M. *J. Am. Chem. Soc.* **2000**, *122*, 12389-12390.
(70) McQuade, D. T.; Pullen, A. E.; Swager, T. M. *Chem. Rev.* **2000**, *100*, 2537-2574.
(71) Zhou, Q.; Swager, T. M. *J. Am. Chem. Soc.* **1995**, *117*, 12593-12602.
(72) Moses, D. *Appl. Phys. Lett.* **1992**, *60*, 3215-3216.
(73) Yang, Y.; Pei, Q. *J. Appl. Phys.* **1995**, *77*, 4807-4809.
(74) Kido, J.; Hongawa, K.; Okuyama, K.; Nagal, K. *Appl. Phys. Lett.* **1994**, *64*, 815-817.
(75) Yang, Y.; Heeger, A. J. *Appl. Phys. Lett.* **1994**, *64*, 1245-1247.
(76) Karg, S.; Scott, J. C.; Salem, J. R.; Angelopoulos, M. *Synth. Met.* **1996**, *80*, 111-117.
(77) Scott, J. C.; Carter, S. A.; Karg, S. *Polym. Prepr.* **1997**, *38*, 384-385.
(78) Carter, S. A.; Angelopoulos, M.; Karg, S.; Brock, J.; Scott, J. C. *Appl. Phys. Lett.* **1997**, *70*, 2067-2069.
(79) Groenendaal, L. B.; Jonas, F.; Feitag, D.; Pielartzik, H.; Reynoldes, J. R. *Adv. Mater.* **2000**, *12*, 481-494.
(80) Barta, P.; Cacialli, F.; Friend, R. H.; Zagorska, M. *J. Appl. Phys.* **1998**, *84*, 6279-6284.
(81) Marsella, M. J.; Fu, D. K.; Swager, T. M. *Adv. Mater.* **1995**, *7*, 145-147.
(82) Kraft, A.; Grimsdale, A. C.; Holmes, A. B. *Angew. Chem. Int. Ed.* **1998**, *37*, 402-428.
(83) Leising, G.; Tasch, S.; Graupner, W. In *Fundamentals of electroluminescence in paraphenylene-type conjugated polymers and oligomers*; Skothein, T. A., Elsenbaumer, R. L., Reynoldes, J. R., Eds.; Marcel Dekker: New York, 1998, p 847-880.
(84) Shirakawa, H. *Angew. Chem., Int. Ed. Engl.* **2001**, *40*, 2575-2580.
(85) Holliday, B. J.; Swager, T. M. *Chem. Commun.* **2005**, 23-36.
(86) Atwood, J. D. *Inorganic and Organometallic Reaction Mechanisms*; Wiley: New York, 1997.
(87) Rodgers, G. E. *Introduction to Coordination, Solid State, and Descriptive Inorganic Chemistry*; McGraw-Hill: New York, 1994.
(88) Ley, K. D.; Li, Y. T.; Johnson, J. V.; Powell, D. H.; Schanze, K. S. *Chem. Commun.* **1999**, 1749-1750.
(89) Walters, K. A.; Ley, K. D.; Schanze, K. S. *Chem. Commun.* **1998**, 1115-1116.
(90) Ley, K. D.; Whittle, C. E.; Bartberger, M. D.; Schanze, K. S. *J. Am. Chem. Soc.* **1997**, *119*, 3423-3424.

(91) Catellani, M.; Destri, S.; Porzio, W.; Themans, B.; Bredas, J. L. *Synth. Met.* **1988**, *26*, 259-265.
(92) Bolognesi, A.; Catellani, M.; Destri, S.; Porzio, W. *Synth. Met.* **1987**, *18*, 129-132.
(93) Aldissi, M.; Nyitray, A. M. *ACS Symp. Ser.* **1987**, *346*, 559-567.
(94) Bredas, J.-L. In *Handbook of conducting polymers*; Skotheim, T. A., Ed.; Marcek Dekker: New York, 1986, p 859-913.
(95) Kanbara, T.; Yamamoto, Y. *Macromolecules* **1993**, *26*, 3464.
(96) Saito, N.; Tanbara, T.; Nakamura, Y.; Yamamoto, Y.; Kubota, K. *Macromolecules* **1994**, *27*, 756-761.
(97) Sato, K.; Kanbara, T.; Kushida, T.; Kubota, K.; Yamamoto, Y. *Chem. Lett.* **1992**, 1153.
(98) Genin, H.; Hoffmann, R. *Macromolecules* **1998**, *31*, 444-455.
(99) Ishibashi, T.; Ichimura, M.; Tamura, S. In *EP1072668* 2001.
(100) Swager, T. M.; Gil, C. J.; Wrighton, M. S. *J. Phys. Chem.* **1995**, *99*, 4886-4893.
(101) Ofer, D.; Swager, T. M.; Wrighton, M. S. *Chem. Mater.* **1995**, *7*, 418-425.
(102) Heller, C. A.; Henry, R. A.; McLaughl.Ba; Bliss, D. E. *J. Chem. Eng. Data* **1974**, *19*, 214-219.
(103) Zweig, A.; Maurer, A. H.; Roberts, B. G. *J. Org. Chem.* **1967**, *32*, 1322-1329.
(104) Gu, J.; Kawabe, M.; Masuda, K.; Namba, S. *J. Appl. Phys.* **1977**, *48*, 2493-2494.
(105) Tasch, S.; List, E. J. W.; Hochfilzer, C.; Leising, G.; Schlichting, P.; Rohr, U.; Geerts, Y.; Scherf, U.; Müllen, K. *Phys. Rev. B* **1997**, *56*, 4479-4483.
(106) Tasch, S.; Brandstatter, C.; Meghdadi, F.; Leising, G.; Froyer, G.; Athouel, L. *Adv. Mater.* **1997**, *9*, 33-36.
(107) Rehahn, M.; Schluter, A.-D.; Wegner, G.; Feast, W. J. *Polymer* **1989**, *30*, 1054-1059.
(108) Rehahn, M.; Schluter, A.-D.; Wegner, G. *Makromol. Chem.* **1990**, *191*, 1991-2003.
(109) Scherf, U.; Müllen, K. *Makromol. Chem. Rapid. Commun.* **1991**, *12*, 489-497.
(110) Grüner, J.; Wittmann, H. F.; Hamer, P. J.; Friend, R. H.; Huber, J.; Scherf, U.; Müllen, K.; Moratti, S. C.; Holmes, A. B. *Synth. Met.* **1994**, *67*, 181-185.
(111) Haugeneder, A.; Lemmer, U.; Scherf, U. *Chem. Phys. Lett.* **2002**, *365*, 366-368.
(112) Jacob, J.; Sax, S.; Piok, T.; List, E. J. W.; Grimsdale, A. C.; Müllen, K. *J. Am. Chem. Soc.* **2004**, *126*, 6987-6995.
(113) Neher, D. *Macromol. Rapid Commun.* **2001**, *22*, 1366-1385.
(114) Panozzo, S.; Vial, J. C.; Kervella, Y.; Stephan, O. *J. Appl. Phys.* **2002**, *92*, 3495-3502.
(115) Haugeneder, A.; Lemmer, U.; Scherf, U. *Chem. Phys. Lett.* **2002**, *351*, 354-358.
(116) Scherf, U.; List, E. J. W. *Adv. Mater.* **2002**, *14*, 477-487.
(117) List, E. J. W.; Guentner, R.; de Freitas, P. S.; Scherf, U. *Adv. Mater.* **2002**, *14*, 374-378.
(118) Gaal, M.; List, E. J. W.; Scherf, U. *Macromolecules* **2003**, *36*, 4236-4237.

Chapter 2 Synthesis, Metal Complexation and Conductivity Studies on Bisthiazole Analogues to Polyaniline

In this chapter, the synthesis and characterization of materials based on bisthiazol-2-yl-amine (**BTA**) as well as their complexes through coordination with transition metals are presented. The focus of this work has been to examine whether the introduction of coordinating metal ions onto the polymer backbone can enhance the conductivity of the material. Previous unpublished work by Dr. Josemon Jacob within our group on dithiophen-2-yl-amine derivatives will be briefly mentioned for comparison. The synthesis, optical and redox properties of *N*-substituted poly(5,5'-bisthiazol-2-yl-amine) are described and the effect of metal-ion coordination on the conducting properties of **BTA**-based polymers and copolymers are discussed.

Proposed Synthetic Approach

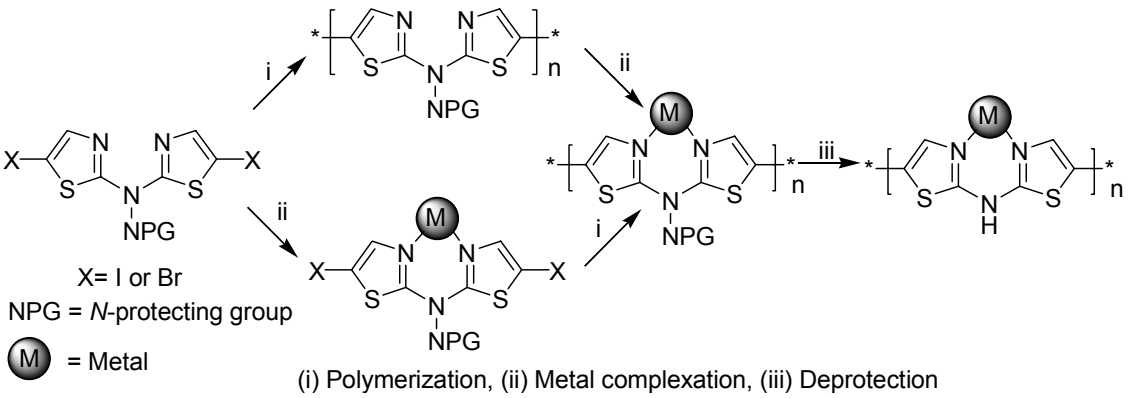

2.1 Uncomplexed Conducting Materials

Polyaniline (PANI) **1**, synthesized by the chemical or electrochemical oxidative polymerization of aniline, is one of the most widely studied among conducting materials.[1,2] A general formula for its structure is shown in Chart 2.1. It is known to exist in various oxidation states, for example, leucoemeraldine refers to the fully reduced form of the material, emeraldine to the 50 % oxidized material and pernigraniline to the fully oxidized form.[3,4] In other words, the ratio of the imine nitrogen atoms to amine nitrogen atoms varies depending on the extent of oxidation of the material. Irrespective of its oxidation state, PANI in its undoped state is an insulator. Upon doping with acid, a process where the number of electrons on the polymer backbone remains the same but the protons are increased, the conductivity is found to increase by approximately ten orders of magnitude.[5-8] Undoped PANI is an insoluble material; however with suitable choice of dopants, PANI becomes soluble and processable. PANI finds commercial applications in anticorrosion coatings for steel,[9] electromagnetic interference shielding[10] and rechargeable organic batteries.[7]

Several other classes of conducting polymers have been identified over the years, the most extensively studied ones include polyacetylene, polypyrrole (PPy), polythiophene (PT) and poly(thiophenealkanesulfonate)s. Although many of these materials show conductivities in the semiconducting or metallic regime upon doping, the stability of these materials is limited. In the past two decades, conducting polymers have found increasing use as components in optoelectronic devices. Hence there is an increasing need to identify new classes of materials with improved conductivity and long term stability that can be readily synthesized as well. It is surmised that replacing benzene with thiophene in polyaniline as in **2** would generate a hitherto unknown material that is more electron rich than PANI; thiophene is more electron rich than benzene since its six π-electrons are distributed over only five atoms. The synthesis and doping studies on two new classes of semiconducting materials analogous to polyaniline viz. poly(5,5'-dithiophen-2-yl-amine) and poly(5,5'-bisthiazol-2-yl-amine) are here explored.

Chart 2.1. Oxidation state of conducting materials (PANI and poly(5,5'-dithiophen-2-yl-amine)

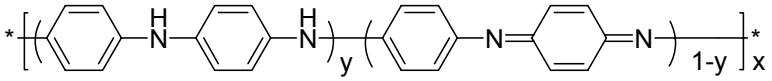

1

PANI **y = 1** **leucoemeraldine**
y = 0.5 **emeraldine**
y = 0 **pernigraniline**

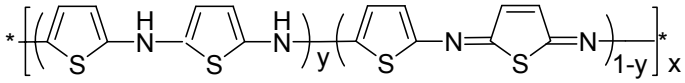

2

Thiophene analogue of PANI

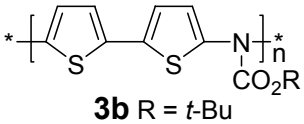

3b R = *t*-Bu
3c R = $C_{12}H_{25}$

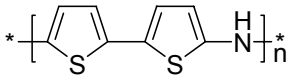

4

2.1.1 Synthesis and Characterization

Although coupling of a secondary amine to the 2-position of thiophene is documented in literature,[11-15] to the best of our knowledge, there exists no reports on the introduction of a primary amine at the 2-position. The initial synthetic approach was to use a precursor route towards the synthesis of a thiophene analogue to polyaniline by a Buchwald-type amination reaction[15] where the *N*-atom bears an easily removable protecting group (equation 1). Starting with 2-bromothiophene, several attempts to introduce a carbamate group at the 2-position of the thiophene under palladium catalyzed conditions were unsuccessful. However, when copper iodide was used as the coupling reagent, di-thiophen-2-yl-carbamic acid ethyl ester (**5a**) was isolated in 34 % yield (equation 2).[12,16,17] For R = *t*-Bu, the corresponding carbamate **5b** was isolated in 35 % yield. 3° alkyl substituents are particularly desirable in that they are easily cleaved off under mild acidic conditions or by thermal elimination. This serendipitous synthesis of **5** prompted us to alter our target polymer to one where an amine linkage exists between two thiophene units as in **3** (Chart 2.1). The carbamate group can then be removed either thermally or under mild acidic conditions to generate a poly(5,5'-dithiophen-2-yl-amine) as in **4**. It should be pointed out that **5a** and **5c** are stable for months at room temperature whereas **5b** slowly starts decomposing after 48 hours.

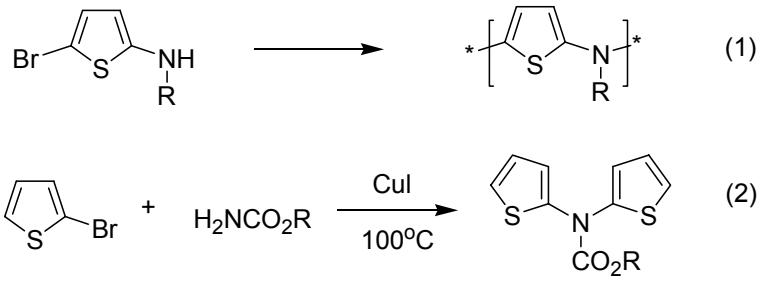

5a R = C_2H_5
5b R = *t*-Bu
5c R = $C_{12}H_{25}$

Treatment of **5b** with two equivalents of *N*-bromosuccinimide (NBS) generated di-(5-bromo-thiophen-2-yl)-carbamic acid *tert*-butylester (**6b**) in 89 % isolated yield (Scheme 2.1). Again, this compound is only stable for a few days at room temperature and should be used for the next step soon after isolation. Compound **6b** was subjected to polymerization under standard Yamamoto-type conditions using stoichiometric nickel(0) reagent. A black material, insoluble in common organic solvents was obtained after polymerization.

FT-IR analysis of the insoluble polymer **3b** demonstrated that the carbamate group had been completely cleaved off (as evidenced by the disappearance of the carbonyl stretch at 1720 cm^{-1} for the monomer **6b**) and one can conclude that the polymer structure matched with the polymer **4** in Chart 2.1. Conductivity measurements on a pellet made from this polymer showed the material to be an insulator (10^{-12} Scm^{-1}). This material was subjected to oxidative iodine doping and the resulting material was again insoluble in common organic solvents. The material developed a bluish tinge upon doping. Conductivity studies on a pellet made from the doped sample show an increase in conductivity to 10^{-6} Scm^{-1}. In attempts to make a soluble and processable polymer, a bithiopheneaminecarbamate **5c** with R = *n*-$C_{12}H_{25}$ as a long solubilizing group was synthesized. Bromination using two equivalents of NBS generated the monomer which was then subjected to Yamamoto type polymerization to generate the polymer **3c** (Chart 2.1). Surprisingly, this polymer is completely insoluble as well in common organic solvents although the carbamate group is still intact as evidenced by the carbonyl stretch at 1715 cm^{-1} by FT-IR. This probably suggests that under the reaction conditions, in addition to the anticipated carbon-carbon bond formation to generate the polymers, there

are some undesirable cross-linking reactions going on rendering the polymer insoluble. Also, attempts were made to isolate the dithiophen-2-yl-amine as its hydrochloride salt by deprotection of **5b** with hydrochloric acid in ether. However, this only led to an insoluble blue material suggesting the formation of cross-linked material after deprotection possibly by oxidative coupling.

Scheme 2.1. Synthetic route to poly(5,5'-dithiophen-2-yl-amine)

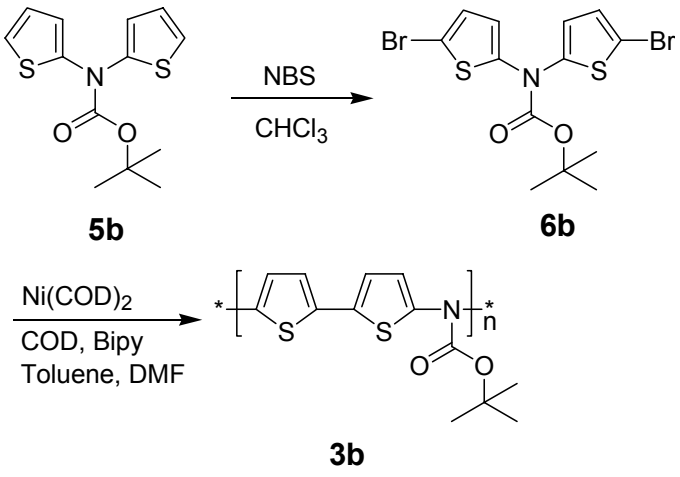

5b **6b** **3b**

Scheme 2.2. Synthetic route to poly(5,5'-bisthiazol-2-yl-amine)

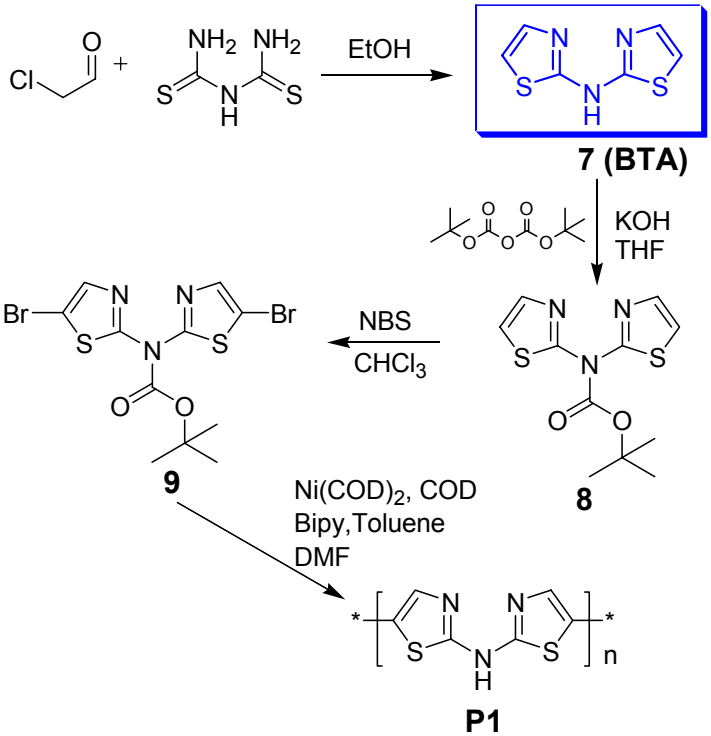

7 (BTA) **8** **9** **P1**

Carbamates **5** were found to be stable when the R group was a primary alkyl group. However, with a tertiary alkyl substituent, the monomer had only limited stability (any deprotection leaves a secondary amine at the 2-position of thiophene which seems inherently unstable). The observed instability of the deprotected monomer suggested that tuning the electron density on the thiophene could potentially lead to a more stable material. Towards this, bisthiazol-2-yl-amine (**BTA**) was chosen as a modified target, the structure and synthesis of which is shown in Scheme 2.2.

Chart 2.2. Synthetic attempts for the preparation of soluble polymers based on **BTA** via (a) Nickel(0)-mediated Yamamoto-type polycondensation or (b) Palladium(0)-mediated Suzuki or Stille-type polycondensation.

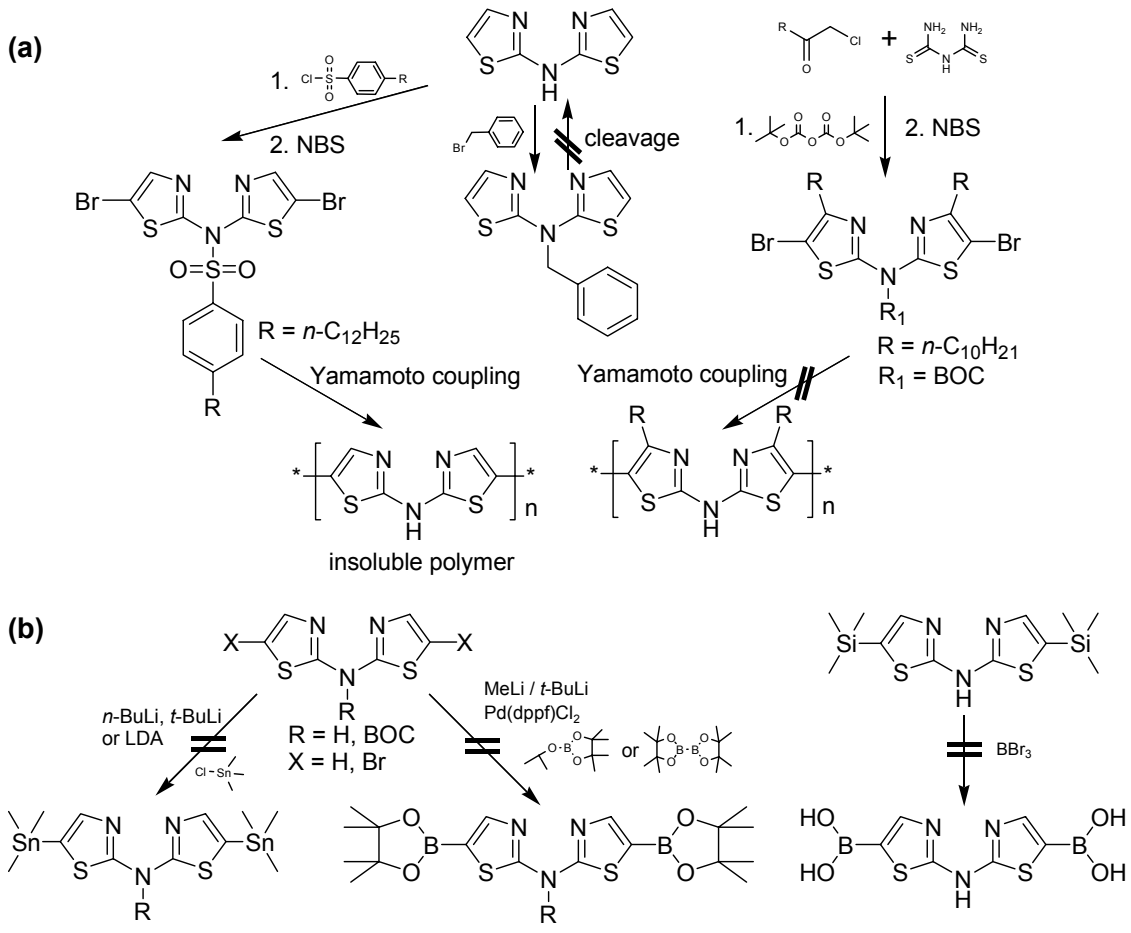

BTA (**7**) was synthesized from chloroacetaldehyde and dithiobiuret in 60 % isolated yield[18] and the carbamate protecting group was introduced in 52 % yield using di-*tert*-

butylcarbonate as depicted in Scheme 2.2. Bromination using NBS gave bis-(5-bromo-thiazol-2-yl)-carbamic acid *tert*-butyl ester (**9**) but the yield was limited to less than 20 % under the reaction conditions used. Poly(5,5'-bisthiazol-2-yl-amine) (**P1**) was synthesized by a nickel(0) mediated Yamamoto-type polycondensation and the resulting red solid was found to be insoluble in common organic solvents. Complete cleavage of the carbamate group occurred upon polymerization as evidenced by the disappearance of the carbonyl stretch at 1763 cm^{-1} for the monomer. Conductivity measurements on a pellet made from this polymer showed a semiconductor (10^{-8} Scm^{-1}) after oxidation (p-type iodine doping). The poor conductivity of the both polymer **4** and **P1** can be attributed to a disordered structure in the main chain or to instability upon doping. It was reported[19] that valence effective calculations show that placing nitrogen atoms in the conduction pathway of poly(α-thiophene) should produce good conductors. Therefore, there was clearly a need for further experimental studies of thiazole-based systems, which prompted us to investigate **BTA** systems further as part of the current work.

For generating a soluble and processable **BTA** based material, use of a sulfonamide protecting group (using *p*-dodecylbenzenesulfonyl chloride[20]) at the nitrogen of **BTA** was explored. However, upon following analogous steps as described in Scheme 2.2, only an insoluble material was obtained. FT-IR analysis gave almost an identical spectrum as for polymer **P1** suggesting that the carbamate group has been completely cleaved off under the reaction conditions. Also, the benzyl group was tried as an alternate protecting group however it was very stable and couldn't be easily removed. Several attempts were made to remove the benzyl group including the use of palladium on charcoal in the presence of various hydrogen donors like hydrazine hydrate, 1,4-cyclohexadiene, and acetic acid, as well as a powerful oxidant like ceric ammonium nitrate (CAN) but to no avail (Chart 2.2).

Long alkyl substituents (decyl) were introduced onto the **BTA** skeleton at 4,4'-positions however Yamamoto-type polymerization of the corresponding dibromide failed to give any polymeric material due to steric hindrance of the bulky alkyl chain at the 4,4'-positions. Also, another approach using a Suzuki or Stille type coupling for polymerization was designed but the synthesis of the bis(borolane) or bis(stannane) of **7** or **8** by lithiation (*n*-BuLi, *t*-BuLi, or LDA) and subsequent reactions of the lithio-derivative with trimethyltin chloride or 2-iopropoxy-4,4,5,5-tetramethyl-1,3,2-

dioxaborolane were not successful (see below).

The synthesis of the *N*-alkylated soluble analogue was then undertaken (Scheme 2.3). *N*-alkylation poly(5,5'-bisthiazol-2-yl-amine) was anticipated to improve solubility while minimizing oxidative degradation.[21,22] **BTA** (**7**) was alkylated at nitrogen using 2-hexyl-1-decyl bromide to generate (2-hHexyl-decyl)-bis-thiazol-2-yl-amine (**10**) which was brominated using NBS to give bis-(5-bromo-thiazol-2-yl)-(2-hexyl-decyl)-amine (**11**). Poly(5,5'-(2-hexyl-decyl)-bis-thiazol-2-yl-amine) (**P2**) was synthesized by Yamamoto-type coupling under standard conditions. The resulting polymer, however, shows low solubility in common organic solvents. GPC analysis of the polymer for the THF-soluble part gives a M_n value of 2.70×10^3 g/mol with a polydispersity of 2.2. This corresponds to a degree of polymerization of **6** suggesting that the strong dipoles in dithiazolylamine largely diminish the solubilising effect of the branched alkyl chain. Upon iodine doping, the material showed semiconducting behavior with a measured conductivity of 10^{-7} Scm^{-1} (measured on a pellet). The low conductivity upon *N*-alkylation is not surprising in that the introduction of the branched alkyl chain leads to less effective packing in the solid state as well as reduced conjugation along the polymer chain.[23,24] As one of the factors determining the measured conductivity of the polymers, the extent of iodine doping density has to be considered, which was calculated based on the increase in polymer weight upon doping to be *ca*. 0.25/monomer unit. The low magnitude of doping density in **P2** may explain the poor electric conductivity loss but conductivity may also depend upon other factors.

Scheme 2.3. Synthetic route to poly(5,5'-(2-hexyl-decyl)-bis-thiazol-2-yl-amine) (**P2**).

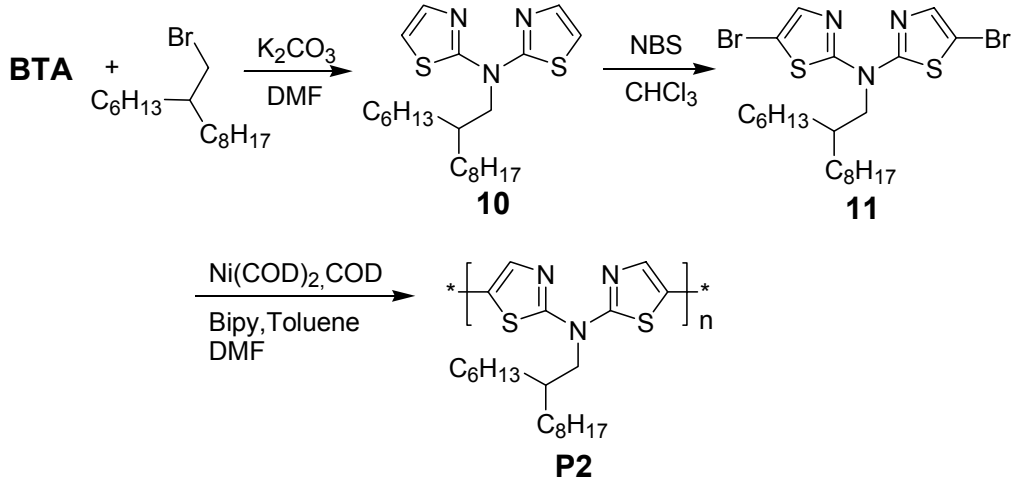

2.1.2 Photophysical and Electrochemical Properties

The UV-vis absorption and photoluminescence (PL) spectra of **P2** in dilute THF solution are shown in Figure 2.1.The spectrum of **P2** has broad absorption bands with a maximum at 390 nm without any vibronic features. The PL spectrum of **P2** in solution shows a blue emission region with a maximum at 444 nm and a shoulder peak at 471 nm.

Even though cyclic voltammetry (CV) against Ag/Ag+ was employed to investigate the redox behavior of **P2** and doped **P2,** the characterization of the doped **P2** was unsuccessful due to its low solubility in common solvents.[25] This film deposited on a platinum plate electrode was scanned both positively and negatively in 0.10 M anhydrous acetonitrile solution of tetrabutylammonium perchlorate (Bu_4NClO_4), using a platinum wire as the counter electrode and Ag/AgCl (0.10 M) as the reference electrode. As shown in Figure 2.2, **P2** exhibits two oxidation peaks at 0.86 V and 1.96 V. The oxidation onset was determined to be 0.71 V and estimating the bandgap from the absorption onset, the HOMO and LUMO energy levels of **P2** are found to be 5.11 eV and 2.90 eV respectively. These results clearly reveal the redox behavior of a **BTA**-based polymer however, **P2** does not show the property of low bandgap-conjugated polymers. This can be attributed in part to the introduction of the branched alkyl chain which leads to less effective packing along the polymer chain.

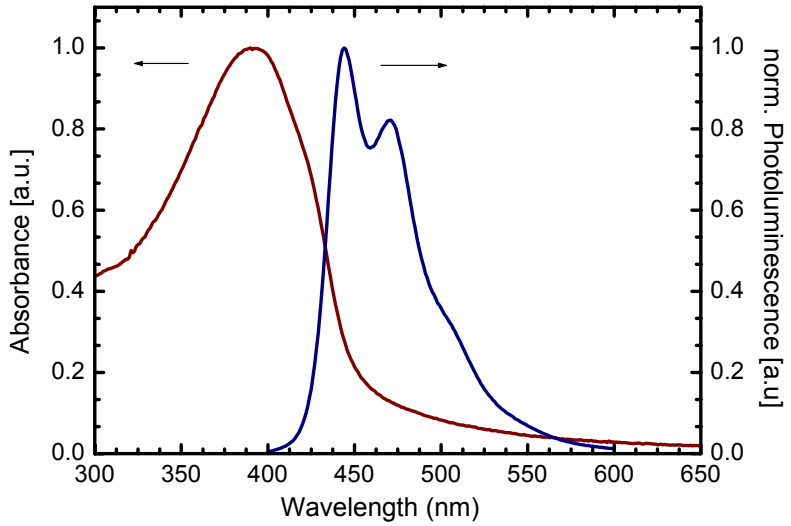

Figure 2.1. UV-vis (solution, THF; red line), photoluminescence (solution, THF; blue line) of **P2**

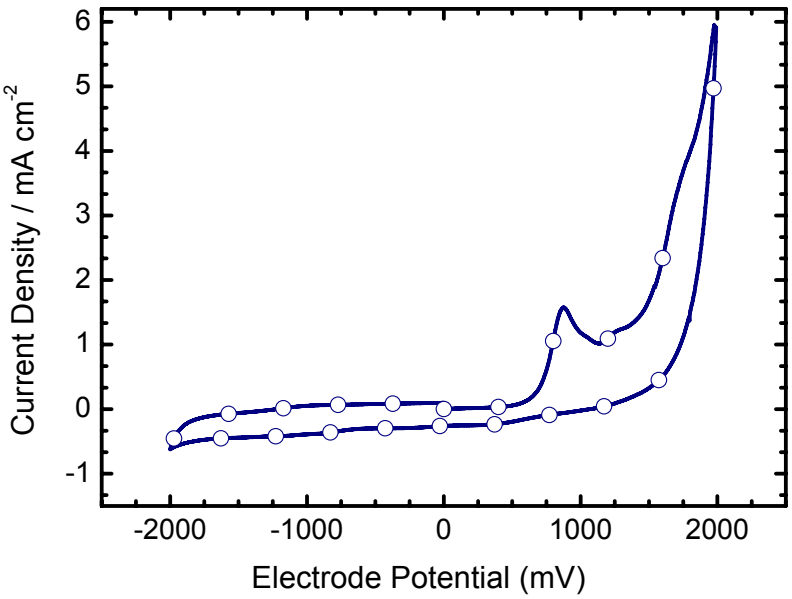

Figure 2.2 Cyclic voltammogram of a drop-cast film of **P2** measured in acetonitrile containing 0.1 M Bu_4NClO_4 at a scan rate 100 mV/s at room temperature

2.2 Complexation Studies

The design of coordination polymers incorporating organic ligands, also called "conjugated metallopolymers", comprise an essential part of contemporary efforts in the field of conducting polymers. Such polymers, while presenting an intriguing challenge for chemists, are of particular interest in areas described earlier. Despite the large variety of known architectures, metals and ligands, the study of their intrinsic properties still remains unsystematic.

BTA-based materials have the potential to bind transition-metal ions, which can be used to tune their electronic, electrochemical and physical properties. Therefore, the coordination of metal centers directly to the conjugated polymer backbone was undertaken. Herein the preparation, the single-crystal X-ray structures and the optical properties of metal complexes with **BTA**-based materials are described. The reaction of **BTA** with Cu(II) triflate gave a purple solid **12** in THF solution at room temperature (Scheme 2.4). It was difficult for this material **12** to be spectroscopically characterized by ^{1}H NMR, ^{13}C NMR or Field Desorption Mass Spectrometry (FD-MS). The NMR spectra of inorganic compounds are often more complicated than simple organics due to

additional splitting from NMR active nuclei. It was found that complex **12** is paramagnetic which was confirmed by electron paramagnetic resonance (EPR) spectroscopy. X-ray diffraction can provide the most unambiguous characterization of such complexes. X-ray structural analysis of **12** reveals two **BTA** units complexed to a copper and a distorted tetrahedral geometry around the copper (Figure 2.3 top).

Scheme 2.4 Cu(II) and Pd(II) complexes with **BTA**.

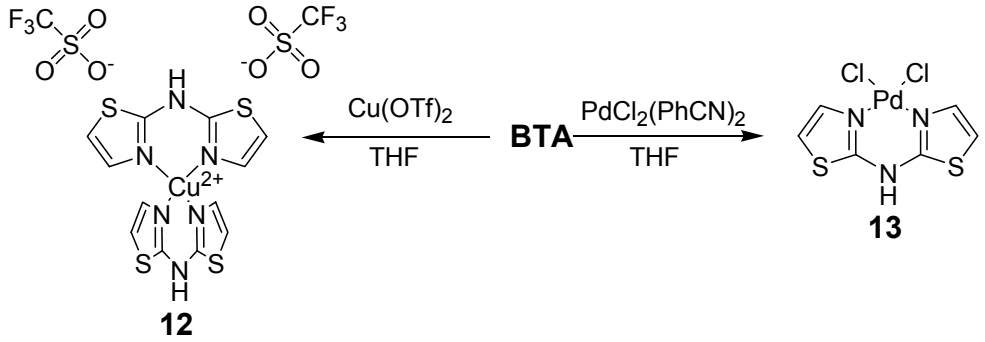

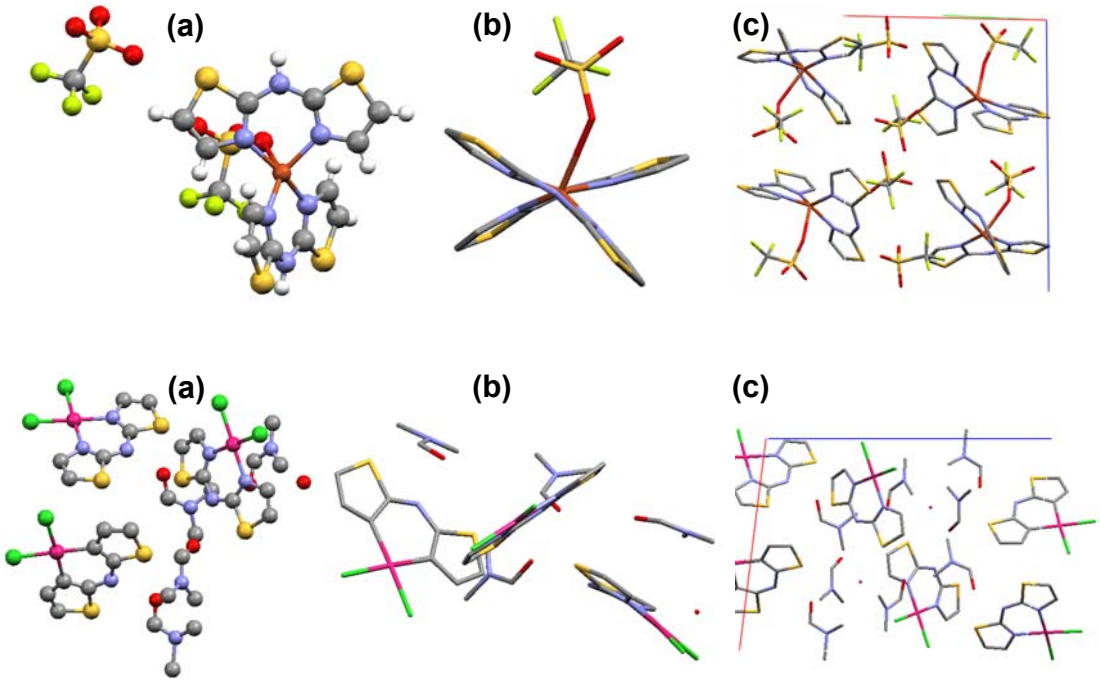

Figure 2.3. X-ray crystal structure of (top) **12** and (bottom) **13**. (a) top view (it is colorized by elements) (b) side view and (c) packing projection.

In further studies on complexation behavior, $Pd(II)Cl_2(PhCN)_2$ was reacted with **BTA** and an orange single crystal was obtained by slow diffusion of ether into a *N,N*-dimethylformamide solution of the Pd(II) complex **13** and analyzed by X-ray crystallography. In contrast, the resulting data displays one **BTA** unit coordinated to one palladium and a square-planar geometry around the palladium (the bottom of Figure 2.3).

The optical properties of the metal free compound **7** and metal complexes (**12** and **13**) were investigated in dimethylsulfoxide (DMSO) solution by UV-vis spectroscopy. As depicted in Figure 2.4, the absorption bands of **7** were broad with a maximum centered at 339 nm which can be clearly attributed to a π-π^* transition. In contrast, both the complexes **12** and **13** reveal an absorption peak centered at 352 nm and shoulder peaks at 362 and 372 nm respectively. The downhill energy transfer in UV-vis spectra of metallated derivatives (**12** and **13**) is attributed to more extended conjugation systems in the metal complex due to their increased planarity.

The metal complexed compounds (**12** and **13**) possess only limited solubility in common organic solvents. As a realistic approach to improve the solubility of **7** without decreasing the planarity, introduction of metal with a bulky ligand was considered. In doing so, the metal complexation was anticipated to enforce planarity, which could lead to better π-overlap in the polymer thereby decreasing the bandgap and increasing conductivity and the bulky ligands could enhance the solubility. In an initial study, 1,3-bis(diphenylphosphine)propane nickel(II) chloride was used as the metal complex but the incorporation of Ni(II) with big ligands on **BTA** did not give satisfactory solubility (in fact there was no improvement in solubility). It is postulated that the enhanced planarity due to metal complex also increases the intrinsic rigidity and so lowers the solubility of the material.

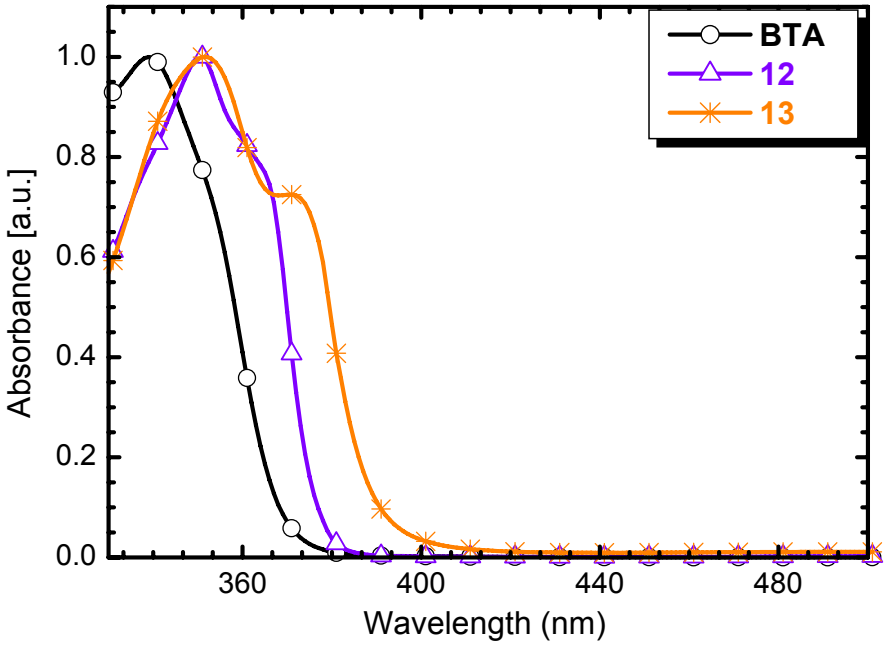

Figure 2.4 UV-vis absorption spectra of **7**, **12** and **13** in DMSO solution.

2.2.1 Ambipolar p-Type and n-Type Oligomer

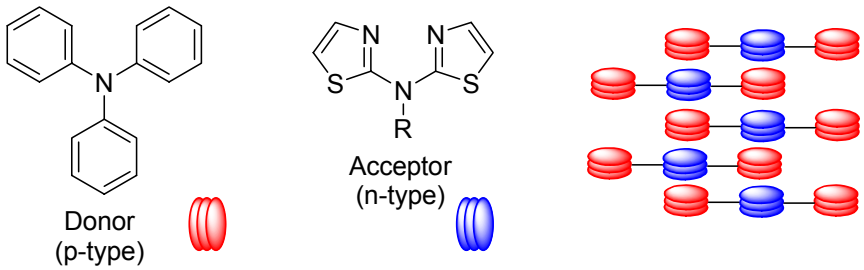

Figure 2.5. Triphenylamine donor, *N*-alkylated **BTA** acceptor unit and schematic organization of donor-acceptor.

The design of systems incorporating both donor and acceptor chromophores is of particular interest in applications in bipolar field effect transistors and solar cells. The synthesis of a donor-acceptor type oligomer using diphenylamine and **BTA** as p- and n-type moieties was first carried out. However, the Buchwald amination with diphenylamine and bis-(5-bromo-thiazol-2-yl)-octyl-amine (**14**) was not successful even using diphenylamine with more electron donating substituents such as methoxyl at *para*

positions under various conditions because the major product was mono amino **BTA** which was inseparable from the diadduct. Instead, a system consisting of a donor and an acceptor unit within the same molecule was undertaken using triphenylamine units. This molecule in which thiazole rings having a high electron affinity, *i.e.* n-type character was incorporated with triphenylamine units having p-type character, is schematically illustrated in Figure 2.5.

Scheme 2.5. Synthetic route to donor and acceptor compound based on 5,5'-triphenylamino-2,2'-bithiazole (**16**).

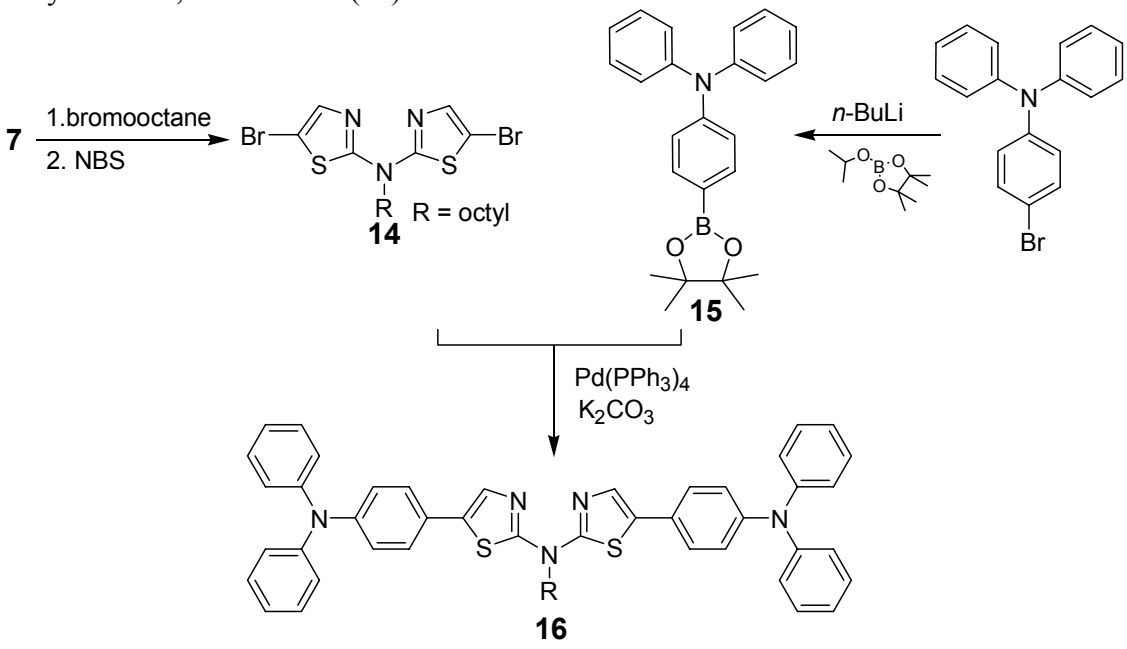

7 was alkylated at nitrogen using 1-bromooctane (yield = 95 %) and subsequently brominated using NBS to give bis-(5-bromo-thiazol-2-yl)-octyl-amine (**14**) as previously mentioned (yield = 97 %). 4-Bromo-*N,N*-diphenylaniline was converted into *N,N*-diphenyl-4-(4,4,5,5-tetramethyl-1,3,2-dioxaborolan-2-yl)aniline (**15**) by lithiation and subsequent reaction with 2-isopropoxy-4,4,5,5-tetramethyl-1,3,2-dioxaborolane. The synthesis of 5-(4-(diphenylamino)phenyl)-*N*-(5-(4-(diphenylamino)phenyl)thiazol-2-yl)-*N*-octylthiazol-2-amine (**16**) by using **14** and **15** was successful via Suzuki coupling[26] under $Pd(PPh_3)_4/K_2CO_3$ in isolated overall yield of 30 % (Scheme 2.5).

Scheme 2.6. Metal complexes of compound (**16**) with Cu(II) and Pd(II).

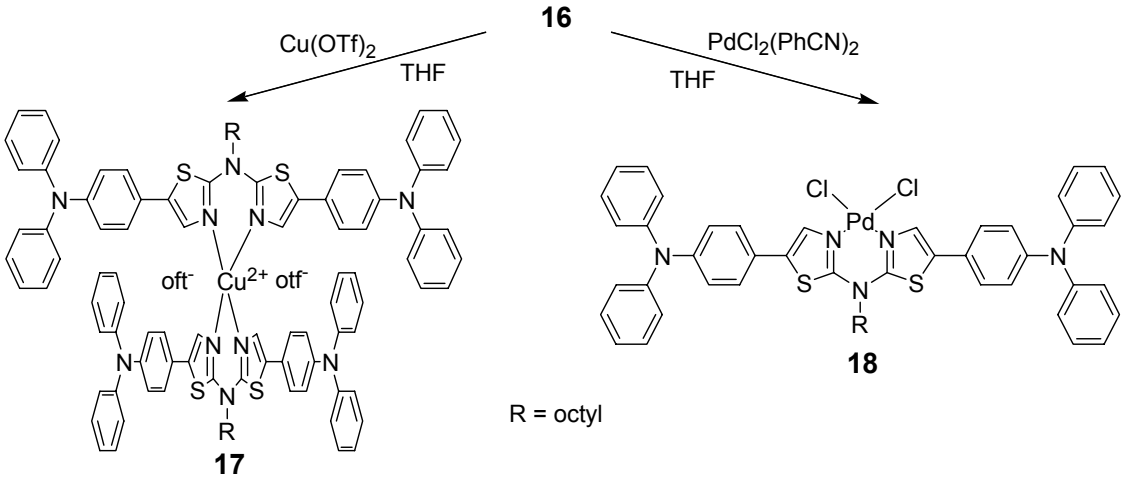

Since **16** consisting of bidentate N-donor sites could complex with transition metals, the metallation of **16** was explored. The reaction of Cu(II) triflate and Pd(II)$Cl_2(PhCN)_2$ with **16** in THF solution provided greenish and orange powdery materials respectively but their paramagnetic nature limited any characterization by NMR spectroscopy (FD-MS analysis is not be sensitive to paramagnetic behavior). For characterization, attempts to grow single crystals were not successful but their geometrical structures are predicted to be as shown on Scheme 2.6 based on earlier results. Scheme 2.6 depicts the anticipated configurations of the Cu(II) complex **17** and the Pd(II) complex **18** calculated using SPARTAN PRO.

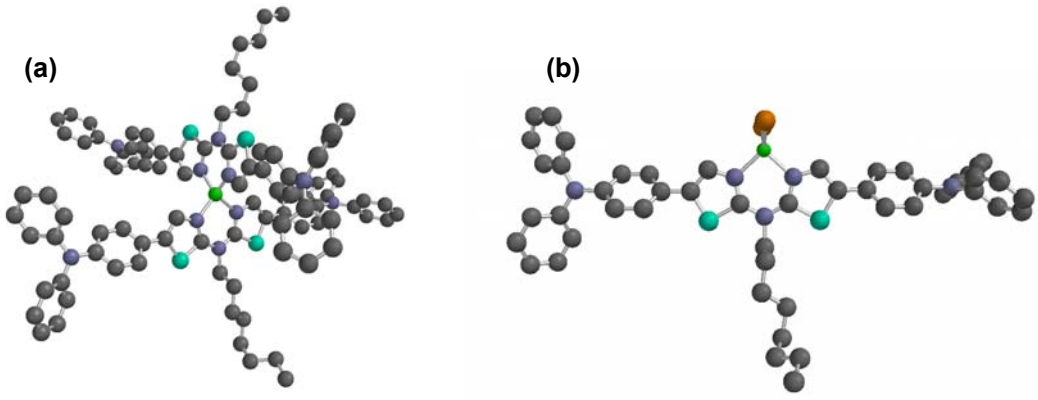

Figure 2.6. Metal complexes simulation using SPARTAN for (a) Cu(II) **17** and (b) Pd(II) **18**.

Photophysical Properties. Figure 2.7 displays the absorption and emission spectral data of the compound **16**, **17**, and **18** in THF solution and the data are summarized in Table 2.1. The absorption maxima for **16**, **17**, and **18** are at 385, 405, and 402 nm respectively, arising from π-π* transition from the conjugated polymer backbone. In the PL spectra of **16** in solution, the emission spectrum consists of two well distinguishable contributions: two peaks at 431 and 457 nm arising from the conjugated backbone. In general, the presence of vibronic structures indicates that the compound has a rigid and well-defined backbone structure.[27] The bathochromic shifts in solution as compared to unmetallated compound **16** are observed for the metal complex compounds **17** at 470 nm and **18** at 475 nm in solution respectively.

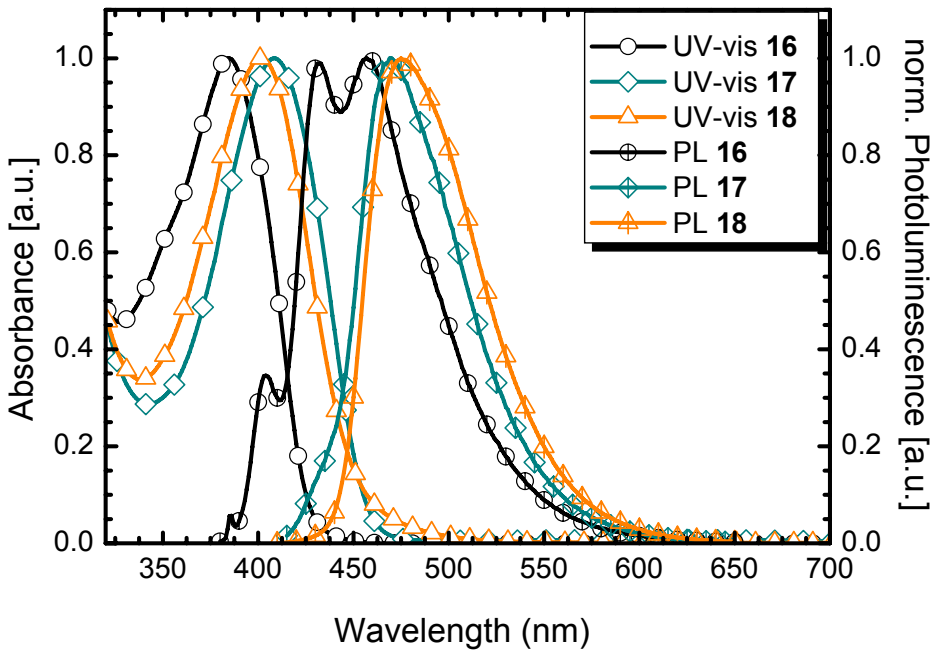

Figure 2.7 UV-vis and PL spectra of **16**, **17** and **18** (λ_{exc} = 350 nm) in THF solution.

Table 2.1. Optical data of **16**, **17** and **18**

compound	solution λ_{max} (nm)		[a]Stokes shift (nm)
	absorption	emission	
16	385	431, 457	90
17	405	470	65
18	402	475	63

[a]Stokes shift = PL $_{solution}$ / nm – UV $_{solution}$ / nm

2.2.2 Metallopolymers

To date, the major challenge in the characterization of polymers containing **BTA** units has been the insolubility of the materials such as poly(5,5'-(2-hexyl-decyl)-bis-thiazol-2-yl-amine) (**P2**). This has also largely limited the scope of the complexation studies using transition metal ions of varying geometry. However, upon iodine doping, all the above materials showed semiconducting behavior. As a result, the generation of suitable copolymers with improved solubility was explored.

Thiophene-based linear π-conjugated systems have attracted a great deal of attention due to their stability, structural versatility, and potential applications in next-generation electronic and optical materials.[28] Poly(cyclopentadithiophene)s exhibit high conductivity in the doped state[29] and the low oxidation potentials (0.1 - 0.2 V) of these polymer are compatible with electronic devices. Therefore, the heteroaromatic electron-rich cyclopentadithiophene structural unit (full name: 4H-cyclopenta[2,1-b:3,4-b']dithiophene; **CPDT**) was selected as a comonomer for **BTA**. Moreover, the resulting copolymer of electron-rich (**CPDT**) and -poor (**BTA**) units in the polyconjugated backbone would have donor–acceptor character and so should be an exceptionally low bandgap material, which might induce high conductivity. The synthesis of **CPDT** was undertaken as Scheme 2.7.[30,31] The first synthesis step was a one-pot process involving the formation of 3-thienyllithium (prepared via metal halogen exchange between 3-bromothiophene and *n*-BuLi) followed by a reaction with thiophene-3-carboxaldehyde (3-ThCHO) to generate an intermediate lithium dithienylmethoxide. The methoxide was then reacted with two equivalents of *n*-butyllithium and three equivalents of iodine which yielded after hydrolysis the 2,2'-diiodoalcohol **19**. In the second step, alcohol **19** was oxidized with pyridinium chlorochromate (PCC) giving the 2,2'-diiodoketone **20**, which was subjected to an Ullmann coupling reaction which afforded the cyclopentadithiophenone **21**. Reduction of **21** according to the Huang-Minlon modification of the Wolf-Kischner procedure afforded **22** in satisfactory yield. The reaction of **22** with 1-bromohexadecane under sodium hydroxide as base tetrabutylammonium chloride as phase-transfer catalyst produced the diaddition product **23**. The desired 2,7-dibromo-4,4-dihexadecylcyclopentaditiophene (**24**) was obtained after treatment with bromine in acetic acid/chloroform in 91 % isolated yield.

Scheme 2.7. Synthetic route to **CPDT** and the random copolymer **P3**.

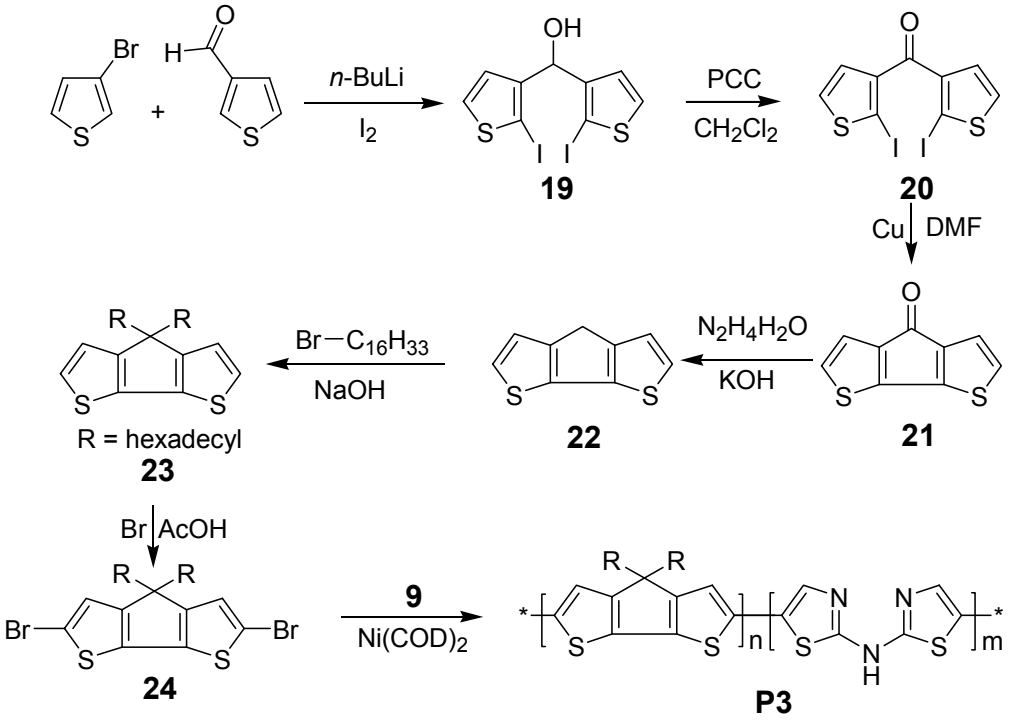

The copolymerization of **BTA** with **24** (50 % mol) was performed by Yamamoto polycondensation in the presence of nickel(0). As expected, FT-IR analysis of this polymer **P3** demonstrated that the carbamate group had been completely cleaved off. However, **P3** was completely insoluble in common organic solvents even with two long solubilizing groups (hexadecyl) at the 4,4-positions of the **CDPT** moiety. On the basis of this unexpected result, the **BTA** moieties along the polymer backbone cannot be utilized as post-polymerization metal coordination sites due to its insolubility. In an alternate approach, initial metallation of the **BTA** unit was carried out to obtain the desired metal/conjugated polymer product. The solubility of the metallated copolymer could be anticipated to be higher in polar solvents. In a preliminary study, $Pd(II)Cl_2(PhCN)_2$ ligand was selected and the reaction with **9** in THF solution provided a dark brown powdery material which showed good solubility in polar solvents (Scheme 2.8). Even though the complete structural characterization of **25** could not be conducted due to failure to obtain single crystals, the Pd(II) complexation can be inferred from the complete change in solubility and color between **9** and **25**. The Pd(II)-metallated random copolymer **P4** was

synthesized from **24** and **25** (50 % mol) using Yamamoto-type type cross-coupling. The metallated copolymer **P4** again has limited solubility in organic solvents (both polar and non-polar). Due to the poor solubility of metal free copolymer **P3** and metal-organic hybrid copolymer **P4**, further studies on their photophysical properties were limited. It was expected that **P4** would show higher conductivity than **P3** since Pd species should increase order in the polymer. Upon iodine doping, however, both the polymers (**P3** and **P4**) show only semiconducting behavior with measured conductivities of 10^{-5} and 10^{-6} Scm^{-1} respectively (measured on a pellet). It is postulated that the instability of the polymers after iodine doping can account for the observed low conductivity. Also, we propose that the observed decrease in the conductivity of **P4** upon binding with Pd(II) is the result of diminished delocalization of charge carriers compared to the parent polymer **P3**.

Scheme 2.8. Synthetic route to Pd(II) complex and its random copolymer with **24**.

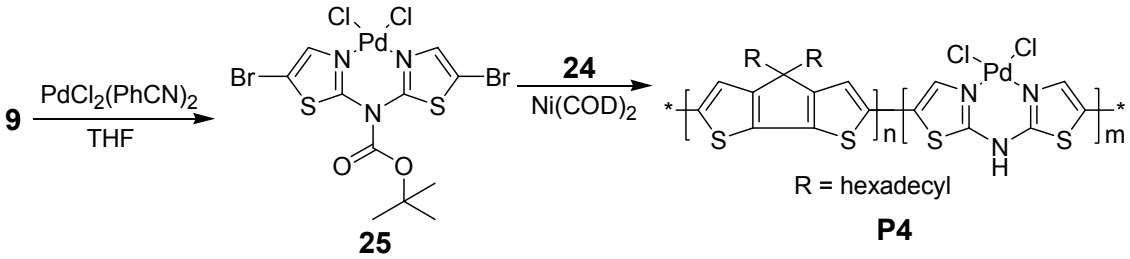

2.3 Conclusion

In efforts to develop five member heterocyclic analogues to polyaniline, a series of poly(5,5'-dithiophen-2-yl-amine) (**4**), poly(5,5'-bisthiazol-2-yl-amine) (**P1**), and *N*-substituted poly(5,5'-bisthiazol-2-yl-amine) (**P2**) have been prepared by nickel(0) mediated Yamamoto-type coupling. Conductivity measurements after oxidative iodine doping show all the materials to be semiconductors with a measured conductivity of 10^{-6} Scm^{-1} for **4**, 10^{-8} Scm^{-1} for **P1** and 10^{-7} Scm^{-1} for **P2**. Alkylation at nitrogen renders **P1** soluble and poly(5,5'-(2-hexyl-decyl)-bis-thiazol-2-yl-amine) **P2** show an emission maximum at 444 nm and its HOMO and LUMO levels are estimated to be 5.11 eV and 2.90 eV respectively. These results disclose the optical and redox properties of the first example of a **BTA**-based polymer. The **BTA** unit has coordination sites to incorporate

metals, which allowed us to study the properties of the metal-organic hybrid materials and compare them with the parent materials. Metal complexes with (Cu(II) and Pd(II)) were synthesized which showed paramagnetic behavior. The crystal structure of the Cu(II) complex **12** with **BTA** comprises **BTA** and copper in a 2:1 ratio with tetrahedral geometry around the copper while the Pd(II) complex **13** displays a 1:1 ratio with square-planar geometry. From the interesting donor-acceptor concept, a material comprising **BTA** representing n-type unit and triphenylamine representing p-type unit was prepared. Additionally, its metal complexes with Cu(II) and Pd(II) were obtained. In attempts to get soluble polymers based on **BTA**, the copolymer **P3** containing **BTA** and **CPDT** with long solubilizers at 4,4'-position and its Pd(II) complexed polymer **P4** were synthesized but this did not improve the overall solubility. The conductivity difference between the unmetallated copolymer **P3** and metallated copolymer **P4** is found to be small when measured after iodine doping (measured on a pellet) but this result is contrary to the theoretical concept of coordinating a metal atom directly into the long-range π-system of a conjugated polymer as a means of enhancing conductivity. This observed low conductivity can be explained by two possible effects: (1) The doping state is not stable; (2) The conductivity of polymers is likely limited by chain-to-chain charge transport events when there is significant delocalization along the chain. Both inter- and intrachain charge transport events can be significant in governing the "conductivity." Therefore, the random copolymers (**P3** and **P4**) are both less delocalized than the parent homopolymer (**CDPT**). This work marks the first time an attempt has been made to use the conjugated metal hybrid strategy to build conducting polymers containing **BTA** unit. These studies provide a basis for understanding the photophysical properties of metal-organic based **BTA**, which in turn will guide the design of new materials based on **BTA** that find application as the active materials in electronic and photonic devices in the future.

2.4 References

(1) Macdiarmid, A. G.; Chiang, J. C.; Richter, A. F.; Epstein, A. J. *Synth. Met.* **1987**, *18*, 285-290.

(2) Huang, W. S.; Humphrey, B. D.; Macdiarmid, A. G. *J. Chem. Soc., Faraday Trans.* **1986**, *82*, 2385-2400.

(3) Kang, E. T.; Neoh, K. G.; Tan, K. L. *Prog. Polym. Sci.* **1998**, *23*, 277-324.

(4) Focke, W. W.; Wnek, G. E.; Wei, Y. *J. Phys. Chem.* **1987**, *91*, 5813-5818.
(5) Epstein, A. J.; Ginder, J. M.; Zuo, F.; Bigelow, R. W.; Woo, H. S.; Tanner, D. B.; Richter, A. F.; Huang, W. S.; Macdiarmid, A. G. *Synth. Met.* **1987**, *18*, 303-309.
(6) Ginder, J. M.; Richter, A. F.; Macdiarmid, A. G.; Epstein, A. J. *Solid State Commun.* **1987**, *63*, 97-101.
(7) Macdiarmid, A. G.; Chiang, J. C.; Halpern, M.; Huang, W. S.; Mu, S. L.; Somasiri, N. L. D.; Wu, W. Q.; Yaniger, S. I. *Mol. Cryst. Liq. Cryst.* **1985**, *121*, 173-180.
(8) Chiang, J. C.; Macdiarmid, A. G. *Synth. Met.* **1986**, *13*, 193-205.
(9) Wessling, B. *Synth. Met.* **1997**, *85*, 1313-1318.
(10) Joo, J.; Epstein, A. J. *Appl. Phys. Lett.* **1994**, *65*, 2278-2280.
(11) Hartmann, H.; Gerstner, P.; Rohde, D. *Org. Lett.* **2001**, *3*, 1673-1675.
(12) Hartwig, J. F. *Synlett* **1997**, 329-340.
(13) Hartwig, J. F.; Kawatsura, M.; Hauck, S. I.; Shaughnessy, K. H.; Alcazar-Roman, L. M. *J. Org. Chem.* **1999**, *64*, 5575-5580.
(14) Watanabe, M.; Yamamoto, T.; Nishiyama, M. *Chem. Commun.* **2000**, 133-134.
(15) Wolfe, J. P.; Tomori, H.; Sadighi, J. P.; Yin, J. J.; Buchwald, S. L. *J. Org. Chem.* **2000**, *65*, 1158-1174.
(16) Jiang, L.; Job, G. E.; Klapars, A.; Buchwald, S. L. *Org. Lett.* **2003**, *5*, 3667-3669.
(17) Wolfe, J. P.; Wagaw, S.; Marcoux, J. F.; Buchwald, S. L. *Acc. Chem. Res.* **1998**, *31*, 805-818.
(18) Beyer, H.; Berg, G. *Chem. Ber.* **1956**, *89*, 1602-1608.
(19) Bredas, J.-L. In *Handbook of conducting polymers*; Skotheim, T. A., Ed.; Marcek Dekker: New York, 1986, p 859-913.
(20) Fujita, S. *Synthesis* **1982**, 423-424.
(21) Kabumoto, A.; Shinozaki, K.; Watanabe, K.; Nishikawa, N. *Synth. Met.* **1988**, *26*, 349-355.
(22) Kobayashi, T.; Yoneyama, H.; Tamura, H. *J. Electroanal. Chem.* **1984**, *177*, 281-291.
(23) Chevalier, J. W.; Bergeron, J. Y.; Dao, L. H. *Macromolecules* **1992**, *25*, 3325-3331.
(24) Watanabe, A.; Mori, K.; Iwabuchi, A.; Iwasaki, Y.; Nakamura, Y.; Ito, O. *Macromolecules* **1989**, *22*, 3521-3525.
(25) Janietz, S.; Bradley, D. D. C.; Grell, M.; Giebeler, C.; Inbasekaran, M.; Woo, E. P. *Appl. Phys. Lett.* **1998**, *73*, 2453-2455.
(26) Miyaura, N.; Suzuki, A. *Chem. Rev.* **1995**, *95*, 2457-2483.
(27) Braun, D.; Heeger, A. J. *Appl. Phys. Lett.* **1991**, *58*, 1982-1984.
(28) Müllen, K.; Wegner, G. In *Electronic Materials: The Oligomer Approach*; Wiley-VCH: New York, 1998.
(29) Zotti, G.; Schiavon, G.; Berlin, A.; Fontanna, G.; Pagani, G. *Macromolecules* **1994**, *27*, 1938-1942.
(30) Coppo, P.; Cupertino, D. C.; Yeates, S. G.; Turner, M. L. *Macromolecules* **2003**, *36*, 2705-2711.
(31) Brzezinski, J. Z.; Reynolds, J. R. *Synthesis* **2002**, 1053-1056.

Chapter 3 Polymeric Materials Containing 9,10-Anthrylene Units

In this chapter, the synthesis and characterization of a series of materials based on polyphenylenes and poly(phenyleneethynylene)s with 9,10-anthrylene subunits are presented. Some anthracene-based materials are known to be efficient blue emitters and the goal here is to develop a suitable anthracene-based material which is readily synthesized and polymerized with other suitable comonomers. Towards this end, 9,10-dibromo-2,6-di(2-octyldecyl)-anthracene (**30**) bearing a branched alkyl chain is obtained. A PPP-type copolymer based on anthracene repeat units with branched alkyl side-chains and *p*-terphenyl units (**P5**) as well as two PPE analogues obtained by copolymerization of the anthracene repeat unit with *p*-diethynylbenzene (**P6**) and diphenylacetylene (**P7**) are discussed. Besides, the synthesis and characterization of step-ladder and ladder poly(*p*-phenylene-*alt*-anthrylene)s (**SLPPPA** and **LPPPA** respectively) containing 9,10-anthrylene building groups within the main chain are explored (see below). The step-ladder derivatives are found to form endoperoxides in the presence of visible light in a thermally reversible process whereas the ladder derivatives undergo irreversible photooxidation.

9,10-Linked anthrylene copolymers

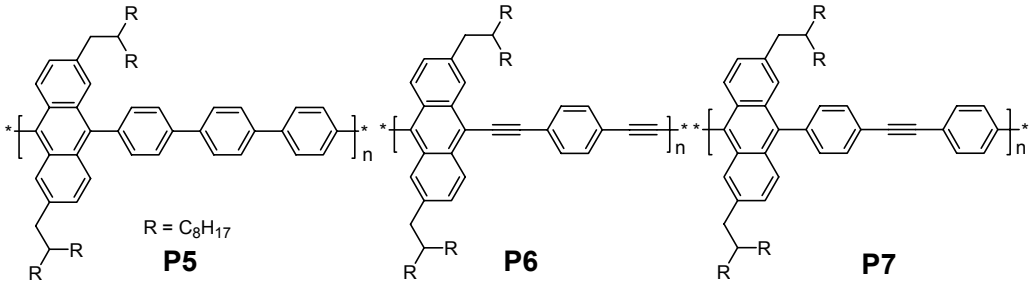

9,10-Linked anthrylene-based ladder polymers

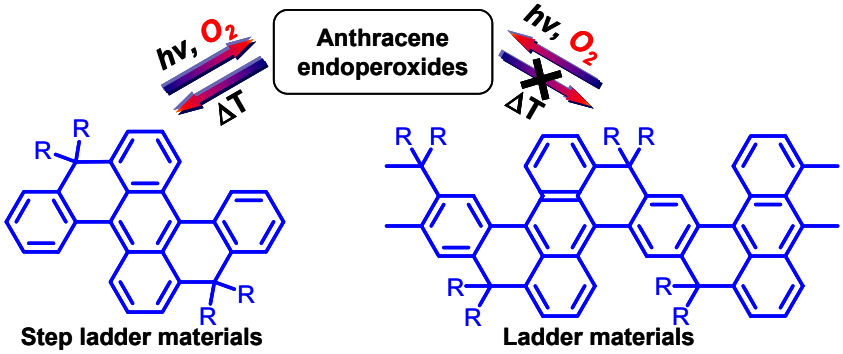

3.1 Polyphenylenes and Polyphenyleneethynylenes with 9,10-Anthrylene Subunits

Modifying the electronic structure and properties of conjugated polymers is a major challenge in the design of new materials. Poly(*p*-phenylene)s (PPP)s[1-6] constitute a particularly important class of polymers in that they emit in the blue and can act as hosts for downhill energy transfer to generate green and red emitters in polymer light emitting diodes (PLEDs).[7-9] Poly(*p*-phenyleneethynylene) (PPE), another fully conjugated system, exhibits high solution-state quantum yields and typically possesses wider bandgaps than its poly(*p*-phenylenevinylene) (PPV) counterpart, allowing for a bluer emission.[4] To date, however, PPE based materials have received only limited attention as light emitting materials[10-13] due to aggregation phenomena[14] attributed to strong π-π stacking of the

PPE polymer backbone.

To overcome these disadvantages, we directed our attention to the anthracene moiety which is known as a blue light emitter[15,16] with good hole and electron transport properties. 9,10-Disubstituted anthracene derivatives were investigated as some, *e.g.* 9,10-diphenylanthracene (DPA) and 9,10-bis(phenylethynyl)anthracene (BPEA), exhibit very high photoluminescence quantum yields[17-20] and are thus some of the "strongest" fluorophores known. Therefore, it was expected that copolymers containing 9,10-linked anthrylene and suitable phenylene or phenyleneethynylene moieties would be materials with promising optical properties for use in LEDs. However, all previous reports on copolymers containing 9,10-linked anthrylene and phenylene have solubilizing groups such as alkoxy or alkyl on the phenylene backbone which cause high torsion between anthrylene and phenylene units resulting in reduced conjugation along the chain. One way to minimize this undesirable twist is to introduce the solubilizing group on the anthracene unit. Furthermore, the introduction of branched alkyl side chains as solubilizers can prevent undesirable stacking in the solid state, and eliminate long wavelength emission.

Only one paper has described a synthesis of 9,10-dibromoanthracene with branched alkoxy side chains.[21] Herein, we present a facile synthetic protocol for the preparation of 9,10-dibromo-2,6-di(2-octyldecyl)-anthracene (**30**) as a building block for copolymers. The synthesis and characterization of a PPP-type blue-emitting copolymer containing **30** and *p*-terphenyl units (**P5**), both inherent blue-emitters on their own, are described. Also, we report on the synthesis of two PPE analogues obtained by copolymerization of **30** with *p*-diethynylbenzene (**P6**) and diphenylacetylene (**P7**) (Chart 3.1). **P5** showed the best solubility and film forming ability among the three copolymers, and was

incorporated into devices. The unoptimized OLEDs exhibit deep blue electroluminescence, however, the efficiency of unoptimized devices is below 0.1 cd/A and the device stability is only in the range of minutes for the best devices.

Chart 3.1. Anthracene based copolymers

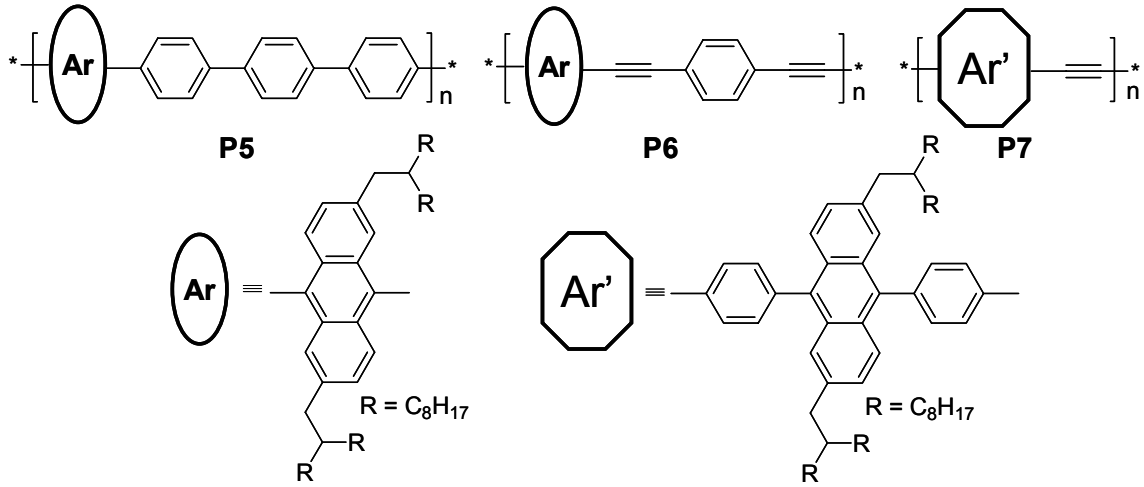

3.1.1 Synthesis and Characterization

Scheme 3.1 outlines the synthesis of the 9,10-dibromoanthracene monomer **30** with branched alkyl side chains (2-octyldecyl) and of its copolymer using the *p*-terphenyl moiety. Commercially available 2,6-diaminoanthraquinone was converted into 2,6-dibromoanthraquinone (**27**) via a Sandmeyer reaction using *tert*-butyl nitrite and anhydrous copper(II) bromide in 85% yield.[22] The branched alkyl side chain was introduced through a Suzuki-type coupling reaction. First, 1,1-dioctylethylene (**28**) was synthesized from 9-heptadecanone by a Wittig reaction.[23] Then, in a one-pot reaction, **28** was first transformed into the corresponding terminal diboronic ester by treatment with 9-BBN and then coupled with **27** under palladium catalysis to generate 2,6-di(2-octyldecyl)anthraquinone (**29**) in 35 % isolated yield.

Scheme 3.1. Synthesis of alternating copolymer **P5**.

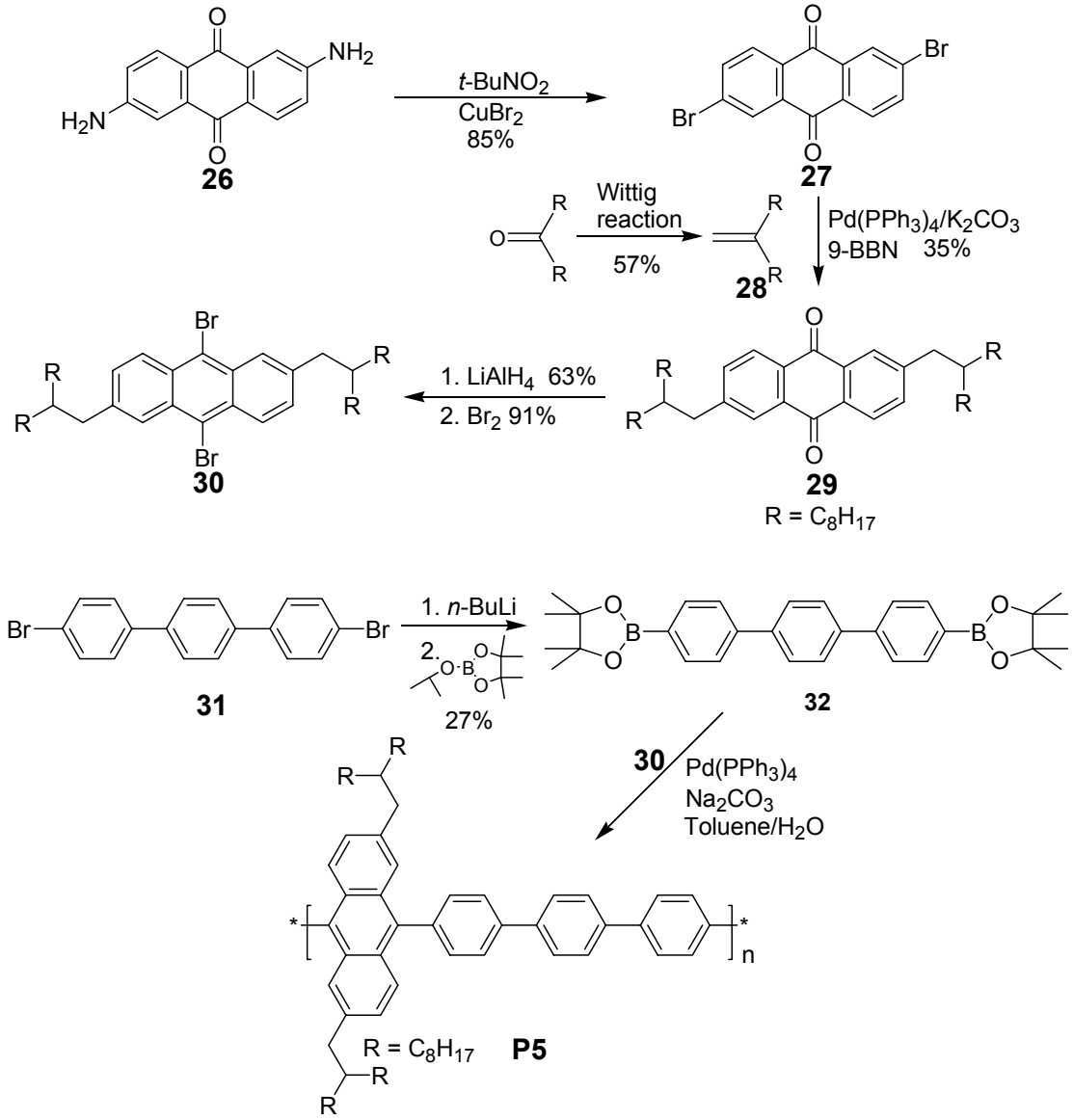

The poor solubility of **27** mostly accounts for the observed low yield. The reduction of **29** was performed by treatment with $LiAlH_4$ and the desired 9,10-dibromo-2,6-di(2-octyldecyl)anthracene (**30**) was obtained after treatment with bromine in acetic acid in 91 % isolated yield. Prior to this preparation of **30**, the 9,10-dibromo-2,6-didodecyl-anthracene monomer with linear solubilizers was successfully synthesized from the same

procedure above using 1-dodecene instead of **28**. Since the solubility of this monomer is limited in organic solvents at room temperature due to the intrinsic rigidity of the anthracene unit, the monomer **30** is preferential for copolymerization, where it should induce improved solubility and suppress stacking in the solid state. 4,4"-Dibromo-*p*-terphenyl (**31**)[24] was converted into the corresponding diboronic ester **32** to generate the comonomer. The copolymer **P5** was synthesized by Suzuki polycondensation of **30** and **32** under palladium catalyzed conditions. **P5** is readily soluble in common organic solvents (THF, toluene, dichloromethane, etc.) and shows pure blue emission in solution.

A PPE-type copolymer of anthracene **P6** was synthesized from **30** and *p*-diethynylbenzene using a Sonogashira-Hagihara-type cross-coupling reaction (Scheme 3.2). **P6** has limited solubility in organic solvents (THF, toluene, dichloromethane, etc.) and exhibits green emission in solution. The poor solubility of **P6** can be attributed in part to the presence of two ethynyl bonds per repeat unit in the main chain. A modified PPE-analogous copolymer of anthracene **P7** was then chosen in order to improve its solubility. It has been reported that steric interactions of 9,10-phenyl substituents with hydrogen atoms in the *peri*-positions of the anthracene unit (1,8 and 4,5) in DPA cause an out-of-plane twisting.[25] Hence, DPA based **P7** is expected to give a blue shift in absorption and emission and at the same time improve solubility in comparison with **P6**. The Suzuki polycondensation to **P7** is preferred over a Hagihara-type reaction to eliminate the possibility of diyne defect formation. Di(4-bromophenyl)acetylene (**33**)[26] was transformed into the corresponding diboronic ester **34** via lithiation and subsequent reaction with 2-isopropoxy-4,4,5,5-tetramethyl-1,3,2-dioxaborolane (57%). Suzuki polycondensation of monomers **30** and **34** under standard conditions generated the target copolymer **P7**. The copolymer **P7** shows improved solubility in organic solvents (THF,

toluene, dichloromethane, etc.) when compared with **P6** and pure blue emission (λ_{max} = 449 nm). Gel-permeation chromatography (GPC) analysis against PPP standard[27] exhibits a number-averaged molecular mass (M_w) of 6.62×10^3, 1.25×10^4 and 4.89×10^4g/mol, for **P5**, **P6** and **P7** respectively with a polydispersity of 1.24, 2.60 and 3.04.

Scheme 3.2. Synthesis of alternating copolymers **P6** and **P7**

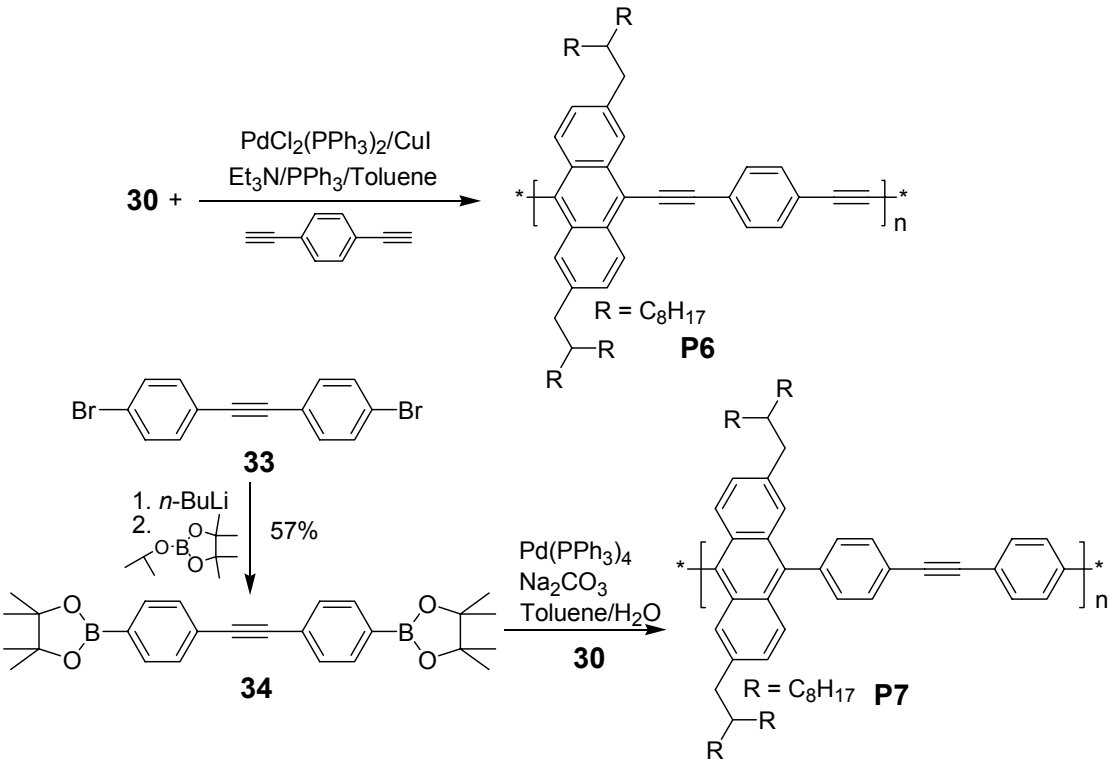

It has previously been reported that 9,10-dibromoanthracene itself does not undergo Ni(0) mediated Yamamoto-type polycondensation.[28] The logical reason was that in the case of 9,10-dibromoanthracene, its reaction with $Ni(COD)_2$ in presence of PPh_3 as a ligand affords the complex $L_mNiX(C_6H_4X)$ which has high thermal and chemical stability. In fact, it was found to be stable in boiling toluene for several hours in air and also as

dispersion in hydrochloric acid. In the case of this complex, the steric effect of the bulky anthryl group as well as back-bonding between nickel and the aromatic group accounts for the high stability of the Ni-C bond. Addition of bipyridine instead of PPh_3 as the neutral ligand does not afford the polymer either. Hence, the Suzuki polycondensation approach towards generating a soluble poly(9,10-anthracene diyl) from **30** having solubilizing substituents was undertaken (Scheme 3.3). When polymerization conditions analogous to the synthesis of **P5** or **P7** were used, no polymers were obtained. In Suzuki reactions involving sterically hindered substrates, limited success has been realized so far.[29-33] New generation ligands which facilitated Suzuki coupling reaction of two hindered arenes have recently been reported.[34,35] Dicyclohexyl-(2-phenanthren-9-yl-phenyl)-phosphine as a ligand was chosen, reported to be highly active for the Suzuki coupling reaction toward sterically hindered biaryls,[34] however, no polymerization was observed. A microwave-assisted (300 W) polymerization did not succeed either.[36] Analysis by Field Desorption Mass Spectrometry (FDMS) of the resulting substrates reveals four strong intense peaks which stem from the parent anthracene and its dimer as well as the corresponding anthraquinones.

Scheme 3.3. Attempts towards poly(9,10-anthracene diyl)

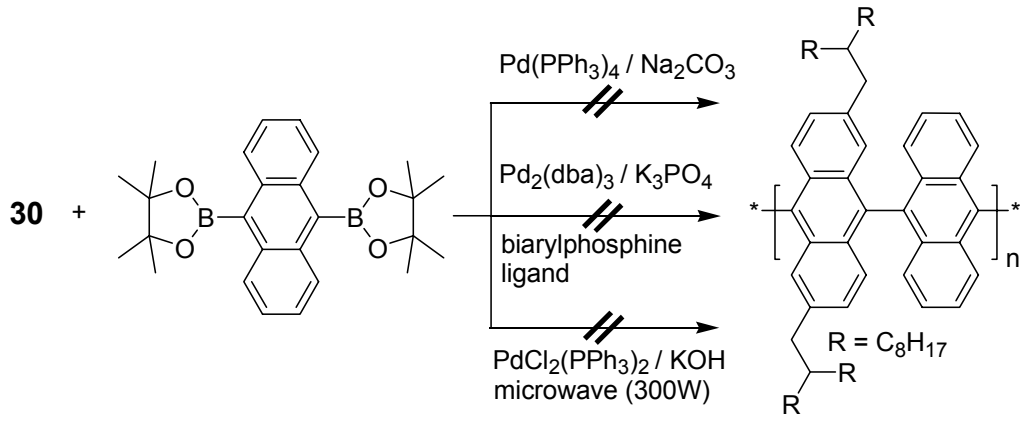

We conclude that these failures are due to the large inherent steric hindrance between the anthracene units and/or the reduced stability of the intermediate palladium complexes involving the 9,10-conjugated anthracene moiety.

TGA thermograms of all the polymers (**P5**, **P6**, and **P7**) exhibit good thermal stability up to 370 °C, which is essential for fabrication of stable PLEDs. Weight loss (5 %) starts at 410, 387, and 401 °C for **P5**, **P6**, and **P7** respectively. The phase transition of the polymers are investigated by differential scanning calorimetry (DSC) in a nitrogen atmosphere at a heating rate of 10 °C/min, but we observed neither a glass transition process (T_g) nor other thermal processes (such as liquid crystalline phase) between - 50 °C and 200 °C.

3.1.2 Electrochemical Properties

The redox behavior of the polymers (**P5**, **P6**, and **P7**) was investigated by cyclic voltammetry (CV) on thin films against Ag/Ag+. All the polymers show an irreversible oxidation, with oxidation onset values ranging from 2.88 V vs Ag/Ag+ for **P5**, 2.24 V for **P6**, 2.87 V for **P7** and the oxidation potential slightly increases in the order **P6** < **P5** < **P7** (Figure 3.1). Calculating the energy level of Ag/AgCl to -4.4 eV from the ferrocene/ferrocenium standard,[37,38] and determining the bandgap from the absorption onset, the HOMO and LUMO values for **P5** are estimated to be -5.52 eV and -2.64 eV respectively.[39,40] The corresponding values for **P6** are -5.41 and -3.17 eV and for **P7**, -5.57 and -2.70 eV respectively.

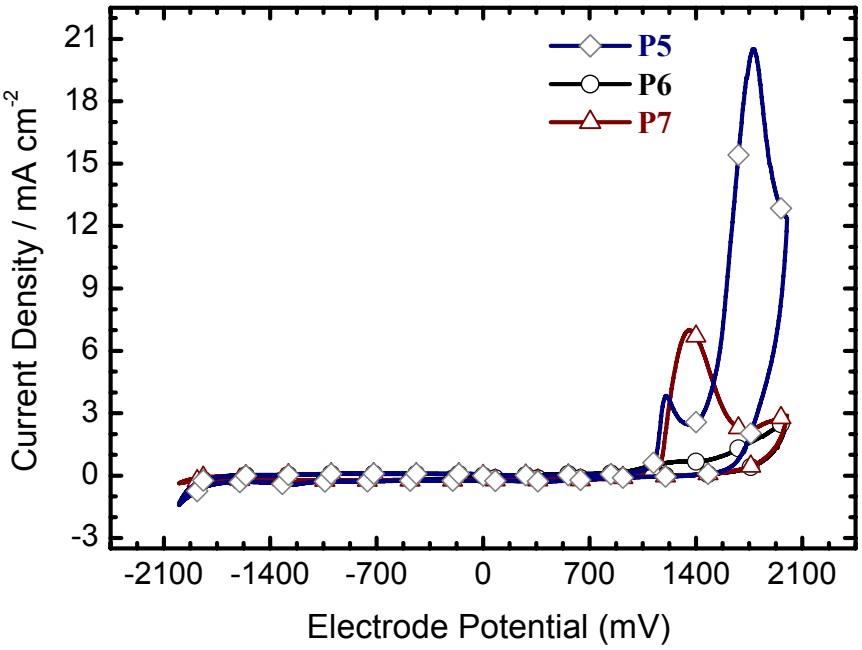

Figure 3.1. Cyclic voltammetry curves of drop-cast films of **P5, P6,** and **P7** measured in acetonitrile containing 0.1 M Bu_4NClO_4 solution at a scan rate 100 mV/s at room temperature.

3.1.3 Photophysical Properties

Table 3.1 summarizes the molecular weights of the three copolymers containing anthracene (THF, PPP standards). The UV-vis absorption and photoluminescence of the polymers (**P5**, **P6**, and **P7**) were investigated both in THF solution and in thin solid films as depicted in Figures 3.2-3.4. Transparent and uniform polymer films were prepared on quartz by spin-casting from their respective THF solutions at room temperature. The absorption and PL spectral data for all the polymers are summarized in Table 3.2. The absorption maxima for **P5**, **P6**, and **P7** are at 403, 490, and 404 nm respectively, arising due to π-π* transitions from the conjugated polymer backbone.

Table 3.1. Physical properties of the copolymers (**P5**, **P6**, and **P7**)

copolymer	M_n	M_w	PDI	$T_d{}^b$(°C)
P5	5.33×10^3	6.62×10^3	1.24	410
P6[a]	4.82×10^3	1.25×10^4	2.60	387
P7	1.67×10^4	4.89×10^4	3.04	401

Estimated from GPC (eluent = THF, poly *p*-phenylene standards). [a] For the THF-soluble part. [b] Onset decomposition temperature (5 % weight loss).

In the case of **P5**, the absorption consists of three well distinct peaks at 364, 383, and 403 nm, which can be associated with anthracene moieties in the main chain because these values for absorption and shape are similar to those of pure anthracene in solution. The PL spectrum of **P5** in THF solution displays pure blue emission with a peak centered at 444 nm without any shoulder peaks. The position of the emission maximum is very close to that of a semiladder-type poly(pentaphenylene) (445 nm)[27] and lies between those of poly(tetraalkylindenofluorene) (430 nm)[41] and fully ladder-type polyphenylene (460 nm),[42] which are some of the best candidates as blue emitters in PLEDs. The PL spectrum of **P5** in film is almost identical to that in solution, and no bathochromic shift is observed. This suggests that there is almost no change in the conformation of the polymer backbone when going from solution to the solid state.

Table 3.2. Optical data of the copolymers (**P5**, **P6**, and **P7**).

copolymer	solution λ_{max} (nm)		film λ_{max} (nm)	[a]Stokes shift (nm)
	absorption	emission	emission	
P5	364, 383, 403	444	458	41
P6	324, 490	540	540 (572)	50
P7	366, 384, 404	449	449	45

[a]Stokes shift = $PL_{solution}$ / nm – $UV_{solution}$ / nm

Peaks that appear as shoulders or weak bands are shown in parentheses

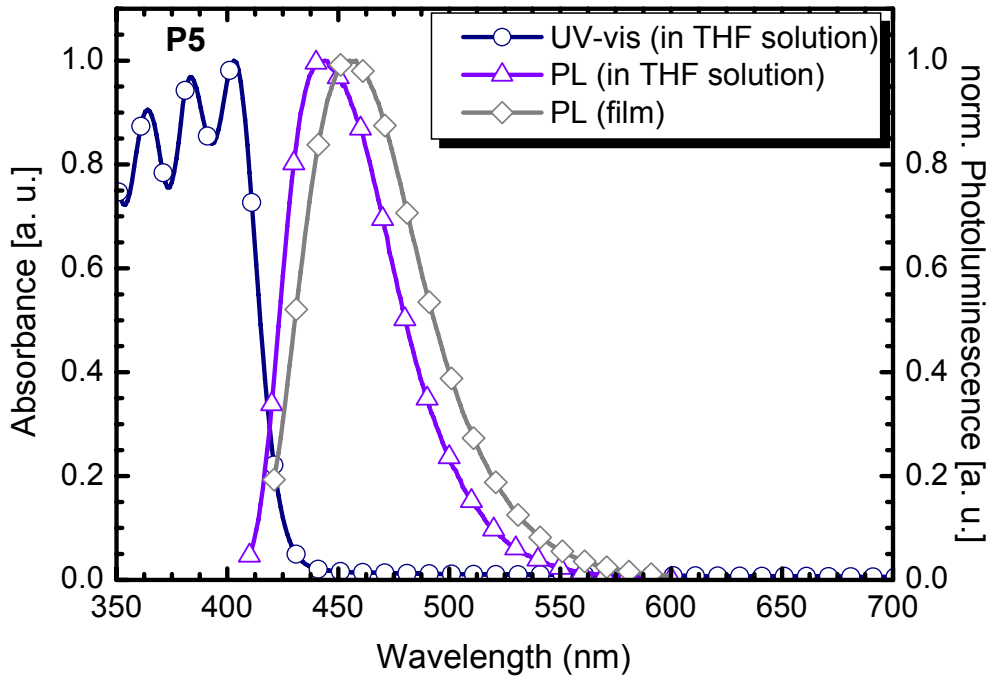

Figure 3.2. UV-vis (THF solution; –○–, ε_{max} : 13920 $M^{-1}cm^{-1}$) and PL (THF solution; –△–, film; –◇–, λ_{exc} = 410 nm) spectra of **P5**.

The PPE-type copolymer **P6** in solution displays an absorption maximum at 490 nm and emits in the green (λ_{max} = 540 nm). The observation of a pronounced bathochromic shift is a clear indication that the PPE-type **P6** has improved π-conjugation when compared to PPP-type copolymer **P5**. This is not unexpected due to the ethynyl units in the main chain since BPEA and its derivatives are bathochromically shifted toward the green when compared to DPAs. For PPE-analogous **P7** in dilute solution, absorption maxima are seen at 366, 384, 404 nm. The PL spectrum both in solution and thin film exhibit an emission maximum at 449 nm when excited at 400 nm.

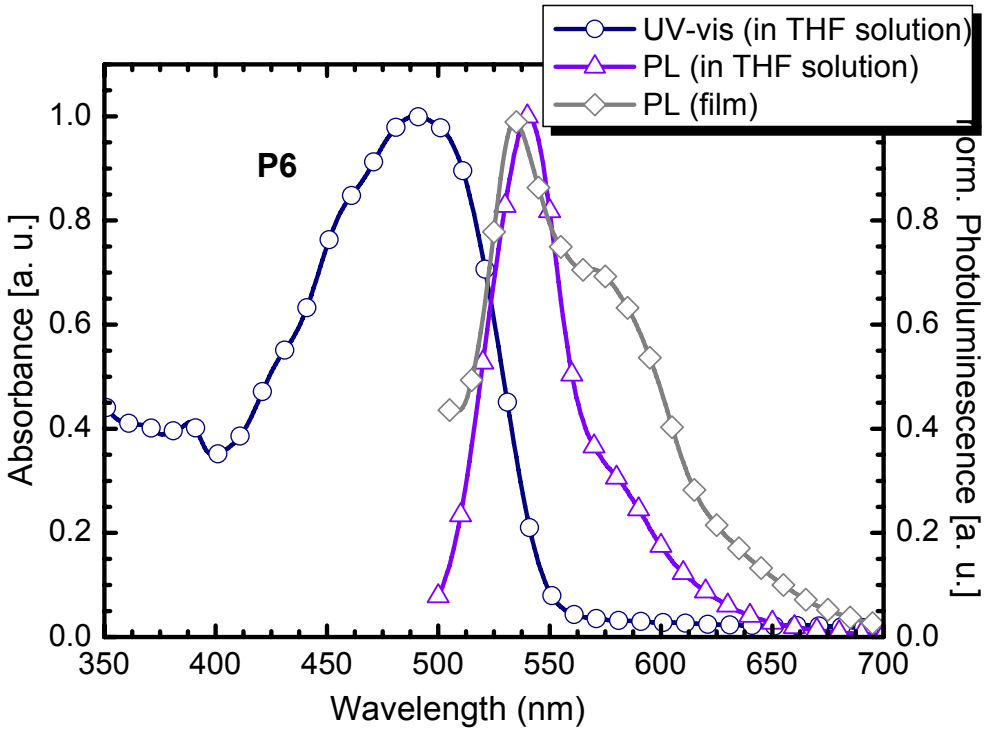

Figure 3.3. UV-vis (THF solution; –○–, ε_{max} : 3520 $M^{-1}cm^{-1}$) and PL (THF solution; –△–, film; –◇–, λ_{exc} = 490 nm) spectra of **P6**.

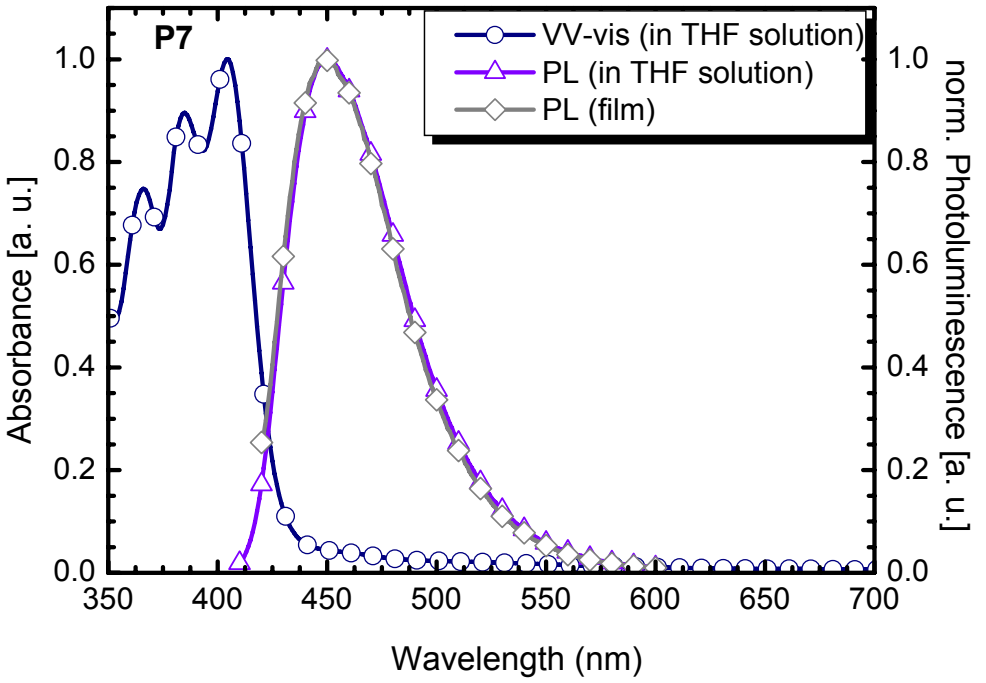

Figure 3.4. UV-vis (THF solution; –○–, ε_{max} : 13800 $M^{-1}cm^{-1}$) and PL (THF solution; –△–, film; –◇–, λ_{exc} = 410 nm) spectra of **P7**.

The absorption and PL spectra reveal remarkable similarities between **P5** and **P7**. The nearly identical PL spectra in solution and film for **P5** and **P7** rule out any aggregation in the solid state for these polymers. However, the PPE-analogous **P6** shows an emission maximum at 540 nm and a shoulder at 572 nm in the film. The strong shoulder peak in the film spectrum can be ascribed to solid state interactions between the polymer chains due to increased backbone planarity as well as self-absorption in the film. However, no significant bathochromic shift is observed. Notably, the absorption and emission maximum at 490 and 540 nm for **P5** are substantially hypsochromically shifted compared to the alternating copolymer containing 9,10-linked anthrylene and phenylene bearing solubilizing groups as alkoxy-side chains on the phenylene backbone (λ_{abs} = 543 nm and λ_{em} = 590 nm) by Swager *et al*.[43,44] It has been suggested that the strong electron-donating characteristic of alkoxy side chains causes bathochromical shift.

The absence of stacking phenomena in the solid state for the copolymers prompted us to investigate the color and thermal stability over an extended temperature range. For degradation studies on a thin film, copolymer **P5** which showed the best solubility and film forming ability among the three copolymers was tested (Figure 3.5). The PL spectra of the film were recorded after 30 minutes at each increased temperatures until 210 °C. All emission bands show the same featureless character as in solution with a little red-shift at 210 °C. This result confirms the color stability of **P5** in PL spectra.

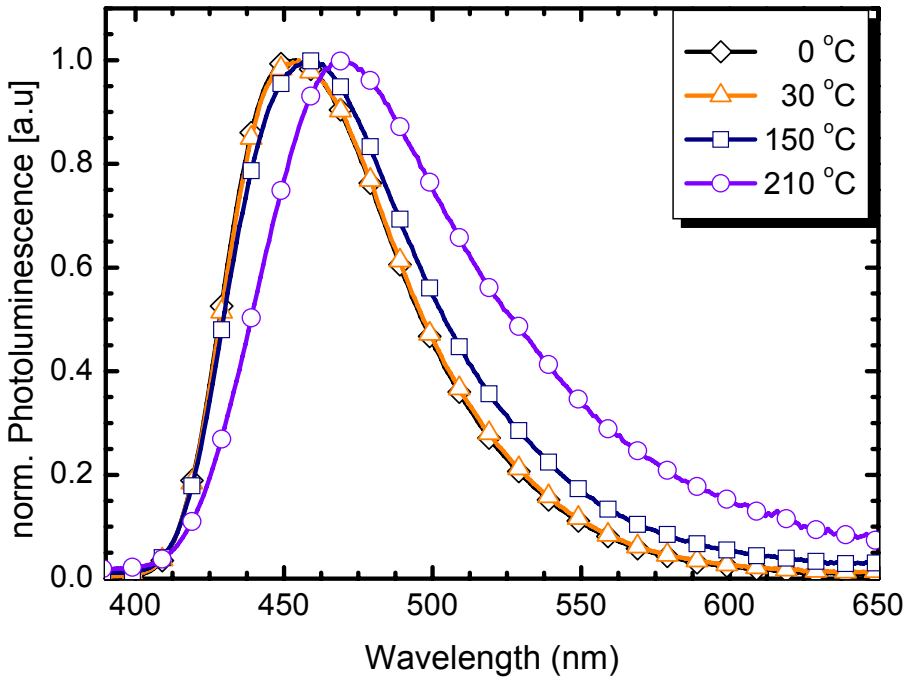

Figure 3.5. PL spectra of **P5** film heated at different temperatures (λ_{exc} = 365 nm).

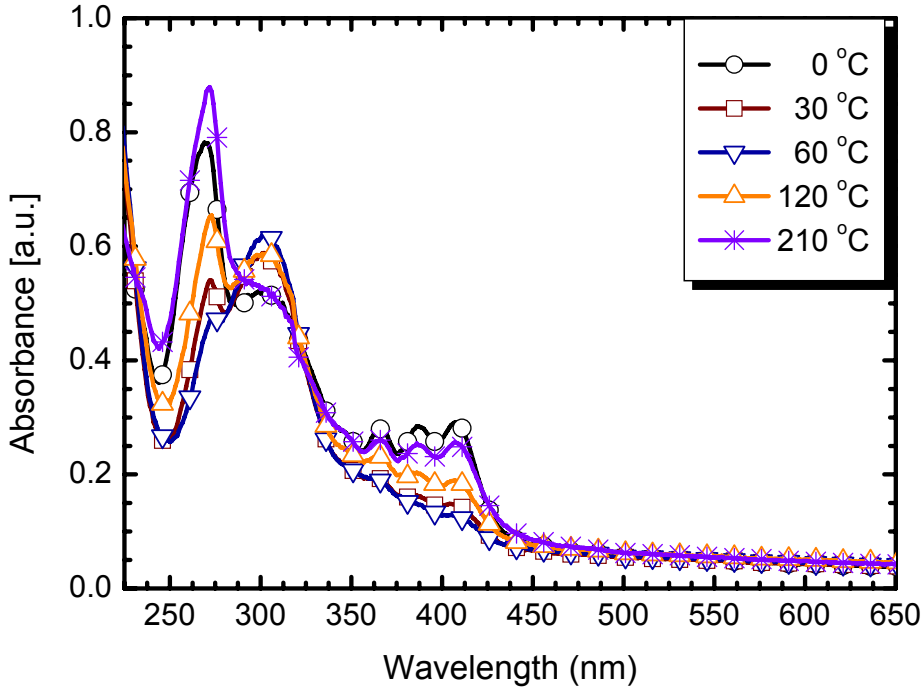

Figure 3.6 Absorption spectra of **P5** films heated at different temperatures.

During the degradation test on **P5**, the absorption spectra changed reversibly (Figure 3.6). The first measurement shows well resolved vibronic structures typical of anthracene between 350 and 400 nm. These structures can not be seen in the second measurement but reappeared at higher temperatures. This observation can be explained by two possible effects: (a) The loss of the well resolved absorption features might be caused by the well known dimerisation of anthracene, which is caused by UV light and can be reversed thermally.[45,46] Also, the ratio of the two peaks at 260 nm and 300 nm changes which can also be attributed to the dimerisation (Figure 3.7a). The PL, however, is not strongly altered by these effects and (b) to the formation of an endoperoxide for example, DPA reacts with oxygen rapidly to give the corresponding endoperoxide under light and can be restored upon heating (Figure 3.7b).[47,48]

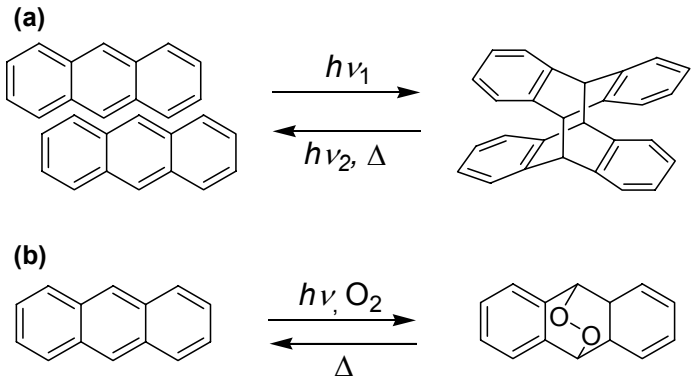

Figure 3.7. Dimerisation (a) and endoperoxide (b) formation in anthracene

3.1.4 Electroluminescence (EL) Properties

Light emitting devices were fabricated in a standard ITO/PEDOT:PSS/**P5**/Al configuration. The devices show a blue emission (CIE coordinates 0.19, 0.18) with a luminance of *ca*. 10 cd/m^2 and an electroluminescence onset at *ca*. 10 V. In this device configuration, the emission is only stable for less than a minute before degradation of the

device sets in. The degradation is probably a consequence of the unoptimized device configuration. Initial tests using electron transport layers and/or Ca electrodes did not result in any drastic improvement of the device performance.

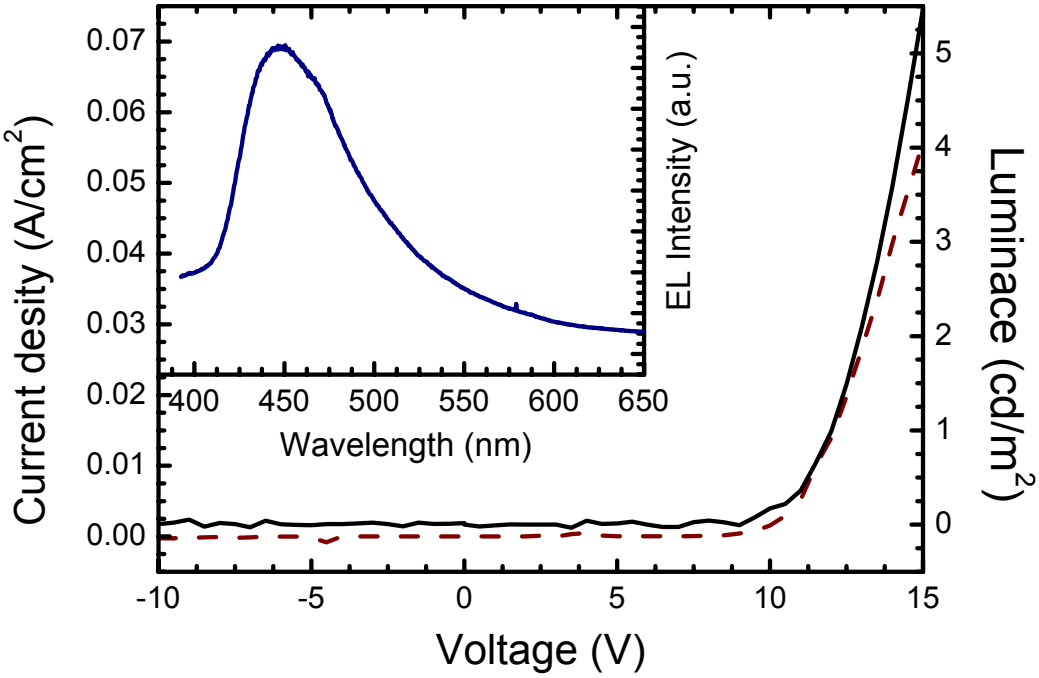

Figure 3.8 Voltage/current and voltage/Electroluminescence characteristics of a typical ITO/PEDOT/**P5**/Al device. The inset shows the EL spectrum recorded at 15 V after turn on.

3.1.5 Conclusion

A new 9,10-dibromoanthracene monomer with branched, solubilizing alkyl side chains (2-octyldecyl) at the 2,6-positions using a facile and short synthetic strategy was prepared. Upon copolymerizing this with *p*-terphenyl units, the resulting polymer **P5** shows pure blue emission both in solution and the solid state with a maximum centered around 450 nm. PPE analogues **P6** and **P7**, emit in the green and blue respectively both in solution and as films. The branched alkyl substituents inhibit the solid-state stacking in these copolymers as evidenced by the absence of any significant bathochromic shift

between the solution and film spectra. Degradation studies of **P5** reveal excellent color stability in PL spectra even on annealing at 200 °C. The attractive properties such as the suppression of the solid-state stacking and color stability of the photoluminescene establish them as good candidates for PLEDs and other polymer based optical and electrooptical applications. The unoptimized single-layer OLEDs with **P5** produces blue emission (*ca*. 448 nm) but the efficiency of unoptimized devices is below 0.1 cd/A and the device stability is only in the range of minutes for the best devices.

3.2 Synthesis and Photochemical Properties of Ladderised Poly(*p*-phenylene-*alt*-9,10-anthrylene)s

Recently, much research into π-conjugated polymeric materials has centered on poly-*p*-phenylene-based polymers such as step-ladder-type polyphenylenes[27,41,49,50] and fully ladder-type polyphenylenes[51] because they possess a unique set of optoelectronic properties due to their planarized molecular structures. The optoelectronic effects of conjugated polymers (including color tuning) are highly dependent on the nature of the building blocks, the pattern in which they are linked, and the type and position of the substituents.[36,52] Anthracene derivatives have been widely studied as organic light emitters due to their high fluorescence quantum yields.[17-19] In copolymers containing 9,10-linked anthrylene and phenylene moieties, however, steric interactions with the hydrogen atoms in the *peri*-positions of the anthracene cause a strong out-of-plane twisting (Chart 3.2).[25] Attempts to enhance the solubility by substitution of the rings force the consecutive phenylene and 9,10-anthrylene units even further out of a common plane resulting in reduced conjugation along the chain. Therefore, utilizing methylene bridges between 9,10-anthrylene and phenylene units in the main chain can offer a simple

alternative to minimize this twist along the polymer backbone and at the same time provide a site to attach solubilizing groups.

Chart 3.2. The molecular structures planarized by methylene bridges between 9,10-anthrylene and phenylene units in order to maximize the extended π-system. The R groups permit solubility of the ladderised system.

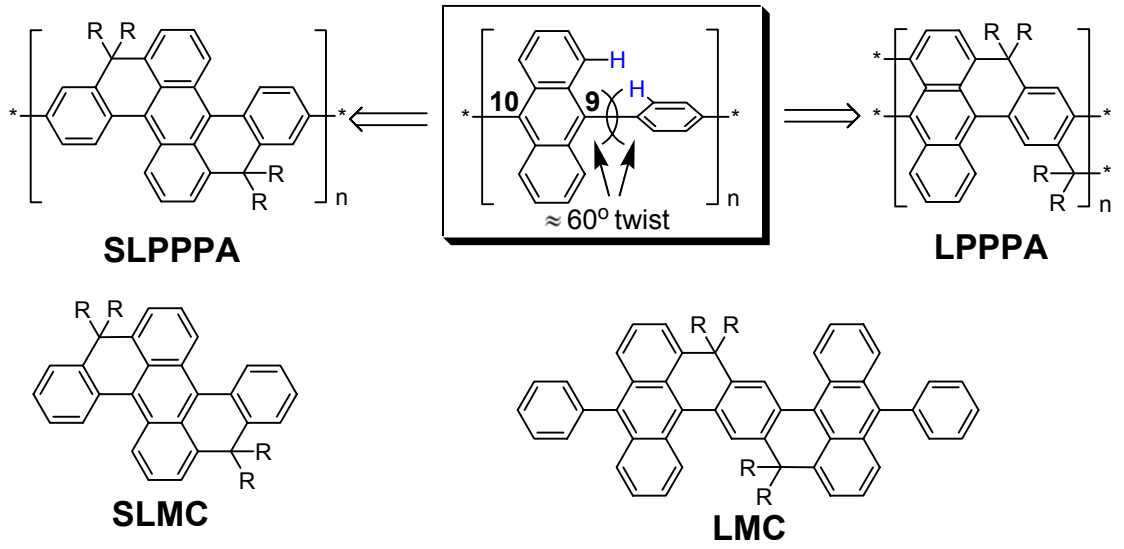

In addressing this issue, we direct our attention toward ladderised PPP-type polymers incorporating 9,10-anthrylene units as higher benzenoid building blocks, which should generate unique electronic and optical properties. While one paper has described a similar approach using 1,5-linked naphthylenes,[36] the step-ladder and ladder poly(*p*-phenylene-*alt*-anthrylene)s (**SLPPPA** and **LPPPA** respectively) containing 9,10-anthrylene units within the main chain are the first examples of the 9,10-linked anthrylene-based ladder-type polymers. The structural and spectroscopic properties of the resulting polymers are thus of great interest. In addition to the synthesis and characterization of **SLPPPA** and **LPPPA**, the methylene bridged 1,4-di(10-phenylanthracen-9-yl)benzene **LMC** and bis-methylene bridged 9,10-diphenylanthracene **SLMC** are described which serve as model compounds

for spectroscopic characterization of the polymers. Finally, the unique thermal and photochemical behavior of the title materials is presented.

3.2.1 Synthesis and Characterization

The synthesis of the step-ladder polymer, poly(*p*-phenylene-*alt*-anthrylene) containing 9,10-anthrylene building groups (**SLPPPA**) was carried out as depicted on Scheme 3.4. Starting from 5-bromo-2-iodo-benzoic acid, 5-bromo-2-iodo-4'-decylbenzophenone (**35**) was prepared by $AlCl_3$ promoted Friedel-Crafts acylation of decylbenzene with 5-bromo-2-iodo-benzoyl chloride in 85 % yield. Suzuki coupling of 9,10-di(4,4,5,5-tetramethyl-1,3,2-dioxaborolan-2-yl)anthracene (**36**) and **35** gave 9,10-di(5-bromo-4'-decylbenzophenon-2yl)anthracene (**37**) (97 %). This was converted into the corresponding anthracene diboronic ester **38** by treatment with bis(pinacolato)diboron under $Pd(OAc)_2$/KOAc/DMF (60 %) and subsequent Suzuki polycondensation of **37** and **38** generated the 9,10-anthrylene linked polyketone precursor **39** (M_n = 6.11 × 10^3 g/mol and M_w = 8.75 × 10^3 g/mol, PPP standards). Addition of 4-octylphenyllithium gave the corresponding polyalcohol **40** and the desired **SLPPPA** was obtained by ring closure with boron trifluoride etherate. Prior to this transformation, **39** was purified by Soxhlet extraction overnight using acetone to remove low molecular oligomeric components. **SLPPPA** is readily soluble in organic solvents like THF, toluene and dichloromethane. Gel-permeation chromatography (GPC) analysis with PPP standards shows a M_n value of 7.24 × 10^3 g/mol and M_w = 1.19 × 10^4 g/mol with a polydispersity of 1.35. To prove that the polymer analogous ring closure had gone to completion, the polymers were characterized by a combination of FT-IR and ^{13}C NMR spectroscopy. The FT-IR spectrum of **39** displays a strong absorption band at 1665 cm^{-1}

due to the carbonyl group and the ^{13}C NMR spectrum shows the carbon signal of the carbonyl group at δ = 196.5 ppm. In the FT-IR spectrum of **SLPPPA**, the carbonyl band at 1665 cm^{-1} is not observed (Figure 3.9).

Scheme 3.4. Synthesis of step-ladder poly(*p*-phenylene-*alt*-anthrylene) containing 9,10-anthrylene units (**SLPPPA**).

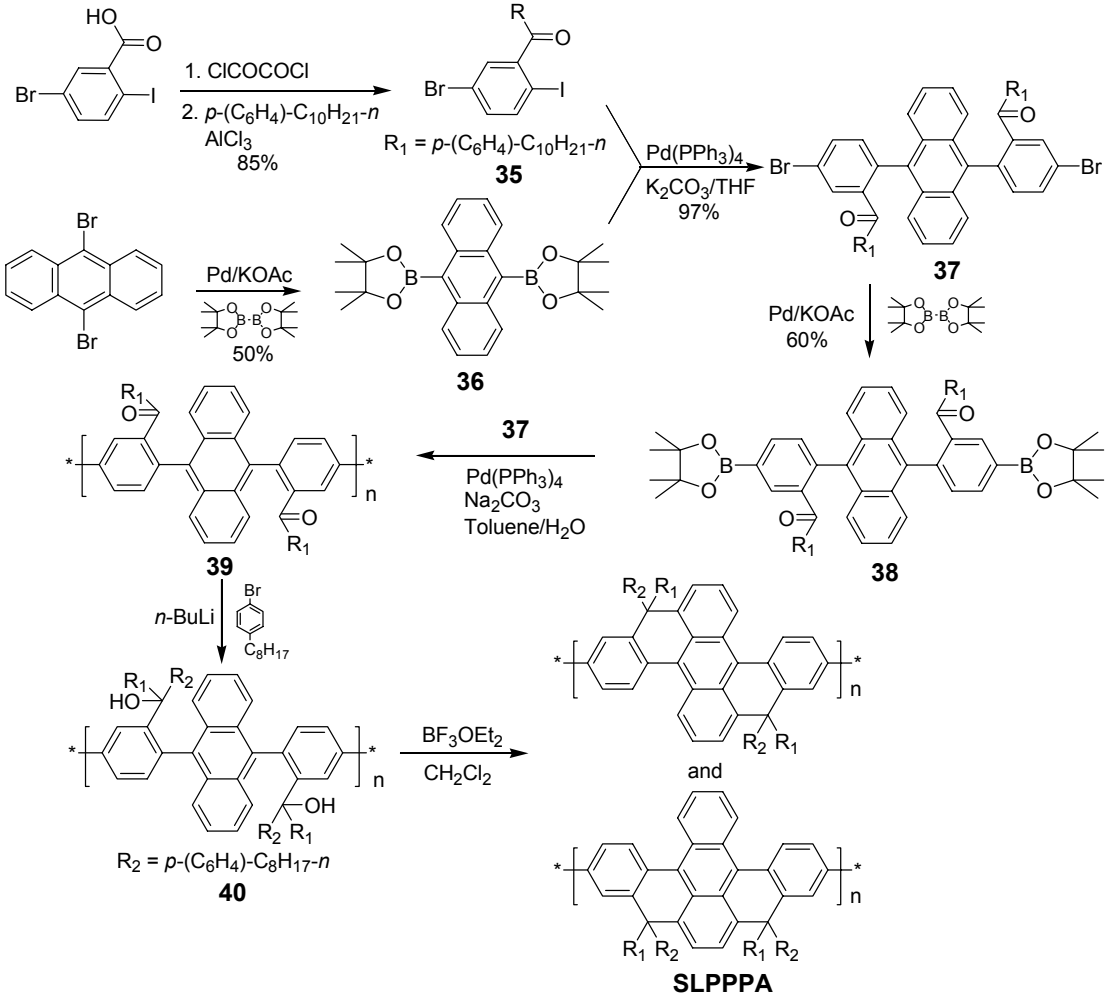

An inspection of ^{13}C NMR spectrum of **SLPPPA** fails to reveal any carbonyl signals which would point toward the presence of incomplete ring closure. In view of the signal to noise ratio achieved we can conclude that the amount of structural defects is below

1 %. Notably, the ^{13}C NMR spectrum of **SLPPPA** has a new signal at δ = 59.8 ppm corresponding to the quaternary bridging carbon of the methylene bridge obtained upon cyclization. As described in Scheme 3.4, mixtures of two regioisomers can be formed because of the rotation between phenylene and anthrylene units in the polymer main chain. However, the ratio of the syn- and anti-ring closure reaction products can not be determined by NMR or other spectroscopic methods.

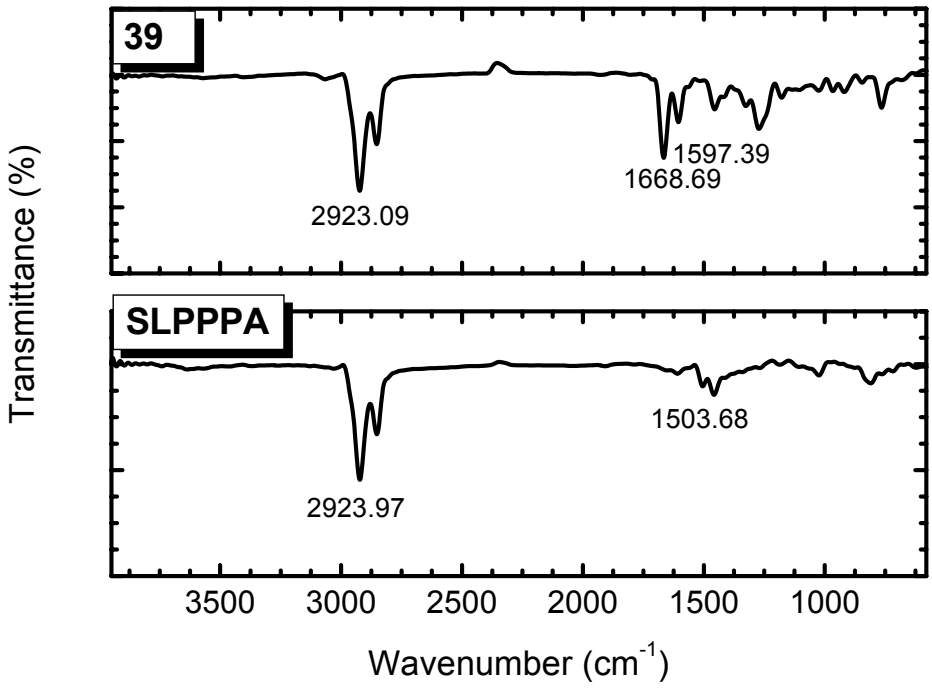

Figure 3.9. FT-IR spectra of **39** and **SLPPPA**.

In order to synthesize ladder poly(*p*-phenylene-*alt*-anthrylene) containing 9,10-anthrylene units (**LPPPA**), a precursor approach was taken as shown in Scheme 3.5. The precursor polyketone **42** was synthesized via Suzuki polycondensation of the anthracene diboronic ester **36** and 2',5'-dibromo-4-decyl-4'-(4-decylbenzoyl)benzophenone (**41**).[53]

Addition of an excess of 4-octylphenyllithium produced the corresponding polyalcohol **43** which underwent facile ring closure with boron trifluoride etherate to generate the target polymer **LPPPA**. This polymer has good solubility in organic solvents. GPC analysis of this polymer exhibits a M_n value of 5.77×10^3 g/mol and M_w of 8.19×10^3 g/mol (THF, PPP standards). The completion of the ring closure was verified by FT-IR (Figure 3.10) and ^{13}C NMR spectroscopy as detailed earlier for **SLPPPA** and showed the amount of structural defects to be below 1 %.

Scheme 3.5. Synthesis of ladder poly(*p*-phenylene-*alt*-anthrylene) containing 9,10-anthrylene units (**LPPPA**).

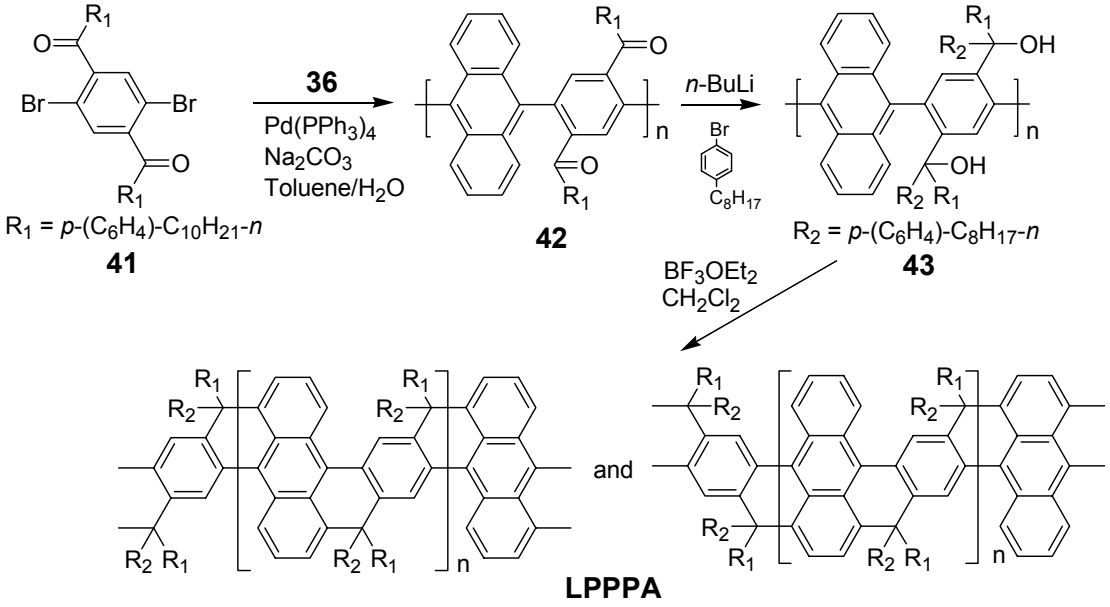

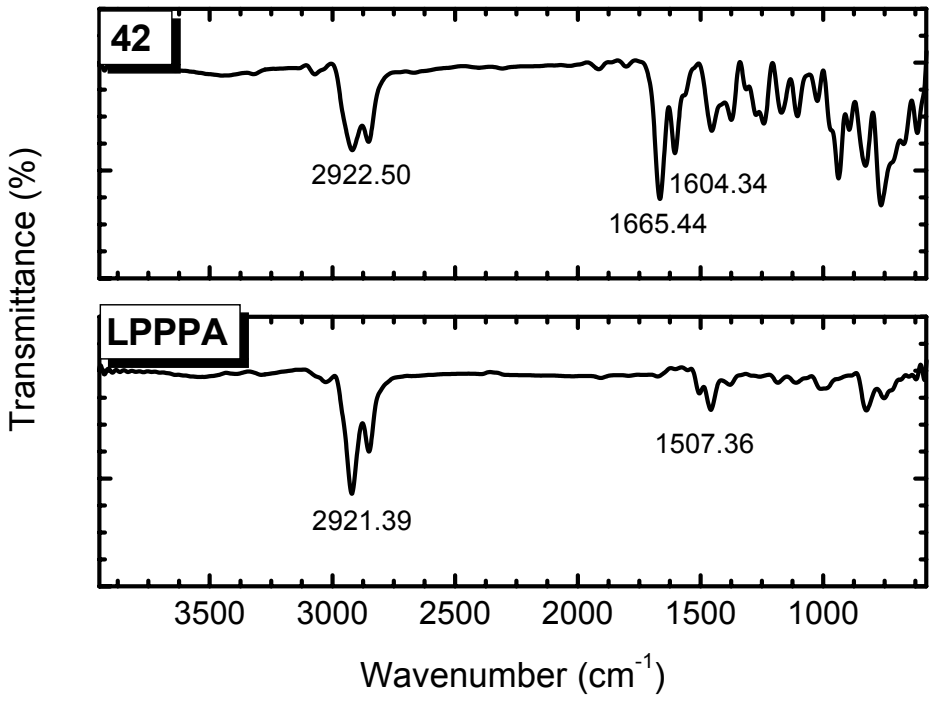

Figure 3.10. FT-IR spectra of **42** and **LPPPA**.

TGA thermograms of the two polymers exhibit good thermal stability up to 400 ˚C. Weight loss (5 %) starts at 420 ˚C and 430 ˚C for **SLPPPA** and **LPPPA** respectively. DSC analysis of the polymers shows neither a glass transition process (T_g) nor other thermal processes (such as liquid crystalline phases) between -50 ˚C and 280 ˚C.

3.2.2 Synthesis of model compounds (SLMC and LMC)

In order to more precisely assess the intrinsic properties of step-ladder and ladder poly(*p*-phenylene-*alt*-anthrylene)s (**SLPPPA** and **LPPPA**) containing 9,10-anthrylene linkage, it is necessary to prepare model compounds, as presented in Scheme 3.6. The bromination of 9-phenylanthracene in acetic acid gave 9-bromo-10-phenylanthracene

(91 %) which was transformed to 4,4,5,5-tetramethyl-2-(10-phenylanthracen-9-yl)-1,3,2-dioxaborolane (**44**) via lithiation and subsequent reaction with 2-isopropoxy-4,4,5,5-tetramethyl-1,3,2-dioxaborolane. Suzuki coupling of **44** and **41** under palladium catalysis generated (2,5-di(10-phenylanthracen-9-yl)-1,4-phenylene)di-4'-decylbenzophenone (**45**).

Scheme 3.6. Synthesis of ladder and step-ladder model compounds (**LMC** and **SLMC**).

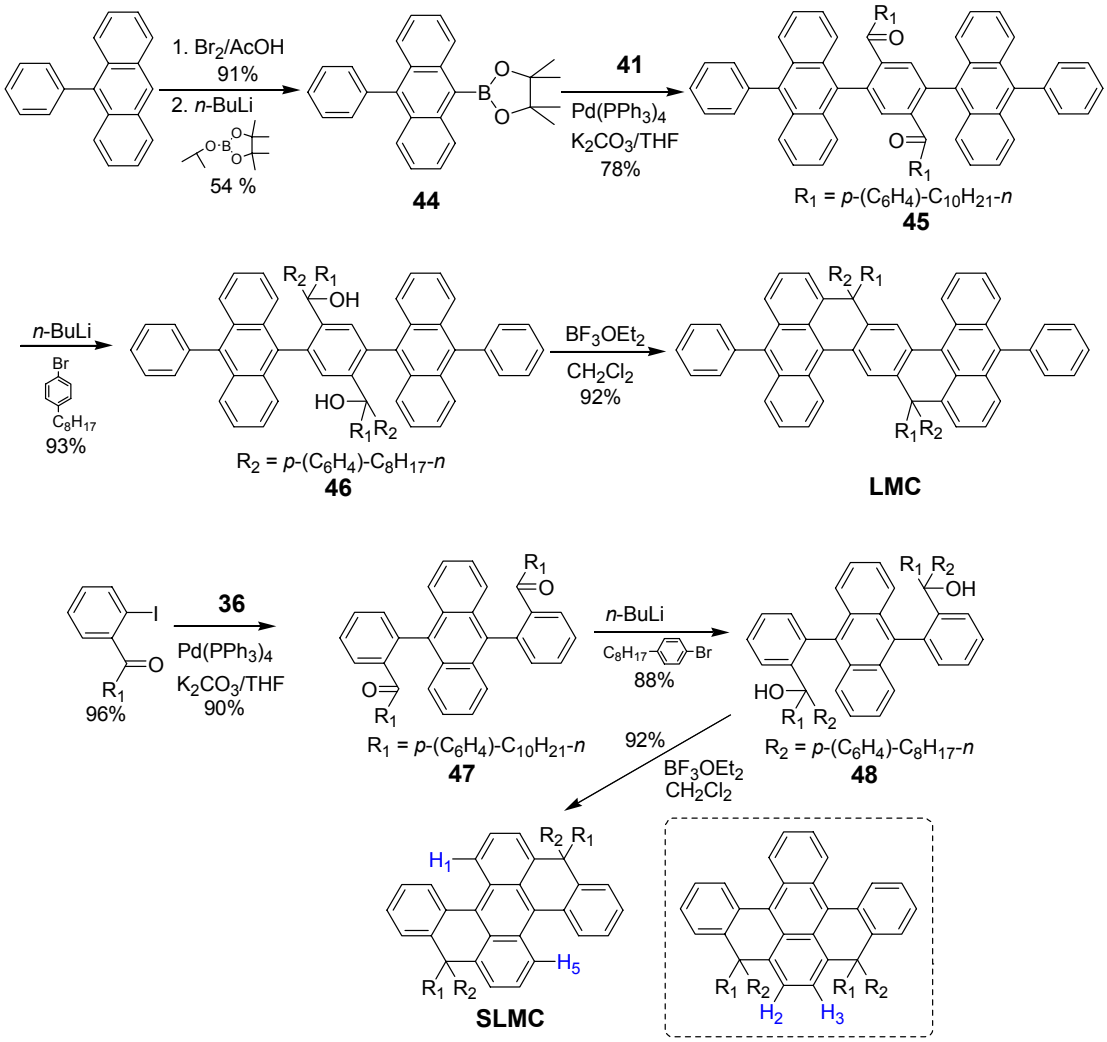

The methylene bridged 1,4-di(10-phenylanthracen-9-yl)benzene **LMC** was synthesized in an analogous fashion to the ladder polymers in 86 % overall yield (2 steps). A similar

procedure was adopted for the synthesis of the bis-methylene bridged 9,10-diphenylanthracene **SLMC** starting from 2-iodo-benzoic acid (acylation, Suzuki coupling, generation of diol, and subsequent ring closure). The cyclization of **48** can generate two regioisomers (syn and anti), analogous to those in the polymers. The ^{1}H NMR spectrum of **SLMC** shows a doublet of doublets at 8.52 ppm with coupling constants of 6.7 and 3.3 Hz (Figure 3.11). This signal is assigned to the two aromatic protons at the 1 and 5-positions of the anthrylene unit. If the syn-ring closed product has been formed, the protons at the 2 and 3-positions of the anthrylene unit would give a singlet, which is not observed in the ^{1}H NMR spectrum of **SLMC**. Therefore, it is concluded that the anti ring-closed isomer was formed. This result also suggests that the polymers (**SLPPPA** and **LPPPA**) contain predominantly anti ring-closed isomers.

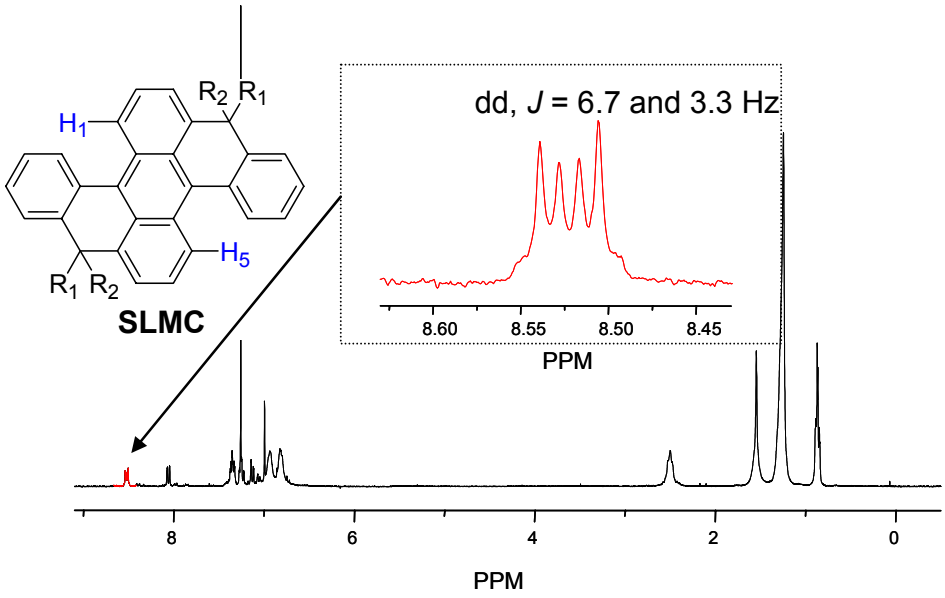

Figure 3.11. ^{1}H NMR spectrum of **SMLC** recorded at room temperature in dichloromethane-d^{2}.

3.2.3 Photophysical Properties

Figures 3.12 and 3.13 depict the UV-vis absorption and photoluminescence characteristics of the two polymers (**SLPPPA** and **LPPPA**) and their model compounds (**LMC** and **SLMC**). The absorption and PL spectral data for all compounds are also summarized in Table 3.3. As shown in Figures 3.12 and 3.13, **SLPPPA** in solution displays a broad absorption with a maximum around 520 nm with no vibronic features. The absorption maximum of **LPPPA** in solution is bathochromically shifted compared to that of **SLPPPA**, to 659 nm. The UV-vis and PL spectra of the ladder-type model compound **LMC** are also bathochromically shifted compared to the step-ladder type model compound **SLMC**, which suggests the notion that **LPPPA** has a more extended π-system relative to **SLPPPA**.

The optical properties of **LPPPA** are unexpectedly strong bathochromically shifted, which prompted us to have a careful look into the presence of any complex formation of **LPPPA** with Lewis acid since 1,5-naphthylene ladder polymers are characterized by a blue-green fluorescence in solution with maximum at 480 nm with sidebands at 513 and 554 nm.[36] The solution of **LPPPA** was again extracted with water and then treated with hydrazine, however the optical spectra of **LPPPA** remained unchanged and the elemental analysis of **LPPPA** gave good agreement with the calculated CH values. Thus one can conclude the observed optical behavior to be an inherent property of 9,10-conjugated anthrylene based fully-ladder type polymer. This notion is supported by two papers[54,55] in which the bridged compound between 9,10-anthrylene and naphthylene is reported to have an absorption maximum around 628-643 nm.

The large Stokes shift (*ca*. 64 nm for **SLPPPA** and *ca*. 34 nm for **LPPPA**) and the lack of any vibrational resolution are in contrast to most step-ladder or ladder-type

poly(*p*-phenylene)-based polymers (LPPPs) which show narrow and well-resolved absorption bands. This large Stokes shift can be attributed to the deviation from the coplanarity caused by the methylene bridges between phenylene and anthrylene units. The six-membered ring containing the sp^3 carbon is not expected to be fully planarized and the attachment of bulky solubilizing groups further distorts the repeat units in the main chain due to steric hindrance. This assumption is supported by the AM1 force field simulation studies, implemented using HyperChem 6.0 (Hypercurb Inc.). The simulated structure of the ladderised compound between 9,10-anthrylene and phenylene with phenyl substituents as solubilizers shows a pronounced steric stain along the main chain when compared to that of the corresponding compound with methyl substituents (Figure 3.14). **SLPPPA** in solution shows a yellow emission (λ_{max} = 584 nm) whereas **LPPPA** exhibits a red emission (λ_{max} = 693 nm). The enhanced π-system induced by the methylene bridges between phenylene and 9,10-anthrylene units accounts for the observed unique optical properties.

Table 3.3. Optical data of **SLPPPA**, **LPPPA** and the model compounds (**LMC** and **SLMC**).

Compound	λ_{max} (nm)		Stokes shift (nm)	λ_{max} (nm)[a]	
	absorption	emission		absorption	emission
LMC	472, 501	536	35	400, 423, 449 (500)	474, 529
SLMC	430, 455, 488	518	30	430, 457, 488	518
SLPPPA	520	584	64	518	580
LPPPA	620, 659	693	34	467, 501	637

Peaks that appear as shoulders or weak bands are shown in parentheses

[a]Absorption and emission after heating at 120 °C directly after irradiation

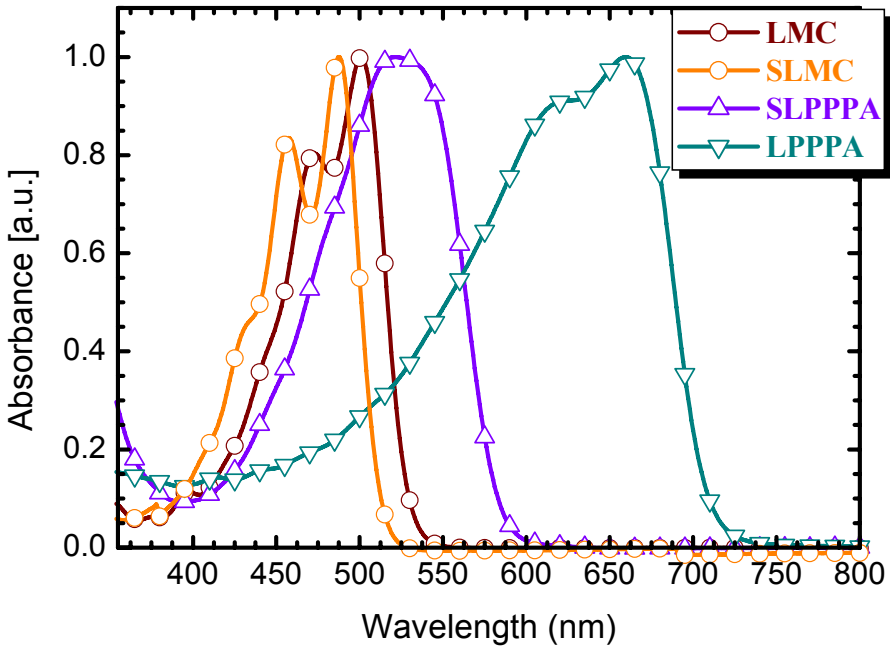

Figure 3.12. UV-vis spectra of **LMC**, **SLMC**, **SLPPPA**, and **LPPPA** in chloroform solution.

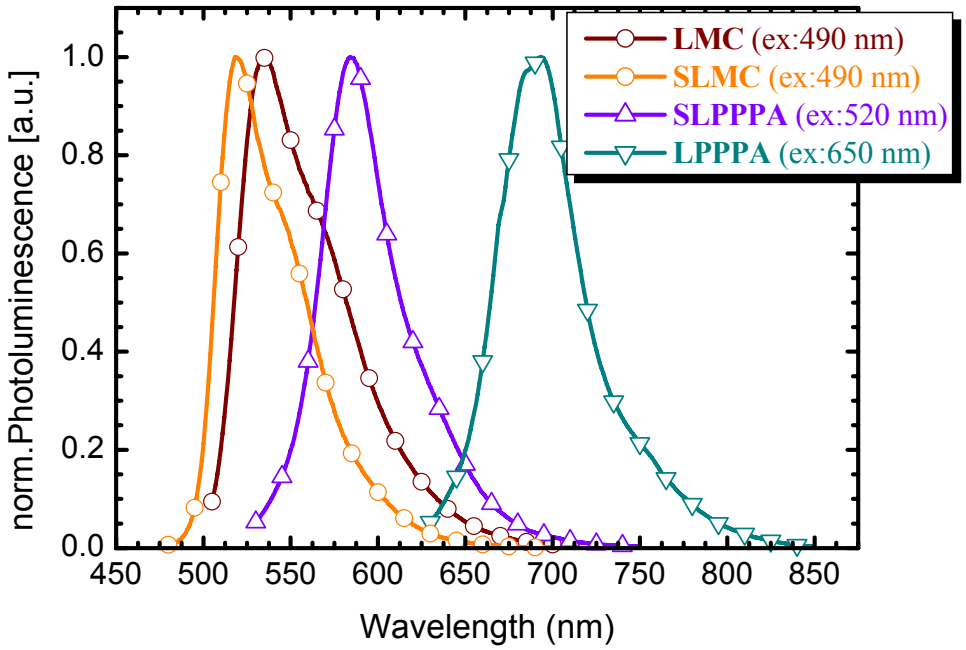

Figure 3.13. PL spectra of **LMC**, **SLMC**, **SLPPPA**, and **LPPPA** in chloroform solution.

(a) **(b)**

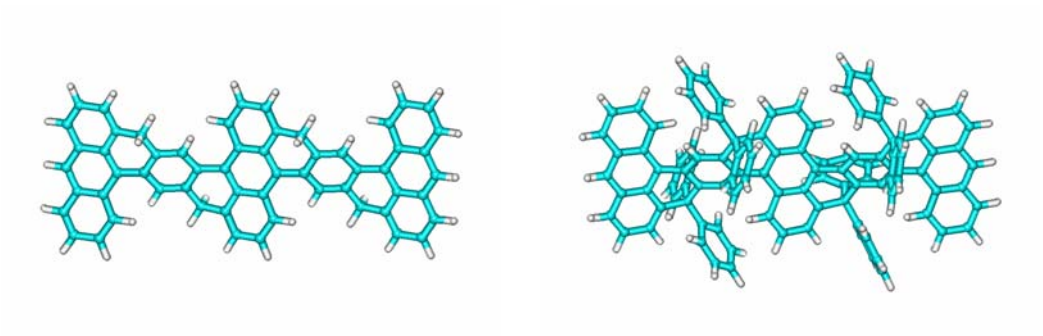

Figure 3.14. The simulated structures of ladderised compounds between 9,10-anthrylene and phenylene with (a) methyl (b) phenyl substituents as solubilizing groups, using the AM1 force field, as implemented by HyperChem 6.0.

3.2.4 Thermal and Photochemical Properties

It has been previously reported[56] that structurally related hydrocarbons such as perylenes and terylenes that are substituted in the bay positions exhibit considerable deviations from planarity, which results in reduced photostability. Furthermore, it has been observed that the anthracene derivatives react rapidly with oxygen to form the corresponding endoperoxides in solution which can provide interesting thermal and photochemical properties.[48,57-60] This prompted us to investigate the photostability of all the materials (**LMC**, **SLMC**, **SLPPPA**, and **LPPPA**).

After irradiation with sunlight in the presence of air, UV-vis absorption and PL spectra of all the compounds (**LMC**, **SLMC**, **SLPPPA** and **LPPPA**) were taken in chloroform solution (1×10^{-5} M) to follow the course of the photooxidation (Figure 3.16). Both the absorption and emission intensity drop drastically upon irradiation, indicating that the anthracene chromophore has undergone chemical transformation. Field Desorption Mass Spectrometry (FD-MS) of the irradiated model compounds (**LMC** and **SLMC**) shows an increase in mass by 32 Dalton, supporting the formation of the

endoperoxides. On heating the step-ladder derivatives (**SLMC** and **SPPPA**) at 120 °C, the initial absorption and emission spectra reappear with little loss of intensity whereas the ladder-type derivatives (**LMC** and **LPPPA**) display significant changes in their spectra.

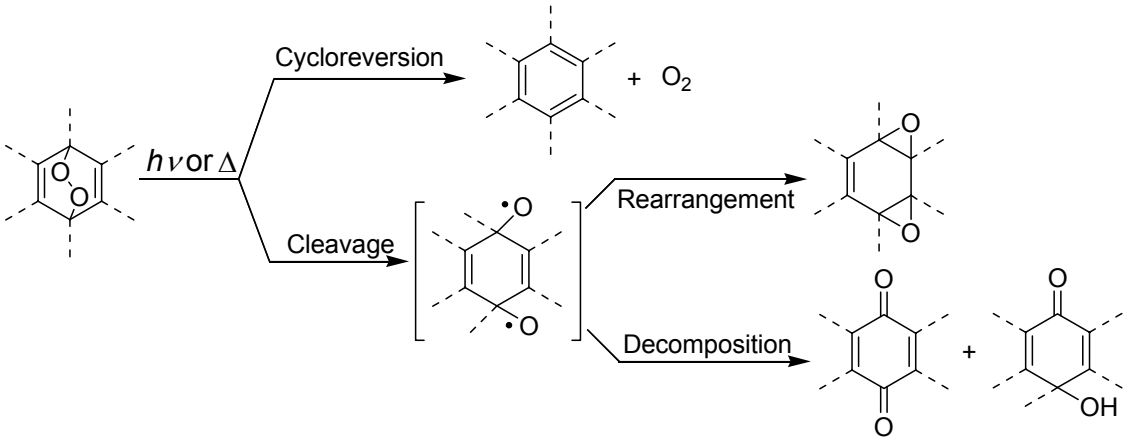

Figure 3.15. Transformation of endoperoxides during thermolysis or photolysis.

It has been described[61] that two primary pathways of transformation can compete during thermolysis of aromatic endoperoxides: cycloreversion, leading to parent substrate and oxygen in a singlet or triplet state, and homolytic cleavage of the peroxidic bond, followed by rearrangement to more or less stable diepoxides or decomposition, leading to hydroxy-ketones or quinones (Figure 3.15). The relative importance of both processes depends on the structure. Therefore, it is postulated that in the 9,10-anthrylene based step-ladder materials (**SLMC** and **SPPPA**), the reversibility of the photooxygenation to the endoperoxides and subsequent thermal cleavage of oxygen suggests a single photoreaction pathway involving $^1O_2$ as the sole oxidizing species (Type II photooxidation)[60-62] whereas in the 9,10-anthrylene based ladder materials (**LMC** and

LPPPA), the mechanism involves electron transfer processes resulting in the anthracene cation radical (Type I photooxidation)[60,63,64] as their products are irreversibly formed. After heating the endoperoxides from the **LMC** and **SLMC**, the FD-MS of **SLMC** reveals an intense peak at 1162 Dalton for the parent compound whereas the parent peak of **SLMC** is clearly not observed. This can support the proposed interpretation and suggest a different dissociation of endoperoxides for step-ladder and ladder derivatives respectively.

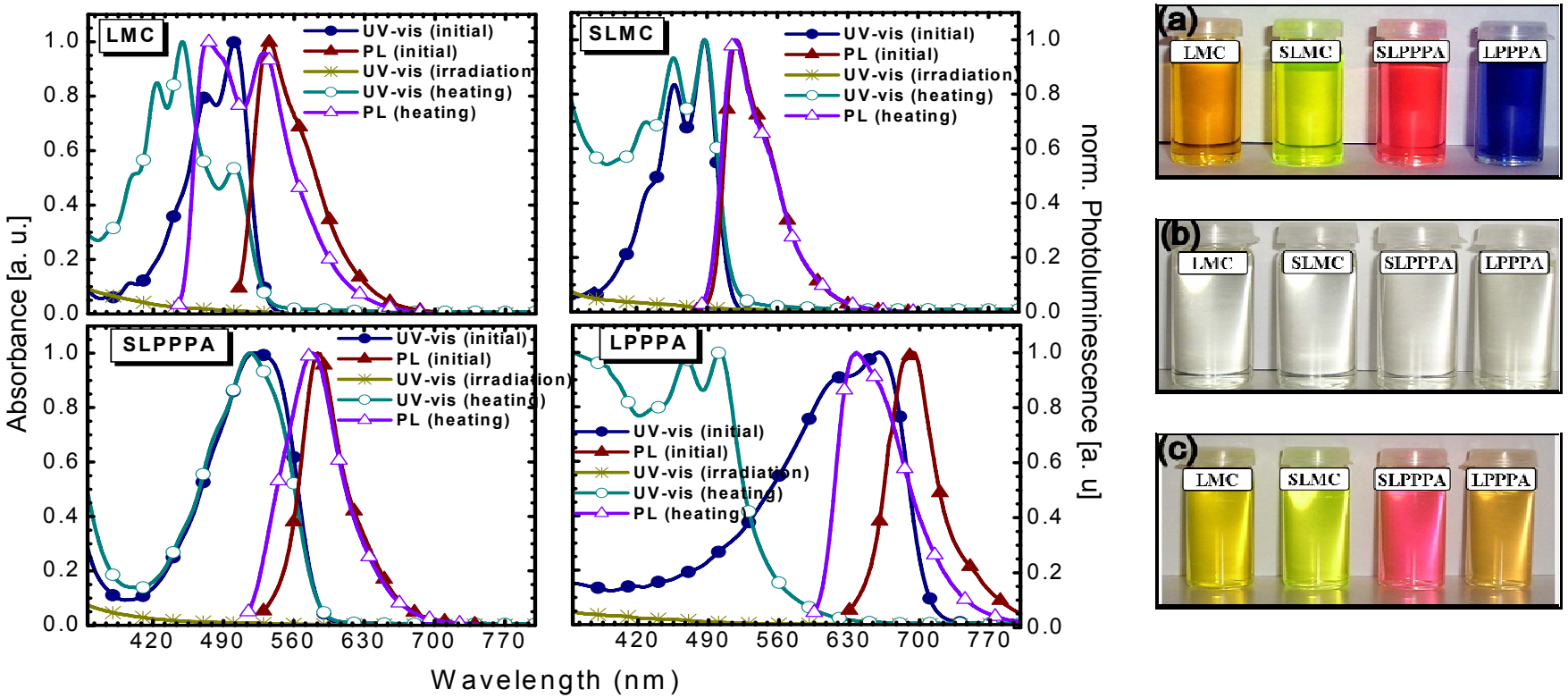

Figure 3.16. UV-vis and PL spectra of **LMC**, **SLMC**, **SLPPPA**, and **LPPPA** in chloroform solution (left). (a) Before, (b) after irradiation with visible light in the presence of air, and (c) heating at 120 °C directly after irradiation (right).

3.2.5 Electrochemical Properties

The redox behavior of the two polymers (**SLPPPA** and **LPPPA**) is investigated by cyclic voltammetry (CV) against Ag/Ag+. As shown in Figure 3.17, the polymers exhibit clear reversibility in both the p-doping and n-doping processes. The oxidation and reduction potentials are summarized in Table 3.4. Electrochemical reduction starts at about -1.38 V with a peak at E_{red} = -1.62 V vs Ag/Ag+ for **SLPPPA** and -1.73 V for **LPPPA**. The corresponding oxidation (n-dedoping) peak is observed at -1.55 V vs Ag/Ag+ for **SLPPPA** and -1.53 V for **LPPPA**. The electron affinity (EA) values derived from the reduction onset potentials are at 3.0 eV for **SLPPPA** and 2.9 eV for **LPPPA**.[65,66] In the oxidative region, both **SLPPPA** and **LPPPA** display reversible oxidation characterized by peaks at E_{ox} = 1.15 V vs Ag/Ag+ for **SLPPPA** and at 0.99 V for **LPPPA** and the corresponding reduction (p-dedoping) peaks are observed at 1.06 V and 0.93 V respectively.

Table 3.4. Electrochemical data for **SLPPPA** and **LPPPA**.

polymer	E^{re}_{onset} [V]	E^{ox}_{onset} [V]	E_{HOMO} [eV]	E_{LUMO} [eV]
SLPPPA	-1.45	1.06	-5.5	-3.0
LPPPA	-1.05	0.88	-5.3	-2.9

$E^{ox/re}_{onset}$ = onset oxidation/reduction potential. E_{LUMO} = lowest unoccupied molecular orbital (LUMO) energy level; E_{HOMO} = highest occupied molecular orbital (HOMO) energy level.

The estimated ionization potential (IP = E_{onset}^{ox} + 4.4 eV, HOMO levels) values are 5.5 eV for **SLPPPA** and 5.3 eV for **LPPPA**. These energy levels (HOMO and LUMO) and the observed reversible redox processes suggest that both compounds (**SLPPPA** and **LPPPA**) have enhanced hole and electron injection compared to LPPPs and have potential for use in hole and electron transport layers.

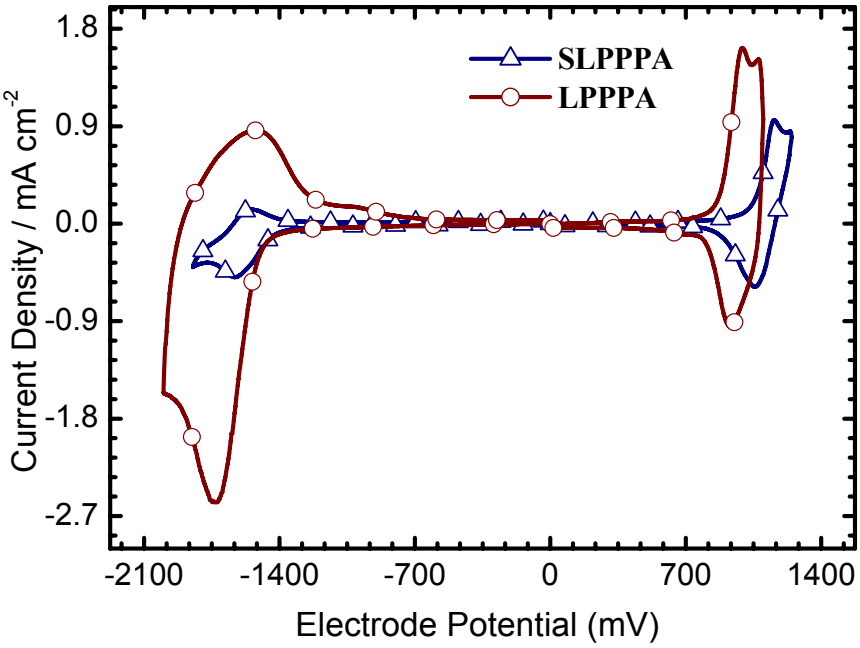

Figure 3.17. Cyclic voltammograms of the polymer films (**SLPPPA** and **LPPPA**) coated on platinum electrodes measured in acetonitrile containing 0.1 M Bu_4NClO_4 solution at a scan rate of 100 mV/s at room temperature.

3.2.6 Conclusion

A series of step-ladder and ladder poly(*p*-phenylene-*alt*-anthrylene)s containing 9,10-anthrylene building sets have been synthesized by Suzuki polycondensation. The resulting polymers (**SLPPPA** and **LPPPA**) are the first examples of 9,10-linked

anthrylene based ladder-type polymers consisting of alternating six-membered rings prepared by polymer analogous cyclization of polyketone precursors. Through the structural manipulation of the methylene bridge at the 9,10-anthrylene unit, it is possible to tune the optical properties of the target polymers (λ_{em} = 584 nm for **SLPPPA** and λ_{em} = 693 nm for **LPPPA**). Even though the variations in the optical properties of the bridged conjugated oligomers and polymers have been attributed to the mutual distortion of the building blocks due to steric effects, the strong bathochromic shift of **LPPPA** when compared to that of 1,5-naphthylene ladder-type polymers was unpredicted. However, one can conclude that the phenomenon is an intrinsic property of 9,10-conjugated anthrylene based fully-ladder type polymers since the optical properties of **LPPPA** do not change even the treatment with hydrazine. Unlike, LPPPs, a significant Stokes shift between absorption and emission is observed for the both polymers (**SLPPPA** and **LPPPA**) which is attributed to the twist of the polymer backbone along the sp^3 methylene bridges. Cyclic voltammetry studies reveal that both polymers (**SLPPPA** and **LPPPA**) have low lying LUMO levels at 3.0 and 2.9 eV respectively with fully reversible p- and n-doping. These results suggest that both polymers can be utilized as electron injecting and electron transporting components in OLEDs. In the photochemical studies, we have demonstrated that the photooxygenation of all materials with visible light gives the colorless endoperoxide structures. Upon thermal treatment, the step-ladder derivatives (**SLMC** and **SLPPPA**) recover their initial optical properties of the starting materials (Type II photooxidation) whereas the ladder derivatives (**LMC** and **LPPPA**) undergo irreversible Type I photooxidation. We conclude that structural features in conjugated polymers containing 9,10-anthrylene units can play an important role in determining photoreaction pathways.

3.3 References

(1) Yang, Y.; Pei, Q.; Heeger, A. J. *J. Appl. Phys.* **1996**, *79*, 934-939.

(2) Staring, E. G. J.; Demandt, R.; Braun, D.; Rikken, G. L. J.; Kessener, Y.; Venhuizen, A. H. J.; Vanknippenberg, M. M. F.; Bouwmans, M. *Synth. Met.* **1995**, *71*, 2179-2180.

(3) Mitschke, U.; Bauerle, P. *J. Mater. Chem.* **2000**, *10*, 1471-1507.

(4) Kraft, A.; Grimsdale, A. C.; Holmes, A. B. *Angew. Chem. Int. Ed.* **1998**, *37*, 402-428.

(5) Scherf, U.; List, E. J. W. *Adv. Mater.* **2002**, *14*, 477-487.

(6) List, E. J. W.; Guentner, R.; de Freitas, P. S.; Scherf, U. *Adv. Mater.* **2002**, *14*, 374-378.

(7) Ego, C.; Marsitzky, D.; Becker, S.; Zhang, J. Y.; Grimsdale, A. C.; Müllen, K.; MacKenzie, J. D.; Silva, C.; Friend, R. H. *J. Am. Chem. Soc.* **2003**, *125*, 437-443.

(8) List, E. J. W.; Tasch, S.; Hochfilzer, C.; Leising, G.; Schlichting, P.; Rohr, U.; Geerts, Y.; Scherf, U.; Müllen, K. *Opt. Mater.* **1998**, *9*, 183-187.

(9) Tasch, S.; Brandstatter, C.; Meghdadi, F.; Leising, G.; Froyer, G.; Athouel, L. *Adv. Mater.* **1997**, *9*, 33-36.

(10) Arias, E.; Maillou, T.; Moggio, I.; Guillon, D.; Le Moigne, J.; Geffroy, B. *Synth. Met.* **2002**, *127*, 229-231.

(11) Pschirer, N. G.; Miteva, T.; Evans, U.; Roberts, R. S.; Marshall, A. R.; Neher, D.; Myrick, M. L.; Bunz, U. H. F. *Chem. Mater.* **2001**, *13*, 2691-2696.

(12) Schmitz, C.; Posch, P.; Thelakkat, M.; Schmidt, H. W.; Montali, A.; Feldman, K.; Smith, P.; Weder, C. *Adv. Funct. Mater.* **2001**, *11*, 41-46.

(13) Tasch, S.; List, E. J. W.; Hochfilzer, C.; Leising, G.; Schlichting, P.; Rohr, U.; Geerts, Y.; Scherf, U.; Müllen, K. *Phys. Rev. B* **1997**, *56*, 4479-4483.

(14) Cotts, P. M.; Swager, T. M.; Zhou, Q. *Macromolecules* **1996**, *29*, 7323-7328.

(15) Gu, J.; Kawabe, M.; Masuda, K.; Namba, S. *J. Appl. Phys.* **1977**, *48*, 2493-2494.

(16) Kim, Y.; Kwon, S.; Yoo, D.; Rubner, M. F.; Wrighton, M. S. *Chem. Mater.* **1997**, *9*, 2699-2701.

(17) Oyama, M.; Okazaki, S. *Anal. Chem.* **1998**, *70*, 5079-5084.

(18) Heller, C. A.; Henry, R. A.; McLaughl.Ba; Bliss, D. E. *J. Chem. Eng. Data* **1974**, *19*, 214-219.

(19) Zweig, A.; Maurer, A. H.; Roberts, B. G. *J. Org. Chem.* **1967**, *32*, 1322-1329.

(20) Maulding, D. R.; Roberts, B. G. *J. Org. Chem.* **1964**, *34*, 1734-1736.

(21) Zheng, S. Y.; Shi, J. M. *Chem. Mater.* **2001**, *13*, 4405-4407.
(22) Hodge, P.; Power, G. A.; Rabjohns, M. A. *Chem. Commun.* **1997**, 73-74.
(23) Greenwald, R.; Chaykovsky, M.; Corey, E. J. *J. Org. Chem.* **1963**, *28*, 1128-1129.
(24) Colonge, J.; Buendia, J.; Sabadie, J. *Bull. Soc. Chim. Fr.* **1967**, 4370-4374.
(25) Adams, J. M.; Ramdas, S. *Acta. Crystallogr. B.* **1979**, *35*, 679-683.
(26) Mio, M. J.; Kopel, L. C.; Braun, J. B.; Gadzikwa, T. L.; Hull, K. L.; Brisbois, R. G.; Markworth, C. J.; Grieco, P. A. *Org. Lett.* **2002**, *4*, 3199-3202.
(27) Jacob, J.; Sax, S.; Piok, T.; List, E. J. W.; Grimsdale, A. C.; Müllen, K. *J. Am. Chem. Soc.* **2004**, *126*, 6987-6995.
(28) Yamamoto, T.; Morita, A.; Miyazaki, Y.; Maruyama, T.; Wakayama, H.; Zhou, Z.; Nakamura, Y.; Kanbara, T.; Sasaki, S.; Kubota, K. *Macromolecules* **1992**, *25*, 1214-1223.
(29) Cammidge, A. N.; Crepy, K. V. L. *Chem. Commun.* **2000**, 1723-1724.
(30) Zhang, H. C.; Kwong, F. Y.; Tian, Y.; Chan, K. S. *J. Org. Chem.* **1998**, *63*, 6886-6890.
(31) Kamikawa, K.; Watanabe, T.; Uemura, M. *J. Org. Chem.* **1996**, *61*, 1375-1384.
(32) Watanabe, T.; Miyaura, N.; Suzuki, A. *Synlett* **1992**, 207-210.
(33) Johnson, M. G.; Foglesong, R. J. *Tetrahedron Lett.* **1997**, *38*, 7001-7002.
(34) Yin, J. J.; Rainka, M. P.; Zhang, X. X.; Buchwald, S. L. *J. Am. Chem. Soc.* **2002**, *124*, 1162-1163.
(35) Wolfe, J. P.; Tomori, H.; Sadighi, J. P.; Yin, J. J.; Buchwald, S. L. *J. Org. Chem.* **2000**, *65*, 1158-1174.
(36) Nehls, B. S.; Fuldner, S.; Preis, E.; Farrell, T.; Scherf, U. *Macromolecules* **2005**, *38*, 687-694.
(37) de Leeuw, D. M.; Simenon, M. M. J.; Brown, A. R.; Einerhand, R. E. F. *Synth. Met.* **1997**, *87*, 53-59.
(38) Cervini, R.; Li, X. C.; Spencer, G. W. C.; Holmes, A. B.; Moratti, S. C.; Friend, R. H. *Synth. Met.* **1997**, *84*, 359-360.
(39) Neher, D. *Macromol. Rapid. Commun.* **2001**, *22*, 1366-1385.
(40) Leclerc, M. *Macromol. Rapid. Commun.* **2001**, *39*, 2867-2873.
(41) Grimsdale, A. C.; Leclere, P.; Lazzaroni, R.; Mackenzie, J. D.; Murphy, C.; Setayesh, S.; Silva, C.; Friend, R. H.; Müllen, K. *Adv. Funct. Mater.* **2002**, *12*, 729-733.
(42) Qiu, S.; Lu, P.; Liu, X.; Shen, F. Z.; Liu, L. L.; Ma, Y. G.; Shen, J. C. *Macromolecules* **2003**, *36*, 9823-9829.
(43) Swager, T. M.; Gil, C. J.; Wrighton, M. S. *J. Phys. Chem.* **1995**, *99*, 4886-4893.

(44) Ofer, D.; Swager, T. M.; Wrighton, M. S. *Chem. Mater.* **1995**, *7*, 418-425.
(45) Mery, S.; Haristoy, D.; Nicoud, J. F.; Guillon, D.; Monobe, H.; Shimizu, Y. *J. Mater. Chem.* **2003**, *13*, 1622-1630.
(46) Trancong, Q.; Nagaki, T.; Yano, O.; Soen, T. *Macromolecules* **1991**, *24*, 1505-1510.
(47) Rigaudy, J.; Perlat, M. C.; Cuong, N. K. *Bull. Soc. Chim. Fr.* **1974**, 2521-2526.
(48) Dabestani, R.; Ellis, K. J.; Sigman, M. E. *J. Photochem. Photobiol. A: Chem.* **1995**, *86*, 231-239.
(49) Setayesh, S.; Marsitzky, D.; Müllen, K. *Macromolecules* **2000**, *33*, 2016-2020.
(50) Jacob, J.; Zhang, J. Y.; Grimsdale, A. C.; Müllen, K.; Gaal, M.; List, E. J. W. *Macromolecules* **2003**, *36*, 8240-8245.
(51) Scherf, U. *J. Mater. Chem.* **1999**, *9*, 1853-1864.
(52) Burn, P. L.; Holmes, A. B.; Kraft, A.; Bradley, D. D. C.; Brown, A. R.; Friend, R. H.; Gymer, R. W. *Nature* **1992**, *356*, 47-49.
(53) Scherf, U.; Müllen, K. *Makromol. Chem., Rapid Commun.* **1991**, *12*, 489-497.
(54) Nakatsuka, M. In *JP 2000044498* Feb. 15, 2000.
(55) Rauhut, M. M.; Boberts, B. G.; Maulding, D. R.; Bergmark, W.; Coleman, R. *J. Org. Chem.* **1975**, *40*, 330-335.
(56) Anton, U.; Golter, C.; Müllen, K. *Chem. Ber.* **1992**, *125*, 2325-2330.
(57) Wasserma.Hh; Scheffer, J. R.; Cooper, J. L. *J. Am. Chem. Soc.* **1972**, *94*, 4991-&.
(58) Jesse, K.; Comes, F. J. *Journal of Physical Chemistry* **1991**, *95*, 1311-1315.
(59) Clennan, E. L.; Foote, C. S. In *Orgainc peroxides*; Ando, W., ed.; John Wiley & Sons: Chichester, England, 1992, p 225-318.
(60) Donkers, R. L.; Workentin, M. S. *J. Am. Chem. Soc.* **2004**, *126*, 1688-1698.
(61) Aubry, J. M.; Pierlot, C.; Rigaudy, J.; Schmidt, R. *Acc. Chem. Res.* **2003**, *36*, 668-675.
(62) Fudickar, W.; Fery, A.; Linker, T. *J. Am. Chem. Soc.* **2005**, *127*, 9386-9387.
(63) Clennan, E. L. *Tetrahedron* **1991**, *47*, 1343-1382.
(64) Sigman, M. E.; Zingg, S. P.; Pagni, R. M.; Burns, J. H. *Tetrahedron Lett.* **1991**, *32*, 5737-5740.
(65) Zhu, Y.; Alam, M. M.; Jenekhe, S. A. *Macromolecules* **2003**, *36*, 8958-8968.
(66) Tonzola, C. J.; Alam, M. M.; Kaminsky, W.; Jenekhe, S. A. *J. Am. Chem. Soc.* **2003**, *125*, 13548-13558.

Chapter 4 Polymeric Materials Containing Phenanthrylene Units

In this chapter, polymeric materials based on phenanthrylene units are presented. The synthesis of a series of soluble conjugated 2,7- and 3,6-poly(phenanthrylene)s analogous respectively to poly(*p*-phenylene)s (PPP) and poly(*p*-phenylenevinylene) (PPV) is discussed. This enables the effects of the conjugation mode of a polymer, *i.e.* PPP-like versus PPV-like, as a function of the coupling of the repeat unit at different positions to be investigated. The different optical properties and photostability of these step-ladder polymers containing the phenanthrylene moiety are described. Additionally, it was found that a Yamamoto-type polycondensation of 3,6-dihalophenanthrenes predominantly leads to the formation of a macrocyclic trimer, which can be isolated by column chromatography. The thermal behavior and self-organization of the macrocyclic trimer is also investigated.

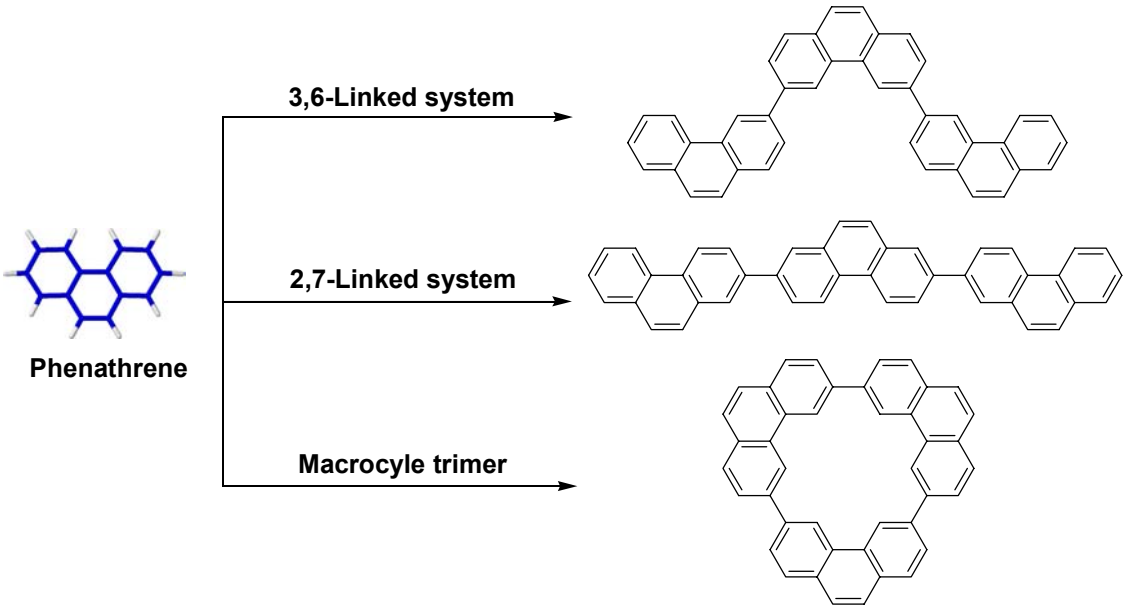

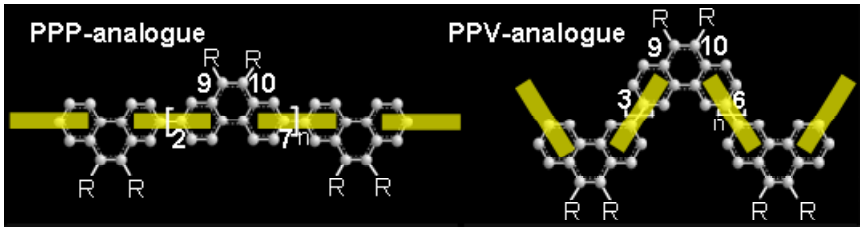

4.1 Poly-2,7- and 3,6-phenanthrylenes as Polyphenylene and Polyphenylenevinylene Analogues

Recent research into polymer-based organic light-emitting diodes (OLEDs) has focused on the use of conjugated polymers, such as poly(*p*-phenylenevinylene)s (PPVs) and poly(*p*-phenylene)s (PPPs), owing to their high photoluminescence efficiency in thin films. PPV (**P1a**) and its derivatives have several advantages as emitting materials such as high thermal stability, good film forming ability, and color tunability (Figure 4.1).[1-6] PPP (**P2a**) and its derivatives constitute a particularly important class since they emit in the blue[7-9] and are suitable hosts for upconversion emission which is significant for the development of blue lasers.[10,11] However, the PPP backbone has a 23° twist between

consecutive phenylene units due to ortho-hydrogen interactions.[12,13] Introduction of solubilizing side chains leads to steric interactions, which cause a marked increase in the phenylene-phenylene torsional angles, with a concurrent loss of π-overlap and a significant blue-shift in the emission wavelength.[14-16] To overcome this, totally planarized ladder-type PPP (LPPPs, **P3a**)[17] and the so-called angular poly(acene)s, **P4a**,[18,19] were developed. These materials, however, show blue-green emission in solution (λ_{em} = 450–470 nm for **P3a** and λ_{em} = 478–516 nm for **P4a**) and tend to form aggregates which adversely affect their solid-state optical properties. As a result, considerable attention has been paid to step-ladder polymers in which the PPP backbone is only partially planarized by methine-bridges such as poly(dialkylfluorene)s (PFs, **P5a**)[20-22] and poly(tetraalkylindenofluorene)s (PIFs, **P6a**).[23,24] These materials exhibit efficient blue emission in solution from 420 nm to 450 nm with the emission color red-shifting with increasing chain rigidity. However, the blue emission of these derivatives in the solid state appears to be unstable due to the rapid appearance of long-wavelength emission bands (Figure 4.1).

A step-ladder polymer containing the phenanthrylene moiety can offer three major advantages: (1) the attachment of alkyl or aryl solubilizing groups at the 9,10-positions enhances solubility without disturbing the conjugation along the chain; (2) the partial planarization of the π-system in the aromatic repeat unit should produce an emission in the pure blue region of the electromagnetic spectrum, comparable to the emission from the parent PPP (**P2a**); (3) the interruption of the planarity within the step-ladder polymers would reduce aggregation which has been observed for LPPP-based OLEDs.

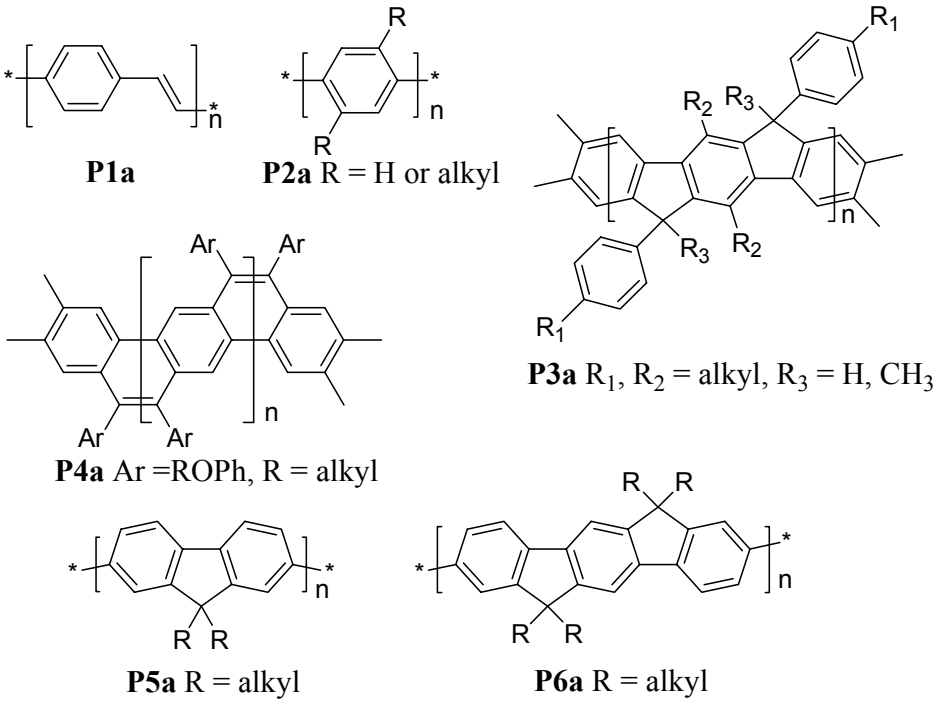

Figure 4.1. Structures of phenylene-based polymers.

Considering these advantages, the synthesis of phenanthrylene-based polymers as potential blue emitters in OLEDs was investigated. The synthesis and detailed characterization of a series of novel polyphenanthrylenes, which can be viewed either as PPP- or PPV-analogues is described. Phenanthrylenes can be polymerized from either a 2,7-substituted monomer to generate a linear, rod-like PPP-type chain or from a 3,6-substituted monomer to create a kinked PPV-analogue (Scheme 4.1). Additionally, the synthesis of 2,7- and 3,6-linked trisphenanthrylenes (**2,7-MT** and **3,6-MT**) is described which serve as model compounds for the spectroscopic characterization of the corresponding polymers.

Two synthetic approaches were utilized to generate the target polymers (Scheme 4.1): (i) by a nickel(0)-mediated Yamamoto-type coupling of 2,7- or 3,6-dihalophenanthrene monomers and (ii) by initial polymerization of a diketone precursor monomer and

subsequent polymer-analogous ring closure. Notably, while a Yamamoto-type polycondensation of 3,6-dihalophenanthrenes predominantly leads to the formation of a macrocyclic trimer **MCT** (Scheme 4.1), a Suzuki-Miyaura-type polycondensation can afford PPV-type polyphenanthrylenes with improved molecular weights due to the avoidance of the formation of **MCT**.

Scheme 4.1. Synthetic protocols for the preparation of the polyphenanthrylenes and the structures as (a) PPP-analogue and (b) PPV-analogue. (i) Nickel(0)-mediated Yamamoto-type polycondensation; (ii_a) polymer-analogous cyclization by McMurry-type coupling; (ii_b) cyclization with B_2S_3 generated in situ.

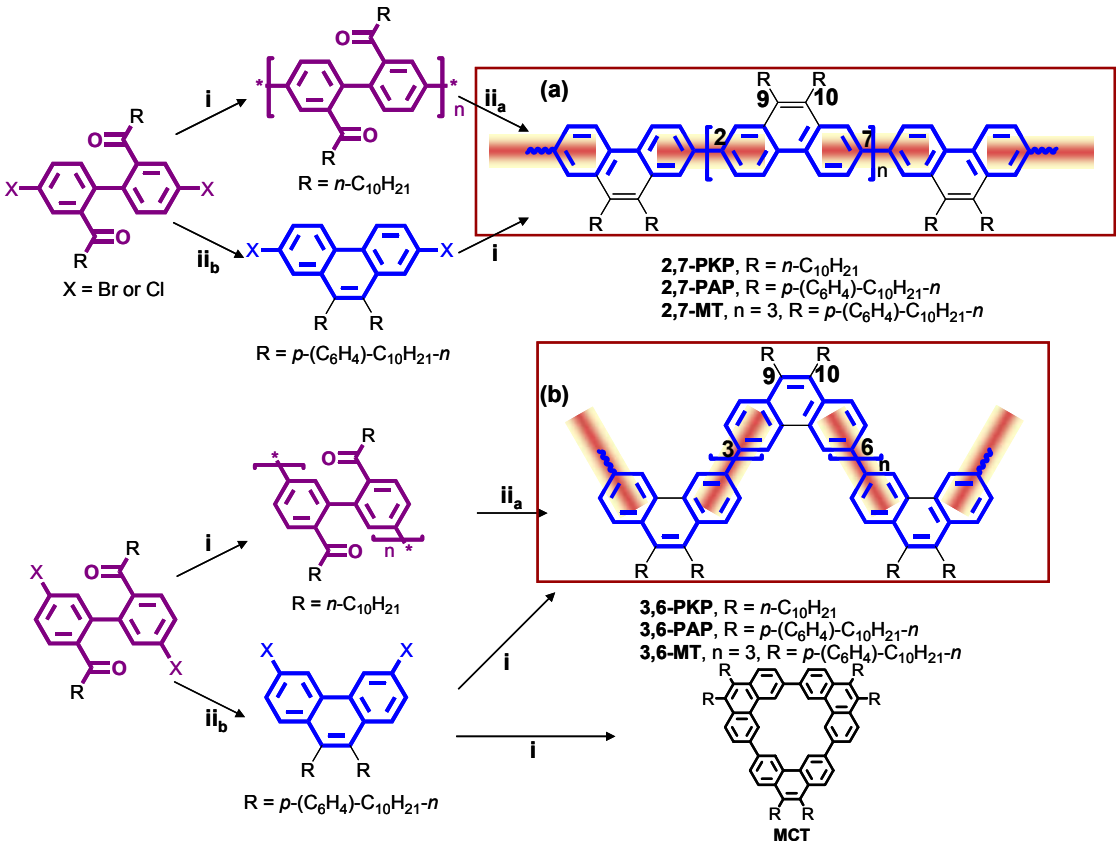

4.1.1 Synthesis and Characterization

Scheme 4.2. Synthesis of poly-2,7-(9,10-dialkylphenanthrylene)

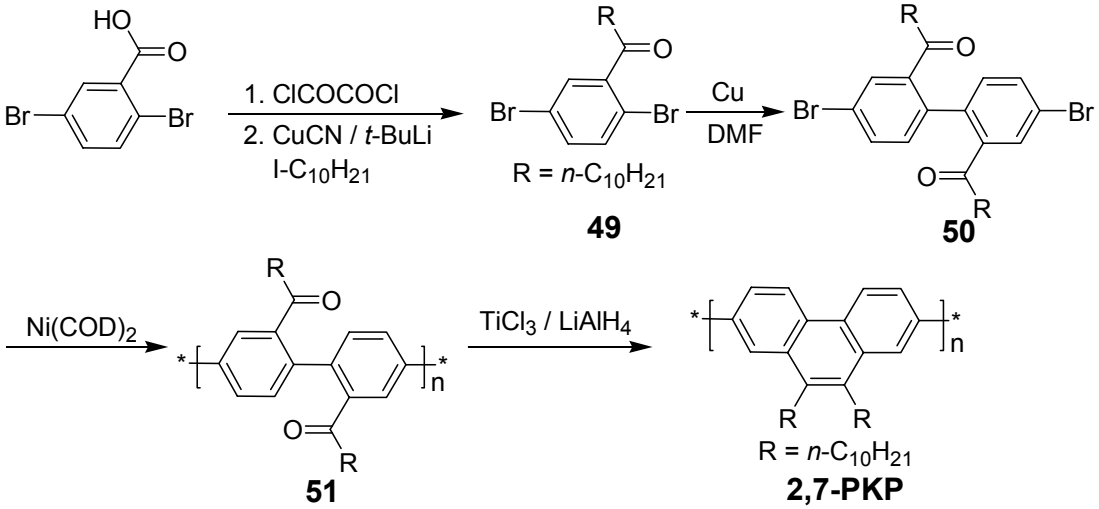

The synthetic approach to poly-2,7-(9,10-dialkylphenanthrylene) is depicted in Scheme 4.2. 2,5-Dibromobenzoic acid was first converted to the 2,5-dibromobenzoyl chloride by treatment with oxalyl chloride, which was then coupled with decyllithium in the presence of copper(I) cyanide to generate 2',5'-dibromo-undecylphenone (**49**) in 70% isolated yield.[13] Ullmann coupling of **49** in the presence of copper powder gave 4,4'-dibromo-2,2'-di(undecyloyl)-1,1'-biphenyl (**50**) (43%). Reductive cyclization of this compound using either tricyclohexyltin sulfide and trichloroborane, or with hydrazine in a polar solvent (acetic acid) in a modified Wolff-Kishner reaction, was not successful. Although McMurry-type coupling with $TiCl_3/LiAlH_4$ led to ring closure,[25] simultaneous debromination was observed. Hence, the target polymer **2,7-PKP** was prepared by initial polymerization of **50** and subsequent polymer-analogous McMurry coupling. The biphenyl polymer **51** was synthesized by a nickel(0)-mediated Yamamoto-type polycondensation. It is readily soluble in organic solvents like THF, toluene, chloroform,

and dichloromethane (M_n = 2.32 × 10^4 g/mol, M_w = 4.25 × 10^4 g/mol, THF, PPP standards). Following cyclization of **51**, the target polymer **2,7-PKP** possesses an M_n of 4.68 × 10^4 g/mol and M_w of 9.78 × 10^4 g/mol by gel-permeation chromatography (GPC) analysis against PPP standards.[26] To ensure that the polymer-analogous ring closure had gone to completion, the polymers were characterized by FT-IR and ^{13}C NMR spectroscopy. The strong peak at 1690 cm^{-1} in the FT-IR spectrum of **51**, which is assignable to the carbonyl group, is not observed in the spectrum of **2,7-PKP** (Figure 4.2). An inspection of the ^{13}C NMR spectrum of **2,7-PKP** fails to reveal any carbonyl signals which would point toward the presence of uncyclized precursor **51**. In view of the signal to noise ratio achieved we can conclude that the amount of structural defects is below 1%. This polymer has limited solubility in common organic solvents (THF, toluene, dichloromethane, etc.) and shows greenish-blue emission in solution.

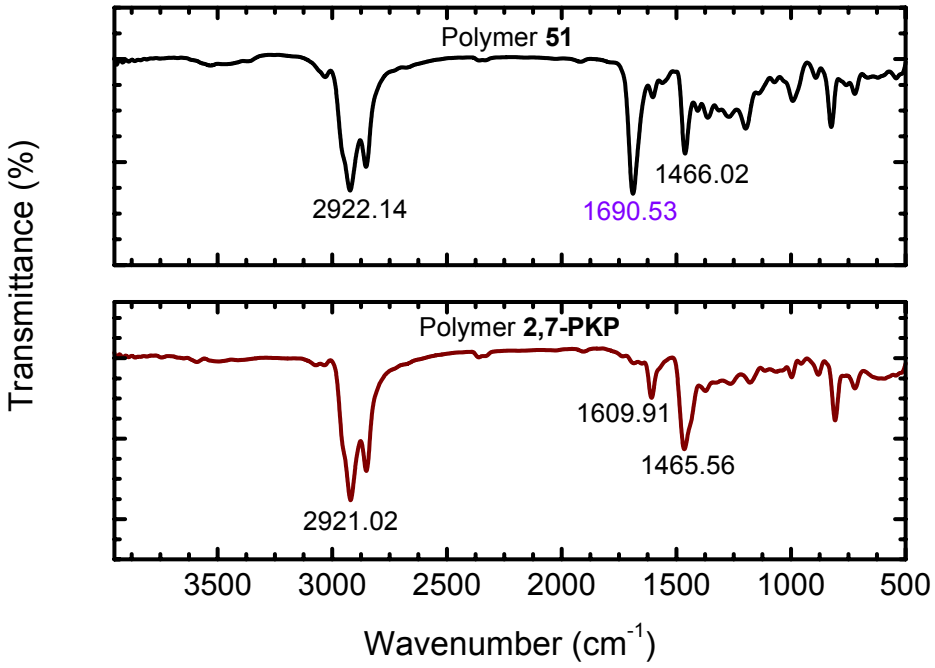

Figure 4.2. FT-IR spectra of **51** and **2,7-PKP**.

Scheme 4.3. Synthesis of poly-3,6-(9,10-dialkylphenanthrylene)

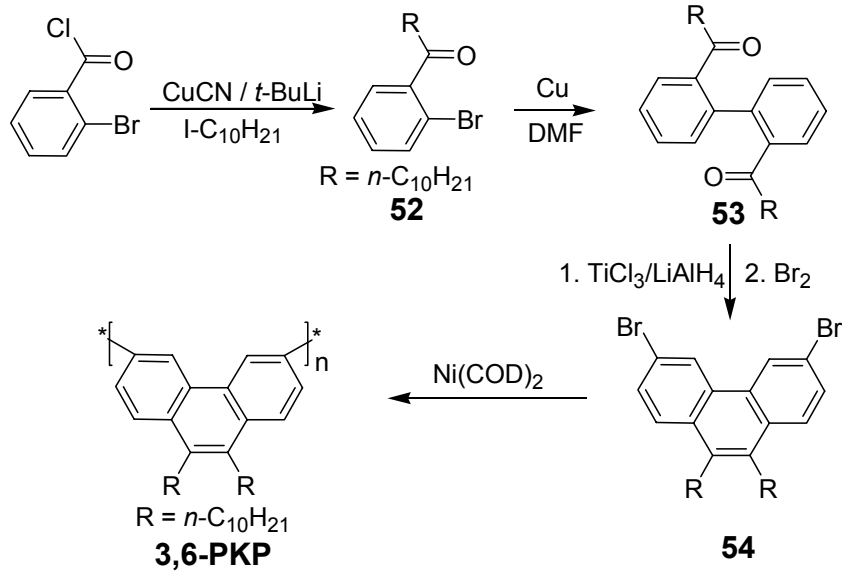

The analogous 3,6-linked polymer **3,6-PKP** was synthesized starting from 2-bromobenzoyl chloride as shown in Scheme 4.3. The synthetic sequences are similar to the one described earlier (acylation, Ullmann, and McMurry) and the dibromide monomer **54** was isolated in an overall yield of 38 %. The yield-limiting step of the synthetic scheme is the bromination of the phenanthrene moiety. To avoid overbromination, which resulted in an inseparable mixture of di-, tri- and tetra-bromophenanthrenes, less than two equivalents of bromine were added to the reaction vessel. The desired product **54** could then be isolated from the underbrominated side-products. **3,6-PKP** was synthesized by a Yamamoto-type polycondensation and is readily soluble in organic solvents. GPC analysis of **3,6-PKP** exhibits a M_n value of 3.15×10^3 g/mol and M_w of 5.10×10^3 g/mol (THF, PPP standards). Although attempts were made to improve the molecular weight by varying the monomer concentration as well as the mode of mixing the solutions of the nickel reagent and the monomer,[27] the

polymerization always resulted in low molecular weight (M_n = 3000 – 4000 g/mol) materials.

Scheme 4.4. Synthesis of poly-3,6-(9,10-diarylphenanthrylene)

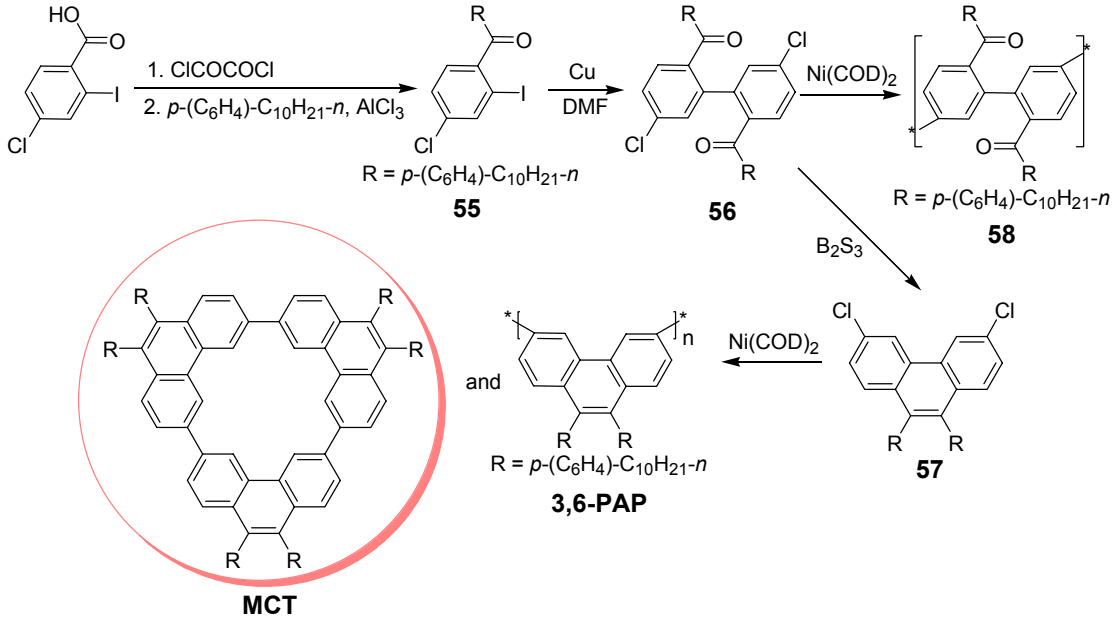

We proceeded to prepare the corresponding 9,10-diaryl substituted polymers to explore the reason for the observed low molecular weight of 3,6-linked system and to compare their solubility as well as long term stability in particular. These results can offer a key of the reason and approach detailed studies between 2,7- and 3,6-linked polymers. Scheme 4.4 illustrates the synthetic approach towards **3,6-PAP**. 4-Chloro-2-iodo-4'-decylbenzophenone (**55**) was prepared by $AlCl_3$-promoted Friedel-Crafts acylation of decylbenzene with 4-chloro-2-iodo-benzoyl chloride in 91% yield. Ullmann-type coupling followed by cyclization of **56** using tricyclohexyltin sulfide and trichloroborane generated **57** in an overall yield of 55%. Although dichloro substitution was believed to

be more suitable for Yamamoto-type polymerization[28] than the dibromo case, polymerization of **58** gave only a low molecular weight polymer (M_n = 3.25 × 10^3 g/mol and M_w = 4.66 × 10^3 g/mol, THF, PPP standards). The low molecular weight polymer obtained from the polymerization of **57** can readily be attributed to the formation of a macrocyclic trimer **MCT** during polymerization (Scheme 4.1). This follows from the intrinsic angle of the phenanthrylene unit which facilitates **MCT** instead of linear polymers. This was, indeed, proven by Staab *et al*. who reported the synthesis of **MCT** (R = H) via the Ullmann coupling of 3,6-diiodophenanthrene.[29] The GPC curve of **3,6-PAP** reveals a large amount of low molecular weight polymer (*ca*.> 2500 g/mol) due to a significant amount of **MCT** in the reaction.[30]

The GPC curve of **3,6-PAP** shows a peak corresponding to a large amount of low molecular fraction (*ca*. 2500 g/mol) as shown on Figure 4.3 and MALDI-TOF mass spectrometry turns out to be an ideal tool for the analysis of the oligomeric fraction (Figure 4.4). The MALDI spectrum of **3,6-PAP** displays one significant strong intense peak at 1,827 Dalton and a number of small peaks up to 15,000 Dalton. The peak at 1,827 Dalton stems from **MCT**. These results clearly indicate that **MCT** is formed predominantly via Yamamoto polymerization and interestingly, it can be isolated in high purity by preparative TLC. Furthermore, when the Yamamoto polymerization of **57** in very dilute solution was carried out, only oligomers were formed with **MCT** being the predominant product which was isolated by column chromatography. It shows strong pure blue emission in solution. This structure has been assigned by a combination of techniques including ^{1}H and ^{13}C NMR and Field Desorption Mass Spectrometry (required *m/z*: 1826.8; found *m/z*: 1825.0 ($M^{+\bullet}$)). The various characterization and investigation of **MCT** are independently discussed in the next section because it shows distinctly different

chemistry as compared to the polymeric materials based on phenanthrylenes. The polymerization of precursor **56**, a monomer that does not possess the intrinsic angle due to rotation between the phenyl units of the monomer, did not yield a high molecular weight polymer either (M_n = 2.14 × 10^3 g/mol, THF, PPP standards). Although concrete evidence is lacking at this stage, we attribute this to the possibility of cyclization or the inherent instability of the oxidative addition product formed by the metal-complex with **56**.

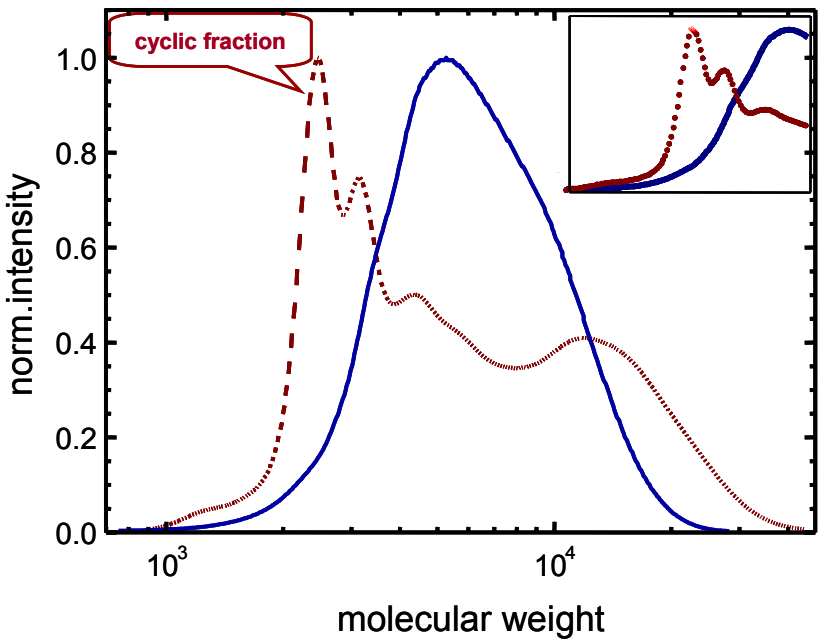

Figure 4.3. GPC curves (standard PPP) of **3,6-PAP** via Yamamoto (dash red line) and **3,6-LPAP** via Suzuki polymerization (solid blue line).

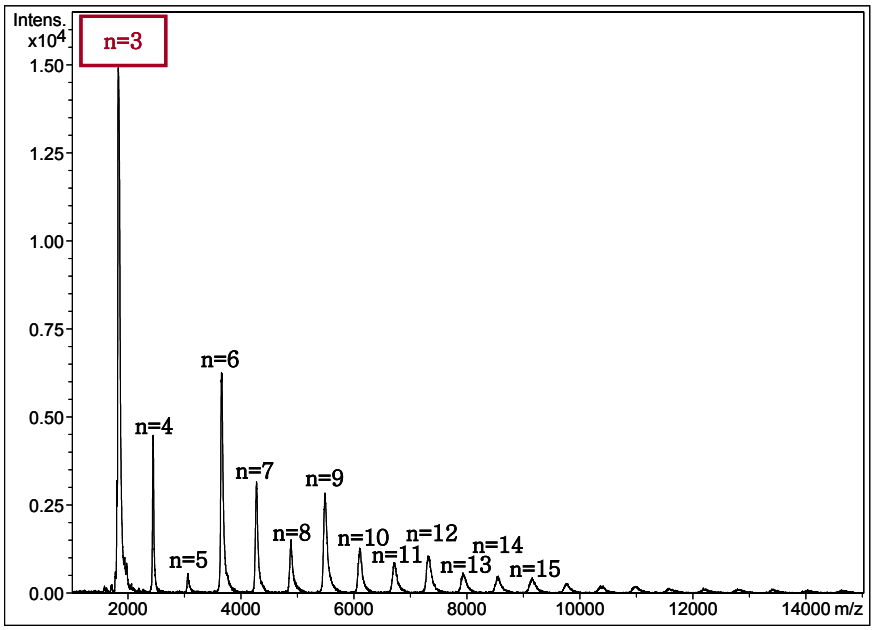

Figure 4.4. MALDI-TOF mass spectrum of the **3,6-PAP**.

The preparation of poly-3,6-phenanthrylene via Suzuki polycondensation was undertaken to improve the molecular weight, because from mechanistic considerations this suppresses the formation of **MCT**, since as shown in Scheme 4.5, the endgroups of a trimer will be identical, and the boron-bromine exchange necessary to allow cyclisation will be much slower than the coupling to another unit. The 3,6-diboronic ester of phenanthrene **62** was prepared by a palladium-catalyzed coupling reaction of **57** with bis(pinacolato)diboron under $Pd_2(dba)_3/PCy_3$/KOAc (see below) and the 3,6-dibromide **61** was synthesized from 2-iodo-benzoyl chloride in an analogous approach as discussed earlier. The Suzuki polycondensation of **61** and **62** gave the linear polymer **3,6-LPAP** with improved molecular weights (M_n = 5.33 × 10^3 g/mol and M_w of 6.82 × 10^3 g/mol, PPP standards). This polymer has good solubility in common organic solvents and exhibits pure blue emission in solution.

Scheme 4.5. Synthesis of linear poly-3,6-(9,10-diarylphenanthrylene) via Suzuki coupling

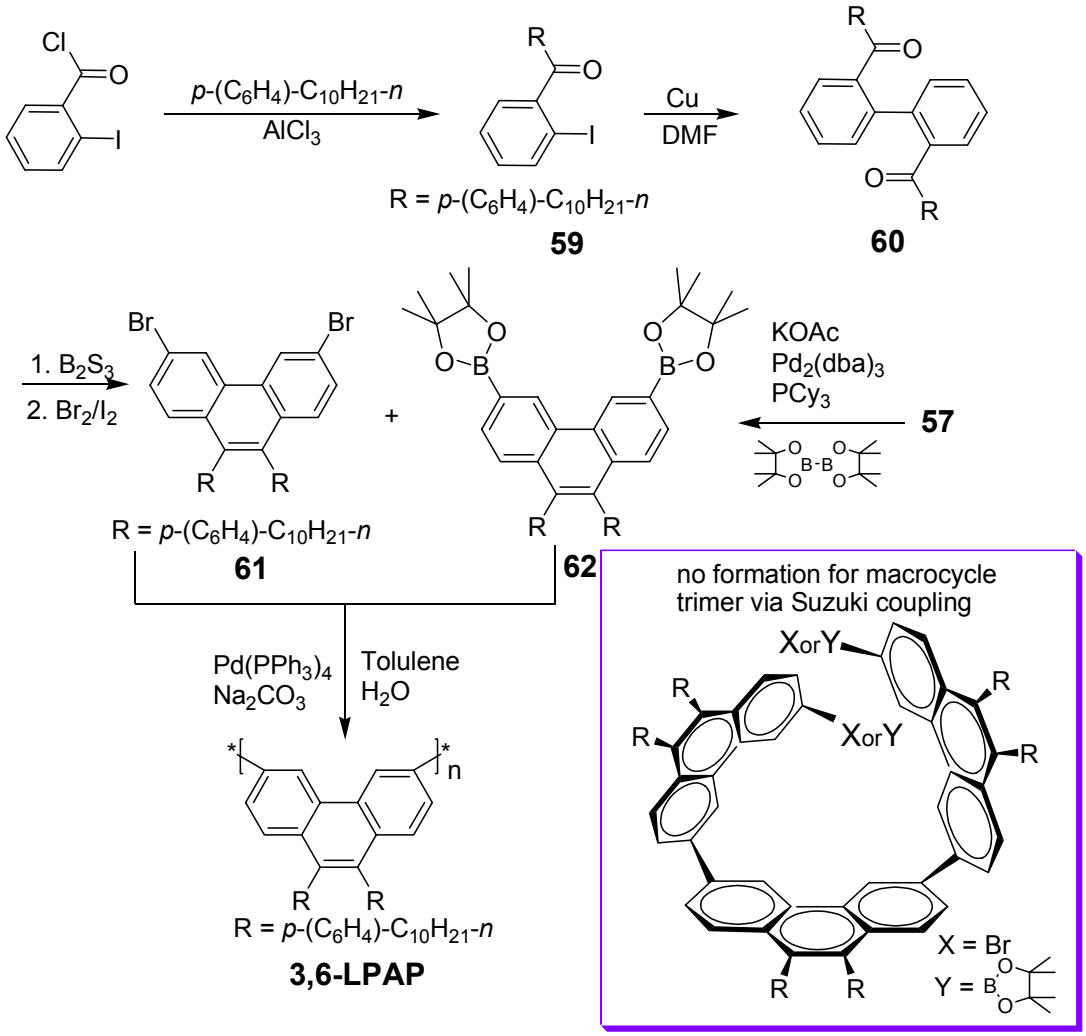

To complete the series, **2,7-PAP** was synthesized starting from 5-bromo-2-iodo-benzoic acid as depicted on Scheme 4.6 by similar procedures as detailed before. **2,7-PAP** is readily soluble in common solvents and displays a pure blue emission in solution (M_n = 1.13 × 10^4 g/mol, M_w = 5.26 × 10^4 g/mol, D = 4.66, PPP standards). This high polydispersity index prompted us to have a careful look at the resulting GPC elution curve of **2,7-PAP** and this revealed a bimodal molecular weight distribution (Figure 4.5).

We assume that it is due to the low molecular weight oligomeric components which cannot be separated by Soxhlet extraction overnight using acetone. More detailed studies including dynamic light scattering are separately discussed in the next section to explore the behavior of poly-2,7-and 3,6-phenanthrylenes.

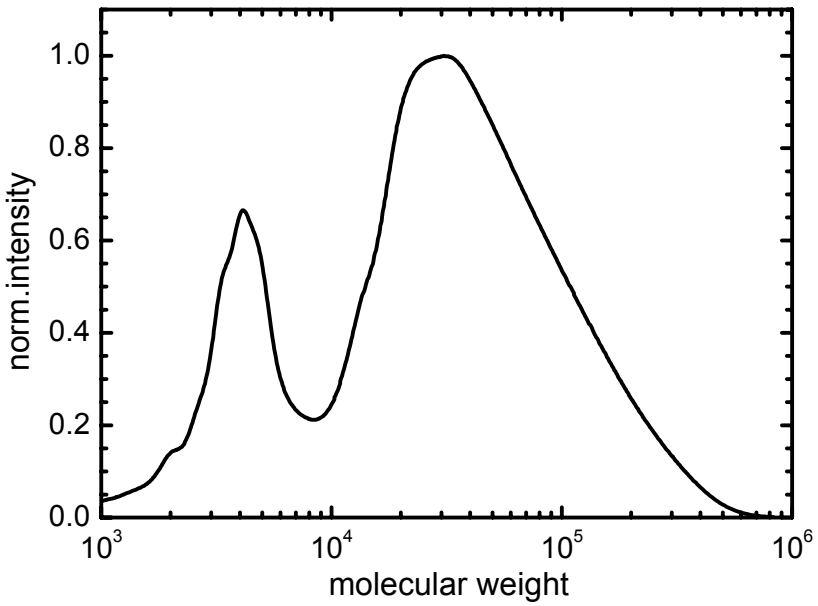

Figure 4.5. GPC curves (standard PPP) of **2,7-PAP** via Yamamoto polymerization.

TGA thermograms of all polymers reveal good thermal stability up to 350 ˚C, which is essential for fabricating stable OLED devices. Weight loss (5%) starts at 380, 425, 445, and 430 ˚C for polymers **2,7-PKP**, **2,7-PAP**, **3,6-PKP**, and **3,6-LPAP** respectively. DSC analysis of the polymers shows neither a glass transition process (T_g) nor other thermal processes (such as liquid crystalline phase) from -50 ˚C to 200 ˚C.

Scheme 4.6. Synthesis of poly-2,7-(9,10-diarylphenanthrylene)

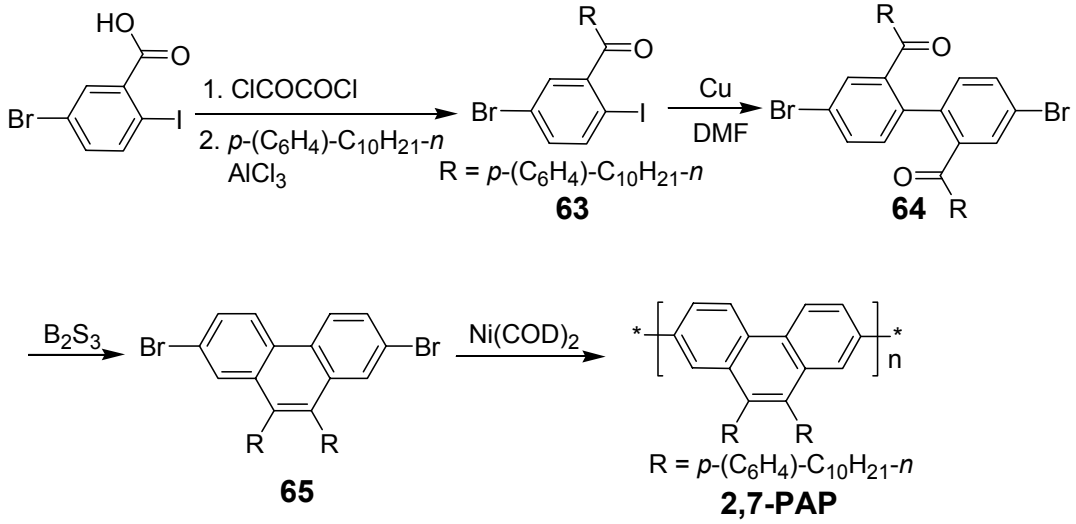

4.1.2 Synthesis of 2,7- and 3,6-Linked Model Trimers and Their Characterization

To more precisely assess the different modes of π-conjugation between poly-2,7-and 3,6- phenanthrylenes, 2,7- and 3,6-linked model trimers were prepared according to Schemes 4.7 and 4.8. 5-Chloro-2-iodo-4'-decylbenzophenone (**66**) was coupled with the boronic ester **67** (50%) by Suzuki reaction, subsequent cyclization of **68** gave 2-chloro-9,10-bis-(4-decyl-phenyl)-phenanthrene **(69**) (89%). The compound **69** was converted to the corresponding boronic ester **70** under $Pd_2(dba)_3$/KOAc with tricyclohexylphosphine as a ligand (72%). Suzuki coupling of **70** with **65** afforded 2,7-linked trimer **2,7-MT** (26%). The synthesis of the 3,6-linked analogue **3,6-MT** was achieved via Suzuki coupling of **71** with **62** (71%).

Scheme 4.7. Synthesis of 2,7-linked 9,10-diarylphenanthrylene trimer

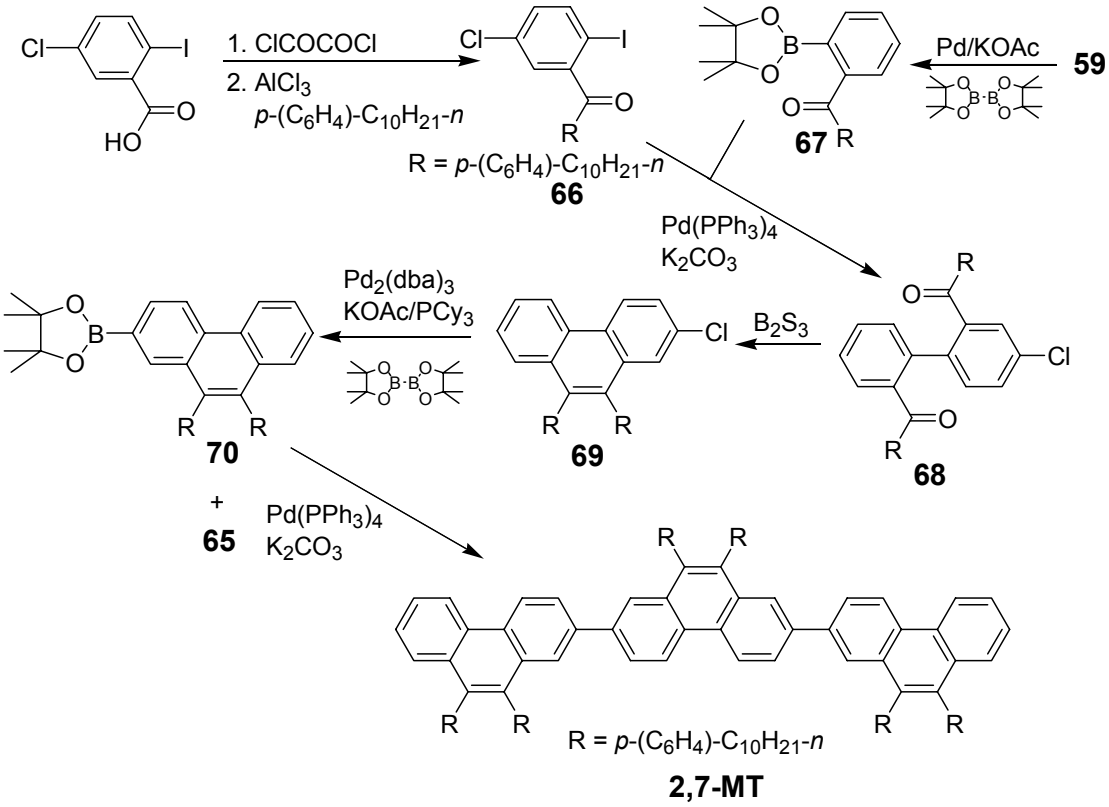

Scheme 4.8. Synthesis of 3,6-linked 9,10-diarylphenanthrylene trimer

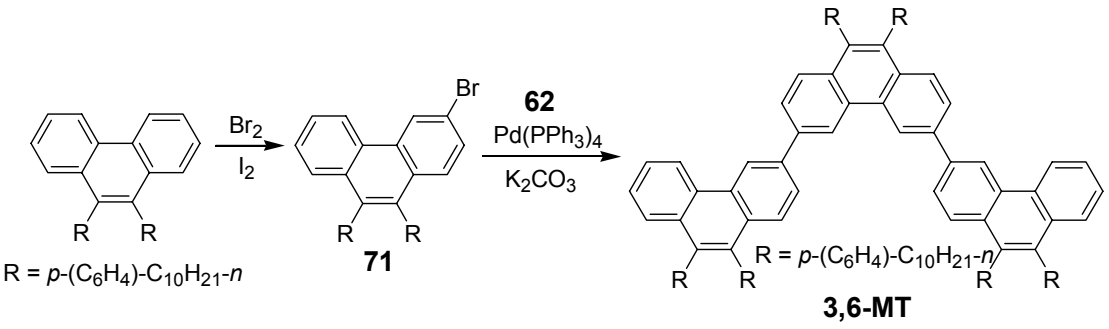

4.1.3 Electrochemical Properties

The redox behavior of thin films of **2,7-PKP**, **2,7-PAP**, **3,6-PKP**, and **3,6-LPAP** was investigated by cyclic voltammetry (CV) against Ag/Ag+. As shown in Figure 4.6, all the

polymers show an irreversible oxidation, with oxidation onset values of 1.54 V vs Ag/Ag+ for **3,6-PKP,** 1.57 V for **3,6-LPAP**, 1.61 V for **2,7-PKP**, and 1.64 V for **2,7-PAP**. The CV data listed in Table 1 point toward a slight increase in the oxidation onset for the 2,7-linked polymers (**2,7-PKP** and **2,7-PAP**). Calculating the energy level of Ag/AgCl to be -4.4 eV from the ferrocene/ferrocenium standard,[31,32] and determining the bandgap from the absorption onset, the HOMO and LUMO values for **3,6-PKP** are estimated to be -5.55 eV and -2.45 eV respectively. The corresponding HOMO and LUMO values are -5.71 and -2.65 eV for **3,6-LPAP**, -5.56 and -2.72 eV for **2,7-PKP**, -5.89 and -2.81 eV for **2,7-PAP**, respectively.[20]

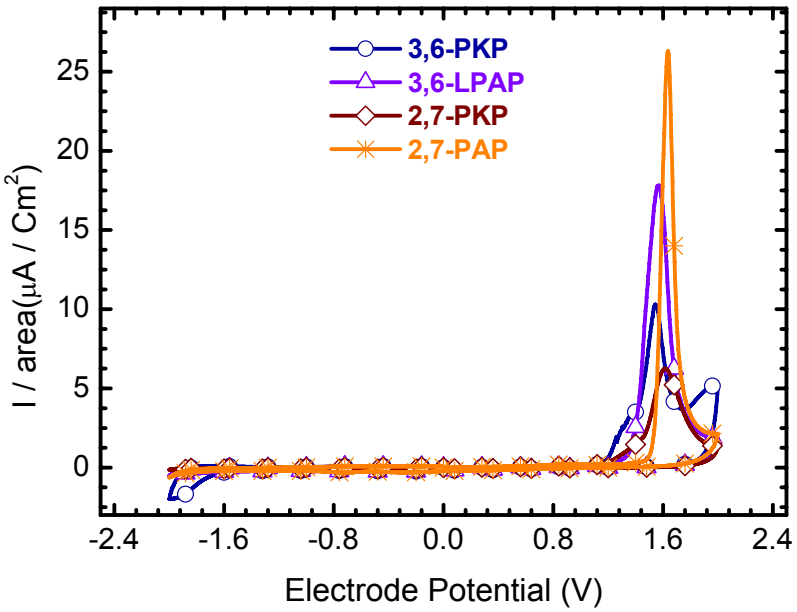

Figure 4.6. Cyclic voltammograms of the polymer films coated on platinum electrodes measured in acetonitrile containing 0.1 M Bu_4NClO_4 solution at a scan rate of 100 mV/s at room temperature.

4.1.4 Photoluminescence Properties

The UV-vis absorption and photoluminescence properties of all polymers (**2,7-PKP**, **2,7-PAP**, **3,6-PKP**, and **3,6-LPAP**), as well as the model compounds (**2,7-MT** and **3,6-MT**), were investigated in THF solution and in thin films. Transparent and uniform polymer films were prepared on quartz by spin-casting from toluene, THF chloroform, or DCM solutions at room temperature. The physical, optical and electrochemical data for all materials are summarized in Table 4.1 and Table 4.2.

Table 4.1 Physical properties of the copolymers (**2,7-PKP**, **2,7-PAP**, **3,6-PKP**, and **3,6-LPAP**)

polymer	M_n	M_w	PDI	T_d[b](°C)
2,7-PKP[a]	4.68×10^4	9.78×10^4	2.09	380
2,7-PAP	1.13×10^4	5.26×10^4	4.46	425
3,6-PKP	3.15×10^3	3.15×10^3	1.62	445
3,6-LPAP	5.33×10^3	6.82×10^3	1.28	430

Estimated from GPC (eluent = THF, poly *p*-phenylene standards). [a] For the THF-soluble part. [b] Onset decomposition temperature (5 % weight loss).

2,7-MT and **3,6-MT**. The absorption spectra of **2,7-MT** and **3,6-MT** in THF solution are similar in shape, exhibiting a shoulder at 340 nm and 355 nm and a peak at 306 nm and 325 nm for **2,7-MT** and **3,6-MT**, respectively. The emission spectra from both compounds show a clear vibronic fine structure with a spacing of *ca*. 150-160 meV for all transitions (stretching vibration of the C=C–C=C bonds). The observation of a systematic bathochromic shift of 50 meV between **2,7-MT** and **3,6-MT** in absorption and emission is a clear indication that the linear PPP-analogue has reduced conjugation when compared to the PPV-analogue, consisting of linked, planarized *cis*-stilbene units.

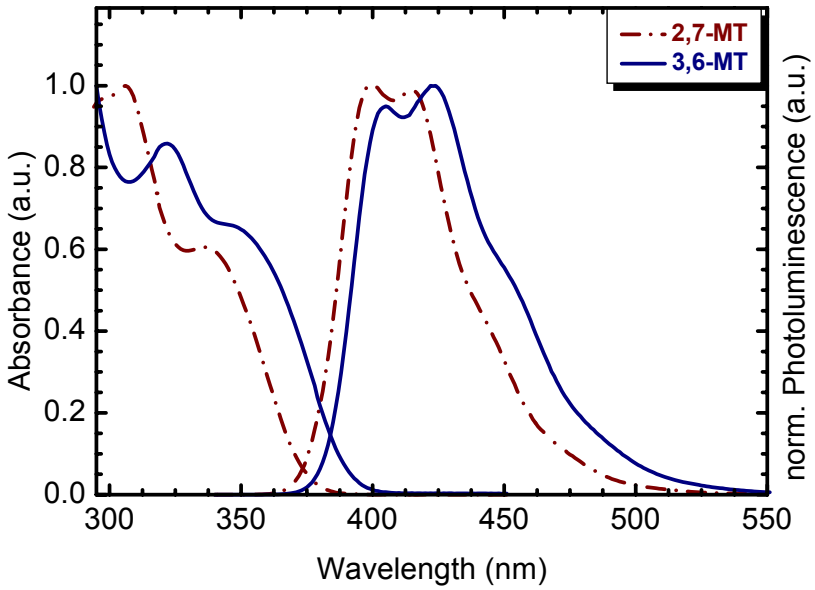

Figure 4.7. UV-vis absorption and photoluminescence spectra (λ_{exc} = 370 nm) of **2,7-MT** and **3,6-MT** in THF solution.

2,7-PKP and **3,6-PKP** in solution and as thin film. The absorption maxima in solution for **2,7-PKP** and **3,6-PKP** are at 392 and 343 nm respectively, arising from π-π* transitions in the conjugated polymer backbone (Figure 4.8 and 4.9). In the film of **2,7-PKP**, a large bathochromic shift of the onset of the emission of *ca*. 150 meV is observed, with an additional broad, long wavelength emission band. This low energy emission can be due to aggregation or a more planar configuration of the 9,10-dialkyl substituted phenanthrylene units, in comparison with the analogous polymer with 9,10-aryl substituents. (vide infra). A bathochromic shift of the onset of emission between 50 and 150 meV is typical for linear PPP-type polymers[7] as a consequence of the reduced inter-ring twist in the solid-state. In the case of **3,6-PKP**, the thin film emission and absorption spectra are similar to those recorded in solution, with a typical bathochromic shift of *ca*. 130 meV. This compound exhibits a long-wavelength tail emission, which starts to make

a dominant contribution for wavelengths above 500 nm. This can be attributed to aggregation of the phenanthrylene units with alkyl substituents at the 9,10-positions.

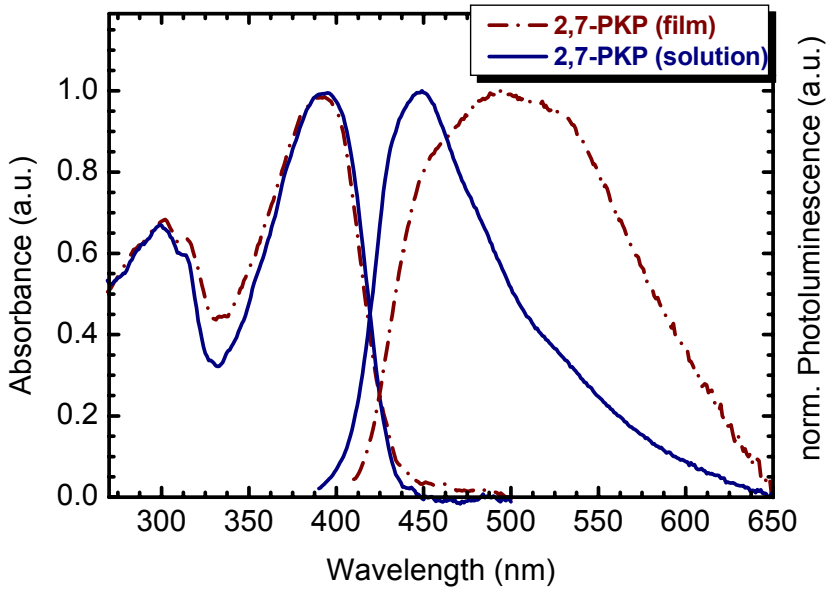

Figure 4.8. UV-vis absorption and photoluminescence spectra (λ_{exc} = 370 nm) of **2,7-PKP** film and in THF solution.

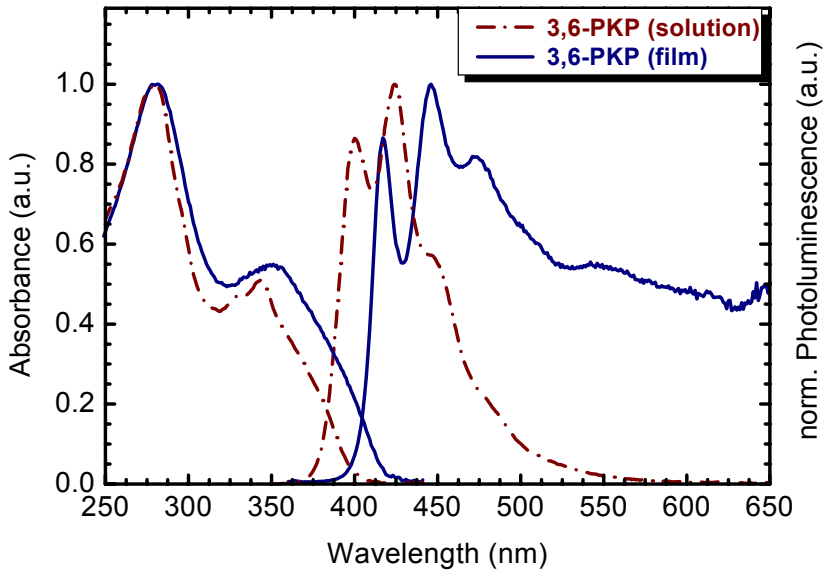

Figure 4.9. UV-vis absorption and photoluminescence spectra (λ_{exc} = 370 nm) of **3,6-PKP** film and in THF solution.

2,7-PAP and **3,6-LPAP** in solution and as thin films. The poly(9,10-dialkylphenanthrylene)s presented so far, **2,7-PKP** and **3,6-PKP**, show a broad, long wavelength emission band in the solid state. This is due to increased interaction of the polymer chains in the solid-state masking the intrinsic properties of the polymers. To study the influence of the 2,7- and 3,6-conjugation on the properties of excited states, the corresponding aryl-substituted compounds **2,7-PAP** and **3,6-LPAP** are better suited because they do not exhibit any long wavelength emission, suggesting suppression of aggregation in the solid-state. In addition to suppressing the unwanted long wavelength emission bands, **2,7-PAP** and **3,6-LPAP** exhibit much better film forming properties, allowing for the ready fabrication of light emitting devices. (vide infra) As depicted in Figure 4.10, the absorption spectrum of **3,6-LPAP** in THF solution has one distinguishable broader band when compared to that of **2,7-PAP**. Additionally, the excitation spectra of all polymers (**2,7-PKP, 3,6-PKP, 2,7-PAP,** and **3,6-LPAP**) in THF solution are almost identical to the absorption spectra, which implies that these absorptive features mainly contribute to the emissions from the backbone by excitation energy transfer (Figure 4.12).

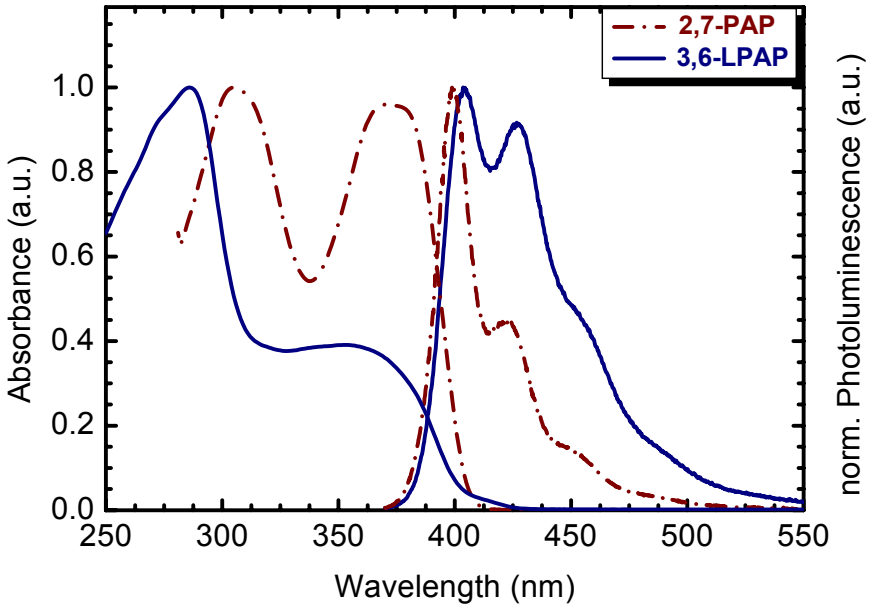

Figure 4.10. UV-vis absorption and photoluminescence spectra (λ_{exc} = 370 nm) of **2,7-PAP** and **3,6-LPAP** in THF solution.

A comparison of the absorption and emission spectra of **2,7-PAP** and **3,6-LPAP** in solution reveals a significant broadening of the bands in **3,6-LPAP**, in addition to a bathochromic shift in emission by ~10 meV for the PPV-analogue. This is accompanied by a less pronounced 0-0 transition and an increased Huang-Rhys factor. This observation indicates that in the linear 2,7-linked compound there is less vibronic coupling due to the rigid-rod nature of the polymer when compared to the PPV-analogue.

In the film, **2,7-PAP** displays only a slight red shift of *ca*. 45 meV. In contrast to the alkyl substituted **2,7-PKP**, **2,7-PAP** fails to suggest any aggregation in the solid-state, as depicted in Figure 4.11. Conversely, for **3,6-LPAP** the solid-state emission spectrum reveals a more pronounced red shift of *ca*. 120 meV as compared to the solution spectrum.

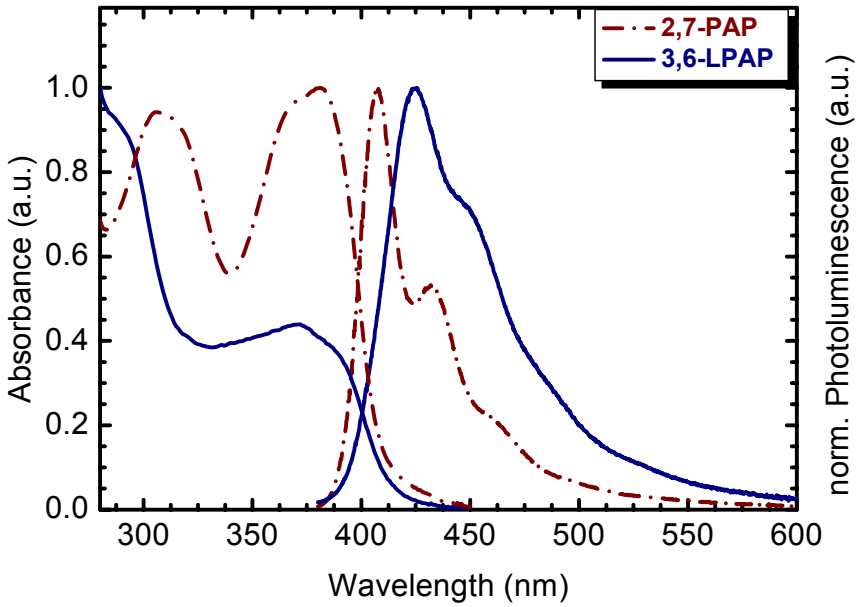

Figure 4.11. UV-vis absorption and photoluminescence spectra (λ_{exc} = 370 nm) of **2,7-PAP** and **3,6-LPAP** films.

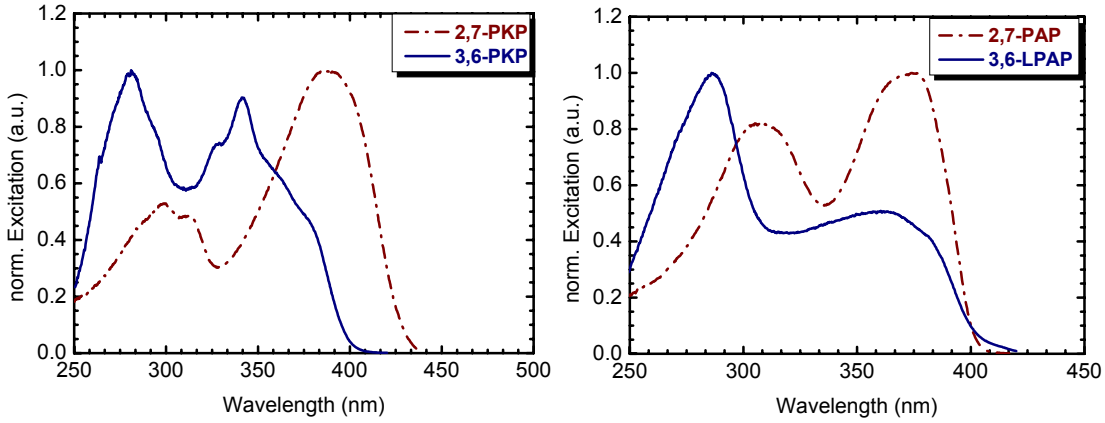

Figure 4.12. PL excitation spectra (λ_{em} = 400 nm) of **2,7-PKP, 3,6-PKP, 2,7-PAP,** and **3,6-LPAP** in THF solution.

To explore the optical properties in detail, the absorption and emission of all polymers (**2,7-PKP, 3,6-PKP, 2,7-PAP,** and **3,6-LPAP**) were investigated in various solvents and no significant solvatochromic effects were observed. The PL film spectra of alkyl

substituted polymers (**2,7-PKP** and **3,6-PKP**) reveal a broad, long wavelength emission in all solvents whereas the corresponding aryl-substituted polymers (**2,7-PAP** and **3,6-LPAP**) do not display any such emission in films from various solvents (Figure 4.13), confirming the suppression of the aggregation in the solid state. The observed slight differences in the thin film PL spectra of **2,7-PAP** cast from different solvents can be attributed to the fact that spin-coating from THF and toluene solutions yield remarkably thinner films compared to chloroform and DCM (~ 30 nm compared to 10 nm for toluene films) (Figure 4.13top). Therefore, the spectra from the latter two can be to a certain degree influenced by self-absorption.

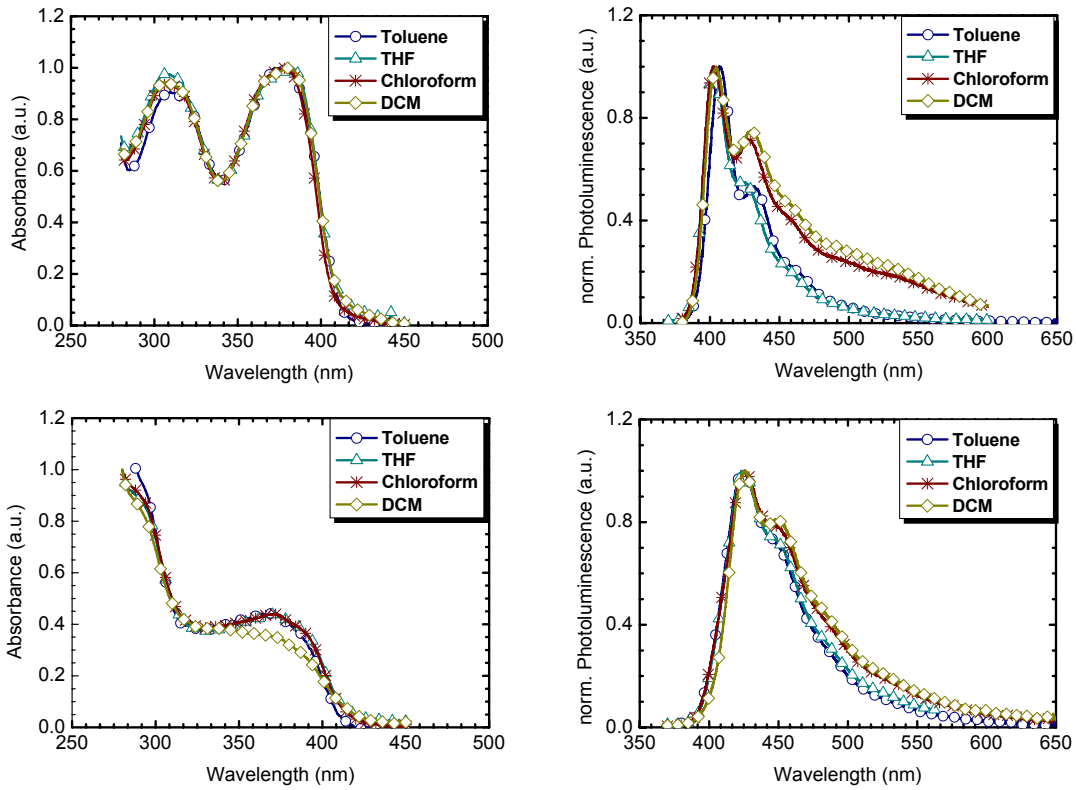

Figure 4.13. UV-vis absorption and photoluminescence spectra (λ_{exc} = 370 nm) of **2,7-PAP** (top) and **3,6-LPAP** (bottom) as the films fabricated in various solvents.

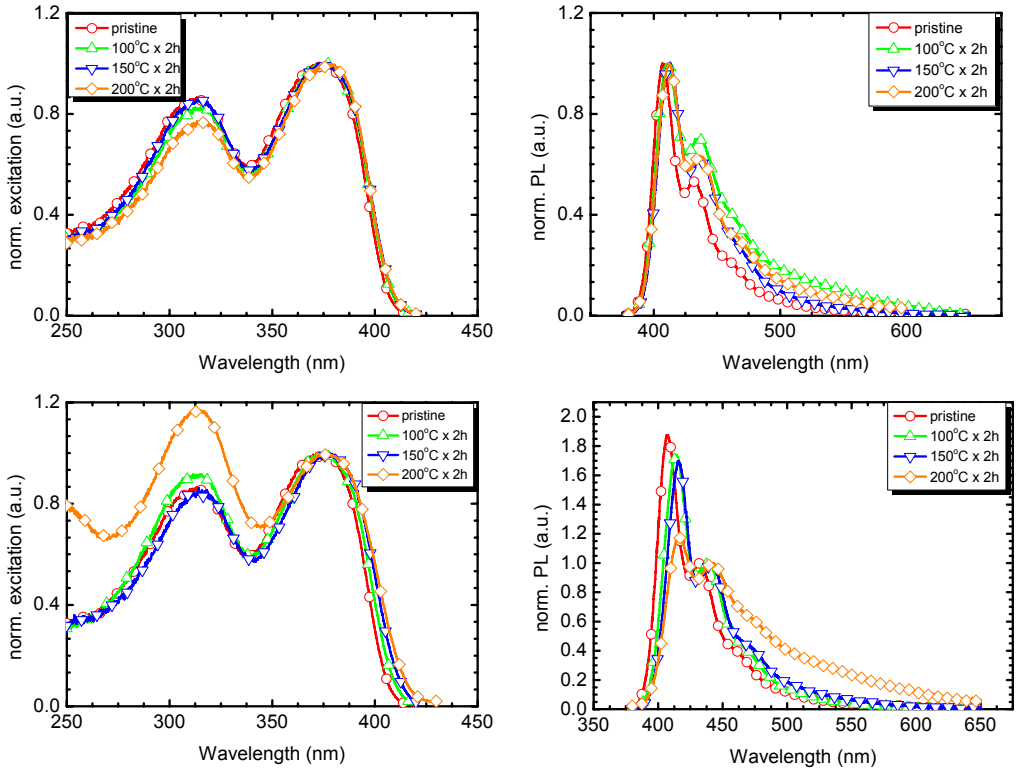

Figure 4.14. Excitation and photoluminescence spectra (λ_{exc} = 370 nm) of pristine and thermally degraded **2,7-PAP** film in vacuum (top) and in air (bottom). The PL spectra are normalized on the second vibronic in order to show the reduction of intensity of the first peak and the emergence of the tail at 200 °C.

To study the different behavior of polyphenanthrylenes (**2,7-PAP** and **3,6-LPAP**) and PF-type polymers upon heating, the thermal degradation studies were done on baked films spun from toluene at 200 °C in vacuum and air, respectively. Both polymers show only slight degradation in vacuum but baking in air yields strong deviations from the original spectra (Figure 4.14 and 4.15). The observed reduction in PL intensity is common to PF-type polymers with alkyl substituents where the emission (π-π* transition bands, *ca.* λ_{em} = 420-450 nm) is reduced on continued heating.[33] A second broad emission band appears in PF-type polymers around 530-550 nm attributed to the formation of

fluorenone defects,[22,34-36] however the formation of any such oxidative defects is not seen in **2,7-PAP** and **3,6-LPAP**. This suggests that the aryl-substituents on polyphenanthrylenes suppress the long-wavelength emission due to both a lower susceptibility toward oxidation of the arylated bridgeheads and to hindrance of exciton migration to any defect sites that may arise.

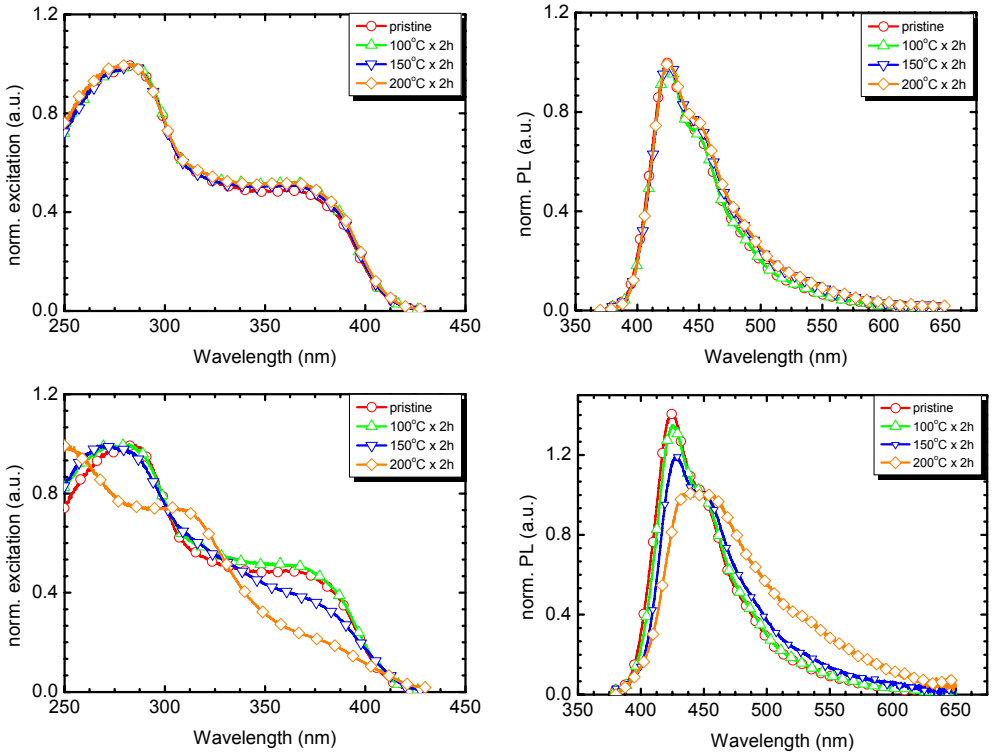

Figure 4.15. Excitation and photoluminescence spectra (λ_{exc} = 370 nm) of pristine and thermally degraded **3,6-LPAP** film in vacuum (top) and in air (bottom). The PL spectra are normalized on the second vibronic in order to show the reduction of intensity of the first peak and the emergence of the tail at 200 °C.

In case of **2,7-PAP,** a drastic reduction in air of the 0-0 vibronic emission peak at 407 nm compared to the 0-1 peak at 440 nm is observed when heated in air. The decrease in PL intensity was about 80 %, which is attributed to attack of the polymer by oxygen

and/or water since these effects are not observed for the films baked in vacuum. Film spectra show a moderate red shift, which can be assigned to relaxation during baking. This behavior is very similar to that of PF-type polymers. As shown in Figure 4.15, thermal degradation of **3,6-LPAP** in air appears close to **2,7-PAP** such as the strong decrease of the 0-0 peak and is even stronger. However, a new peak emerges around 307 nm, which is presumably originated from the cracking of bonds in the polymers.

In summary, the thermal degradation experiments show (i) a large drop of π-π* transition band upon heating in air for all polymers and (ii) no long wavelength broadening or a ketonic defect formation.

4.1.5 Steady State Photoexcitation Dynamics

To further elucidate the difference in the photoexcited states of **2,7-PAP** and **3,6-LPAP**, the photoinduced absorption (PA) spectra of films have been recorded by Horst Scheiber of the group of Dr. Emil J. W. List at TU Graz (Figure 4.16). The samples for PA measurements were prepared by spin-coating on Infrasil substrates. The pump beam is produced by an Ar^+ laser with a laser power of approximately 100 mW, which is mechanically chopped at ~17 Hz, providing the reference for the lock-in amplifier. The sample is mounted in an optically accessible cryostat under a dynamic vacuum of less than 10^{-5} mbar. A 50 W tungsten halogen lamp was the light source for the transmission measurements. All PA spectra are measured at 100 K and are corrected for PL and the optical throughput of the setup.

2,7-PAP displays one dominant band at 880 nm (1,4 eV) with a shoulder at 789 nm (1,6 eV). The 1.4 eV feature has an obvious similarity to the PA spectra of other PPP type derivatives,[33,34] such as methyl substituted ladder-type poly(*p*-phenylene) (MeLPPP),

where this characteristic was observed at 1.3 eV, with the entire absorption band having a very similar shape. Therefore, this band can be assigned to absorptions within the triplet manifold (T1 → Tn absorption). The high-energy shoulder is also caused by a T1 → Tn absorption, as the lifetime of this absorptive mark is identical to the dominant peak at 1.4 eV. Because of its energetic separation to the main characteristic it is tentatively assigned to a vibronic progression of the absorption. No explicit polaronic absorption is observed.

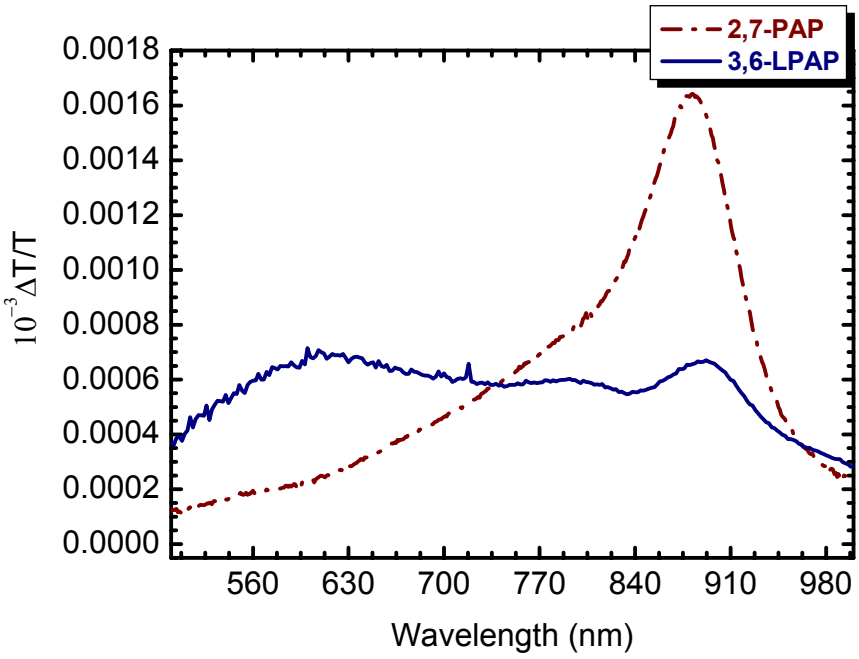

Figure 4.16. Photoinduced absorption spectra of **2,7-PAP** and **3,6-LPAP** films recorded at 100K.

In contrast, the PA spectrum of **3,6-LPAP** demonstrates a shift of the two T1 → Tn absorption bands to lower energies, to 892 nm and 785 nm. This is accompanied by a reduction of the signal intensity to about 30 % of the signal intensity of **2,7-PAP**. The PA spectrum of **3,6-LPAP** displays a broad band at 615 nm, which is absent in **2,7-PAP**. The

observed shift can be explained by the overall lowering of the optical bandgap in **3,6-LPAP** as compared to **2,7-PAP**, whereas the additional band at 615 nm is untypical for any PPP-type polymer.[33,34] However, comparing this characteristic to PPV-type polymers, a resemblance to the typically observed broad polaronic absorption may be recognised.[35,36] This again points toward the similarity in the properties of **3,6-LPAP** to PPV-type polymers.

Table 4.2. Optical and electrochemical data of **2,7-PKP**, **2,7-PKP**, **3,6-PKP**, **3,6-LPAP**, and the model trimers (**2,7-** and **3,6-MT**).

compound	solution λ_{max} (nm)		film λ_{max} (nm)		HOMO (eV)	LUMO (eV)	optical bandgap[a] (eV)
	absorption	emission	absorption	emission			
2,7-MT	306 (340)	406 (416)					
2,7-PKP	392	448	392	500	-5.56	-2.92	2.84
2,7-PAP	306, 375	400 (424, 451)	381	403(429)	-5.89	-2.81	3.08
3,6-MT	325 (355)	410, 422					
3,6-PKP	343	398, 425 (450)	351	417, 446 (473)	-5.69	-2.59	3.10
3,6-LPAP	343-357	403, 426 (456)	365-378	424 (451)	-5.71	-2.65	3.08

[a]Estimated from a combination of CV data and the onset wavelength of optical absorption in THF solution.
Peaks that appear as shoulders or weak bands are shown in parentheses

4.1.6 Electroluminescence (EL) Properties

2,7-PAP and **3,6-LPAP** exhibit the best film forming properties of the presented polymers and therefore the electroluminescent properties of these two polymers have been tested in a functional device. OLEDs were prepared add in by the group of Dr. Emil J. W. List at TU Graz under an inert atmosphere, with the configuration ITO/PEDOT:PSS/**polymer**/Ca/Al (Figure 4.17).

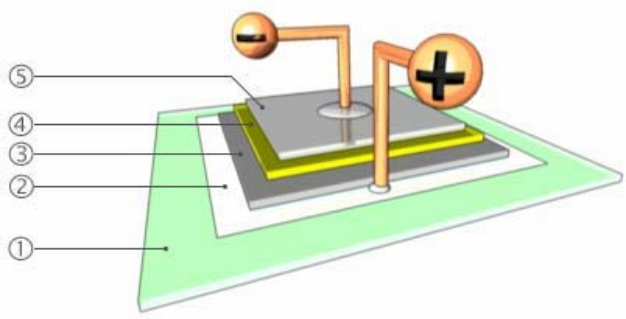

Figure 4.17. Device architecture used in the EL experiments. (1) Transparent substrate; (2) Hole injection electrode (ITO); (3) Hole transporting layer(PEDOT/PSS); (4) Light emitting polymer; (5) Electron injecting electrode (Ca/Al).

As depicted in Figure 4.18, OLEDs fabricated from **2,7-PAP** show a deep blue electroluminescence spectrum with a maximum at 403 nm and a spectral shape identical to the thin film PL spectrum. The luminance values are found to be *ca*. 200 cd/m^2 at a bias voltage of 15 V and color coordinates of the emission are in the deep blue range at x=0.19, y=0.14, according to the CIE standard 1931. The devices display the electroluminescence onset at *ca*. 4 V in forward bias direction and exhibit stable blue emission within the first minutes of operation under glove box conditions and when operated in air. Driving the device at constant current leads to a 50 % reduction in luminescence after 10 min., however, without a significant change in the emission spectrum of the device.

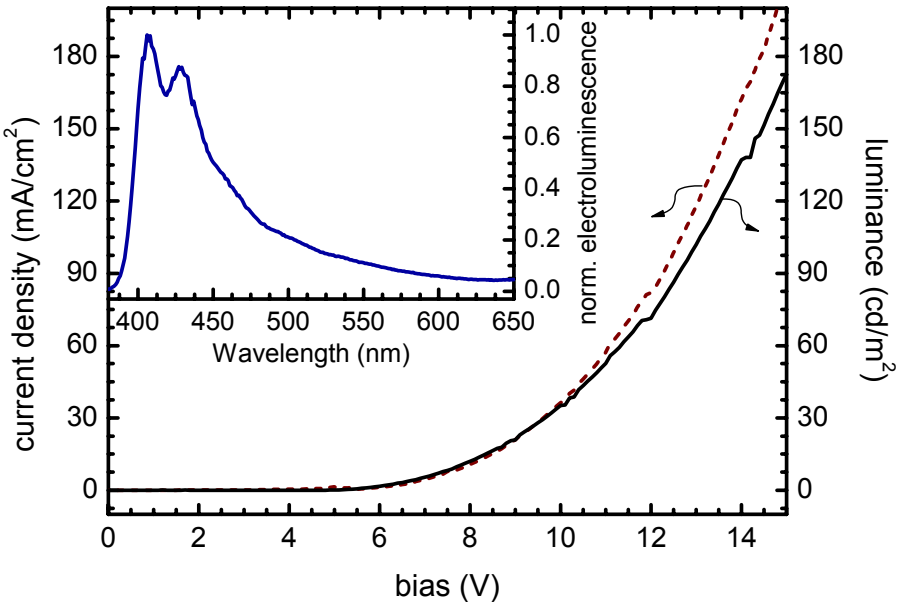

Figure 4.18. Bias/current and bias/electroluminescence characteristics and normalized electroluminescence of an ITO/PEDOT/**2,7-PAP**/Ca/Al device.

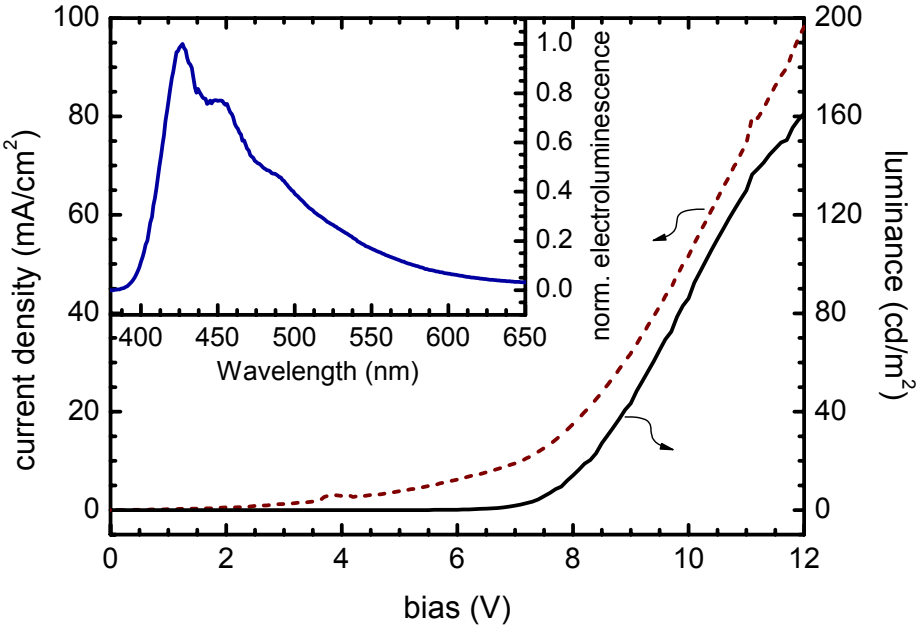

Figure 4.19. Bias/current and bias/electroluminescence characteristics and normalized electroluminescence of an ITO/PEDOT/**3,6-LPAP**/Ca/Al device.

OLEDs prepared from **3,6-LPAP** also exhibit an electroluminescence spectrum identical to the PL spectrum in the film, with luminance values of *ca*. 200 cd/m^2, however at a slightly lower bias voltage of 10 V. The color coordinates are also in the deep blue range at x = 0.18, y = 0.16 according to the CIE standard 1931. These devices are slightly less stable under operation compared to **2,7-PAP** since at constant current over 10 min a 70 % reduction in luminescence is observed, but also no spectral degradation of the material is seen during operation under glove box conditions, as well as under operation in air. These unoptimized single-layer devices show only moderate efficiencies (0.25-0.5 cd/A), indicating that electron-transporting layers are required to obtain maximum efficiency in the devices.

4.1.7 Thermal Stability of EL Devices

A detailed investigation into the long term stability on the EL devices of the two polymers, **2,7-PAP** and **3,6-LPAP** in air and vacuum was undertaken. The ITO covered substrate was etched using oxygen plasma, and then the PEDOT/PSS layer was subsequently applied by spin-coating then heated at 100°C, 150 °C and 200 °C for two hours respectively. The device performance of the two polymers reveals some similarities to their thermal degradation behaviors. Use of toluene instead of THF as solvent does not show any major improvements. The only significant difference is a decrease of the onset voltage by approximately 1 V. But this can be assigned to a lower thickness of the emissive layer when spin cast from toluene. Besides, both polymers display a red shift and decrease of the 0-0 peak, as well as the emergence of low energy tails with increasing voltage and operation time. Operation in argon atmosphere shows no significant improvements as compared to the devices operated in air (Figure 4.20 for **2,7-PAP** and

3,6-LPAP). This suggests that elimination of the disturbing effects of oxygen and water does not yield satisfying color stability. This degradation can be due to chemical or electrochemical reactions of the evaporated cathode material with the conjugated polymers, suggesting that a buffer layer can enhance device lifetimes.

As depicted in Figure 4.20, the EL intensity (0-0 vibronic peak) of **2,7-PAP** decreases upon driving the device at high voltages and 0-1 peak (427 nm) becomes more dominant with a red shift to 440 nm during operation 15 V. Overall luminance reduces by 80 % during the first minute of operation (Figure 4.21a). A similar trend is observation in PL as well.

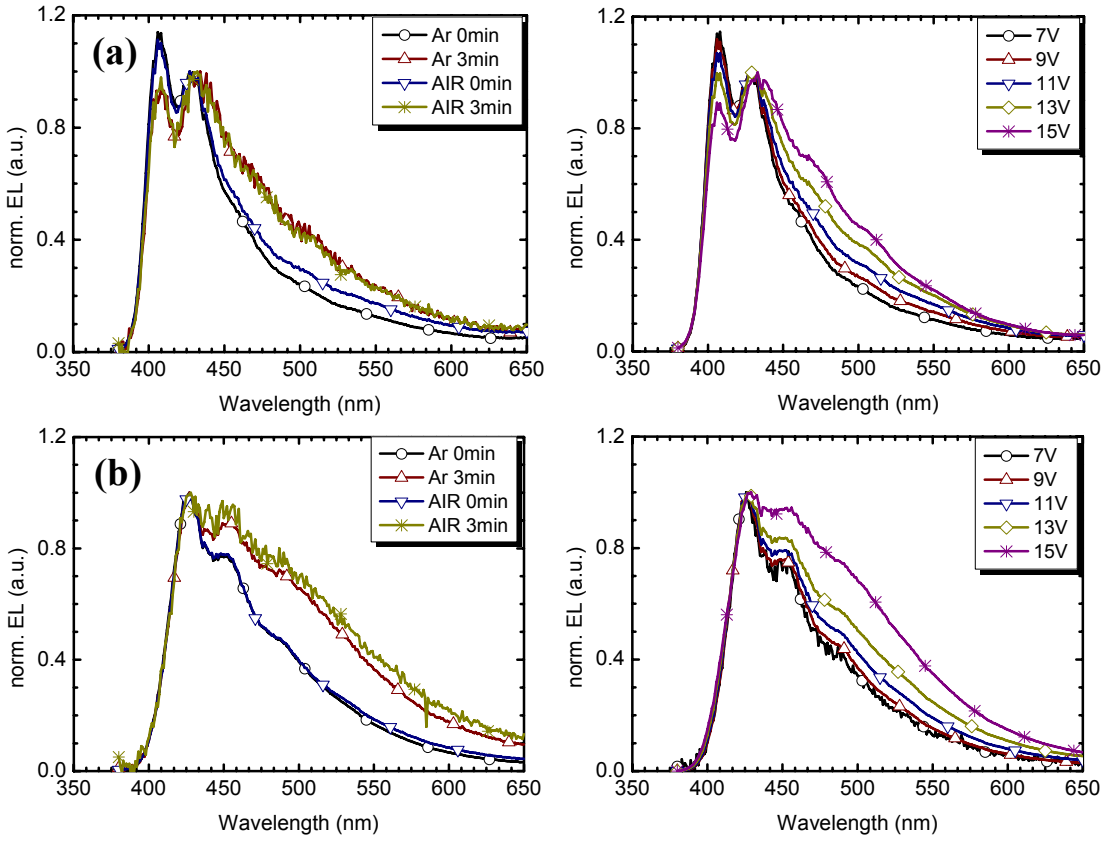

Figure 4.20. EL spectra of (a) **2,7-PAP** and (b) **3,6-LPAP** devices.

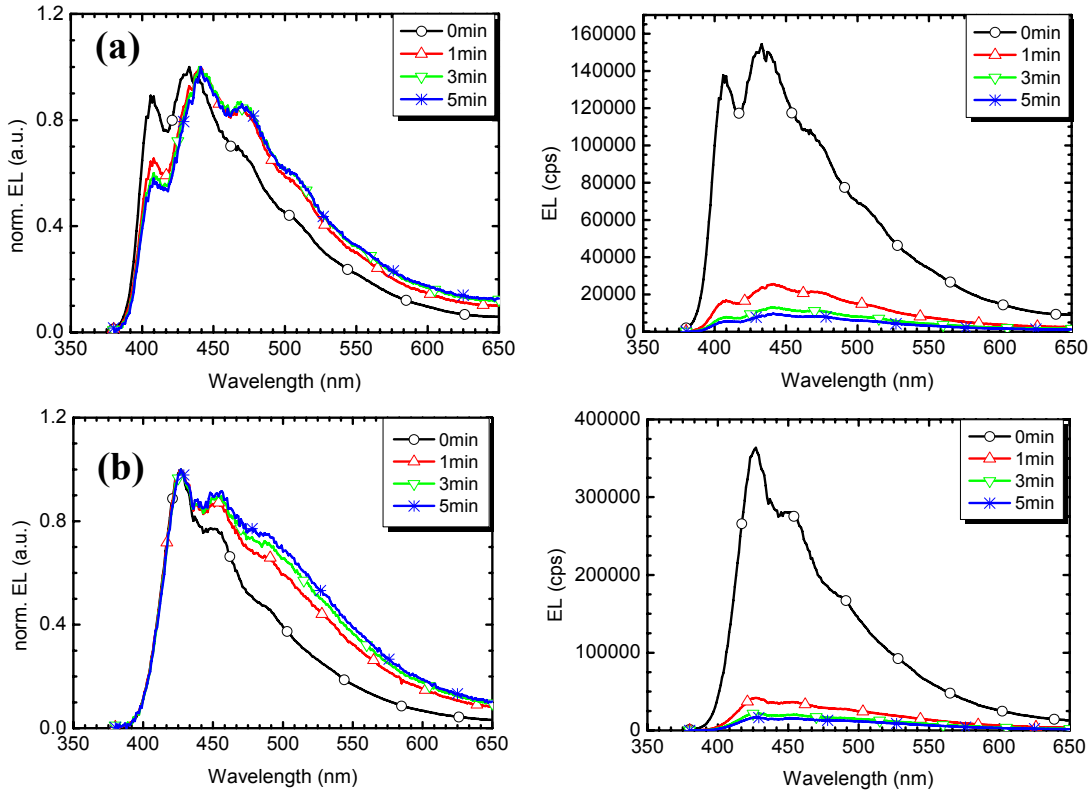

Figure 4.21. Normalized (left) and absolute (right) EL spectrum of (a) **2,7-PAP** and (b) **3,6-LPAP** device operated at 15 V and 10 V for 5 min respectively.

Similarly, in the case of **2,7-PAP**, **3,6-LPAP** device displays that the primary peak decreases and the second peak at 450 nm becomes more dominant with a red shift to 465 nm during operation at higher voltages. Overall luminance decreases even more (85-90 %) during the first minute of operation (Figure 4.21b). The red shift and relative increase of the second peak are more sensitive to operational voltage than that of **2,7-PAP**.

In summary, (i) the thermal degradation experiments show that both polymers (**2,7-PAP** and **3,6-LPAP**) reveal remarkable degradation when heated in air, which can be correlated to reaction with oxygen and/or water. On the X-ray experiments, no crystalline structures can be identified either in pristine or in degraded films. This implies that any

form of packing crystallographic rearrangement can be excluded as a reason for spectral changes during thermal degradation experiment. However, the reason for the severe reduction of the 0-0 vibronic emission peak can not fully be interpreted at this time. (ii) Both polymers display similar behavior at high voltage when operated in PLEDs compared to those of thermal degradation (significant decrease of 0-0 peak). PF-type polymers exhibit the unwanted long-wavelength bands which can be attributed to the formation of ketonic sites however, long-wavelength bands broadening is not observed in the case of **2,7-PAP** and **3,6-LPAP**.

4.1.8 Dynamic Light Scattering Studies

4.1.8.1 Behavior of 3,6-PAP

Dynamic light scattering studies were performed by Antje Larsen of the group of Prof. George Fytas in Greece. For very small polymers or particles with $qR_g<1$ in extremely dilute solution, where q is the scattering wave vector and R_G the radius of gyration, the scattering intensity is q-independent. From the value of the normalized intensity R_{VV} at q=0 and c→0 and with the measured dn/dc = 0.1446 mL/g, the molecular weight can be calculated M_w = 19.6 kg/mol, which is about three times larger than the value from GPC analysis (M_w = 6.29 kg/mol, against PS).

$$M_W = \frac{R_{VV}(q=0)}{c \cdot H} \tag{6}$$

$$H = \left(\frac{dn}{dc}\right)^2 \frac{4\pi^2 n^2}{N_A \lambda_0^4} \tag{7}$$

Where c is the concentration, H the optical constant, N_A the Avogadro-number and λ_0 the wavelength of the incident laser beam.

In dilute solution c→0 from the diffusion coefficient D_0 the hydrodynamic radius R_h

can be calculated with the Stokes-Einstein relation

$$R_k = \frac{k_B T}{6\eta\pi D_0} \tag{8}$$

where k_B is the Boltzmann constant, T the temperature in Kelvin and η the viscosity of the solvent. We obtained by dynamic light scattering, D = 1.5×10^{-6} cm^2/s and with eq.8 a R_h=2.5nm.

This value corresponds to a rodlike structure with length L = 15 nm (assuming a thickness d = 1-1.5 nm). The significant depolarized light scattering intensity supports this rigid structure since the optical anisotropy $\langle\gamma^2\rangle$ is about 7300 times larger than β^2 of toluene. The effective monomer optical anisotropy $\langle\gamma^2\rangle/N$ is about 230 β^2.

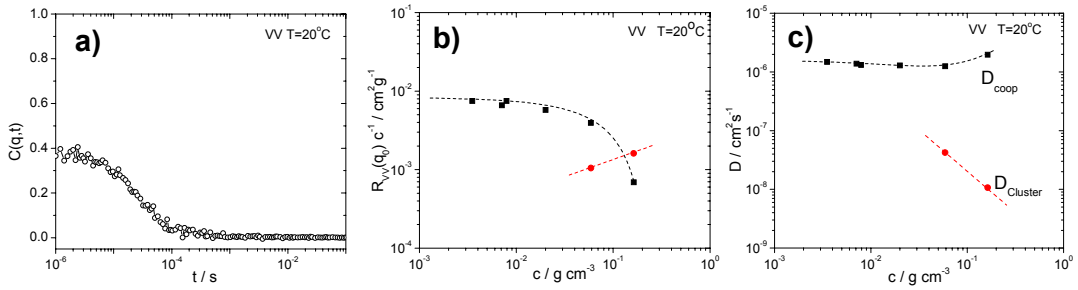

Figure 4.22. (a) Correlation function c = 0.0035 g/mL VV at q = 0.0135 nm^{-1} of **3,6-PAP** in toluene; (b) Intensity vs. concentration of **3,6-PAP** in toluene; (c) Diffusion vs. concentration of **3,6-PAP** in toluene

Based on the M_w and R_h values, the overlap concentration c* = $M_w/(4/3\pi N_A R_h^3)$, where M_w is the molecular weight and N_A is the Avogadro number, lie in the vicinity of 8 %. In fact this concentration, the translational diffusion (Fig.4.22 c) of the rigid chains become cooperative diffusion due to the interactions between chains. At about this c-range, clusters are formed as indicated by the presence of an additional second process

with increasing intensity and much slower diffusion coefficient. The cluster size has R_h = 90 nm.

4.1.8.2 Behavior of 2,7-PAP

Noticeable is the high intensity and q-dependence with c for as low as 0.006 g/L suggestive of high M_w since the measured dn/dc = 0.144 mL/g remains essentially unaltered relative to **3,6-PAP**. From the inset plot of Figure 4.23a, R_g = 93 nm, and M_w = 2-4 × 10^6 g/mol (obtained from three dilute concentrations). The strong variation of the intensity $R_{vv}(q)$ of this polydisperse system can be described (solid line) by a semiflexible chain conformation (Koyama model) with a contour length L_n = 750 nm and Kuhn segment length b = 50 nm (Figure 4.23a) and polydispersity M_w/M_n = 3. These numbers suggest a) significantly larger M_w than GPC result (M_w = 107 kg/mol, against PS standard), b) **2,7-PAP** assumes a semiflexible shape with considerable persistent length, that suggests c) the **3,6-PAP** is rigid *i.e.* L< b.

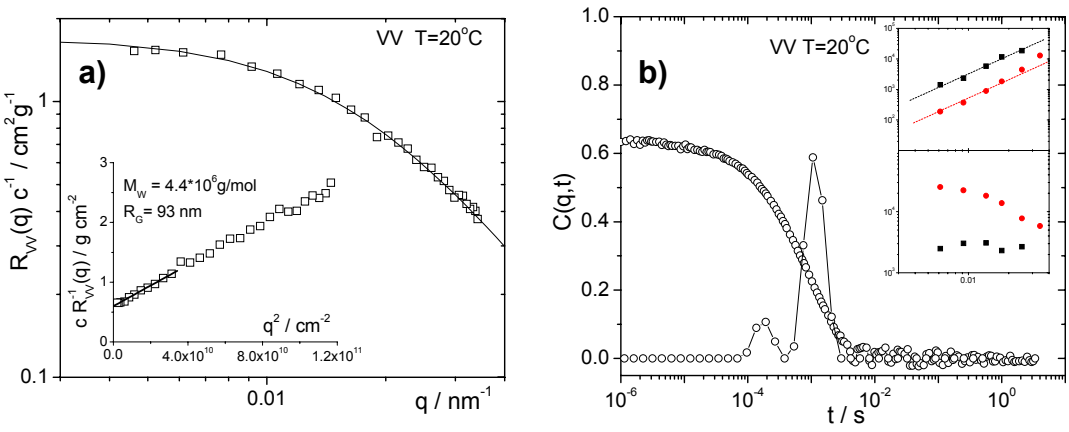

Figure 4.23. (a) Intensity vs. q (Form factor) at c = 0.0000607 g/mL VV of **2,7-PAP**, Inset Ornstein-Zernicke plot for estimation of M_w and R_g (inverse intensity vs. q^2); (b) Correlation function at q = 0.0135 nm^{-1} VV with Inverse Laplace transformation (the two peaks-curve) at c = 0.0000607 g/mL of **2,7-PAP**; upper Inset: Relaxation rate Gamma vs. q with slope of 2 (for translational diffusion) and lower Inset: Intensity vs q.

Additional information on the chain conformation can be obtained by dynamic light scattering. Even at very dilute solutions (in the absence of chain interactions) the correlation functions reveal two populations as shown in Figure 4.23b. The GPC-curve the molecular weight distribution function is expectedly bimodal characterized by the diffusion coefficients $D_S = 3.4 \times 10^{-7}$ cm^2/s and $D_L = 4.1 \times 10^{-8}$cm^2/s. An estimation of the concentrations (in g/mL) of the two populations can be obtained from the diffusion coefficients: $D_S/D_L \sim (N_L/N_S)^{0.6} \sim 8$ and the ratio $M_L/M_S \sim 32$ should be contrasted to the value of 10 (inset of Figure 4.23b). This apparent discrepancy is due to about three times higher concentration of the lower molecular weight fraction. Therefore, the solution contains two populations with $c_L/c_S = 0.3$ and $M_S \sim 80$ kg/mol. The static intensity represents the high molecular weight fraction due to its much stronger scattering power (Figure 4.23a). The value of D_L can be described by a semiflexible model (Yamakawa-Fujii) using b = 50 nm and $L_Z = 2000$ nm. To more precisely assess the two populations, separation by GPC was attempted however, the two fractions could not be separated. An inspection of MALDI-TOF spectrum shows some strong peaks corresponding to oligomeric components (*ca*. 3590 – 4800 Dalton) which stem from repeating units of about 6-8. Even though further detailed investigation can not be carried out due to failure of separation for two species, this supports our earlier conclusion.

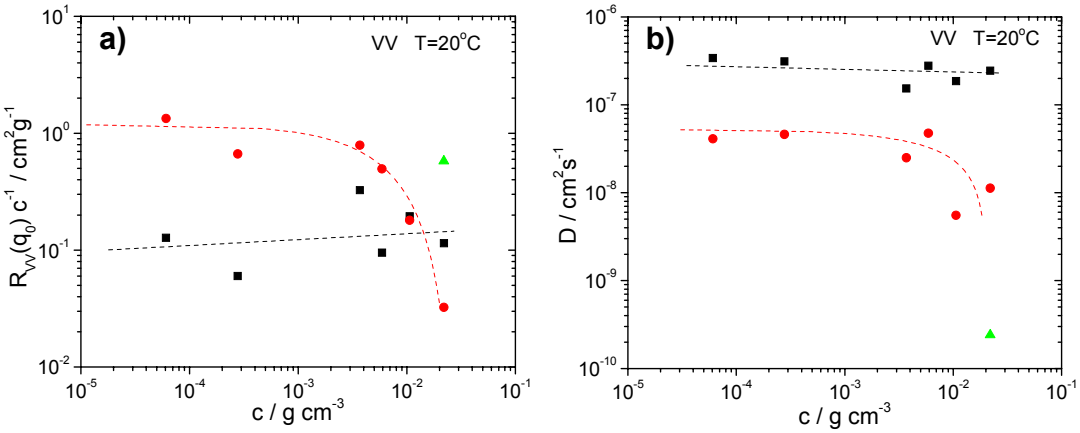

Figure 4.24. (a) Concentration dependence of the intensity VV of **2,7-PAP**; (b) Concentration dependence of the diffusion VV of **2,7-PAP**.

As Figure 4.24 depicted, the overlap concentration of the solution is determined by the large molecular weight fraction estimated to be about c*~0.2 % in agreement with the decrease of the intensity above 0.1 % (red curve). The slow diffusion coefficient (red symbol) becomes self-diffusion in this bimodal solution above that concentration. Cluster formation occurs above 3 % (green symbol). The semiflexible character with relatively large persistent length of this polymer allows the precise measurement of orientational correlation functions. This is one of the few examples where translational-rotational coupling is observed.[41-43] The relaxation function shown in Figure 4.25a is slower at high scattering angle albeit the difference is weaker probably due to the large polydispersity (internal plasticization). The concentration dependence of the rotational diffusion coefficient can be followed at low scattering angles as shown in Figure 4.25b.

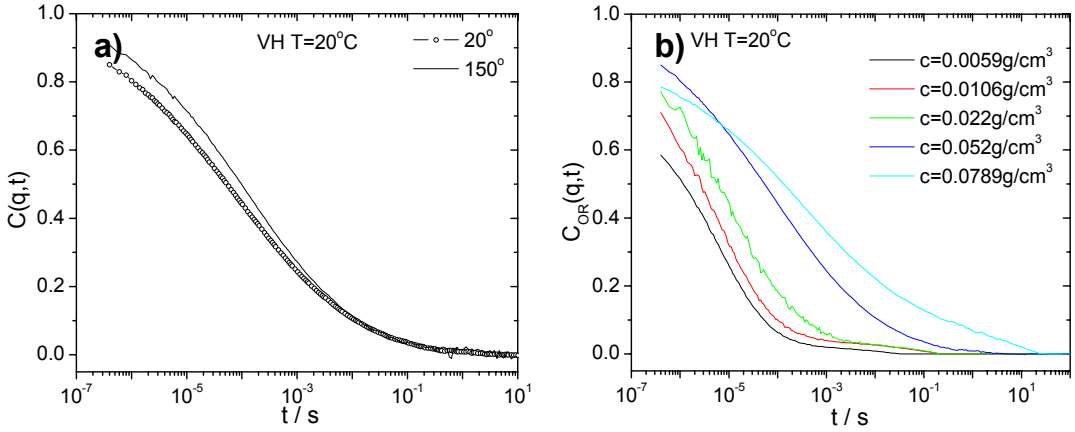

Figure 4.25. (a) Depolarized LS (VH) Orientation correlation function at angle 20° and 150° of **2,7-PAP**; (b) Orientation correlation functions at angle 20° for several concentrations of **2,7-PAP**.

The orientation correlation functions show strong concentration dependence for both shape and dynamics. The rotational diffusion is obtained from the fit $C(q,t) = \alpha \exp(-(t/\tau)^{\beta})$ at a low scattering angle (20°) where α is amplitude, τ a characteristic relaxation time, and the shape parameter (β) is a measure of width of the distribution of relaxation time. The rotational diffusion coefficient, $D_R = 1/(6\tau)$ decreases with c and the shape parameter β decreases from 0.55 to 0.3 over the concentration range 0.0035 g/mL to 0.08 g/mL. Information about the complex rotational dynamics can extracted from Figure 4.25b and Figure 4.26a.

At the lowest concentration, $D_R = 13000\ s^{-1}$ which is quite fast for these very long chains. The only way to account for this high value is to attribute it to the segmental rotational motion with a length of the order of the Kuhn segment. Indeed, the rigid rod expression leads to b~130 nm. In contrast an overall chain rotation even for semiflexible chains (L~2000 nm) would require a $D_R < 100\ s^{-1}$; for rigid chains with the same L, D_R would be even smaller. The polarized and depolarized light scattering experiments

suggest a semiflexible chain with a Kuhn segment length of the order of 80 nm which means they are not flexible as a coil or stiff as a cylinder.

In this consideration $C_{OR}(q,t)$ should be single exponential ($\beta = 1$), in contrast to the experiment. This finding implies distribution of the Kuhn segment length b, which can be feasible only by the presence of the short chains. For example, chains with molecular weight less than 100 kg/mol have length L of the order of the Kuhn segment length b.

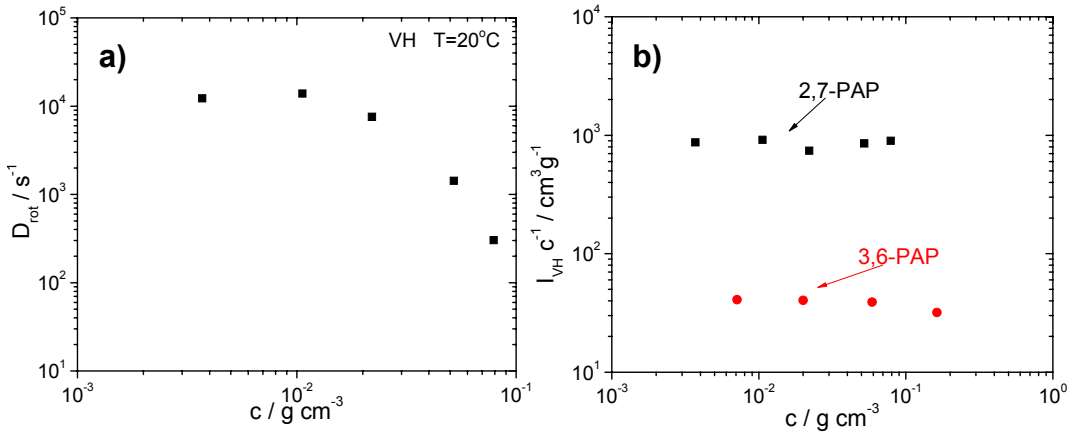

Figure 4.26. (a) Concentration dependence of the rotational diffusion of **2,7-PAP**; (b) Concentration dependence of the depolarized scattered intensity of **3,6-PAP** and **2,7-PAP**.

The concentration dependence of D_R reflects the increase of the solution viscosity. The increased broadening of the $C_{OR}(q,t)$ with c is a pertinent observation, which implies enhanced interactions affecting the cooperativity of the rotational dynamics. The depolarized light scattering intensity, which measures the collective optical anisotropy, could provide evidence on the origin (thermodynamic/kinetic) of these interactions.

The reduced I_{VH}/c (relative to the toluene) intensity is found to be insensitive to the concentration variation (up to a clouding point) where I_{VH} is the depolarized light scattering intensity. This suggests negligible static pair orientation correlations since $I_{VH} \sim c \langle\gamma^2\rangle$ is proportional to c. The effective monomer optical anisotropy is about 4600

β^2 (the optical anisotropy of the neat toluene) or about 20 times more than **3,6-PAP**.

The conformational freedom of these phenanthrylene based chains is constrained, which can give rise to the observed largest persistence length. The chain rigidity allows the study of the unexplored behavior in concentrated solution with interesting rotational-translational coupling.

4.1.9 Conclusion

In summary, a series of poly(2,7-and 3,6-phenanthrylene)s as PPP- and PPV-analogues respectively, have been synthesized by either Yamamoto or Suzuki-type polycondensation. The spectroscopic and electroluminescent properties of the two different types of π-conjugation were compared. The introduction of alkyl or aryl substituents at 9,10-positions of phenanthrene renders these materials soluble and processable. In the case of 2,7-linked polymers, it is found that alkyl substituents at 9,10-positions lead to the appearance of an unwanted low energy emission band in the solid state, which is suggestive of aggregation. The introduction of aryl substituents at the 9,10-positions completely suppresses this long wavelength emission, suggesting that the steric bulkiness of the substituents hinders the solid-state packing of the polymers. In the case of 3,6-linked polymers, the Yamamoto-type polycondensation led to the formation of substantial amounts of a macrocyclic trimer **MCT**. When using a Suzuki-type polycondensation, the formation of **MCT** was mechanistically unfavorable and resulted in improved molecular weight polymers. Both the 2,7- and 3,6-linked poly(phenanthrylene)s with 9,10-aryl substituents display blue emission in solution and film. The PL spectra of **3,6-LPAP** as PPV-analogue in both solution and film are bathochromically shifted as compared to the PPP-analogous **2,7-PAP**, which can be

attributed to the solid-state packing of the polymers. A qualitative comparison of the emission and absorption spectra indicates that the 2,7-linked compounds have less vibronic coupling in emission due to the rigid-rod nature of the polymers when compared to the 3,6-linked compounds. The photoinduced absorption features of **2,7-PAP** are similar to those of PPP-type polymers, whereas the **3,6-LPAP** exhibits characteristics only found in the spectra of PPV-type polymers. **2,7-PAP** and **3,6-LPAP** were incorporated into a single layer OLED as the active emitting material. A peak brightness of the devices of 200 cd/m^2 and good spectral stability is observed while operating under glove box as well as ambient conditions. However, both polymers (**2,7-PAP** and **3,6-LPAP**) display significant degradation at 200 °C in air. This is attributed to reaction with oxygen at elevated temperatures leading to the decomposition of the polymer backbones. Due to the good film forming properties and the stable blue electroluminescence in vacuum, both **2,7-PAP** and **3,6-LPAP** are attractive candidates as the emissive material for OLED-based flat panel display applications. The presented classes of 3,6- and 2,7-conjugated polyphenanthrylenes allow for a unique photophysical investigation, illustrating the PPP-type properties of the 2,7-linked polymers in comparison with the PPV-type properties of the 3,6-linked polymers, thereby further elucidating the structure-property relationships in conjugated polymers.

4.2 Columnar Mesophase Formation of Cyclohexaphenylene-based Macrocycles

The cyclohexa-*meta*-phenylene (**CHP**) was prepared by a colleague (Marcel Kastler) in a single step using a bimolecular coupling via Yamamoto-type cross coupling. The self-organization of two different macrocycles (**CHP** and **MCT**) of different conformational

flexibilities is been discussed in solution and in the bulk, since the structural feature of **CHP** is related to that of **MCT**. The supramolecular organization of **CHP** and **MCT** has been studied by 2D wide-angle X-ray scattering experiments performed on oriented filaments prepared by extrusion as well as temperature-dependent ^{1}H NMR measurements. Additionally, the properties of the macrocycles (**CHP** and **MCT**) having a central cavity are not only compared to those of the 3,6-linked trisphenanthrylene (**3,6-MT**) as an acyclic system but also the configuration of the corresponding polymer (**3,6-LPAP**) has been investigated.

4.2.1 Introduction

Macrocycles with rigid, non-collapsible, unsaturated hydrocarbon backbones have attracted great interest in the past few years, due to their novel properties (e.g., aggregation phenomena) and potential applications such as three-dimensional nano-structures, discotic liquid crystals, extended tubular channels, guest-host complexes and porous organic solids.[44-48] These macrocycles consist of a shape-persistent scaffold in a planar or nearly planar conformation, with a minimum of ring strain and a large diameter to thickness ratio. Often they possess an internal void volume because of their toroidal shape. The cyclic backbone of these macrocycles is typically modified with peripheral side chains containing various functionalities, which gives rise to their unique and interesting behavior such as columnar mesophase formation.[49-52] Motivated by the novel properties and potential applications of these self-assembled entities, intense efforts have been made to explore highly efficient methods for preparing such macrocycles with varied structures.[44,48,53-55] Studies into supramolecular organizations of these macrocycles have provided a better understanding of the non-covalent driving force responsible for their self-association.[56-59] However, the

efficient preparation of macrocycles has been a challenging task.

Two theoretical strategies that have been used in our macrocycle synthesis: (1) one step intermolecular coupling between two or more ring fragments followed by unimolecular cyclization in one pot; (2) oligomerization/cyclization. The advantage of these one-step procedures is evident; the starting materials are readily accessible and the target molecule is generated in a single step. On the basic two cyclisation principles, **CHP** was prepared using the protocol for a bimolecular cyclic dimerisation whereas **MCT** was derived via a one pot cyclisation methodology using Yamamoto type cross coupling under dilute condition as mentioned earlier. The development of the supramolecular chemistry of the intriguing macrocyclic structures (**CHP** and **MCT**) based on the cyclohexa-*meta*-phenylene was investigated because it was anticipated that **CHP** shows substantially different in the properties from **MCT** since **CHP** is a more flexible system compared to **MCT** which has a double-bonded bridging unit between some of the phenylene moieties.

It is important to correlate the molecular design to the supramolecular packing. In this study, the self-assembly in solution and in the solid state of macrocycles based on cyclohexa-*meta*-phenylene (**CHP** and **MCT**) are compared, whereby the structures differed in planarity (Scheme 4.9). Additionally, the organization of 3,6-linked trisphenanthrylene (**3,6-MT**) was investigated as an acyclic system. The self-assembly of the three synthesized ring-type structures was elucidated by means of temperature-dependent ^{1}H NMR spectroscopy and X-ray scattering experiments. Additionally, the phase formation at different temperatures in the solid state was investigated by X-ray scattering experiments which gave an insight into the supramolecular organization.

Scheme 4.9. Chemical structures of the investigated compounds: a) cyclohexa-*meta*-phenylene (**CHP**), b) cyclo-3,6-trisphenanthrylene (**MCT**) and c) linear-3,6-trisphenanthrylene (**3,6-MT**).

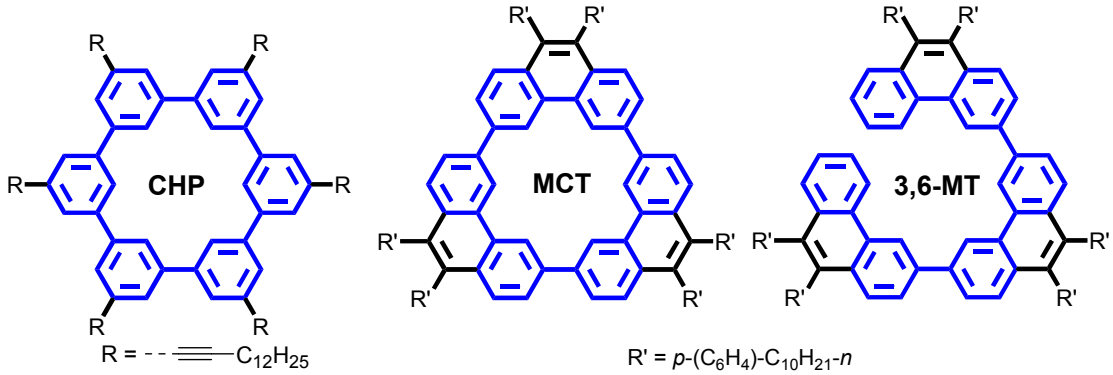

4.2.2 Thermal Characterization

The thermal behavior of all three derivatives (**CHP, MCT and 3,6-MT**) was determined by differential scanning calorimetry (DSC) (Figure 4.27). Only a relatively low melting point of 45 °C was found for the ring molecule **CHP**. For **MCT**, the DSC trace showed only one endothermic peak at 148 °C, corresponding to a transition into the mesophase. The open ring structure **3,6-MT** revealed a very small peak at 43 °C in the DSC trace, which could not be assigned to a phase transition. Thermogravimetric analysis (TGA) showed high thermal stability for both compounds **MCT** and **3,6-MT** with onset decomposition temperatures (T_d, 5 % weight loss) of 420-450 ˚C under nitrogen.

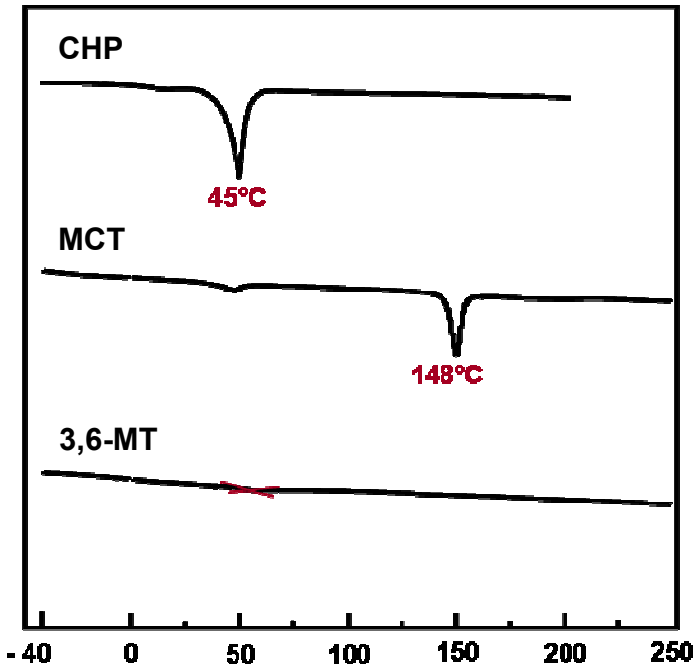

Figure 4.27. Differential scanning calorimetry (DSC) of compounds **CHP**, **MCT** and **3,6-MT**.

4.2.3 Photophysical Studies

In order to access the optical properties between cyclo-3,6-trisphenanthrylene (**MCT**) and linear 3,6-trisphenanthrylene (**3,6-MT**), the UV-vis absorption and photoluminescence were investigated in THF solution. The absorption of **3,6-MT** in THF shows a broad peak centered at 322 nm without the well-resolved vibrational energy bands, while **MCT** displays as shifted toward low energy (λ_{max} = 347 nm). The PL spectra of **MCT** and **3,6-MT** in THF illustrate a blue emission with a peak centered at 436 nm for **MCT** and at 422 nm for **3,6-MT**. The observation of a pronounced bathochromic shift is a clear indication that **MCT** has an efficient π-conjugation due to the cyclized structural feature when compared to the non-cyclic system **3,6-MT**.

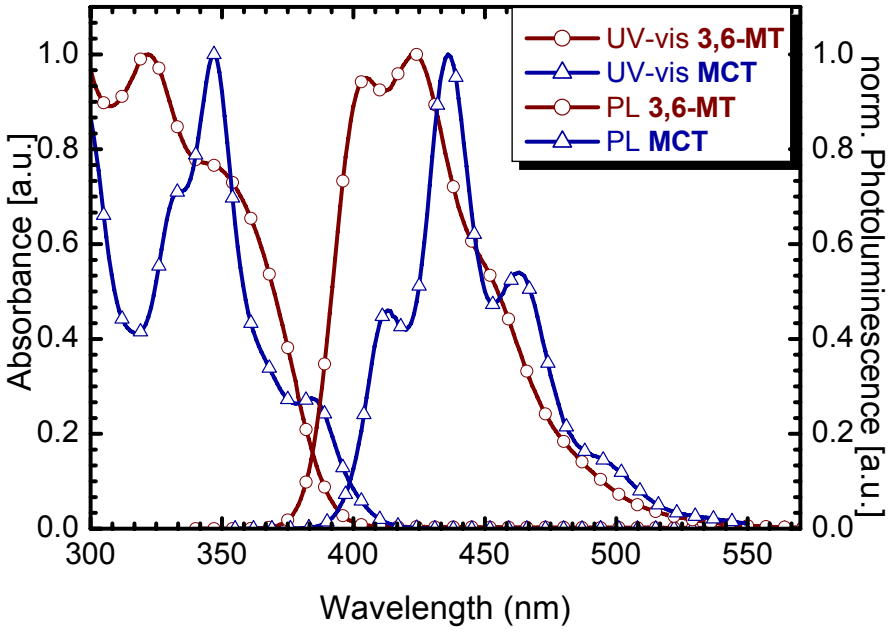

Figure 4.28. UV-vis absorption and PL spectra (λ_{exc} = 370 nm) of compounds **MCT** and **3,6-MT** in THF solution.

4.2.4 Self-assembly Behavior

The self-assembly behavior of the cyclophenylene derivatives (**CHP**, **MCT** and **3,6-MT**) in solution was investigated using the temperature-dependence of the ^{1}H NMR chemical shifts. ^{1}H NMR spectroscopy is the most frequently used technique for the investigation of aggregation in solution due to stacking interaction of nucleic acid and aromatic compounds. Furthermore, it has a great advantage because of its ease, precision, and the fact that the chemical shift data provide insight not only into the structural arrangement of individual molecule, but also into their interactions with surrounding molecules. The aggregation of all three compounds (**CHP**, **MCT** and **3,6-MT**) in solution is only slightly temperature-dependent, (Figure 4.29) which is commonly observed for disc-like aromatic systems.[47,56,59-63] In a face-to-face aggregate, the protons of one molecule are localized in the

secondary magnetic field of the neighboring aromatics, resulting in a shielding, and such a shielding effect depends on the size of the aggregates since the size of the aggregates in solution decreased at higher temperatures. The ^{1}H NMR study of the three compounds illustrated weak π-stacking interactions in solution. The small change in the observed chemical shift by ~0.1 ppm for all the protons is suggestive of the formation of dimers.[64]

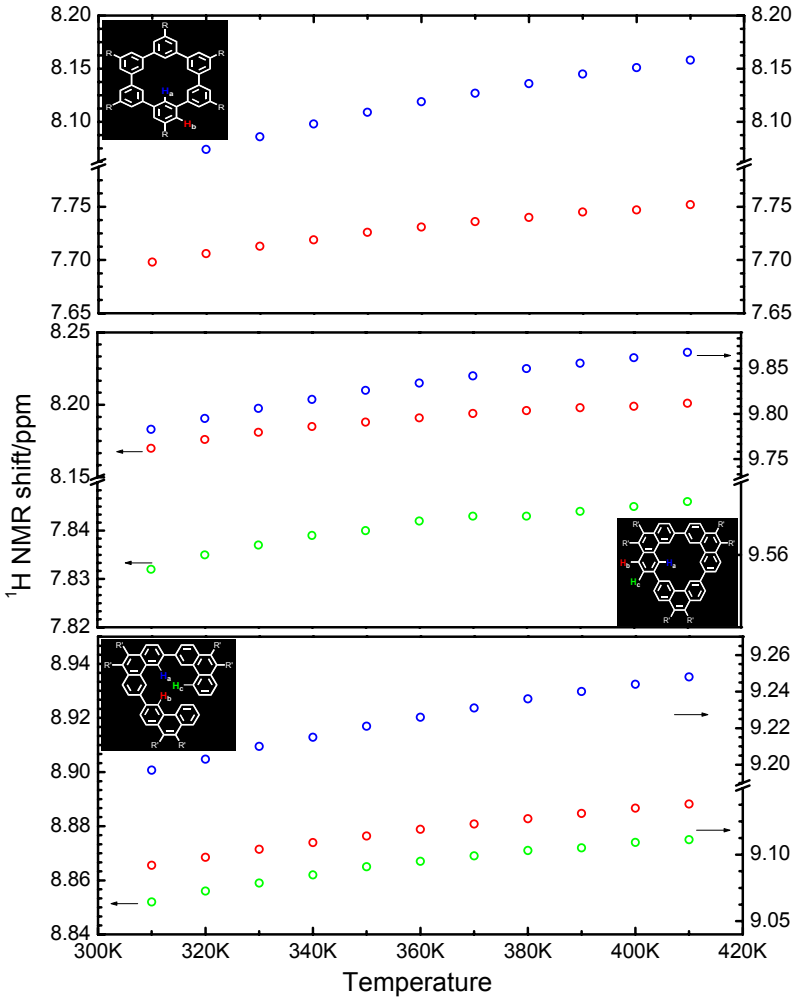

Figure 4.29. Temperature dependent ^{1}H NMR chemical shifts of the investigated phenylene derivatives (**CHP**, **MCT** and **3,6-MT**), recorded in 1,1,2,2-tetrachloroethane-d^{2}.

4.2.5 Supramolecular Organization

The supramolecular organization of the three compounds(**CHP**, **MCT** and **3,6-MT**) at the room temperature and at the mesophase was analyzed on the basis on the structural data obtained from 2D-WAXS experiments performed on mechanically extruded filaments.[65] The 2D-WAXS pattern of **CHP** after extrusion exhibited only anisotropic reflections at room temperature indicating a poor macroscopic alignment of the sample (Figure 4.30a). The small-angle reflections in the range of 2.34 nm implied a mesogenic columnar structure formed by the ring-shaped molecules, whereby wide-angle peaks correlate to a stacking distance of 0.41 nm of the single building blocks within the columns. The columnar organization of **CHP** is illustrated in Figure 4.30a. However, the residual flexibility and the non-planarity of the central ring weakened the intermolecular interactions leading to a poorly ordered macroscopic ordered self-assembly. This is in accordance with the low melting point of 45 °C confirming the poor intermolecular attractive forces in the case of **CHP**.

By contrast, the orientation of the extruded fibers of **MCT** and **3,6-MT** was more pronounced at room temperature as displayed in the patterns in Figure 4.30b,c. The 2D-WAXS showed reflections at identical positions suggesting a quite similar organization for both materials **MCT** and **3,6-MT**. Equatorial reflections indicated the self-assembly of both types of molecules into columnar structures which were aligned in the shearing direction. Such supramolecular organization was expected for **MCT**. But the columnar order of **3,6-MT** was rather surprising, since the conformation of the molecule was not predicted as ring-like.

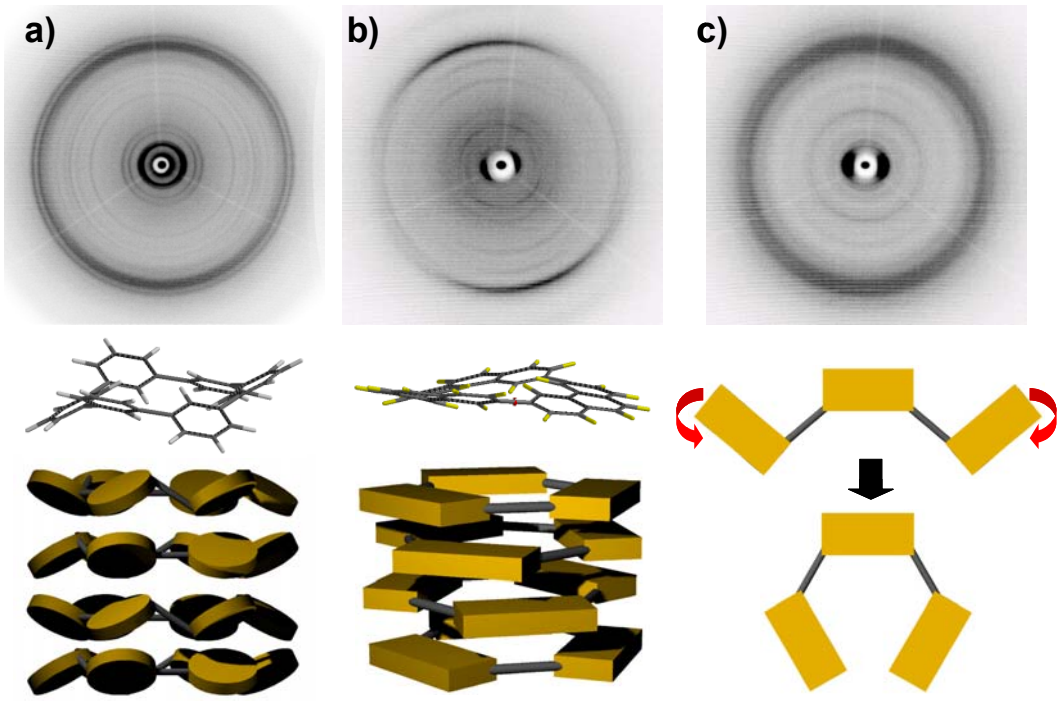

Figure 4.30. Room temperature 2D-WAXS patterns, calculated molecular geometries using SPARTAN PRO and schematic illustrations of the intracolumnar organization of a) **CHP**, b) **MCT** and c) **3,6-MT**.

It is assumed that the nanophase separation between the aromatic core and the flexible side chains of **3,6-MT** results in a conformation change into a the ring-like design as displayed schematically in Figure 4.30c. On the other hand, the non-closed structure **3,6-MT** did not reveal such planarity as the planar ring **MCT** in the packing. Indeed, sharper and more anisotropic meridional reflections were observed for compound **MCT** (π-stacking distance of 0.44 nm) in comparison to **3,6-MT**. Additional meridional reflections appeared for both **MCT** and **3,6-MT** at corresponding distances of 0.62 nm and 1.2 nm (as example for **MCT**) and were related to correlations between every 4th ring along the columnar structures. Thereby, the molecules are rotated successively by 120°/4 = 30° leading to a helical pitch containing three molecules as schematically shown in Figure

4.30b. The steric hindrance of the phenyls, attached at the ring out-of-plane rotated, induced the rotation of the rings towards each other.

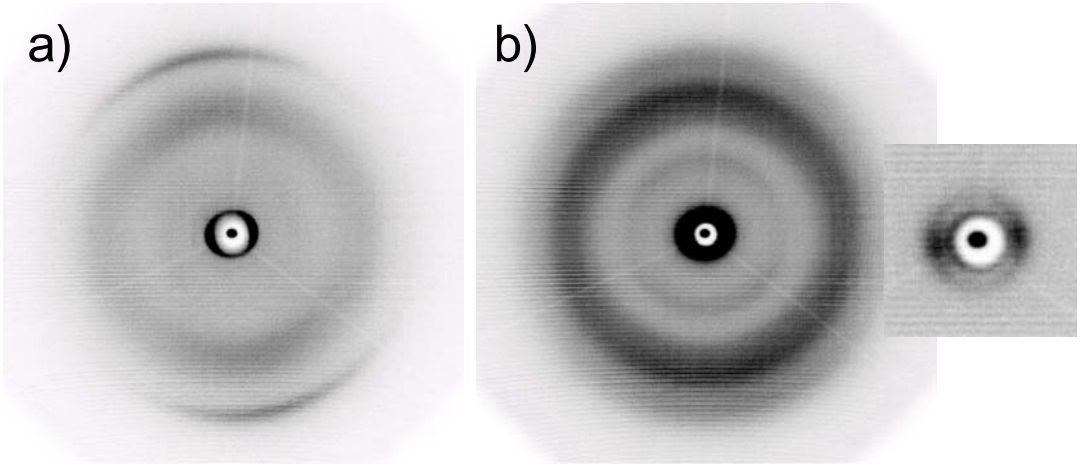

Figure 4.31. 2D-WAXS pattern of a) **MCT** at 160 °C and b) **3,6-LPAP** at room temperature.

The equatorial reflections corresponding to large periodicities of 3.50 nm for a hexagonal unit cell for **3,6-LPAP** indicated an organization of the polymer chain, not quite ordinary along the alignment direction. In general, conjugated polymers with a higher molecular weight orient with their molecular axes along the shearing direction giving rise to small equatorial distances. In this case, these large periodicities indicate a columnar organization of the conjugated chain folding into a helical arrangement. The two meridional reflections relate to 0.84 nm and 0.38 nm confirming this assumption. The smaller period corresponds to the packing of single phenanthrylene units, whereby the appearance of the additional reflection in the pattern was related to the helical arrangement.

Heating of **MCT** above the phase transition at 148 °C to the mesophase was accompanied by a significant change of the intracolumnar arrangement (Figure 4.31). The

helical packing disappeared due to higher molecular dynamics, which is characteristic for different types of columnar mesogenes.[66] In the mesophase, **MCT** arranged with its molecular plane perpendicular to the columnar axes with an intracolumnar distance of 0.37 nm, whereby the columns were organized in a hexagonal array with a packing parameter of 3.2 nm. This columnar mesophase was stable up to 500 °C, before which the isotropic phase was not reached.

The introduction of flexible side chains attached to the cyclohexaphenylene-based macrocycles enhanced the solubility of the compounds, as described in the previous section, but also opened the opportunity to the control the thermal behavior and thus the supramolecular self-assembly. All three investigated materials showed a columnar organization due to the π-interaction between the aromatic cores accompanied by the nanophase-separation between the aliphatic chains and the better ordered cyclic skeletons. The structural analysis revealed a great influence of the core planarity on the supramolecular order. It was indicated that the less planar flexible cyclic oligomer **CHP** displayed only a self-organization, whereas the cyclic compound **MCT** revealed an excellent columnar formation and a stable discotic phase at high temperatures.

4.2.6 Conclusion

Two cyclohexaphenylene-based macrocycles bearing different planarity have been synthesized in a straightforward fashion. Additionally, a linear oligomer (**3,6-MT**) has been prepared as a non-cylcic model system. The solution association propensity of all synthesized molecules was weak indicating the formation of only dimeric species. The bulk organization revealed a poor macroscopic ordering of the flexible cyclohexa-*meta*-phenylene (**CHP**), whereas the cis-stilbene bridged cyclohexaphenylene macromcycle

(**MCT**) formed well oriented columnar superstructures with a striking thermal stability. The latter **CHP** possessed also a larger π-stacking area in comparison to the cyclo-3,6-trisphenanthrylene (**MCT**) resulting in a more pronounced intermolecular interaction. The mesophase window ranged from 148 °C up to 500 °C, where the thermal decomposition set in. To our knowledge, this is the highest observed mesophase stability. Surprisingly, the linear model system 3,6-trisphenanthrylene (**3,6-MT**) formed similar columnar superstructures, which however were less well organized as indicated by the diffuse reflection in the X-ray pattern. This can be attributed to a back-folding into a ring-like molecular structure. The study revealed the importance of an attractive intermolecular interaction which allows well-defined superstructures to be established. Therefore, more planar disc-like molecules form better organized structures.

4.3 References

(1) Burroughes, J. H.; Bradley, D. D. C.; Brown, A. R.; Marks, R. N.; Mackay, K.; Friend, R. H.; Burns, P. L.; Holmes, A. B. *Nature* **1990**, *347*, 539-541.
(2) Braun, D.; Heeger, A. J. *Appl. Phys. Lett.* **1991**, *58*, 1982-1984.
(3) Bradley, D. D. C. *Adv. Mater.* **1992**, *4*, 756-758.
(4) Clery, D. *Science* **1994**, *263*, 1700-1702.
(5) Gill, R. E.; Malliaras, G. G.; Wildeman, J.; Hadziioannou, G. *Adv. Mater.* **1994**, *6*, 132-135.
(6) Kraft, A.; Grimsdale, A. C.; Holmes, A. B. *Angew. Chem. Int. Ed.* **1998**, *37*, 402-428.
(7) Grem, G.; Leditzky, G.; Ullrich, B.; Leising, G. *Synth. Met.* **1992**, *51*, 383-389.
(8) Balanda, P. B.; Ramey, M. B.; Reynolds, J. R. *Macromolecules* **1999**, *32*, 3970-3978.
(9) Yang, Y.; Pei, Q.; Heeger, A. J. *Synth. Met.* **1996**, *78*, 263-267.
(10) Baluschev, S.; Jacob, J.; Avlasevich, Y. S.; Keivanidis, P. E.; Miteva, T.; Yasuda, A.; Nelles, G.; Grimsdale, A. C.; Müllen, K.; Wegner, G. *Chemphyschem* **2005**, *6*, 1250-1253.
(11) Baluschev, S.; Keivanidis, P. E.; Wegner, G.; Jacob, J.; Grimsdale, A. C.; Müllen,

K.; Miteva, T.; Yasuda, A.; Nelles, G. *Appl. Phys. Lett.* **2005**, *86*.

(12) Elsenbaumer, R. L.; Shacklette, L. W. In *Handbook of Conducting Polymers*; Skotheim, T. A. ed.; Dekker: New York, 1986.

(13) Lamba, J. J. S.; Tour, J. M. *J. Am. Chem. Soc.* **1994**, *116*, 11723-11736.

(14) Rehahn, M.; Schluter, A. D.; Wegner, G. *Makromol. Chem. Macromol. Chem. & Phys.* **1990**, *191*, 1991-2003.

(15) Rehahn, M.; Schluter, A. D.; Wegner, G.; Feast, W. J. *Polymer* **1989**, *30*, 1060-1062.

(16) Rehahn, M.; Schluter, A. D.; Wegner, G.; Feast, W. J. *Polymer* **1989**, *30*, 1054-1059.

(17) Scherf, U. *J. Mater. Chem.* **1999**, *9*, 1853-1864.

(18) Chmil, K.; Scherf, U. *Acta Polymerica* **1997**, *48*, 208-211.

(19) Kirstein, S.; Cohen, G.; Davidov, D.; Scherf, U.; Klapper, M.; Chmil, K.; Müllen, K. *Synth. Met.* **1995**, *69*, 415-418.

(20) Neher, D. *Macromol. Rapid Commun.* **2001**, *22*, 1366-1385.

(21) List, E. J. W.; Guentner, R.; de Freitas, P. S.; Scherf, U. *Adv. Mater.* **2002**, *14*, 374-378.

(22) Scherf, U.; List, E. J. W. *Adv. Mater.* **2002**, *14*, 477-487.

(23) Setayesh, S.; Marsitzky, D.; Müllen, K. *Macromolecules* **2000**, *33*, 2016-2020.

(24) Grimsdale, A. C.; Leclere, P.; Lazzaroni, R.; Mackenzie, J. D.; Murphy, C.; Setayesh, S.; Silva, C.; Friend, R. H.; Müllen, K. *Adv. Funct. Mater.* **2002**, *12*, 729-733.

(25) Dams, R.; Malinowski, M.; Westdorp, I.; Geise, H. Y. *J. Org. Chem.* **1982**, *47*, 248-259.

(26) Jacob, J.; Sax, S.; Piok, T.; List, E. J. W.; Grimsdale, A. C.; Müllen, K. *J. Am. Chem. Soc.* **2004**, *126*, 6987-6995.

(27) Zhang, Z. B.; Fujiki, M.; Tang, H. Z.; Motonaga, M.; Torimitsu, K. *Macromolecules* **2002**, *35*, 1988-1990.

(28) Hagberg, E. C.; Olson, D. A.; Sheares, V. V. *Macromolecules* **2004**, *37*, 4748-4754.

(29) Staab, H. A.; Braunlin.H *Tetrahedron Lett.* **1965**, 45-49.

(30) Kim, Y.-H.; Ahn, J.-H.; Sin, D.-C.; Kwon, S.-K. *polymer* **2004**, *45*, 2525-2532.

(31) Cervini, R.; Li, X. C.; Spencer, G. W. C.; Holmes, A. B.; Moratti, S. C.; Friend, R. H. *Synth. Met.* **1997**, *84*, 359-360.

(32) de Leeuw, D. M.; Simenon, M. M. J.; Brown, A. R.; Einerhand, R. E. F. *Synth. Met.* **1997**, *87*, 53-59.

(33) Gamerith, S.; Gaal, M.; Romaner, L.; Nothofer, H. G.; Guntner, R.; de Freitas, P. S.; Scherf, U.; List, E. J. W. *Synth. Met.* **2003**, *139*, 855-858.

(34) Sims, M.; Bradley, D. D. C.; Ariu, M.; Koeberg, M.; Asimakis, A.; Grell, M.;

Lidzey, D. G. *Adv. Funct. Mater.* **2004**, *14*, 765-781.
(35) Gong, X. O.; Iyer, P. K.; Moses, D.; Bazan, G. C.; Heeger, A. J.; Xiao, S. S. *Adv. Funct. Mater.* **2003**, *13*, 325-330.
(36) Gaal, M.; List, E. J. W.; Scherf, U. *Macromolecules* **2003**, *36*, 4236-4237.
(37) Cadby, A. J.; Lane, P. A.; Mellor, H.; Martin, S. J.; Grell, M.; Giebeler, C.; Bradley, D. D. C.; Wohlgenannt, M.; An, C.; Vardeny, Z. V. *Phys. Rev. B* **2000**, *62*, 15604-15609.
(38) List, E. J. W.; Partee, J.; Shinar, J.; Scherf, U.; Müllen, K.; Zojer, E.; Petritsch, K.; Leising, G.; Graupner, W. *Phys. Rev. B* **2000**, *61*, 10807-10814.
(39) Hsu, J. W. P.; Yan, M.; Jedju, T. M.; Rothberg, L. J.; Hsieh, B. R. *Phys. Rev. B* **1994**, *49*, 712-715.
(40) Leng, J. M.; Jeglinski, S.; Wei, X.; Benner, R. E.; Vardeny, Z. V.; Guo, F.; Mazumdar, S. *Phys. Rev. Lett.* **1994**, *72*, 156-159.
(41) Somma, E.; Loppinet, B.; Fytas, G.; Setayesh, S.; Jacob, J.; Grimsdale, A. C.; Müllen, K. *Colloid and Polym. Sci.* **2004**, *282*, 867-873.
(42) Jian, T.; Vlassopoulos, D.; Fytas, G.; Pakula, T.; Brown, W. *Colloid and Poly. Sci.* **1996**, *274*, 1033-1043.
(43) Petekidis, G.; Fytas, G.; Witteler, H. *Colloid and Poly. Sci.* **1994**, *272*, 1457-1465.
(44) Bunz, U. H. F.; Rubin, Y.; Tobe, Y. *Chem. Soc. Rev.* **1999**, *28*, 107-119.
(45) Faust, R. *Angew. Chem., Int. Ed.* **1998**, *37*, 2825-2828.
(46) Haley, M. M.; Pak, J. J.; Brand, S. C. *Top. Curr. Chem.* **1999**, *201*, 81-130.
(47) Hoger, S.; Meckenstock, A. D.; Pellen, H. *J. Org. Chem.* **1997**, *62*, 4556-4557.
(48) Zhang, J. S.; Pesak, D. J.; Ludwick, J. L.; Moore, J. S. *J. Am. Chem. Soc.* **1994**, *116*, 4227-4239.
(49) Mindyuk, O. Y.; Stetzer, M. R.; Heiney, P. A.; Nelson, J. C.; Moore, J. S. *Adv. Mater.* **1998**, *10*, 1363-1366.
(50) Lehn, J. M.; Malthete, J.; Levelut, A. M. *J. Chem. Soc., Chem. Commun.* **1985**, 1794-1796.
(51) Chandrasekhar, S.; Sadashiva, B. K.; Suresh, K. A. *Pramana* **1977**, *9*, 471-480.
(52) van Nostrum, C. F. *Adv. Mater.* **1996**, *8*, 1027-1030.
(53) McGehee, M. D.; Heeger, A. J. *Adv. Mater.* **2000**, *12*, 1655-1668.
(54) Krouse, S. A.; Schrock, R. R. *Macromolecules* **1989**, *22*, 2569-2576.
(55) Staab, H. A.; Neunhoef.K *Synthesis* **1974**, 424-424.
(56) Shetty, A. S.; Zhang, J. S.; Moore, J. S. *J. Am. Chem. Soc.* **1996**, *118*, 1019-1027.
(57) Venkataraman, D.; Lee, S.; Zhang, J. S.; Moore, J. S. *Nature* **1994**, *371*, 591-593.
(58) Zhang, J. S.; Moore, J. S. *J. Am. Chem. Soc.* **1994**, *116*, 2655-2656.

(59) Zhang, J. S.; Moore, J. S. *J. Am. Chem. Soc.* **1992**, *114*, 9701-9702.

(60) Tobe, Y.; Utsumi, N.; Nagano, A.; Naemura, K. *Angew. Chem. Int. Ed.* **1998**, *37*, 1285-1287.

(61) Lahiri, S.; Thompson, J. L.; Moore, J. S. *J. Am. Chem. Soc.* **2000**, *122*, 11315-11319.

(62) Schutte, W. J.; Sluytersrehbach, M.; Sluyters, J. H. *J. Phys. Chem.* **1993**, *97*, 6069-6073.

(63) Kastler, M.; Pisula, W.; Wasserfallen, D.; Pakula, T.; Müllen, K. *J. Am. Chem. Soc.* **2005**, *127*, 4286-4296.

(64) Martin, R. B. *Chem. Rev.* **1996**, *96*, 3043-3064.

(65) Pisula, W.; Tomovic, Z.; Simpson, C.; Kastler, M.; Pakula, T.; Müllen, K. *Chem. Mater.* **2005**, *17*, 4296-4303.

(66) Wu, J. S.; Watson, M. D.; Zhang, L.; Wang, Z. H.; Müllen, K. *J. Am. Chem. Soc.* **2004**, *126*, 177-186.

Chapter 5 Materials with Donor-Acceptor Architectures

5.1 Random Donor-Acceptor Block Copolymers based on Poly(2,7-carbazoles) (PCz) and Perylene tetracarboxydiimide (PDI)

Photoinduced energy and electron transfer between photoactive and electroactive donor (D) and acceptor (A) moieties continues to be an extremely active area of research.[1-5] Numerous photophysical studies of organic D-A molecules have been performed to elucidate and control resonant energy transfer, charge separation, and recombination processes and to assess the role of intermediates in the deactivation of the initially formed excited states. The intriguing photophysical and photochemical processes that take place in the natural photosynthetic reaction center have stimulated efforts to design and create artificial donor-acceptor architectures in an attempt to mimic the conversion of light into chemical energy or to create electrical power directly.

Photoinduced electron transfer between donor and acceptor materials is also the initial step in organic and polymer solar cells. In these cells, excitations created by the absorption of light, must be able to diffuse to the interface between the two materials where charge generation can occur. However, the exciton diffusion length in organic and polymer materials is often limited to about 10 nm. This implies that an

intimate, nanoscopic mixing of donor and acceptor is favorable for charge creation. Following this principle, the bulk-heterojunction cell, in which a spontaneous phase separation of the two components into a disordered blend is used to create a large interface, has become one of the most promising concepts in the field of polymer solar cells which has resulted in external quantum efficiencies of more than 50 % at the absorption maximum.[6-8] A further increase of performance is expected by designing materials that have an improved overlap of their absorption spectrum with the terrestrial solar radiation, especially in the near-infrared region.

A general drawback of the bulk-heterojunction design is the fact that the transport and collection of charges in a disordered nanoscale blend can be hindered by phase boundaries and discontinuities such as spherical objects and cul-de-sacs. Therefore, the extent, the characteristic dimension, and the contours of the phase separation in polymer-polymer or polymer-molecule blends are essential parameters of bulk-heterojunction solar cells. The actual morphology depends, among other factors, on details of the preparation procedure (*e.g.*, solvent, temperature, drying speed, and substrate). The as-prepared morphology is likely to be kinetically determined rather than thermodynamically stable and subject to further reorganization in time or with temperature.

One way to overcome these drawbacks is by covalently linking the donor and acceptor in a single polymer chain. The covalent bond enables a predefined control over the characteristic distance between donor and acceptor and thereby the extent of phase separation. Two types of covalently linked donor-acceptor polymers have recently been reported. The first consists of a semiconducting polymer as a donor with pendant acceptor groups,[9-13] while the second has extended donor and acceptor units

arranged in a diblock copolymer.[14,15] The latter strategy may have important advantages because the intrinsic tendency of each segment in block copolymers to aggregate in an individual phase provides a means to create a well-ordered nanoscale morphology (*e.g.*, spheres, cylinders, lamellae), governed by the relative volume fractions. While this principle has been utilized in engineering various materials to create fascinating architectures, the use of block copolymers in functional, conjugated polymers has received limited attention.[16-20] Both poly(2,7-carbazoles) (PCz)[21-24] and perylene tetracarboxydiimide (PDI)[25-29] chromophores have been utilized in bulk-heterojunction-like solar cell configurations as donor and acceptor materials, but their combination has received little attention.

Herein is presented the synthesis and properties of a new class of donor-acceptor copolymers, represented by **P8** (Chart 5.1), that consist of PCz and PDI blocks connected via saturated spacers. This design concept is aimed at satisfying two requirements for efficient operation as a photovoltaic material: (1) creating an accessible donor-acceptor interface at which dissociation of excitons into separate charge is promoted, thus reducing the probability of decay along other routes, of which luminescence is one; (2) providing separate pathways for transport of holes (via PCz) and electrons (via PDI), thus reducing the recombination probability. The basic photophysics of the block copolymer and photovoltaic behavior upon incorporation into solar cells in combination with PDI have been studied.

Chart 5.1 Structure of poly(2,7-carbazoles) (PCz) and perylene tetracarboxydiimide (PDI) randomly block copolymer (**P8**)

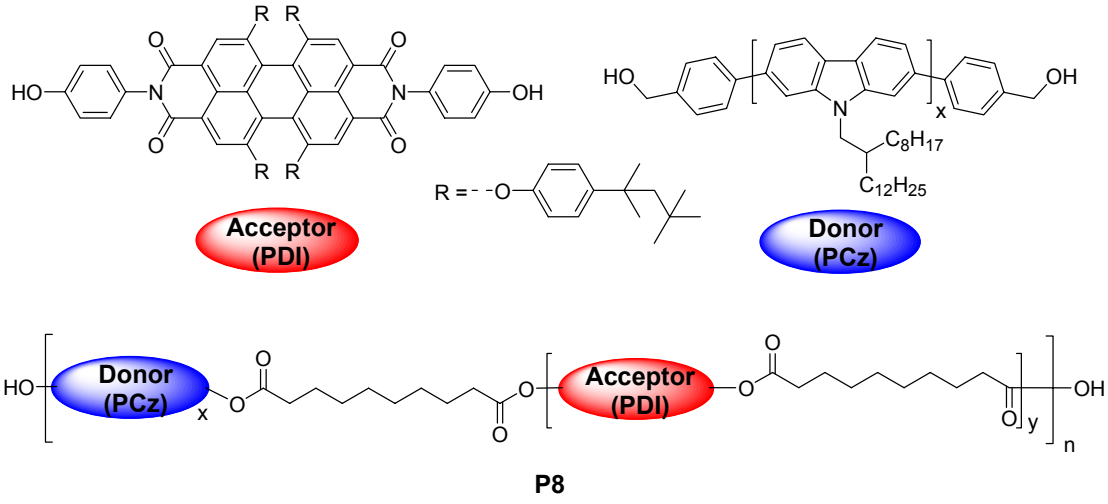

P8

Synthesis and Characterization. The poly-2,7-(carbazole) (PCz)-diol was synthesized by Frank Dierschke starting by an alkylation of 2,7-dibromocarbazole with 2-decyltetradecyl bromide followed by a Yamamoto polymerization carried out in a DMF-toluene mixture by using a Boc protected *p*-bromobenzyl alcohol (0.1 mol/monomer 2,7-dibromo-*N*-(2-decyltetradecyl)carbazole) as an end capper. GPC analysis of the PCz using PPP standards showed a M_n value of 1.55×10^4 g/mol with a polydispersity of 1.7. This correspond to a degree of polymerization of around 31, and ^{1}H-NMR spectroscopy revealed that app. 85 % of all chain ends were bearing an end capper unit. The PCz oligomer possessed excellent solubility in solvents such as dichloromethane, chloroform, and toluene and good film-forming abilities. The Boc protection group was cleaved off by a reduction using an excess of $LiAlH_4$. The removal of the protection group was proven by ^{1}H-NMR and IR spectroscopy.

The monomer dye based on perylene tetracarboxydiimide (PDI) **74** was prepared as shown in Scheme 5.1. Condensation of 1,6,7,12-tetrachloro-perylene tertracarboxylic

acid anhydride with 4-methoxy-phenylamine in refluxing propionic acid gave the diimide **72**, which then underwent nucleophilic substitution of the halides in the bay positions with 4-*tert*-octylphenoxide to produce **73**. A standard reduction using BBr_3 in methylene chloride was performed to give the diol monomer **74** in an overall yield of 29 %. Esterification reactions are commonly assisted by HCl scavenger such as pyridine.

Scheme 5.1. Random poly(2,7-carbazoles) (PCz) and perylene tetracarboxydiimide (PDI) block copolymer (**P8**).

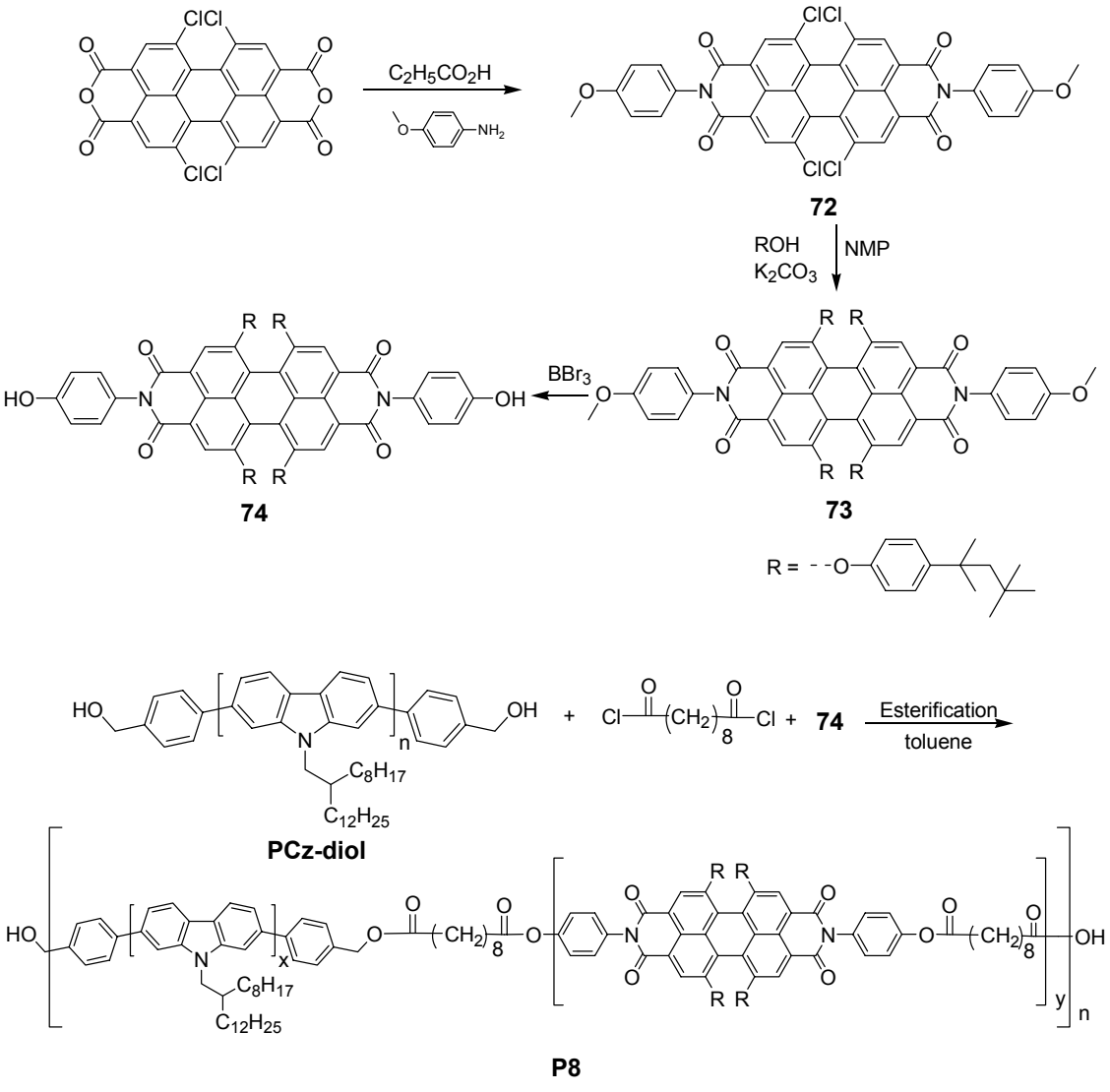

However, the esterification to synthesize the random block copolymer was carried out in efficient yields in the absence of bases. The random block copolyester **P8** (Scheme 5.1) was obtained by the polycondensation of **74**, the PCz-diol (weight ratio PCz : **74**, 1:1) and sebacoyl chloride as a saturated spacer in toluene over 3 days, followed by the addition of an excess of sebacoyl chloride to remove any unreacted terminal alcohol functionality. The copolymer shows excellent solubility in common organic solvents. GPC analysis of this polymer exhibits a M_n value of 1.26×10^4 g/mol and M_w of 3.34×10^4 g/mol with a polydispersity of 2.66 (THF, PPP standards). An inspection of the ^{1}H NMR spectrum of **P8** clearly reveals a new broad peak assigned to the α-protons of the ester at 2.67-2.45 and in addition the OH resonance of **74** at 5.21 ppm is absent, which indicated successful esterification (Figure 5.1). However, the ratio of the structural composition between PCz, PDI and sebacate units can not be determined from the integration of the NMR peaks since the benzyl signals from the end groups of the PCz-diol can not be assigned in the NMR spectrum.

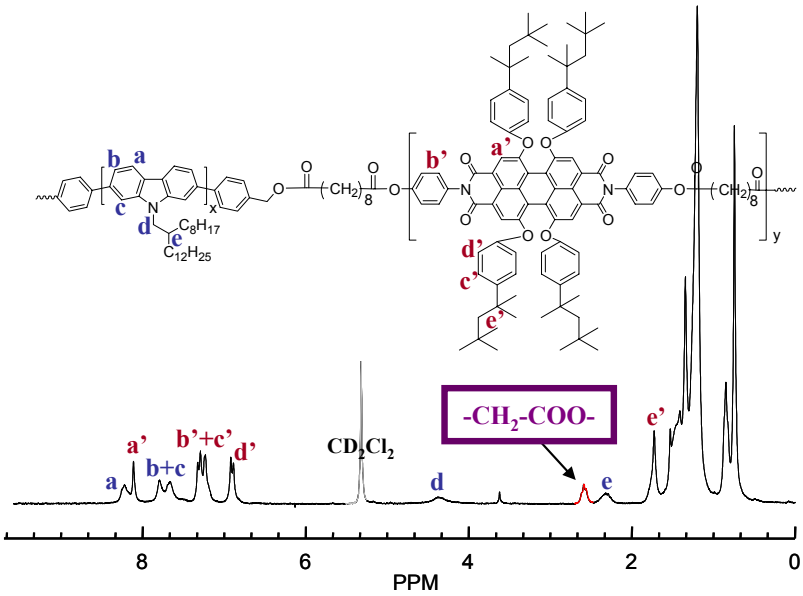

Figure 5.1. ^{1}H NMR spectrum of **P8** recorded at room temperature in dichloromethane-d^2.

Photophysical Properties. The UV-vis and PL properties of the polymer **P8** were investigated in THF solution. As shown in Figure 5.2, **P8** exhibits three dominant absorption bands with 392, 537 and 575 nm. The band at 392 nm can be assigned to the absorption from PCz block, whereas the lower-energy peak is clearly attributed to the PDI block. The PL spectrum of **P8** in solution shows a large blue emission peak (λ_{max} = 420 nm) due to PCz unit and a PDI emission (λ_{max} = 600 nm) when excited at 392 nm. The absorption and PL spectra of **P8** in solution show predominantly absorption and emission from the PCz block. It is postulated that inefficient intramolecular energy transfer to the chromophores in solution occurs so that the emission is predominantly from the PCz backbone, though emission is seen from PDI units.

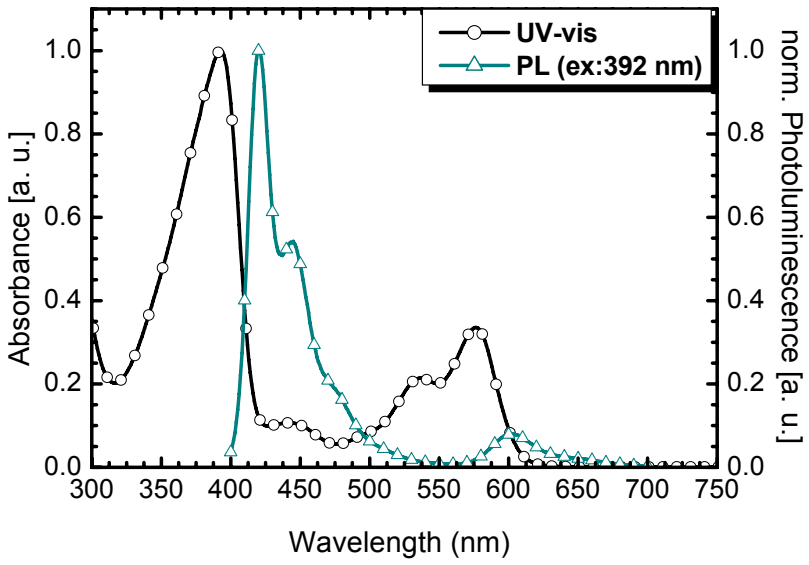

Figure 5.2. UV-vis and PL spectra of polymer **P8** (λ_{exc} = 392 nm) in THF solution.

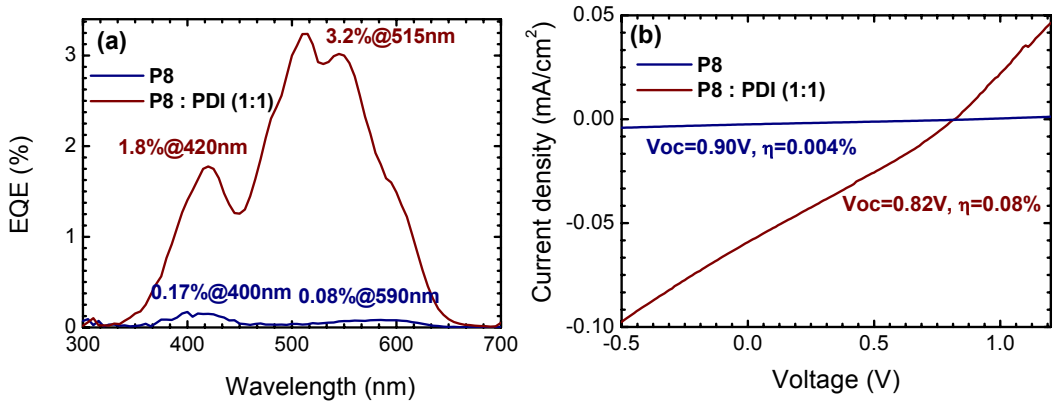

Figure 5.3. EQE-wavelength curves (a) and *I-V* curves (b) under solar light at light intensity of 164 W/m^2 for ITO/**P8** and **P8**:PDI (1:1 wt%).

Photovoltaic Devices. The device fabrication and testing were performed by Jiaoli Li. It has been described[24] when PDI and PCz are blended, a broad absorption between 300 nm and 600 nm coinciding with the strongest emission part of the solar spectrum is achieved, which is highly desirable in a solar cell. In addition, the suitability of the PCz:PDI combination for solar cell applications is confirmed by the position of the molecular orbital energy levels determined from cyclic voltammetry measurements on thin films of PCz and PDI on ITO referenced with Ag/Ag+ and calibrated against ferrocene. From these measurements it has been found that PDI had its HOMO energy level at -5.8 eV, which is below the HOMO level of PCz (-5.6 eV). The corresponding LUMO values are estimated to be -3.8 eV and -2.6 eV calculated from the band-gap found in the absorption spectrum. This indicates that in principle in a solar cell composed of PCz and PDI the 0.2 eV difference in HOMO energies allows for a ready hole transfer from the HOMO level of PDI to the HOMO level of PCz. The 0.8 eV energy difference between the LUMO levels of PCz and PDI means electron migration from PCz to PDI can

also be expected to occur readily.

The photovoltaic devices were prepared to test the performance of **P8** and the **P8**:PDI pair blended with a weight ratio of 1:1 respectively (Figure 5.3). The photovoltaic device data are summarized in Table 5.1. The V_{oc} for **P8** is comparable to or even higher than the V_{oc} of PCz: PDI blends however, the photocurrent (2 μA/cm^2 for **P8**) is much lower than that of PCz:PDI (1:1 wt%) device (70 μA/cm^2), so that the overall efficiency for **P8** is much lower than the devices based on a PCz: PDI blend. Similarly, when the blend (**P8**:PDI, 1:1 wt%) is compared with the device PCz:PDI (1:3 wt%), the short circuit current of the former device (59 μA/cm^2) is much lower than of the latter (300 μA/cm^2). When illuminated with simulated solar light (AM 1.5 Global, light intensity 164 W/m^2), efficiencies of 0.004 % for **P8** and 0.08 % for **P8**:PDI, 1:1 wt% are obtained respectively.

Table 5.1. Photovoltaic device data for **P8** and **P8:**PDI (1:1 wt%)

active layer	I_{sc} (μA/cm^2)	V_{oc} (V)	FF	efficiency (AM 1.5G)	EQE (%)	I_{inc}* (W/m^2)
P8	2	0.90	0.26	0.004	0.08	164
P8:PDI (1:1 wt%)	59	0.82	0.27	0.08	3.2	164

*AM1.5 Global solar light

This result is contrary to the expectations that the inherent tendency of each segment in the block copolymer **P8** to aggregate in an individual phase as a means to achieve a well-ordered morphology. The lower efficiency of devices based on **P8** is understood as

there are no efficient percolation pathways for charge transport. It was observed in the former study on morphology of thin films composed of PCz and PDI that the formation of PDI crystals results in an enhanced photocurrent and charge transport. An increase in domain size of the PDI crystals corresponds to a higher photocurrent. In the copolymer (**P8**), the PDI units bounded with the carbazole blocks lose the mobility for self-organization during the fast spin-coating procedure, thus prohibiting the crystallization and leading to a lower photocurrent. To prove the idea, the devices based on the copolymer (**P8**) and the blend of **P8** and PDI are annealed at 120 °C to facilitate the crystallization of PDI (the phase transition temperature of PDI is 67 °C). The comparison of the devices with and without thermo-treatment is depicted in Figure 5.4. The performance of the blend device is increased by a factor of two after annealing, while the EQE values of the copolymer device remains similar. This indicates that the in the carbazole perylene block polymer the crystallization of PDI is suppressed, and thus charge transport is hampered.

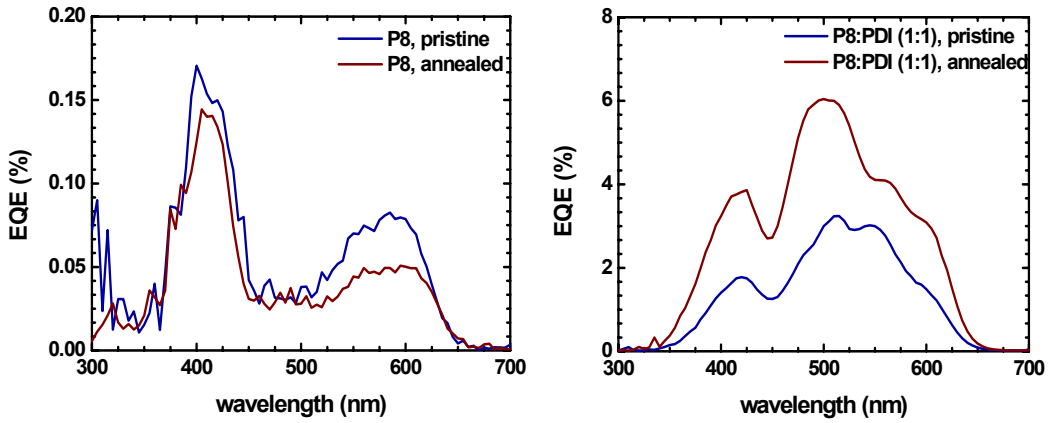

Figure 5.4. Device before and after annealing: (a) **P8**, and (b) **P8**:PDI (1:1 wt%).

Summary. The donor-bridge-acceptor type block copolymer (**P8**) has been synthesized by random condensation of functionalized poly(2,7-carbazoles) (PCz) donor, perylene tetracarboxydiimide (PDI) acceptor and sebacate saturated spacer. **P8** and blend (**P8**: PDI, 1:1 wt%) has been tested in photovoltaic devices. While PDIs as oligomeric acceptors are effective in charge generation, they are less effective in charge transport, due to the tendency of the donor-acceptor domains to organize in a random fashion in the main chain. This is in contrast to the desired morphology involving donor-donor/acceptor-acceptor stacking. In this case, charge generated in solar cell has inefficient pathways to travel to the electrodes, which in part accounts for the observed results. The device results on **P8** can provide an important guideline for design of new block copolymers that could be more effective in polymer photovoltaic cells. To overcome this tendency of donor and acceptor segments to give alternating stacks, stronger antagonistic interactions that direct the microscopic morphology should be introduced. This can be accomplished by introducing anchoring points at the polymer chains (*e.g.*, via interchain hydrogen bonds) that secure the relative positions of donor and acceptor.

5.2 Push-Pull Molecule Based on 2,5-Linked Pyrrole Efficient *n*-Type Material

One of the most challenging goals in semiconducting polymer research has been the synthesis of processable and efficient electron-accepting and transporting (*n*-type) materials. Most organic materials are p-type materials, which accept and transport holes better than electrons, but n-type materials are urgently needed for use in *n*-type transistors, as accepting components in photovoltaic devices, and to increase the efficiency of LEDs by

improving electron injection and transport. Also, small bandgap conjugated materials have attracted much attention in the last few years.[30-36] Such compounds are potentially; (i) intrinsically good electrical conductors or semiconductors without the need of any chemical or electrochemical doping reaction, (ii) transparent in either the neutral or doped state and (iii) of interest as new polymeric materials for nonlinear optics.[37]

Pyrrole based materials are one of the most important classes of conjugated *p*-type materials. Recently, a new push-pull design (polysquaraines and polycroconaines) of small bandgap materials has been initiated by Havinga *et al.,*[38] who proposed bringing together electron-donating and electron-withdrawing groups along a main backbone. According to this concept, one of the most efficient strategies to get *n*-type materials is the introduction of strong electron acceptor groups into the donor backbone, which is also an efficient method to reduce the bandgap and control the HOMO/LUMO levels. In addressing this point, the synthesis and characterization of pyrrole based *n*-type push-pull materials using intramolecular Friedel-Crafts acylation to form ladder-type π-conjugated molecules was explored.

Synthesis and Characterization. The facile synthesis of the target molecule toward the desired bis-carbonyl bridged 1-(4-octyl-phenyl)-2,5-diphenyl-1*H*-pyrrole compound is outlined in Scheme 2. 2,2'-(1,3-Butadiyne-1,4-diyl)bisbenzoic acid dimethyl ester (**77**) was easily prepared in three steps (isolated overall yield = 72 %).[39] The cycloaddition reaction of **77** with *p*-octylphenylamine gave 2,2'-[1-(4-octylphenyl)1-*H*-pyrrole-2,5-diyl]bisbenzoic acid dimethyl ester (**78**) using copper(I) chloride. The corresponding benzoic acid **79** was obtained via hydrolysis by treatment with KOH as strong base (isolated overall yield = 35 %), which is the key intermediate material of the target molecule. **79** was treated with oxalyl chloride and then intramolecular Friedel-Crafts

acylation using aluminium chloride gave the bis-carbonyl bridged 1-(4-octyl-phenyl)-2,5-diphenyl-1*H*-pyrrole **80** (11 %). It has been reported[40] that the method for synthesis of the starting five-membered heterocycle consisting of intramolecular cyclization of 2-hetarylbenzoic acids and their derivatives under various conditions suffer from a number of drawbacks such as low accessibility of these benzoic acids, sometimes unpredictable reaction route,[41] and relatively low yields. The observed low yield for the last step of the synthesis of **80** can be explained by this.

Scheme 5.2. Synthesis of bis-carbonyl bridged 1-(4-octyl-phenyl)-2,5-diphenyl-1*H*-pyrrole.

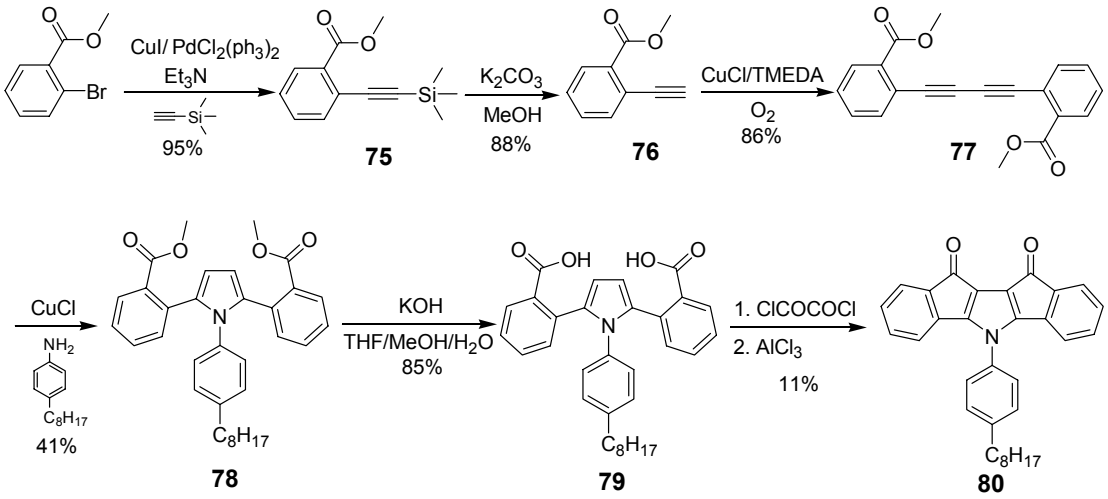

The absorption behavior of **80** was measured in solvents of varying polarity in order to investigate the solvatochromism of these D-A molecules. Two prominent absorption bands along with a shoulder are observed in the spectra of **80** in all solvents: a broad lower intensity band at 500-520 nm range, a higher intensity band at 408-422 nm range, and a shoulder at 429-445 nm range. The high-energy absorption band can be associated with π-π^* transitions of the D-A molecules. As depicted in Figure 5.5a, the absorption

maxima of **80** recorded in various solvents reveal moderate bathochromic shift upon increasing the polarity of solvent from 408 nm in hexane to 422 nm in acetonitrile. This indicates that this molecule possesses unambiguously intramolecular charge transfer from the donor (pyrrole) to the acceptor (ketone) unit.[42-46] It is known that larger solvatochromic shifts are observed in the PL emission spectra compared to those in the absorption spectra because of an excited state with much stronger ICT character and larger dipole moments relative to the ground state.[47,48] However, the PL properties of **80** can not be analyzed in various solvents since the observed PL intensities are too low due to internal quenching units (two ketone).

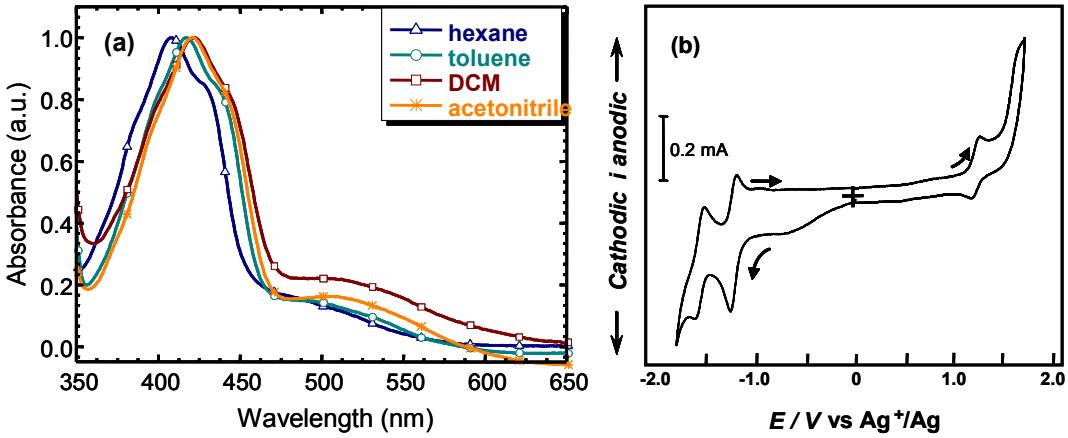

Figure 5.5. UV-vis absorption spectra of **80** in solvents of varying polarity (a) and cyclic voltammogram of **80** in acetonitrile solution (b).

Photophysical Properties. The redox behavior of **80** was investigated by cyclic voltammetry (CV) against Ag/Ag+. As shown in Figure 5.5b, **80** exhibits clear reversibility in both the p-doping and n-doping processes, with two reduction peaks -1.25 and -1.61 V, which can presumably be assigned to the reduction of the diketone to the quinoidal dianion, and an oxidation peak at 1.29 V. The onsets of for reduction and oxidation occurred at -1.15 and 1.18 V, from which the LUMO and HOMO energy levels

were estimated to be 3.25 and 5.58 eV respectively. This corresponds to an electrochemical bandgap of 2.33 eV. The relatively high EA is lower than that of of 2-(4-biphenylyl)-5-(4-*tert*-butylpehnyl)-1,3,4-oxadiazole (PBD) (*ca*. -2.4 eV), one of the most widely used electron injecting/transport materials,[49] and comparable with that of CN-PPV (3.10 eV),[50] which shows good electron transporting ability in polymeric LEDs. Therefore, **80** which shows reversible reduction is a promising electron-transporting material.[51,52] Moreover, the HOMO energy levels of **80** matches well with one of the most widely used hole-transporting materials ((4,4'-bis(4-(*N*-(1-naphthyl)-*N*-phenylamino)phenyl)biphenyl (5.46 eV)).[53] Thus **80** also holds potential as a hole injecting and hole transport material in LEDs.

Summary. The bis-carbonyl bridged 1-(4-octyl-phenyl)-2,5-diphenyl-1*H*-pyrrole compound **80** as push-pull type material was successfully prepared via intramolecular Friedel-Crafts acylation with 2,2'-[1-(4-octylphenyl)1-*H*-pyrrole-2,5-diyl]bisbenzoic acid (**79**). The compound **80** shows good processability from solution. On the redox behaviors, **80** not only shows low-lying LUMO but also displays high-lying HOMO with fully reversible p-and n-doping. Such attractive properties of **80** can establish it as good candidates for use as an electron/hole transporting materials in polymer-based optical and electrooptical applications such as LEDs, FETs, and solar cell devices.

5.3 References

(1) In *Electron Transfer in Chemistry*; Balzani, V., Ed. Weinheim, 2001; Vol. 1-5.
(2) Kavrnos, G. J. In *Fundamentals of Photoinduced Electron Transfer*; Wiley-VCH: Weinheim, 1993.
(3) In *Photoinduced Electron Transfer*; Fox, M. A., Chanon, M., Eds.; Elsevier:

Amsterdam, 1988; Vol. 1-4.
(4) Guldi, D. M. *Chem. Soc. Rev.* **2002**, *31*, 22-36.
(5) Wasielewski, M. R. *Chem. Rev.* **1992**, *92*, 435-461.
(6) Brabec, C. J.; Sariciftci, N. S.; Hummelen, J. C. *Adv. Funct. Mater.* **2001**, *11*, 15-26.
(7) Yu, G.; Gao, J.; Hummelen, J. C.; Wudl, F.; Heeger, A. J. *Science* **1995**, *270*, 1789-1791.
(8) Halls, J. J. M.; Walsh, C. A.; Greenham, N. C.; Marseglia, E. A.; Friend, R. H.; Moratti, S. C.; Holmes, A. B. *Nature* **1995**, *376*, 498-500.
(9) Zhang, F. L.; Svensson, M.; Andersson, M. R.; Maggini, M.; Bucella, S.; Menna, E.; Inganas, O. *Adv. Mater.* **2001**, *13*, 1871-1874.
(10) Zerza, G.; Cravino, A.; Neugebauer, H.; Sariciftci, N. S.; Gomez, R.; Segura, J. L.; Martin, N.; Svensson, M.; Andersson, M. R. *J. Phys. Chem. A* **2001**, *105*, 4172-4176.
(11) Cravino, A.; Zerza, G.; Maggini, M.; Bucella, S.; Svensson, M.; Andersson, M. R.; Neugebauer, H.; Sariciftci, N. S. *Chem. Commun.* **2000**, 2487-2488.
(12) Wang, S.; Yang, J. L.; Li, Y. L.; Lin, H. Z.; Guo, Z. X.; Xiao, S. X.; Shi, Z. Q.; Zhu, D. B.; Woo, H. S.; Carroll, D. L.; Kee, I. S.; Lee, J. H. *Appl. Phys. Lett.* **2002**, *80*, 3847-3849.
(13) Russell, D. M.; Arias, A. C.; Friend, R. H.; Silva, C.; Ego, C.; Grimsdale, A. C.; Müllen, K. *Appl. Phys. Lett.* **2002**, *80*, 2204-2206.
(14) de Boer, B.; Stalmach, U.; van Hutten, P. F.; Melzer, C.; Krasnikov, V. V.; Hadziioannou, G. *Polymer* **2001**, *42*, 9097-9109.
(15) Stalmach, U.; de Boer, B.; Videlot, C.; van Hutten, P. F.; Hadziioannou, G. *J. Am. Chem. Soc.* **2000**, *122*, 5464-5472.
(16) Liu, J. S.; Sheina, E.; Kowalewski, T.; McCullough, R. D. *Angew. Chem., Int. Ed. Engl.* **2002**, *41*, 329-332.
(17) Wang, H. B.; Wang, H. H.; Urban, V. S.; Littrell, K. C.; Thiyagarajan, P.; Yu, L. P. *J. Am. Chem. Soc.* **2000**, *122*, 6855-6861.
(18) Malenfant, P. R. L.; Groenendaal, L.; Frechet, J. M. J. *J. Am. Chem. Soc.* **1998**, *120*, 10990-10991.
(19) Hempenius, M. A.; Langeveld-Voss, B. M. W.; van Haare, J.; Janssen, R. A. J.; Sheiko, S. S.; Spatz, J. P.; Moller, M.; Meijer, E. W. *J. Am. Chem. Soc.* **1998**, *120*, 2798-2804.
(20) Wang, H. B.; Ng, M. K.; Wang, L. M.; Yu, L. P.; Lin, B. H.; Meron, M.; Xiao, Y. N. *Chem. Eur. J.* **2002**, *8*, 3246-3253.
(21) Zotti, G.; Schiavon, G.; Zecchin, S.; Morin, J. F.; Leclerc, M. *Macromolecules* **2002**,

35, 2122-2128.

(22) Morin, J. F.; Beaupre, S.; Leclerc, M.; Levesque, I.; D'Iorio, M. *Appl. Phys. Lett.* **2002**, *80*, 341-343.

(23) Morin, J. F.; Leclerc, M. *Macromolecules* **2001**, *34*, 4680-4682.

(24) Li, J. L.; Dierschke, F.; Wu, J. S.; Grimsdale, A. C.; Müllen, K. *J. Mater. Chem.* **2006**, *16*, 96-100.

(25) Schmidt-Mende, L.; Fechtenkotter, A.; Müllen, K.; Moons, E.; Friend, R. H.; MacKenzie, J. D. *Science* **2001**, *293*, 1119-1122.

(26) Dittmer, J. J.; Marseglia, E. A.; Friend, R. H. *Adv. Mater.* **2000**, *12*, 1270-1274.

(27) Dittmer, J. J.; Petritsch, K.; Marseglia, E. A.; Friend, R. H.; Rost, H.; Holmes, A. B. *Synth. Met.* **1999**, *102*, 879-880.

(28) Angadi, M. A.; Gosztola, D.; Wasielewski, M. R. *J. Appl. Phys.* **1998**, *83*, 6187-6189.

(29) Halls, J. J. M.; Friend, R. H. *Synth. Met.* **1997**, *85*, 1307-1308.

(30) Karpfen, A.; Kertesz, M. *J. Phys. Chem.* **1991**, *95*, 7680-7681.

(31) Bredas, J. L.; Heeger, A. J.; Wudl, F. *J. Chem. Phys.* **1986**, *85*, 4673-4678.

(32) Wudl, F.; Kobayashi, M.; Heeger, A. J. *J. Org. Chem.* **1984**, *49*, 3382-3384.

(33) Hong, S. Y.; Kertesz, M.; Lee, Y. S.; Kim, O. K. *Chem. Mater.* **1992**, *4*, 378-383.

(34) Lorcy, D.; Cava, M. P. *Adv. Mater.* **1992**, *4*, 562-564.

(35) Hanack, M.; Hieber, G.; Dewald, G.; Ritter, H. *Synth. Met.* **1991**, *41*, 507-511.

(36) Hanack, M.; Dewald, G. *Synth. Met.* **1989**, *33*, 409-414.

(37) Agrawal, G. P.; Cojan, C.; Flytzanis, C. *Phy. Rev. B* **1978**, *17*, 776-789.

(38) Havinga, E. E.; Tenhoeve, W.; Wynberg, H. *Polym. Bull.* **1992**, *29*, 119-126.

(39) Acheson, R. M.; Lee, G. C. M. *J. Chem. Research (S)* **1986**, 380-380.

(40) Kashulin, I. A.; Nifant'ev, I. E. *J. Org. Chem.* **2004**, *69*, 5476-5479.

(41) Gattermann, L. *Liebigs Ann. Chem.* **1912**, *393*, 215-233.

(42) Zhang, F. L.; Perzon, E.; Wang, X. J.; Mammo, W.; Andersson, M. R.; Inganas, O. *Adv. Funct. Mater.* **2005**, *15*, 745-750.

(43) Winder, C.; Sariciftci, N. S. *J. Mater. Chem.* **2004**, *14*, 1077-1086.

(44) Brabec, C. J.; Winder, C.; Sariciftci, N. S.; Hummelen, J. C.; Dhanabalan, A.; van Hal, P. A.; Janssen, R. A. J. *Adv. Funct. Mater.* **2002**, *12*, 709-712.

(45) Vangeneugden, D. L.; Vanderzande, D. J. M.; Salbeck, J.; van Hal, P. A.; Janssen, R. A. J.; Hummelen, J. C.; Brabec, C. J.; Shaheen, S. E.; Sariciftci, N. S. *J. Phys. Chem. B* **2001**, *105*, 11106-11113.

(46) Roncali, J. *Chem. Rev.* **1997**, *97*, 173-205.

(47) Jenekhe, S. A.; Lu, L. D.; Alam, M. M. *Macromolecules* **2001**, *34*, 7315-7324.

(48) Herbich, J.; Kapturkiewicz, A.; Nowacki, J.; Golinski, J.; Dabrowski, Z. *Phys. Chem. Chem. Phys.* **2001**, *3*, 2438-2449.

(49) Yu, W. L.; Meng, H.; Pei, J.; Huang, W. *J. Am. Chem. Soc.* **1998**, *120*, 11808-11809.

(50) Greenham, N. C.; Moratti, S. C.; Bradley, D. D. C.; Friend, R. H.; Holmes, A. B. *Nature* **1993**, *365*, 628.

(51) Zhan, X. W.; Wang, S.; Liu, Y. Q.; Wu, X.; Zhu, D. B. *Chem. Mater.* **2003**, *15*, 1963-1969.

(52) Tonzola, C. J.; Alam, M. M.; Jenekhe, S. A. *Adv. Mater.* **2002**, *14*, 1086-1090.

(53) Yu, G.; Yin, S. W.; Liu, Y. Q.; Shuai, Z. G.; Zhu, D. B. *J. Am. Chem. Soc.* **2003**, *125*, 14816-14824.

Chapter 6 Summary and Outlook

The topic of this work was the synthesis, characterisation and investigation of conjugated semiconducting organic materials for electronic applications.

1) Due to the relatively young nature of the field of highly conducting metallopolymers the potential of such systems remains largely unexploited. In addressing this issue, synthesis of bisthiazol-2-yl-amine (**BTA**) based polymers was attempted and their metallation was investigated. **BTA** molecules can form a tetrahedral complex with Cu(II) comprising one copper and two **BTA** units while a Pd(II) complex displays a square-planar geometry with a 1:1 ratio of Pd to **BTA**. However, the conductivity measurements on **BTA**-based polymers (**P1**, **P2** and **P3**) as well as the metallated copolymer (**P4**) after oxidative iodine doping show only semiconductor behavior. Even though these conductivity values are lower than anticipated, these studies provide a basis for understanding the photophysical properties of metal-organic polymers based on **BTA**.

2) Light-emitting conjugated polyphenylenes and polyphenyleneethynylenes have been synthesized, which comprise 9,10-linked anthracene repeat units with branched alkyl side-chains (2-octyldecyl) at the 2,6-positions linked by *p*-terphenyl (**P5**), *p*-diethynylbenzene (**P6**), and diphenylacetylene (**P7**) units. Both Sonogashira-Hagihara and Suzuki-Miyaura-type cross coupling reactions under palladium catalysis were used as polycondensation methods. The branched alkyl side chains not only improve the

solubility of the resulting copolymers but also prevent stacking in the solid state as evident from their almost identical PL spectra in solution and film. The copolymers **P5** and **P7** display pure blue emission while **P6** exhibits green emission due to the more extended π-system along the polymer backbone. All polymers possess high thermal stability and **P5** shows the best solubility and film forming ability among the three copolymers investigated. Furthermore, the enhanced color stability of this material is demonstrated by the almost identical PL spectra obtained on annealing at 200 °C. The unoptimized OLEDs exhibit deep blue electroluminescence, though the efficiency of unoptimized devices was below 0.1 cd/A and the device stability was only in the range of minutes for the best devices.

In related work, the step-ladder and ladder poly(*p*-phenylene-*alt*-anthrylene)s (**SLPPPA** and **LPPPA** respectively) containing 9,10-anthrylene building groups within the main chain was synthesized and characterized. The polyketone ladder polymer precursors were prepared by palladium catalyzed Suzuki-type cross-coupling. The solution optical spectra of **SLPPPA** and **LPPPA** exhibit broad absorption bands with large Stokes shifts unusual for ladder-type polymers, which are usually very rigid. **SLPPPA** shows an intense yellow emission with a maximum at 584 nm while **LPPPA** is more red-shifted in emission with a maximum at 693 nm due to the planarization of the aromatic repeat units. Additionally, the methylene bridged 1,4-di(10-phenylanthracen-9-yl)benzene **LMC** and the bis-methylene bridged 9,10-diphenylanthracene **SLMC** are also synthesized; they serve as ladder and step-ladder model compounds respectively. The step-ladder derivatives (**SLMC** and **SLPPPA**) are found to form endoperoxides in the presence of visible light in a thermally reversible process whereas the ladder derivatives (**LMC** and **LPPPA**) undergo irreversible photooxidation.

3) A series of soluble poly-2,7- and 3,6-phenanthrylenes was synthesized. This enabled us to do a systematic investigation into the optical and electronic properties of PPP-like versus PPV-like. In the case of the 9,10-dialkyl substituted poly-2,7- and 3,6-phenanthrylenes, spectroscopic characterization suggests that polymer aggregation occurs in the solid state, which can be efficiently suppressed by the introduction of aryl substituents to result in a narrow blue emission. The 2,7- or 3,6-coupling of the phenanthrenes has a strong influence on the emission properties of the polymers. The PPP analogues (**2,7-PKP** and **2,7-PAP**) show less vibronic coupling in emission due to the rigid-rod nature of the polymer as compared to the PPV analogue. In the solid state, the PPV analogues (**3,6-PKP** and **3,6-LPAP**) show a more pronounced red-shift of the emission, which is assigned to the solid-state packing of the polymers. The polymers display deep blue electroluminescence and good color stability when tested in a polymer light emitting device. The formation of long wavelength emission bands, typically attributed to keto defects, was not observed.

The self-organization of a macrocyclic trimer (**MCT**) and acyclic 3,6-linked trisphenanthrylene (**3,6-MT**) with different conformational flexibilities has been investigated by 2D wide-angle X-ray scattering experiments performed on extruded filaments in solution and in the bulk. The 2D-WAXS shows reflections at identical positions suggesting a quite similar organization for both materials **MCT** and **3,6-MT** but **3,6-MT** forms less organized columnar superstructures, because of back-folding of the molecule into a ring-like structure. **MCT** is more planar and self-assembled into a well defined columnar superstructure comparable to that of cyclohexa-*meta*-phenylene (**CHP**). The flexible **CHP** ring showed a poor macroscopic ordering and a low isotropization temperature, whereas the more planar **MCT** self-assembled into well defined columnar

superstructures. The larger π-stacking area and the more pronounced intermolecular interactions for **MCT** led to the formation of a mesophase which spanned over a very large temperature range. The surprising columnar organization of the non-closed **3,6-MT** system was explained by a back-folding of the molecule into a ring-like structure.

The progress in investigation of polymeric materials containing anthrylene and phenanthrylene units for electronic applications has been studied here. The scientific background and results are reflected in systematic and logical approaches for the development of new materials for LEDs. One of the most important goals of research on organic materials for electronic applications is the obtaining of blue emission, which can be achieved by the anthrylene and phenanthrylene based polymers. The next most promising application for electroluminescent polymers is general illumination, where high efficiency, stability and the low cost are the major criteria. The efficiency and durability of the devices based on anthrylene and phenanthrylene still can and need to be further improved with respect to high-end applications, if the progress of this work continues then superior polymeric materials for PLEDs can be produced. From the above studies, it has been shown that 9,10-diaryl substitution in polyphenanthrylenes suppress aggregation in the solid state and thereby eliminate undesirable long wavelength emission. However, their emissions are blue-violet in color (emission maxima λ_{max} = 405-430), so poly(5,5,12,13-tetraaryl-dibenzo*[a,h]*anthracen-3,6-diyl) (see below) not only can display a purer blue emission (*ca*. λ_{max} = 445-455 nm) but also produce better desirable properties for PLEDs compared to those of the polyphenanthrylenes. Moreover, upon copolymerizing this with anthrylene units, the resulting polymer can completely avoid the detrimental aggregate formation in solid state and give very high emission efficiency since the 9,10-disubsittued anthracene derivatives are some of the strongest fluorophores

known.

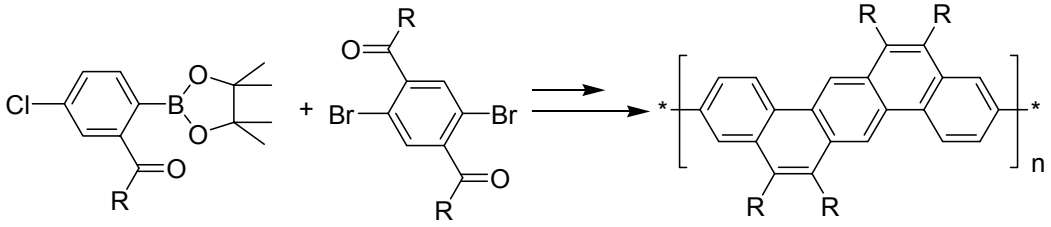

4) From the concept that donor-acceptor diblock copolymer can induce efficient electron transfer, the covalent incorporation of PDI into one block of a poly(2,7-carbazole) (PCz)-based diblock copolymer was achieved. However, copolymer (**P8**) was found not to be an effective material for solar cells, which can be attributed to the formation of an undesirable organization of the donor-acceptor blocks. In order to improve the donor-acceptor morphology, a well defined diblock copolymer is proposed as a promising candidate for future work. (see below). A 2,5-pyrrole based on push-pull type material (**80**) was synthesized, which possessed low-lying LUMO energy and high-lying highest occupied molecular orbital (HOMO) with fully reversible p-and n-doping respectively. This work clearly shows that the incorporation in the molecular main chain of electron-donating and electron-withdrawing groups can play an important role in decreasing the bandgap.

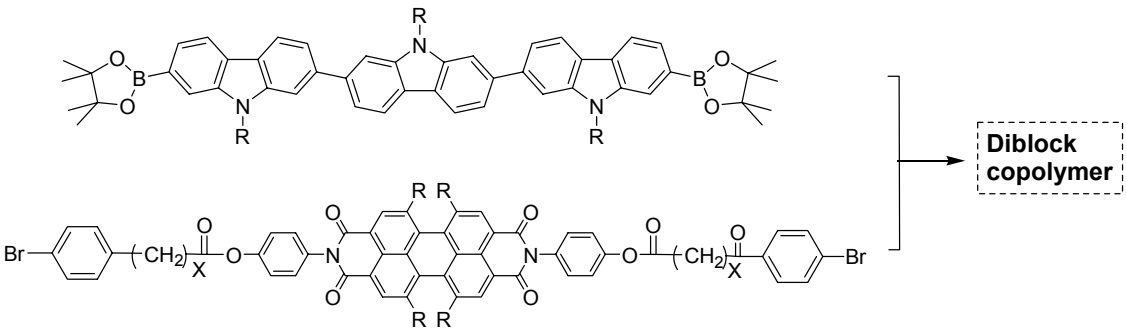

Chapter 7 Experimental Section

7.1 Apparatus for Analysis

^{1}H-NMR and ^{13}C-NMR Spectroscopy

Bruker DPX 250

Brucker AMX 300

Brucker DRX 500

Mass Spectroscopy

FD:VG ZAB 2 SE-FPD (Range: 110-3300)

MALDI – TOF : Brucker Reflex II ; Matrix : 1,8,9-Anthracentriol

Solvents : THF, DCM

UV-vis Spectroscopy

Perkin Elmer Lambda 9

Perkin Elmer Lambda 15

Analytic Gel Permeation Chromatography (GPC)

THF : PSS –GPC: SDV-Gel 10µ (10^{3},10^{5},10^{6} A^{O}) SOMA UV-Detector PL Gel 10µ (10^{4},10^{5} A^{O}), RI – Detector. Calibration with PS or PPP Standards.

Cyclic Voltammetry (CV)

EG&G PARC model 270/250 potensiostat/ Galvanostat

Thermogravimetry (TGA)

Mettler 500 Thermogravimetry Analyzer

Differential Scanning Calorimetry (DSC)

Mettler DSC 30

Elemental Analysis (performed at University of Mainz)

C, H ,N, S : Heraeus Vario EL

7.2 General Procedures

7.2.1 EL Devices

The ITO covered glass substrates for the OLEDs were thoroughly cleaned in a variety of organic solvents and exposed to an oxygen plasma dry cleaning step. PEDOT:PSS (Baytron P from Bayer Inc.) layers were spin-coating under ambient conditions and dried according to specifications by Bayer Inc. under inert atmosphere. The emissive polymer films were spin-cast from solution and dried at 80°C overnight in vacuum. Metal

electrodes were thermally deposited in a vacuum coating mounted in a glove box at a base pressure of below 2 x 10^{-6} mbar.

EL spectra were recorded using an ORIEL spectrometer with an attached CCD camera. The current/luminance/voltage (ILV) characteristics were recorded in a customized setup using a Keithley 236 source measure unit for recording the current/voltage characteristics while recording the luminance using a calibrated photodiode attached to an integrating sphere (Ulbrich).

7.3 Synthetic Procedures

Di-thiophen-2-yl-carbamic acid ethyl ester (5a), Di-thiophen-2-yl-carbamic acid *tert*-butyl ester (5b) and Di-thiophen-2-yl-carbamic acid dodecyl ester (5c)

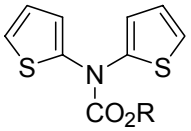

5a R = C_2H_5
5b R = *t*-Bu
5c R = $C_{12}H_{25}$

Copper iodide (4.92 g, 25.8 mmol), K_3PO_4 (21.93 g, 103 mmol) and ethylcarbamate (2.30 g, 25.8 mmol) were nicely powdered in a crucible and then transferred to a 100 mL Schlenk flask. To this, 50 mL of anhydrous dioxane and 3.10 mL of 1,2-diaminocyclohexane were added followed by 2-bromothiophene (5.0 mL, 51.6 mmol). The flask was purged with argon for twenty minutes with stirring and then heated at 100 ˚C for 48 hours under argon. The crude was first filtered through silica using a frit, washed several times with dichloromethane and the combined washings were concentrated. This was then loaded on silica and chromatographed using 0-2 % ethyl acetate in hexane as eluent. Isolated yield of **5a** = 2.20 g as a colorless solid (34 %). ^{1}H NMR: δ 7.07 (d, *J* = 5.4 Hz, 2H) 6.86 (dd, *J* = 5.4, 3.8 Hz) 6.68 (s, br, 2H) 4.24 (q, *J* = 7.3 Hz, 2H) 1.24 (t, *J* = 7.3 Hz, 3H) ppm. FDMS: m/z 253.30. Similar procedure for **5a** and starting with 31 mmol of 2-bromothiophene, the product Di-thiophen-2-yl-carbamic acid *tert*-butyl ester, **5b** was isolated in 35 % yield as a white solid. ^{1}H NMR: δ 7.05 (d, *J* = 5.4 Hz, 2H) 6.84 (dd, *J* = 5.3, 3.8 Hz) 6.63 (s, br, 2H) 1.45 (s, 9H) ppm. Elemental Analysis: Calculated for $C_{13}H_{15}NO_2S_2$: C, 55.49; H, 5.37; N, 4.98; S, 22.79; Found C, 55.64; H, 5.36; N, 4.89; S, 22.60. In the case of Di-thiophen-2-yl-carbamic acid dodecyl ester, **5c** the product was isolated as a colorless solid in 30 % isolated yield. ^{1}H NMR: δ 7.12 (d, *J* = 5.4 Hz, 2H) 6.89 (dd, *J* = 5.4, 3.8 Hz), 6.70 (s, br, 2H) 4.16 (t, *J* = 6.6 Hz) 1.54 (m, 2H) 1.29-1.21 (m, 18H) 0.88 (t, *J* = 7.0 Hz, 3H) ppm. FDMS (m/z) : 393.50 ($M^{+\bullet}$).

Di-(5-bromo-thiophen-2-yl)-carbamic acid *tert*-butylester (6b)

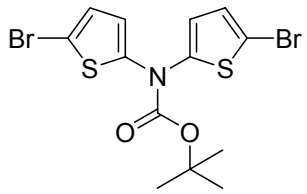

Di-thiophen-2-yl-carbamic acid *tert*-butyl ester, **5b** (0.70 g, 2.49 mmol) was dissolved in 75 mL of chloroform and purged with argon for 15 minutes. Then, N-bromosuccinimide (887 mg, 5.00 mmol) was added and stirred at room temperature for 3 hours. The crude was then concentrated and chromatographed on silica using 0-3 % ethylacetate in hexane as eluent. Isolated yield of **6b** = 0.97 g (89 %) as a colorless solid. FDMS (m/z) : 439.50 ($M^{+\bullet}$).^{1}H NMR: δ 6.83 (d, *J* = 4.1 Hz, 2H) 6.36 (s, br, 2H) 1.45 (s, 9H) ppm. Similar procedure for the synthesis of di-(5-bromo-thiophen-2-yl)-carbamic acid ethyl ester, **6a** 88 % isolated yield. FDMS: m/z = 411.20. ^{1}H NMR: δ 6.84 (d, *J* = 4.1 Hz, 2H) 6.40 (s, br, 2H) 4.25 (q, *J* = 7.0 Hz, 2H) 1.25 (t, *J* = 7.0 Hz, 3H) ppm. For Bis-(5-bromo-thiophen-2-yl)-carbamic acid dodecyl ester, **6c** isolated yield = 83 % FDMS (m/z) : 551.30 ($M^{+\bullet}$). ^{1}H NMR: δ 6.89 (d, *J* = 4.1 Hz, 2H) 6.44 (s, br, 2H) 4.19 (t, *J* = 6.7 Hz, 2H) 1.60 (m, 2H) 1.35-1.24 (m, 18H) 0.89 (t, *J* = 6.3 Hz, 3H) ppm.

Synthesis of Bis-thiazol-2-yl-carbamic acid *tert*-butyl ester (8)

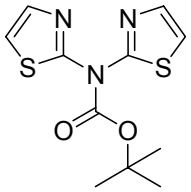

To a solution of **7** (4.0 g, 21.8 mmol) in 88 mL of THF was added di-*tert*-butyl dicarbonate (5 g, 21.8 mmol, 1.0 equivalent) under argon and cooled to 0 ˚C and then a solution of a potassium hydroxide (2.04 g, 36.3 mmol) in 40 mL of water was added and vigorously stirred for 24 hours at room temperature. The product was extracted into dichloromethane, washed twice with brine, dried, and then the crude product was chromatographed on silica gel eluted with 0-20% ethylacetate in hexane. Isolated yield = 52 % as a white solid. ^{1}H NMR ($CDCl_3$, 300 MHz): δ 7.52 (d, *J* = 3.70 Hz, 1H), 7.22 (d, *J* = 5.35 Hz, 1H), 6.92 (d, *J* = 3.70 Hz, 1H), 6.22 (d, *J* = 5.35 Hz, 1H), 1.56 (m, 9H). ^{13}C NMR ($CDCl_3$, 75.46 MHz): δ 170.05, 156.53, 147.14, 138.59, 122.58, 114.48, 104.71, 85.03, 27.51. FDMS (m/z) : 283.20 ($M^{+\bullet}$). Elemental analysis: Calculated for $C_{11}H_{13}N_3O_2S_2$: C, 46.62; H, 4.62; N, 14.83; O, 11.29; S, 22.63; Found: C, 46.65; H, 4.54; N, 15.08; S, 22.71.

Synthesis of Bis-(5-bromo-thiazol-2-yl)-carbamic acid *tert*-butyl ester (9)

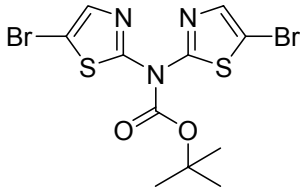

A mixture of (3.24 g, 11.4mmol) of **8**, N-bromosuccinimide (4.05 g, 22.8 mmol, 2.0 equiv.), and chloroform (60 mL) was stirred at room temperature for 48 hours under argon. The solvent was removed under reduced pressure. The crude product was chromatographed on silica gel eluted with 0-5 % ethylacetate in hexane. Isolated yield = 20 % as a light yellow solid. ^{1}H NMR ($CDCl_3$, 300 MHz): δ 7.47 (s, 1H), 7.32 (s, 1H), 1.62 (m, 9H). ^{13}C NMR ($CDCl_3$, 75.46 MHz): δ 169.86, 155.98, 146.31, 139.64, 122.86, 104.05, 95.62, 86.14, 27.73. FDMS (m/z) : 438.80 ($M^{+\bullet}$). Elemental analysis: Calculated for $C_{11}H_{11}Br_2N_3O_2S_2$: C, 29.95; H, 2.51; Br, 36.22; N, 9.52; O, 7.25; S, 14.54; Found: C, 29.96; H, 2.56; N, 9.57; S, 14.54.

Poly(5,5'-bisthiazol-2-yl-amine) (P1)

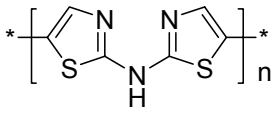

Bis(cyclooctadiene)nickel (1.197 g, 4.34 mmol, 2.4 equiv.), cyclooctadiene (530 mL, 4.34 mmol, 2.4 equiv.), and 2,2'-bipyridine (680 mg, 4.34 mmol, 2.4 equiv.) were dissolved in anhydrous toluene (5 mL) and anhydrous N,N-dimethylformamide (5 mL) in a Schlenk flask in a glovebox. The mixture was heated at 60 ˚C with stirring under argon for 20 min to generate the catalyst, and then a solution of the dibromide **9** (800 mg, 1.81 mmol) in anhydrous toluene (7 mL) was added. The reaction was heated at 75 ˚C for 2 days. Then a mixture of toluene (4 mL) and bromobenzene (0.10 mL) was added and the mixture was heated at 75 ˚C for an additional 12 h. The mixture was then poured into a mixture of methanol and concentrated NH_4OH (1:1, 300 mL) and stirred for 24 h and filtered. The precipitated solid was washed with methanol (200 mL). The resulting solid was filtered off and subjected to Soxhlet extraction for 24 hours in acetone. Isolated yield of **P1** = 215 mg (65 %) as a red solid.

(2-Hexyl-decyl)-bis-thiazol-2-yl-amine (10)

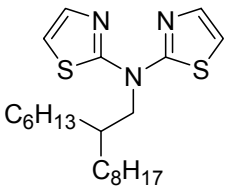

To a solution of **7** (1.0 g, 5.46 mmol) in 20 mL of N,N-dimethylformamide was added K_2CO_3 (1.13 g, 8.17 mmol, 1.5 equiv.) and 7-bromomethyl-pentadecane (2.0 g, 6.54 mmol, 1.2 equiv.) and refluxed at 120 ˚C overnight. The cooled mixture was extracted with diethyl ether, washed with brine and then dried over $MgSO_4$. The crude product was chromatographed on silica using 0-10 % ethylacetate in hexane as eluent. Isolated yield = 0.75 g (34 %) as a yellow liquid. ^{1}H NMR ($CDCl_3$, 300 MHz): δ 7.44 (d, *J* = 3.60 Hz, 2H), 6.85 (d, *J* = 3.60 Hz, 2H), 4.27 (d, *J* = 7.59 Hz, 2H), 2.22-2.10 (m, 1H), 1.31-1.20 (m, 24H), 0.87 (t, *J* = 6.82 Hz, 6H). ^{13}C NMR ($CDCl_3$, 75.46 MHz): δ 163.61, 137.76, 110.96, 56.55, 35.63, 31.63, 31.23, 29.69, 29.36, 29.04, 26.14, 22.42, 13.87. FDMS (m/z) = 407.70 ($M^{+\bullet}$). Elemental analysis: Calculated for $C_{22}H_{37}N_3S_2$: C, 64.81; H, 9.15; N, 10.31; S, 15.73; Found: C, 65.18; H, 9.29; N, 9.74; S, 14.98.

Bis-(5-bromo-thiazol-2-yl)-(2-hexyl-decyl)-amine (11)

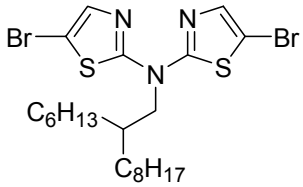

A mixture of **10** (0.637 g, 1.56 mmol) *N*-bromosuccinimide (0.596, 3.354 mmol, 2.15 equiv.) and chloroform (15 mL) was stirred at room temperature for 24 hours under argon. The mixture was then extracted into ether, washed with brine and dried. The crude product was chromatographed on silica using 0-10 % ethylacetate in hexane as eluent. Isolated yield = 0.58 g (65 %) as a yellow oil. ^{1}H NMR ($CDCl_3$, 300 MHz): δ 7.32 (s, 2H), 4.11 (d, *J* = 7.65 Hz, 2H), 2.20-2.11 (m, 1H), 1.32-1.21 (m, 24H), 0.90 (t, *J* = 6.7 Hz, 6H). ^{13}C NMR ($CDCl_3$, 75.46 MHz): δ 162.25, 138.20, 100.16, 55.49, 35.40, 31.43, 30.97, 29.44, 29.02, 28.83, 25.89, 22.23, 13.68. FDMS (m/z) : 565.10 ($M^{+\bullet}$). Elemental analysis: Calculated for $C_{22}H_{35}Br_2N_3S_2$: C, 46.73; H, 6.24; Br, 28.26; N, 7.43; S, 11.34; Found: C, 47.87; H, 6.31; N, 7.41; S, 10.94.

Poly(5,5'-(2-hexyl-decyl)-bis-thiazol-2-yl-amine) (P2)

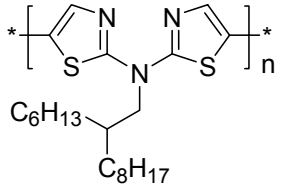

Bis(cyclooctadiene)nickel (589.0 mg, 2.17 mmol, 2.4 equiv.), cyclooctadiene (266.0 mL, 2.17 mmol, 2.4 equiv.), and 2,2'-bipyridine (335 mg, 2.17 mmol, 2.4 equiv.) were dissolved in anhydrous toluene (7 mL) and anhydrous N,N-dimethylformaide (7 mL) in a

Schlenk flask in a glovebox. The mixture was heated at 60 ˚C with stirring under argon for 20 min to generate the catalyst, and then a solution of the dibromide **11** (512 mg, 0.905 mmol) in anhydrous toluene (10 mL) was added. The reaction was heated 75 ˚C for 3 days. Then a mixture of toluene (4 mL) and bromobenzene (0.10 mL) was added and the mixture was heated at 75 ˚C for an additional 12 h. This was then poured into a mixture of methanol and concentrated NH_4OH (1:1, 300 mL) and stirred for 4 h and filtered. The precipitated solid was washed with methanol (200 mL) and subjected Soxhlet extraction for 2 days in acetone. Isolated yield of **P2** = 230 mg (63 %). GPC analysis M_n = 2.38 × 10^3 g/mol, M_w = 4.40 × 10^3 g/mol, and D = 1.85 (against PPP standard); M_n = 2.71 × 10^3 g/mol, M_w = 6.02 × 10^3 g/mol, and D = 2.22 (against PS standard). Only soluble portion was measured by GPC. Elemental analysis: Calculated for $C_{22}H_{35}N_3S_2$: C, 65.14; H, 8.70; N, 10.36; S, 15.81; Found: , 66.05; H, 7.99; N, 9.94; S, 14.48.

Cu(II) complex of BTA (12)

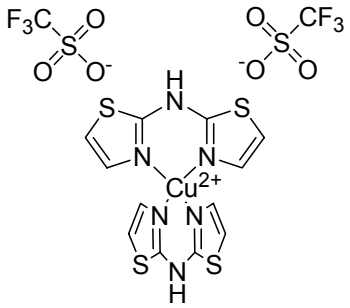

To a solution of **7** (0.5 g, 2.7 mmol) in THF (30 ml) was added copper(II) triflate (1.0 equivalent) solution in THF (30 ml), and stirred for 15 hours at room temperature. Precipitated product was filtered, washed with THF and dried. Isolated yield = 20.1 % as a purple solid. The product was dissolved in N,N-dimethylformamide, and diethyl ether was diffused into the solution, forming a mixture of purple crystals precipitate.

Pd(II) complex of BTA (13)

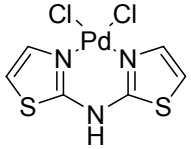

To a solution of **7** (0.5 g, 2.7 mmol) in THF (30 ml) was added dichlorobis(benzonitrile)palladium(II) (1.0 equivalent) solution in THF (30 ml), and stirred for 15 hours at room temperature. Precipitated product was filtered, washed with

THF and dried. Isolated yield = 0.84 g (85.1 %) as an orange solid. The product was dissolved in N,N-dimethylformamide, and diethyl ether was diffused into the solution, forming a mixture of orange crystals precipitate.

Octyl-bis-thiazol-2-yl-amine

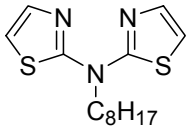

To a mixture solution of **7** (4.0 g, 21.85 mmol) and NaH (60 % in oil, 1.2 equiv) in 25 mL of N,N-dimethylformamide at room temperature was added 1-octylbromide (1.2 equiv) dropwise under argon. This solution was stirred at room temperature for 12 hours. The mixture was then extracted into ether, washed with brine and dried. The crude product was chromatographed on silica gel eluting with 0-10 % ethylacetate in hexane. Isolated yield = 3.12 g (48.4 %, first fraction) as yellow solid and 3.01 (46.5 % second fraction) as a yellow liquid. The first fraction was used for the next step. ^{1}H NMR ($CDCl_3$, 300 MHz): δ 7.45 (d, *J* = 3.62 Hz, 2H), 6.86 (d, *J* = 3.63 Hz, 2H), 4.26 (t, *J* = 7.82 2H*),* 1.87 (td, *J* = 15.56, 7.65, 7.65 Hz, 2H), 1.51-1.16 (m, 10H), 0.87 (t, *J* = 6.70, 6.70 Hz, 3H). ^{13}C NMR ($CDCl_3$, 75.46 MHz): δ 162.80, 137.92, 110.91, 52.70, 31.52, 28.99, 28.93, 26.55, 22.37, 13.83. FDMS (m/z) = 295.30 ($M^{+\bullet}$). Elemental analysis: Calculated for $C_{14}H_{21}N_3S_2$: C, 56.91; H, 7.16; N, 14.22; S, 21.70; Found: C, 59.58; H, 7.29; N, 14.74; S, 21.98.

Bis-(5-bromo-thiazol-2-yl)-octyl-amine (14)

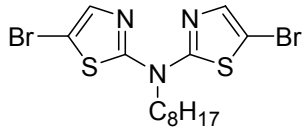

A mixture of octyl-bis-thiazol-2-yl-amine (2.5 g, 8.46 mmol) *N*-bromosuccinimide (3.3, 18.37 mmol, 2.2 equiv.) and chloroform (25 mL) was stirred at room temperature for 24 hours under argon. The mixture was then extracted into ether, washed with brine and dried. The crude product was chromatographed on silica using 0-10 % ethylacetate in hexane as eluent. Isolated yield = 3.7 g (97 %) as a yellow oil. ^{1}H NMR ($CDCl_3$, 300 MHz): δ 7.34 (s, 2H), 4.21-4.07 (m, 2H), 1.81 (td, *J* = 15.43, 7.69, 7.69 Hz, 2H), 1.51-1.17 (m, 10H), 0.88 (t, *J* = 6.72, 6.72 Hz, 3H). ^{13}C NMR ($CDCl_3$, 75.46 MHz): δ 161.69, 138.37, 100.45, 51.90, 31.51, 28.94, 28.90, 26.48, 22.37, 13.85. FDMS (m/z) : 452.90 ($M^{+\bullet}$). Elemental analysis: Calculated for $C_{13}H_{18}Br_2N_3S_2$: C, 35.47; H, 4.12; Br, 36.30; N, 9.54; S, 14.57; Found: C, 35.87; H, 4.51; N, 9.41; S, 14.97.

***N,N*-diphenyl-4-(4,4,5,5-tetramethyl-1,3,2-dioxaborolan-2-yl)aniline (15)**

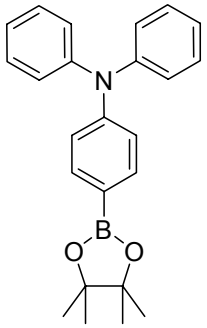

To (4-bromo-phenyl)-diphenyl-amine (2.0g, 6.17 mmol) in a 250 mL Schlnek flask, 30mL of anhydrous THF was added and cooled to -78℃ in an acetone/dry ice bath. To this, 5.78 mL of 1.6 M n-Butyllithium (1.5 equivalent) was added slowly and stirred for 30 minutes. Then 2.14 mL of 2-isopropoxy-4,4,5,5-tetramethyl-1,3,2-dioxaborolane (1.7 equivalent) was added and slowly allowed to warm to room temperature. The reaction was stirred overnight and then quenched with saturated salt, the product was then extracted into ether, washed with brine and dried. The crude product was chromatographed on silica gel eluted with 0-10 % ethylacetate in hexane. Isolated yield = 91.6 % as a yellow oily liquid. ^{1}H NMR ($CDCl_3$, 300 MHz): δ 7.75 (d, *J* = 7.93 Hz, 2H), 7.37-7.26 (m, 5H), 7.18 (d, *J* = 7.20 Hz, 4H), 7.11 (d, *J* = 7.31 Hz, 3H), 1.40 (s, 12H). ^{13}C NMR ($CDCl_3$, 75.46 MHz): δ 150.38, 147.18, 135.67, 129.09, 128.98, 124.76, 123.95, 123.15, 122.45, 121.59, 83.31, 24.66. FDMS (m/z) : 371.20 ($M^{+\bullet}$). Elemental analysis: Calculated for $C_{24}H_{26}BNO_2$: C, 77.64; H, 7.06; B, 2.91; N, 3.77; O, 8.62; Found: C, 77.89; H, 7.55; N, 3.25.

5-(4-(Diphenylamino)phenyl)-*N*-(5-(4-(diphenylamino)phenyl)thiazol-2-yl)-*N*-octylthiazol-2-amine (16)

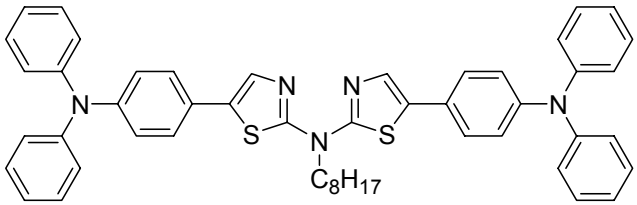

The boronic ester **15** (0.81 g, 2.18 mmol), **14** (0.4 g, 0.88 mmol) were dissolved in THF (20 mL) in a 100 mL Schlenk flask.. To this solution were added aqueous 2 M K_2CO_3 solution (10 mL). The solution was purged with argon for 20 min, and the tetrakis(triphenylphosphine)palladium (61 mg, 0.06 equiv) was added and the reaction was heated with stirring at 85 ℃. The reaction was followed by TCL and was worked up

after 2 days. The cooled mixture was extracted with diethyl ether, and the extract was washed with brine and then dried over $MgSO_4$. The crude product so obtained was purified by chromatography on silica with 0-30 % dichloromethane in hexane as eluent and further purified by recrystallization from TFH in EtOH to afford 0.23 g (33.4 %) of the title compound as yellow powders. ^{1}H NMR ($CDCl_3$, 300 MHz): δ 7.49 (s, 2H), 7.31 (d, *J* = 8.60 Hz, 4H), 7.18 (dd, *J* = 10.36, 5.24 Hz, 8H), 7.10-6.84 (m, 16H), 4.49-4.04 (m, 2H), 2.04-1.65 (m, 2H), 1.51-1.20 (m, *J* = 54.59 Hz, 10H), 0.80 (t, *J* = 6.47, 6.47 Hz, 3H). ^{13}C NMR ($CDCl_3$, 75.46 MHz): δ 160.69, 147.39, 147.27, 131.19, 129.31, 126.79, 125.60, 124.50, 123.71, 123.15, 31.77, 29.27, 29.18, 26.93, 26.80, 22.61, 14.08. FDMS (m/z) : 781.30 ($M^{+\bullet}$). Elemental analysis: Calculated for $C_{50}H_{47}N_5S_2$: C, 76.79; H, 6.06; N, 8.95; S, 8.20; Found: C, 76.99; H, 6.25; N, 6.15; S, 8.57.

Cu(II) complex of 16

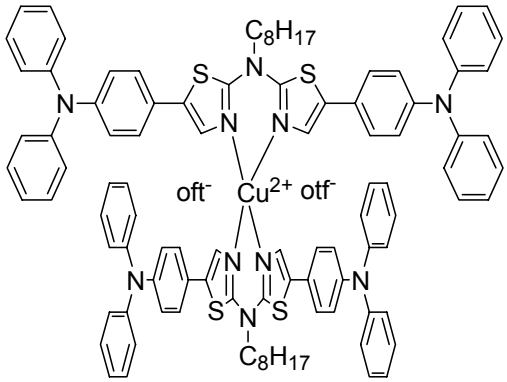

To a solution of **16** (50 mg, 0.063 mmol) in THF (5 mL) was added copper(II) triflate (1.2 equivalent) solution in THF (10 mL), and stirred for 15 hours at room temperature. The solvent was evaporated and then washed with methanol. The crude product was filtered, washed with methanol again and then purified by recrystallization from N,N-dimethylformamide in ether to afford 15 mg (12.6 %) of title compound as a greenish powder.

Pd(II) complex of 16

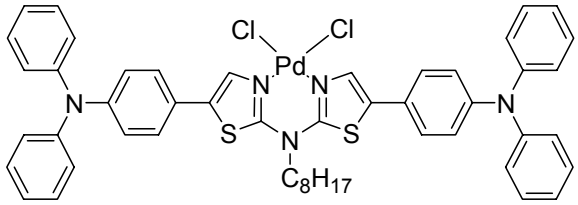

To a solution of **16** (50 mg, 0.063 mmol) in THF (5 mL) was added dichlorobis(benzonitrile)palladium(II) (1.5 equivalent) solution in THF (10 mL), and stirred for 15 hours at room temperature. The solvent was evaporated and then washed with acetone. The crude product was filtered, washed with acetone again and then purified by recrystallization from N,N-dimethylformamide in ether to afford 30 mg (49.5 %) of title compound as orange powders.

Polymer P3

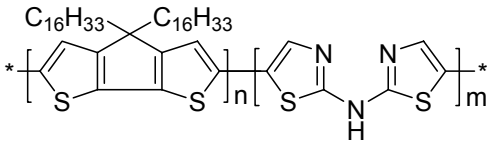

Bis(cyclooctadiene)nickel (430 g, 1.58 mmol, 2.4 equiv.), cyclooctadiene (194 mL, 1.58 mmol, 2.4 equiv.), and 2,2'-bipyridine (245 mg, 1.58 mmol, 2.4 equiv.) were dissolved in anhydrous toluene (7 mL) and anhydrous N,N-dimethylformamide (7 mL) in a Schlenk flask in a glovebox. The mixture was heated at 60 ˚C with stirring under argon for 20 min to generate the catalyst, and then a solution of **9** (145 mg, 0.33 mmol) and **24** (0.259 mg, 0.33 mmol) in anhydrous toluene (10 mL) was added. The reaction was heated at 75 ˚C for 2 days. Then a mixture of toluene (4 mL) and bromobenzene (0.10 mL) was added and the mixture was heated at 75 ˚C for an additional 12 h. The mixture was then poured into a mixture of methanol and concentrated NH_4OH (1:1, 300 mL) and stirred for 24 h and filtered. The precipitated solid was washed with methanol (200 mL). The resulting solid was filtered off and subjected to Soxhlet extraction for 24 hours in acetone. Isolated yield of **P3** = 230 mg (42 %) as a dark brown solid.

Pd(II) complex of 8 (25)

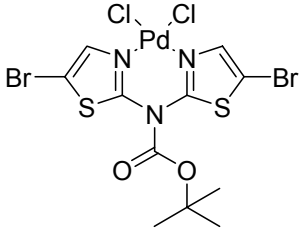

To a solution of **8** (200 mg, 0.453 mmol) in THF (10 mL) was added dichlorobis (benzonitrile) palladium(II) (0.26 g, 0.68 mmol, 1.5 equivalent) solution in THF (50 mL), and stirred for 15 hours at room temperature. The solvent was evaporated and then washed with THF. The crude product was filtered, washed with acetone again and then purified by recrystallization from N,N-dimethylformamide in ether to afford 110 mg (40.0 %) of title compound as brown powders.

Polymer P4

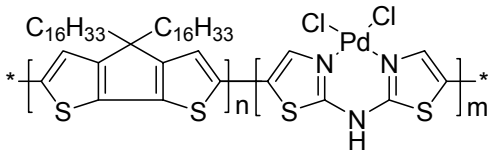

Bis(cyclooctadiene)nickel (215 g, 0.79 mmol, 2.4 equiv.), cyclooctadiene (970 μL, 0.79 mmol, 2.4 equiv.), and 2,2'-bipyridine (123 mg, 0.79 mmol, 2.4 equiv.) were dissolved in anhydrous toluene (7 mL) and anhydrous N,N-dimethylformamide (7 mL) in a Schlenk flask in a glovebox. The mixture was heated at 60 ˚C with stirring under argon for 20 min to generate the catalyst, and then a solution of **24** (0.13 mg, 0.165 mmol) and **25** (102 mg, 0.165 mmol) in anhydrous toluene (10 mL) was added. The reaction was heated at 75 ˚C for 2 days. Then a mixture of toluene (4 mL) and bromobenzene (0.10 mL) was added and the mixture was heated at 75 ˚C for an additional 12 h. The mixture was then poured into a mixture of methanol and concentrated NH_4OH (1:1, 300 mL) and stirred for 24 h and filtered. The precipitated solid was washed with methanol (200 mL). The resulting solid was filtered off and subjected to Soxhlet extraction for 24 hours in acetone. Isolated yield of **P4** = 150 mg (45 %) as a dark brown solid.

Synthesis of 1,1-dioctylethylene (28)

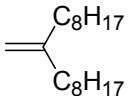

To 40 mL of anhydrous DMSO in a Schlenk flask, NaH (4.0 g, 0.10 mol, 60 % dispersion in mineral oil) was added and heated at 75 ˚C for 20 min under argon. This was then cooled in an ice bath and methyltriphenylphosphonium bromide (35.7 g, 0.10 mol) in 100 mL of warm DMSO was added. The resulting dark red solution was stirred at room temperature for 10 min. To this, 9-heptadecanone (25.4 g, 0.10 mol) was added and the mixture stirred at room temperature overnight under argon. The crude product was then extracted into *n*-pentane, washed with brine and dried. This was then chromatographed on

silica using hexane as eluent. Isolated yield = 14.5 g (58 %) as a colorless liquid. ^{1}H NMR ($CDCl_3$, 300 MHz): δ 4.70 (s, 2H), 2.04 (t, *J* = 7.1 Hz, 4H), 1.37-1.23 (m, 24H), 0.93 (t, *J* = 6.9 Hz, 6H). ^{13}C NMR ($CDCl_3$, 75.46 MHz): δ 150.01, 108.46, 42.81, 36.17, 32.04, 29.66, 27.94, 22.78, 14.08. FDMS (m/z): 252.2 ($M^{+\bullet}$). Elemental analysis: Calculated for $C_{18}H_{36}$: C, 85.63 H, 14.37 Found: C, 85.53 H, 14.37.

Synthesis of 2,6-di(2-octyldecyl)-anthraquinone (29)

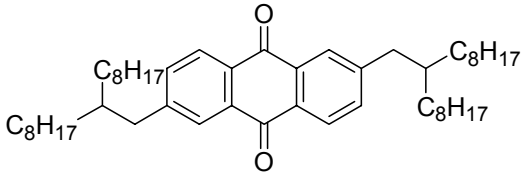

To **28** (14.0 mL, 55.5 mmol) in a 500 mL Schlenk flask, 122.2 mL of a 0.5 M solution of 9-borabicyclo nonane (9-BBN) in THF was added slowly under argon, and then stirred overnight at room temperature. To this solution, 20 mL of aqueous K_2CO_3 (6.4 g, 46.6 mmol) solution was added via a syringe followed by 2,6-dibromoanthraquinone (8.1 g, 22.2 mmol) and $Pd(PPh_3)_4$ (1.03 g, 0.89 mmol). The reaction mixture was stirred under argon at 75 ˚C for 12 h and then extracted into dichloromethane, washed three times with brine and dried over $MgSO_4$. The crude product was then chromatographed on silica gel using 0-25 % dichloromethane in hexane as eluent. Isolated yield = 5.4 g (35 %) as a yellow oil. ^{1}H NMR ($CDCl_3$, 300 MHz): δ 8.22 (d, *J* = 7.9 Hz, 2H), 8.06 (d, *J* = 1.5 Hz, 2H), 7.55 (dd, *J* = 7.9, 1.7 Hz, 2H), 2.70 (d, *J* = 7.0, 4H), 1.81-1.69 (m, 2H), 1.31-1.20 (m, 56H), 0.87 (t, *J* = 6.8 Hz, 12H). ^{13}C NMR ($CDCl_3$, 75.46 MHz): δ 183.14, 139,10, 134.53, 133.18, 131.28, 127.2, 40.69, 39.35, 32.91, 31.61, 29.64, 29.29, 29.02, 26.26, 22.39, 13.81. FDMS (m/z): 712.6 ($M^{+\bullet}$). Elemental analysis: Calculated for $C_{50}H_{80}O_2$: C, 84.21; H, 11.31; O, 4.49; Found: C, 84.22; H, 11.28.

Synthesis of 2,6-di(2-octyldecyl)-anthracene

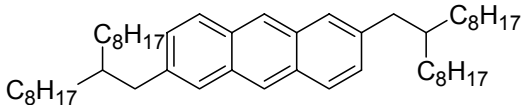

$LiAlH_4$ (18.5 mL of 1.0 M solution in THF, 18.5 mmol) was added dropwise with stirring to a solution of the anthraquinone **29** (5.3 g, 7.4 mmol) in 30 mL of anhydrous THF. After the addition was completed, the mixture was stirred at reflux overnight under argon. Excess $LiAlH_4$ was quenched by the addition of 2.0 M HCl and extracted into dichloromethane and washed with brine. The solvent was evaporated and dried completely. The crude product afforded mixtures of the anthracenes and the anthrones. In

order to convert the anthrones to the anthracenes, the crude product was treated with $LiAlH_4$ (37.0 mL of 1.0 M solution in THF, 37.0 mmol) without further purification and heated at reflux overnight. The mixture was cooled and quenched by the addition of 2.0 M HCl, extracted into dichloromethane, washed with brine and dried over $MgSO_4$. The crude product was chromatographed on silica using hexane as eluent. Isolated yield = 3.2 g (63 %) as a yellow oil. ^{1}H NMR ($CDCl_3$, 300 MHz): δ 8.32 (s, 2H), 7.92 (d, *J* = 8.7 Hz, 2H,), 7.72 (s, 2H), 7.31 (d, *J* = 8.7 Hz, 2H,), 2.74 (d, *J* = 6.9 Hz, 4H), 1.80-1.73 (m, 2H), 1.32-1.28 (m, 56H), 0.90 (t, *J* = 6.7 Hz,12H). ^{13}C NMR ($CDCl_3$, 75.46 MHz): δ 138.76, 131.90, 131.11, 128.26, 128.17, 127.32, 125.40, 41.45, 39.74, 33.72, 32.35, 30.44, 30.06, 29.78, 27.05, 23.11, 14.53. FDMS (m/z): 682.6 ($M^{+\bullet}$). Elemental analysis: Calculated for $C_{50}H_{82}$: C, 87.90; H, 12.10; Found: C, 87.49; H, 11.94.

Synthesis of 9,10-dibromo-2,6-di(2-octyldecyl)-anthracene (30)

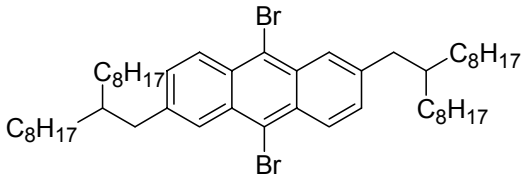

Bromine (1.4 g, 8.8 mmol) in acetic acid (5 mL) was added dropwise over a period of 5 minutes to a vigorously stirred suspension of 2,6-di(2-octyldecyl)-anthracene (3.0 g, 4.4 mmol) in acetic acid (30 mL) at room temperature. The reaction was allowed to stir for 30 minutes during which a canary yellow precipitate formed. The solution was quenched by the addition of $Na_2S_2O_5$, extracted into diethyl ether, washed with water and dried over $MgSO_4$. The crude product was chromatographed on silica using hexane as eluent. Isolated yield = 3.3 g (91 %) as a yellow solid. ^{1}H NMR ($CDCl_3$, 300 MHz): δ 8.48 (d, *J* = 9.0 Hz, 2H), 8.27 (s, 2H,), 7.44 (d, *J* = 9.0 Hz, 2H), 2.80 (d, *J* = 6.9 Hz, 4H), 1.82-1.71 (m, 2H), 1.33-1.23 (m, 56H), 0.88 (t, *J* = 6.9 Hz,12H). ^{13}C NMR ($CDCl_3$, 75.46 MHz): δ 140.66, 130.42, 129.83, 129.65, 127.70, 126.74, 122.14, 40.62, 39.00, 33.03, 31.69, 29.77, 29.41, 29.12, 26.37, 22.46, 13.89. FDMS (m/z): 840.5 ($M^{+\bullet}$). Elemental analysis: Calculated for $C_{50}H_{80}Br_2$: C, 71.41; H, 9.59; Br, 19.00; Found: C, 71.27; H, 9.73.

Synthesis of 4,4''-di(4,4,5,5-tetramethyl-1,3,2-dioxaborolan-2-yl)-*p*-terphenyl (32)

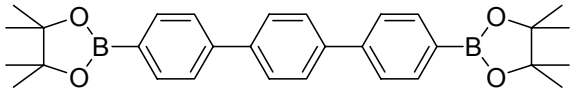

4,4''-Dibromo-*p*-terphenyl (**31**) (1.5 g, 3.86 mmol) was dissolved in 60 mL of anhydrous THF in a 250 mL Schlenk flask and cooled to -78 ˚C in an acetone/dry ice bath. To this, 5.78 mL of 1.6 M *n*-butyllithium (11.58 mmol) was added slowly and stirred for 30

minutes. Then 2.37 mL of 2-isopropoxy-4,4,5,5-tetramethyl-1,3,2-dioxaborolane (12.7 mmol) was added and slowly allowed to warm to room temperature. The reaction was stirred overnight and then quenched with brine, the product was then extracted into dichloromethane, washed again with brine and dried. The crude product was chromatographed on silica using 0-30 % ethylacetate in hexane as eluent. Isolated yield = 0.5 g (27 %) as colorless crystals. ^{1}H NMR ($CDCl_3$, 300 MHz): δ 7.92 (d, J = 8.2 Hz, 4H), 7.71 (s, 4H), 7.67 (d, J = 8.2 Hz, 4H). ^{13}C NMR ($CDCl_3$, 75.46 MHz): δ 143.13, 140.05, 135.15, 127.43, 126.17, 83.67, 24.73. FDMS (m/z): 482.3 ($M^{+\bullet}$). Elemental analysis: Calculated for $C_{30}H_{36}B_2O_4$: C, 74.72; H, 7.52; B, 4.48; O, 13.27; Found: C, 74.31; H, 7.76.

Polymer P5

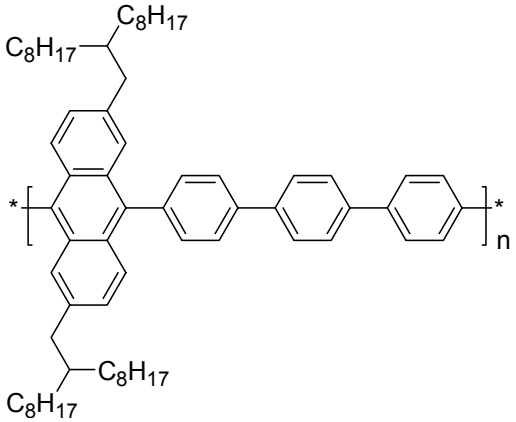

Dibromide **30** (0.252 g, 0.3 mmol), **32** (0.144 g, 0.3 mmol), Aliquat® 336 (0.02 g, 13 mol %), 3.0 mL of aqueous 2.0 M Na_2CO_3 solution and 9.0 mL of toluene were taken together in a Schlenk flask and purged with argon for 15 minutes. Then $Pd(PPh_3)_4$ (0.01 g, 9.0 μmol) was added and the reaction heated under vigorous reflux for 24 h. Phenylboronic acid was added as an end capper (2.0 mg), heated for 6 h and then bromobenzene (5.0 mg) was added and heated again for an additional 6 h. This was then poured into a mixture of methanol and 2.0 M HCl (1:1, 300 mL) and the precipitated product was redissolved in THF (10 mL) and added dropwise to methanol (200 mL). The resulting solid was filtered off and subjected to Soxhlet extraction for a day in acetone and again filtered and dried. Isolated yield of polymer **P5** = 192 mg (70 %). GPC analysis $M_n = 5.33 \times 10^3$ g/mol, $M_w = 6.62 \times 10^3$ g/mol, and D = 1.24 (against PPP standard); $M_n = 6.97 \times 10^3$ g/mol, $M_w = 9.24 \times 10^3$ g/mol, and D = 1.33 (against PS standard). ^{1}H NMR ($CDCl_3$, 300 MHz): δ 8.10-7.81 (m, 6H), 7.73-7.41 (br m, 10H), 7.21-7.10 (m, 2H), 2.67-2.41 (br, 4H), 1.75-1.58 (br, 2H), 1.45-1.15 (br m, 56H), 0.95-0.79 (br, 12H). Elemental analysis: Calculated for $C_{68}H_{92}$: C, 89.80; H, 10.20; Found: C, 90.11; H, 9.79.

Polymer P6

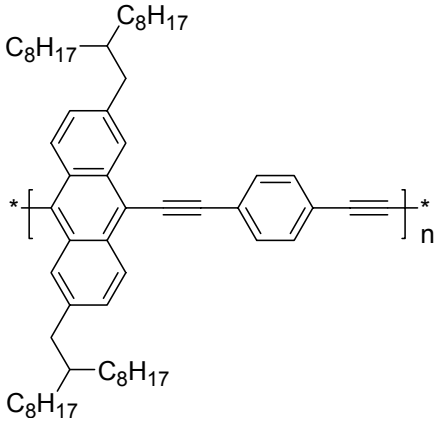

A mixture of *p*-diethynylbenzene (37.8 mg, 0.3 mmol), dibromide **30** (252 mg, 0.3 mmol), $PdCl_2(PPh_3)_2$ (4.2 mg, 6.0 μmol), copper iodide (3.4 mg, 18 μmol), triphenylphosphine (15.7 mg, 0.06 mmol), and triethylamine (1.5 mL, excess) in anhydrous toluene (10 mL) was degassed with argon in a Schlenk tube. This was heated at 90 ˚C for 24 h. Then a mixture of toluene (2 mL) and phenylacetylene (2.0 mg) was added. After 6 h, bromobenzene (5.0 mg) in toluene (2 mL) was added and heated for an additional 12 h. The mixture was then poured into the solution of methanol and concentrated 2.0 M HCl (1:1, 300 mL) and stirred for 4 h. The precipitated reddish solid was redissolved in THF (20 mL) and added dropwise to methanol (200 mL). The resulting solid was filtered off and subjected to Soxhlet extraction for 2 days in acetone. The residue was then redissolved in THF and precipitated again from methanol, filtered, washed with methanol, and dried. Isolated yield of polymer **P6** = 110 mg (46 %). GPC analysis $M_n = 4.82 \times 10^3$ g/mol, $M_w = 1.25 \times 10^4$ g/mol, and D = 2.60 (against PPP standard); $M_n = 6.10 \times 10^3$ g/mol, $M_w = 2.17 \times 10^4$ g/mol, and D = 3.57 (against PS standard). ^{1}H NMR ($CDCl_3$, 300 MHz): δ 8.7-8.10 (m, 4H), 7.91-7.43 (br m, 6H), 2.88-2.71 (br, 4H), 1.88-1.68 (br, 2H), 1.45-1.21 (br m, 56H), 0.89-0.82 (br, 12H). Elemental analysis: Calculated for $C_{61}H_{86}$: C, 89.42; H, 10.58; Found: C, 89.89; H, 9.94.

Synthesis of di(4-(4,4,5,5-tetramethyl-1,3,2-dioxaborolan-2-yl)phenyl)acetylene (34)

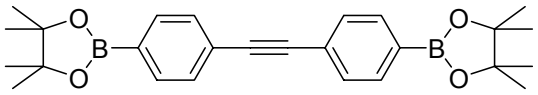

Di(4-bromophenyl)acetylene (**33**) (1.5g, 4.46 mmol) was dissolved in 60 mL of anhydrous THF in a 250 mL Schlenk flask and cooled to -78 ˚C in an acetone/dry ice bath. To this, 8.37 mL of 1.6 M *n*-butyllithium (13.28 mmol) was added slowly and stirred for 30 minutes. Then 3.0 mL of 2-isopropoxy-4,4,5,5-tetramethyl-1,3,2-dioxaborolane (14.7

mmol) was added and slowly allowed to warm to room temperature. The reaction was stirred overnight and then quenched with brine and the product extracted into dichloromethane, washed again with brine and dried. The crude product was chromatographed on silica gel using 0-10 % ethylacetate in hexane as eluent. Isolated yield = 1.1 g (57 %) as a colorless solid. ^{1}H NMR ($CDCl_3$, 300 MHz): δ 7.80 (d, J = 8.2 Hz, 4H), 7.55 (d, J = 8.2 Hz, 2H), 1.35 (m, 24H). ^{13}C NMR ($CDCl_3$, 75.46 MHz): δ 134.15, 130.35, 125.37, 90.40, 83.50, 24.43. FDMS (m/z): 430.3 ($M^{+\bullet}$). Elemental analysis: Calculated for $C_{26}H_{32}B_2O_4$: C, 72.60; H, 7.50; B, 5.03; O, 14.88; Found: C, 72.99; H, 7.33.

Polymer P7

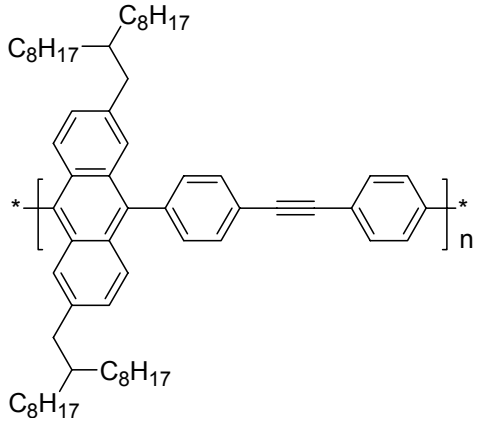

Dibromide **30** (0.252 g, 0.3 mmol), **34** (0.128 g, 0.3 mmol), Aliquat® 336 (0.02 g, 13 mol %) and 3.0 mL of aqueous 2.0 M Na_2CO_3 solution and 9.0 mL of toluene were taken in a Schlenk tube and purged with argon for 15 minutes. Then $Pd(PPh_3)_4$ (0.01 g, 9.0 μmol) was added and the reaction heated under vigorous reflux for 24 h. Phenylboronic acid was added as an end capper (2.0 mg), heated for 6 h and then bromobenzene (5.0 mg) was added and heated again for an additional 6 h. This was then poured into a mixture of methanol and 2.0 M HCl (1:1, 300 mL) and the precipitated product was redissolved in THF (10 mL) and added dropwise to methanol (200 mL). The resulting solid was filtered off and subjected to Soxhlet extraction for a day in acetone and again filtered and dried. Isolated yield of polymer **P3** = 200 mg (76 %). GPC analysis M_n = 1.6 × 10^4 g/mol, M_w = 4.89 × 10^4 g/mol, and D = 3.04 (against PPP standard); M_n = 2.35 × 10^4 g/mol, M_w = 9.98 × 10^4 g/mol, and D = 4.23 (against PS standard). ^{1}H NMR ($CDCl_3$, 300 MHz): δ 7.91-7.81 (m, 3H), 7.71-7.31 (br m, 10H), 7.29-7.20 (m, 1H), 2.77-2.58 (br, 4H), 1.77-1.61 (br, 2H), 1.43-1.21 (br m, 56H), 0.90-0.81 (br, 12H). Elemental analysis: Calculated for $C_{64}H_{88}$: C, 89.65; H, 10.35; Found: C, 89.56; H, 10.43.

Synthesis of 5-bromo-2-iodo-4'-decylbenzophenone (35)

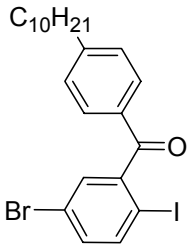

A flask equipped with a reflux condenser and a drying tube was charged with 5-bromo-2-iodo-benzoic acid (5.0 g, 15.33 mmol) and benzene (50 mL). To this mixture was added oxalyl chloride (2.89 g, 23.0 mmol) and one drop of N,N-dimethylformamide (catalyst). The reaction mixture was heated at 80 ˚C overnight (bubbling observed), then the reaction was cooled and the solvent was removed *in vacuo*. The crude solid was dissolved in benzene (20 mL) and stirred with calcium hydride for 1 h and filtered. The solvent was removed in *vacuo* to give 5-bromo-2-iodo-benzoyl chloride and used without further purification. To the benzoyl chloride in 20 mL of dichloromethane, aluminum chloride (3.0 g, 23.0 mmol) and decyl benzene (6.34 g, 29.1 mmol) were added, stirred at room temperature for 12 h and then quenched with aqueous 2 M HCl. The mixture was then extracted into dichloromethane and washed with brine. The crude product obtained was purified by chromatography on silica with 0-10 % ethylacetate in hexane as eluent. Isolated yield = 6.8 g (85 %) as a yellow oil. ^{1}H NMR ($CDCl_3$, 300 MHz): δ 7.73 (dd, J = 10.4 and 8.4 Hz, 3H), 7.40 (d, J = 2.3 Hz, 1H), 7.32-7.28 (m, 3H), 2.66 (t, J = 7.9 Hz, 2H), 1.69-1.58 (m, 2H), 1.37-1.21 (m, 14H), 0.87 (t, J = 6.9 Hz, 3H). ^{13}C NMR ($CDCl_3$, 75.46 MHz): δ 195.53, 150.51, 146.80, 141.32, 134.35, 132.99, 131.44, 130.99, 129.24, 122.75, 90.59, 36.52, 32.24, 31.35, 29.94, 29.90, 29.79, 29.67, 23.03, 14.49. FDMS (m/z): 526.0 ($M^{+\bullet}$). Elemental analysis: Calculated for $C_{23}H_{28}BrIO$: C, 52.39; H, 5.35; Br, 15.15; I, 24.07; O, 3.03; Found: C, 53.11; H, 5.73.

Synthesis of 9,10-di(4,4,5,5-tetramethyl-1,3,2-dioxaborolan-2-yl)anthracene (36)

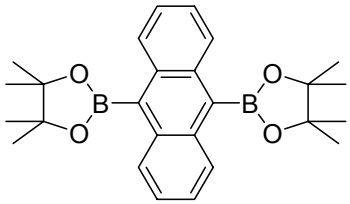

To a 100 mL Schlenk flask, 9,10-dibromoanthracene (4.20 g, 12.5 mmol), bis-(pinacolato)diboron (7.75 g, 30.51 mmol), palladium acetate (0.166 g, 0.74 mmol),

potassium acetate (7.34 g, 75.0 mmol) and 35 mL of anhydrous N,N-dimethylformamide were added. The mixture was degassed by gently bubbling argon for 30 min at room temperature. This was then heated at 70 ℃ under argon overnight. The cooled mixture was extracted with diethyl ether, washed with brine and dried over $MgSO_4$. The crude product was chromatographed on silica using 0-10 % ethylacetate in hexane as eluent. Isolated yield = 2.7 g (50 %) as a yellow solid. ^{1}H NMR ($CDCl_3$, 300 MHz): δ 8.35 (dd, J = 6.8 and 3.3 Hz, 4H), 7.46 (dd, J = 6.8 and 3.3Hz, 4H), 1.58 (m, 24H). ^{13}C NMR ($CDCl_3$, 75.46 MHz): δ 134.91, 128.78, 125.13, 84.44, 25.18. FDMS (m/z): 430.1 ($M^{+\bullet}$). Elemental analysis: Calculated for $C_{26}H_{32}B_2O_4$: C, 72.60; H, 7.50; B, 5.03; O, 14.88; Found: C, 72.11; H, 7.73.

Synthesis of 9,10-di(5-bromo-4'-decylbenzophenon-2yl)anthracene (37)

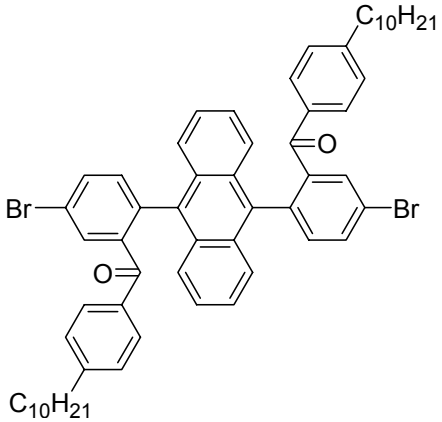

The diboronic ester **36** (0.5 g, 1.16 mmol), and the ketone **35** (1.41 g, 2.67 mmol) were dissolved in THF (20 mL) in a 100 mL Schlenk flask and aqueous 2 M K_2CO_3 solution (10 mL) was added to this solution, purged with argon for 20 min, then tetrakis(triphenylphosphine)palladium (150 mg, 0.129 mmol) was added and the reaction was heated with stirring at 85 ℃. The reaction was followed by TLC and worked up after 2 days. The cooled mixture was extracted with diethyl ether, washed with brine and then dried over $MgSO_4$. The crude product obtained was purified by chromatography on silica with 0-10 % ethylacetate in hexane as eluent and further purified by recrystallization from ethylacetate in hexane to afford 1.1 g (97 %) of the title compound as a yellow solid. ^{1}H NMR ($CDCl_3$, 300 MHz): δ 7.88 (d, J = 2.0 Hz, 1H) 7.80 (m, 3H), 7.47 (m, 4H), 7.24 (m, 8H), 7.11 (d, J = 8.2 Hz, 2H), 6.83 (d, J = 8.2 Hz, 2H) 6.72 (d, J = 8.2 Hz, 2H), 2.34 (m, 4H), 1.35-1.21 (m, 32H) 0.88 (t, J = 5.9 Hz, 6H). ^{13}C NMR ($CDCl_3$, 75.46 MHz): δ 195.65, 148.12, 147.98, 143.21, 142.95, 136.94, 136.83, 134.44, 134.32, 134.08, 133.87, 133.58, 133.36, 133.08, 132.02, 131.31, 129.52, 129.29, 128.87, 127.92, 127.38, 126.63, 126.52, 125.20, 125.06, 121.74, 121.55, 35.84, 31.90, 31.18, 31.02, 29.61, 29.50, 29.44,

29.33, 29.23, 22.67, 14.10. FDMS (m/z): 974.5 ($M^{+\bullet}$). Elemental analysis: Calculated for $C_{60}H_{64}Br_2O_2$: C, 73.76; H, 6.60; Br, 16.36; O, 3.28; Found: C, 73.29; H, 6.73.

Synthesis of 9,10-di(5-(4,4,5,5-tetramethyl-1,3,2-dioxaborolan-2-yl)-4'-decylbenzophenon-2yl)anthracene (38)

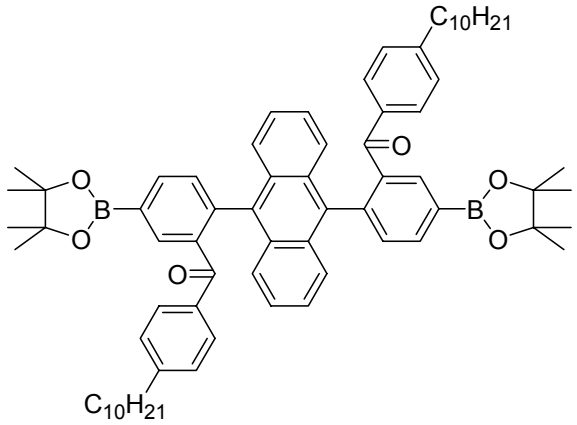

To a 100 mL Schlenk flask, the diketone **37** (0.6 g, 0.61 mmol), bis-(pinacolato)diboron (0.39 g, 1.53 mmol), palladium acetate (0.008 g, 0.037 mmol), potassium acetate (0.36 g, 3.66 mmol) and 10 mL of anhydrous N,N-dimethylformamide were added. The mixture was degassed by gently bubbling argon for 30 min at room temperature. The mixture was then heated at 80 ˚C under argon for overnight. The cooled mixture was extracted with diethyl ether, washed with brine and then dried over $MgSO_4$. The crude product was chromatographed on silica using 0-10 % ethylacetate in hexane as eluent. Isolated yield = 0.39 g (60 %) as a yellow oil. ^{1}H NMR ($CDCl_3$, 300 MHz): δ 8.20 (d, J = 9.0 Hz, 1H), 8.10 (dd, , J = 11.8 and 7.6 Hz, 3H), 7.46 (m, 4H) ppm 7.37 (dd, J = 16.2 and 7.5 Hz, 3H), 7.18 (m, 5H), 6.79 (d, J = 8.1 Hz 2H), 6.67 (d, J = 8.1 Hz, 2H), 2.31 (m, 4H), 1.48-1.40 (m, 32H), 1.29-1.21 (m, 24H), 0.88 (t, J = 6.7Hz, 6H). ^{13}C NMR ($CDCl_3$, 75.46 MHz): δ 197.68, 196.84, 147.42, 147.24, 141.17, 141.02, 140.94, 136.40, 136.10, 135.85, 135.27, 135.20, 135.14, 135.08, 134.91, 134.57, 134.33, 132.13, 130.33, 129.41, 129.37, 129.28, 128.74, 128.32, 127.72, 127.13, 126.84, 126.71, 124.81, 124.69, 84.15, 35.80, 35.76, 31.87, 31.14, 31.03, 29.62, 29.57, 29.48, 29.41, 29.36, 29.29, 29.24, 24.99, 24.90, 24.82, 24.54, 24.49, 22.65, 14.08. FDMS (m/z): 1070.7 ($M^{+\bullet}$). Elemental analysis: Calculated for $C_{72}H_{88}B_2O_6$: C, 80.74; H, 8.28; B, 2.02; O, 8.96; Found: C, 80.27; H, 8.73.

Polymer (39)

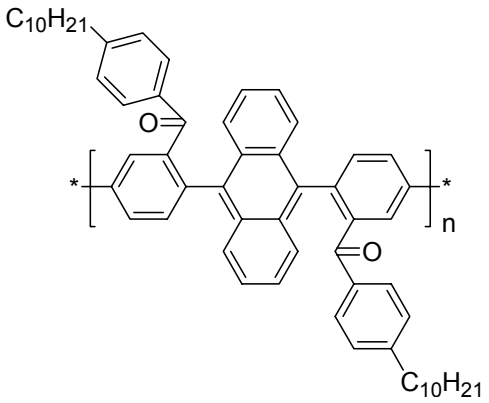

Monomer **37** (117 mg, 0.12 mmol), monomer **38** (128 mg, 0.12 mmol), Aliquat® 336 (0.008 g, 13 mol %), 1.5 mL of aqueous 2.0 M Na_2CO_3 and 4.0 mL of toluene were taken together in a Schlenk flask and purged with argon for 15 minutes. To this, tetrakis(triphenylphosphine)palladium (3.0 mg, 3.6 μmol) was added and the reaction heated at 85 ˚C under vigorous stirring for 48 h. Phenylboronic acid was then added as an end capper (2.0 mg), heated for 6 h, then bromobenzene (5.0 mg) was added and heated again for an additional 6 h. The reaction was poured into a mixture of methanol and 2.0 M HCl (1:1, 300 mL). The precipitated product was redissolved in THF (10 mL) and added dropwise to methanol (200 mL). The resulting solid was filtered off and subjected to Soxhlet extraction for 24 h in acetone and again filtered and dried. Isolated yield of **5** as a dark brown polymer = 130 mg (66 %). GPC analysis M_n = 6.11 × 10^3 g/mol, M_w = 8.75 × 10^3 g/mol, and D = 1.43 (against PPP standard); M_n = 7.30 × 10^3 g/mol, M_w = 1.19 × 10^4 g/mol, and D = 1.63 (against PS standard). ^{1}H NMR (CD_2Cl_2, 500 MHz): δ 8.20-8.11 (br m, 4H), 7.69-7.45 (br m, 8H), 7.34-7.21 (br m, 6H), 6.99-6.81 (br m, 4H), 2.45-2.31 (br m, 4H), 1.47-1.20 (br m, 32H), 0.93-0.81 (br m, 6H). ^{13}C NMR (CD_2Cl_2, 125.75 MHz): δ 196.56, 148.81, 148.71, 142.63, 139.97, 139.95, 139.77, 138.45, 138.24, 135.60, 135.44, 135.25, 134.16, 134.04, 130.35, 130.21, 129.65, 129.56, 128.63, 125.63, 125.47, 36.45, 32.51, 31.74, 30.21, 30.10, 30.01, 29.94, 29.92, 29.28, 14.47. Elemental analysis: Calculated for $C_{60}H_{64}O_2$: C, 88.19; H, 7.89; O, 3.92; Found: C, 88.67; H, 7.11.

Polymer (40)

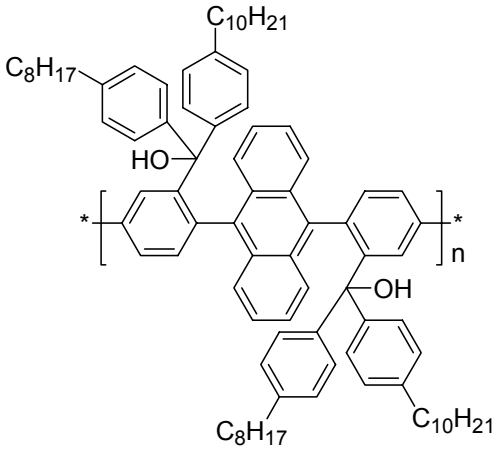

A solution of 4-octylbromobenzene (0.627 mL, 0.7 g, 2.6 mmol) in anhydrous THF (20 mL) in a 250 mL Schlenk flask was cooled to -78 °C in an acetone/dry ice bath. *n*-butyllithium in hexane (1.78 mL, 1.6 M, 2.86 mmol) was then added and the mixture was stirred for 20 min. Then a solution of the diketone polymer **5** (100 mg, 0.122 mmol) in anhydrous THF (5 mL) was added dropwise with stirring and the solution was allowed to slowly warm to room temperature. The mixture was stirred overnight and then quenched with 2 M HCl. The crude product was extracted with dichloromethane, washed with brine and dried over $MgSO_4$. The solvent was evaporated and the crude product was redissolved in THF (10 mL) and added dropwise to methanol (200 mL). The resulting solid was filtered off and dried. Isolated yield of the yellow polymer **6** = 130 mg (89 %). ^{1}H NMR (CD_2Cl_2, 500 MHz): δ 7.75-7.31 (br m, 10H), 7.11-6.81 (br m, 20H), 2.60-2.45 (br m, 8H), 1.69-1.21 (br m, 56H), 0.95-0.81 (br m, 12H). Elemental analysis: Calculated for $C_{88}H_{108}O_2$: C, 88.24; H, 9.09; O, 2.67; Found: C, 88.69; H, 9.43.

Polymer SLPPPA

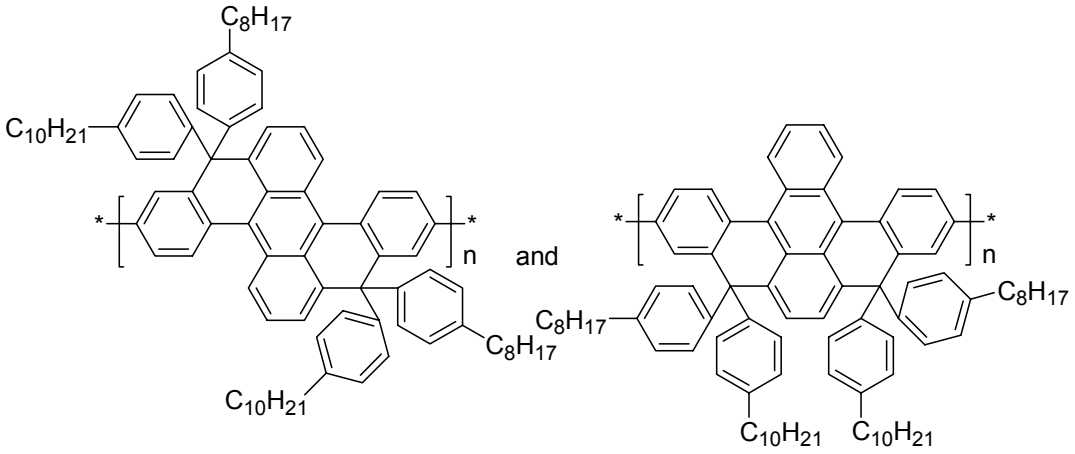

The polyalcohol **40** (0.110 mg, 91.9 μmol) was dissolved in dichloromethane (15 mL), and boron trifluoride etherate (0.736 mL) was added with stirring at room temperature. The greenish colored solution turned deep brown immediately upon addition. The mixture was stirred for 12 h, the mixture was extracted into dichloromethane and washed with water. The organic layer was again washed several times with hydrazine and water. The solvent was removed *in vacuo*, the compound was redissolved in THF (5 mL) and added dropwise to methanol (200 mL). The resulting solid was filtered off and subjected to Soxhlet extraction for 1 day in acetone. Isolated yield of the deep red polymer **SLPPPA** = 85 mg (80 %). GPC analysis $M_n = 7.24 \times 10^3$ g/mol, $M_w = 9.78 \times 10^3$ g/mol, and D = 1.35 (against PPP standard); $M_n = 9.81 \times 10^3$ g/mol, $M_w = 1.45 \times 10^4$ g/mol, and D = 1.48 (against PS standard). ^{1}H NMR ($CDCl_3$, 500 MHz): δ 8.60-8.39 (br m, 2H), 8.01-7.82 (br m, 2H), 7.62-7.31 (br m, 4H), 7.39-6.70 (br m, 20H), 2.63-2.50 (br m, 8H), 1.59-1.45 (br m, 8H), 1.35-1.21 (br m, 48H), 0.91-0.71 (br m, 12H). ^{13}C NMR ($CDCl_3$, 125.75 MHz): δ 145.07, 143.36, 142.96, 140.84, 140.68, 140.51, 140.46, 140.31, 128.74, 128.55, 127.75, 127.51, 127.36, 127.28, 127.17, 126.92, 126.80, 59.77, 35.27, 31.63, 31.02, 30.94, 29.43, 29.35, 29.24, 29.07, 22.40, 13.84. Elemental analysis: Calculated for $C_{88}H_{104}$: C, 90.98; H, 9.02; Found: C, 90.37; H, 9.43.

Polymer 42

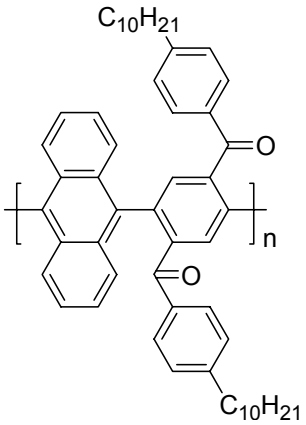

Diboronic ester **36** (0.193 g, 0.45 mmol), diketone **41** (0.326 g, 0.45 mmol), Aliquat® 336 (0.025 g, 13 mol %), 2.0 mL of aqueous 2.0 M Na_2CO_3 and 5.5 mL of toluene were taken together in a Schlenk flask and purged with argon for 15 minutes. To this, tetrakis(triphenylphosphine)palladium (15 mg, 0.013 mmol) was added and the reaction heated at 85 ˚C under vigorous stirring for 24 h. Phenylboronic acid was then added as an end capper (2.0 mg), heated for 6 h and then bromobenzene (5.0 mg) was added and heated again for an additional 6 h. The reaction was poured into a mixture of methanol and 2.0 M HCl (1:1, 300 mL) and the precipitated product was redissolved in THF (10

mL) and added dropwise to methanol (200 mL). The resulting solid was filtered off and subjected to Soxhlet extraction for 24 h in acetone and filtered off and dried. Isolated yield of the brown polymer **42** = 150 mg (45 %). GPC analysis M_n = 3.63 × 10^3 g/mol, M_w = 5.90 × 10^3 g/mol, and D = 1.62 (against PPP standard); M_n = 4.37 × 10^3 g/mol, M_w = 8.25 × 10^3 g/mol, and D = 1.89 (against PS standard). ^{1}H NMR ($CDCl_3$, 500 MHz): δ 7.92-7.75 (br m, 7H), 7.67-7.30 (br m, 8H), 7.04-6.67 (br m, 3H), 2.43-2.11 (br m, 4H), 1.41-1.20 (br m, 32H), 0.91-0.82 (br m, 6H). ^{13}C NMR ($CDCl_3$, 125.75 MHz): δ 196.23, 148.60, 148.50, 148.41, 148.30, 143.12, 142.85, 137.95, 137.80, 135.10, 134.91, 134.53, 134.35, 133.85, 133.66, 133.59, 130.27, 127.91, 127.80, 127.08, 125.85, 125.74, 36.04, 35.96, 32.14, 31.26, 31.20, 29.94, 29.83, 29.74, 29.68, 29.55, 29.45, 29.38, 22.89, 14.27. Elemental analysis: Calculated for $C_{54}H_{60}O_2$: C, 87.52; H, 8.16; O, 4.32; Found: C, 87.15; H, 8.51.

Polymer (43)

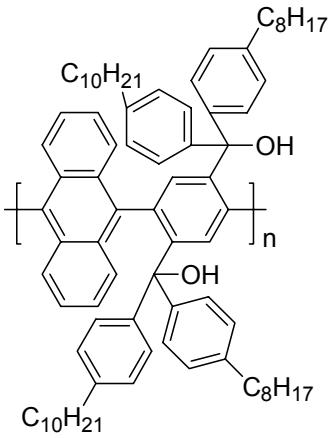

A solution of 4-octylbromobenzene (0.627 mL, 0.7 g, 2.6 mmol) in 10 mL anhydrous THF (20 mL) in a 250 mL Schlenk flask was cooled to -78 ˚C in an acetone/dry ice bath. *n*-Butyllithium in hexane (1.78 mL, 1.6 M, 2.86 mmol) was then added and the mixture was stirred for 20 min. Then a solution of the diketone polymer **42** (100 mg, 0.135 mmol) in anhydrous THF (5 mL) was added dropwise with stirring and the solution was allowed to slowly warm to room temperature. The mixture was stirred overnight and then quenched with 2 M HCl. The crude product was extracted with dichloromethane, washed with brine and dried over $MgSO_4$. The solvent was evaporated and the crude product was redissolved in THF (10 mL) and added dropwise to methanol (200 mL). The resulting solid was filtered off and dried. Isolated yield of the greenish polymer **43** = 120 mg (79 %). ^{1}H NMR ($CDCl_3$, 300 MHz): δ 7.62-7.21 (br m, 6H), 7.17-6.79 (br m, 20H), 2.63-2.41 (br m, 8H), 1.62-1.57 (br m, 8H), 1.49-1.20 (br m, 32H), 0.95-0.82 (br m, 12H).

Elemental analysis: Calculated for $C_{82}H_{104}O_2$: C, 87.80; H, 9.35; O, 2.85; Found: C, 87.32; H, 9.73.

Polymer LPPPA

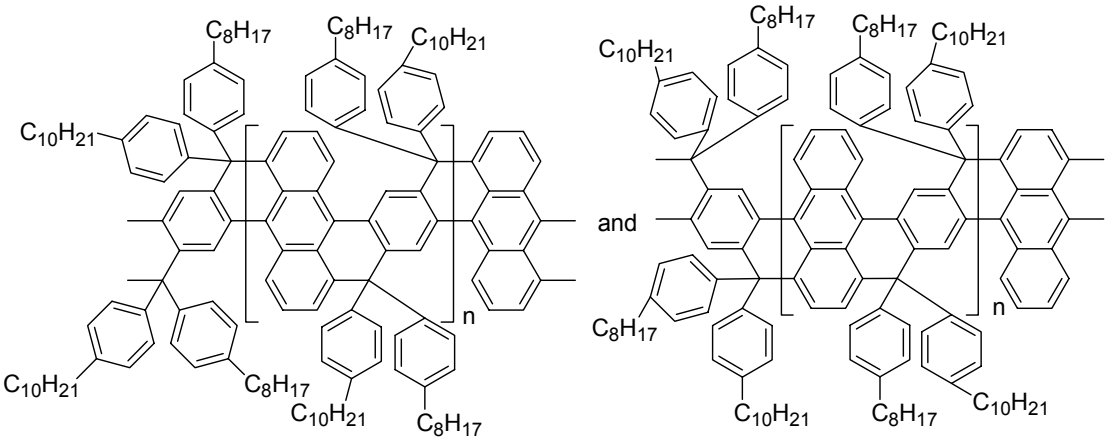

The polyalcohol **43** (0.135 g, 0.12 mmol) was dissolved in dichloromethane (15 mL), and boron trifluoride etherate (0.736 mL) was added with stirring at room temperature. The greenish color solution turned deep brown immediately upon addition. The mixture was stirred for 12 h, then extracted into dichloromethane and washed with water. The organic layer was again washed several times with hydrazine and water. The solvent was removed in *vacuo* and the compound was redissolved in THF (5 mL) and added dropwise to methanol (200 mL). The resulting solid was filtered off and subjected to Soxhlet extraction for 1 day in acetone. Isolated yield of the deep blue polymer **LPPPA** = 130 mg (99.8 %). GPC analysis M_n = 5.77 × 10^3 g/mol, M_w = 8.19 × 10^3 g/mol, and D = 1.42 (against PPP standard); M_n = 7.55 × 10^3 g/mol, M_w = 1.19 × 10^4 g/mol, and D = 1.58 (against PS standard). ^{1}H NMR ($CDCl_3$, 500 MHz): δ 7.91-7.71 (br m, 4H), 7.47-6.50 (br m, 20H), 2.63-2.51 (br m, 8H), 1.51-1.15 (br m, 56H), 0.93-0.72 (br m, 12H). ^{13}C NMR ($CDCl_3$, 125.75 MHz): δ 141.84, 140.18, 131.84, 131.66, 128.64, 128.61, 128.57, 128.38, 127.55, 127.50, 127.40, 126.99, 126.62, 126.57, 125.36, 124.01, 59.40, 35.04, 34.99, 31.37, 30.79, 30.67, 30.53, 29.04, 28.92, 28.84, 28.81, 22.12, 13.48. Elemental analysis: Calculated for $C_{82}H_{100}$: C, 90.72; H, 9.28; Found: C, 90.47; H, 8.99.

Synthesis of 9-bromo-10-phenyl-anthracene.

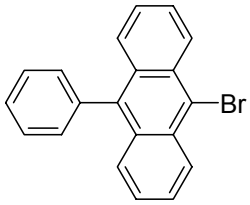

Bromine (3.14 g, 19.65 mmol) in acetic acid (10 mL) was added dropwise over a period of 5 minutes to a vigorously stirred suspension of 9-phenyl-anthracene (5.0 g, 19.65 mmol) in acetic acid (50 mL) at room temperature. The reaction was left to stir for 30 minutes during which a canary yellow precipitate formed. The solution was quenched by the addition of $Na_2S_2O_5$, extracted into diethyl ether, washed with brine and then dried over $MgSO_4$. The crude product was chromatographed on silica using hexane as eluent and further purified by recrystallization from THF in ethanol. Isolated yield = 6.0 g (91 %) as a yellow solid. ^{1}H NMR ($CDCl_3$, 300 MHz): δ 8.32 (d, J = 8.9 Hz, 2H), 7.36 (d, J = 8.7Hz, 2H), 7.29 (m, 3H), 7.08 (m, 4H). ^{13}C NMR ($CDCl_3$, 75.46 MHz): δ 138.35, 137.75, 131.08, 130.99, 130.19, 128.40, 127.80, 127.69, 127.35, 126.89, 125.50, 122.70. FDMS (m/z): 333.1 ($M^{+\bullet}$). Elemental analysis: Calculated for $C_{20}H_{13}Br$: C, 72.09; H, 3.93; Br, 23.98; Found: C, 72.29; H, 3.71.

Synthesis of 4,4,5,5-tetramethyl-2-(10-phenyl-anthracen-9-yl)-dioxaborolane (44).

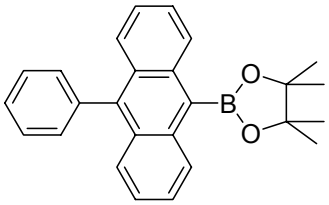

9-Bromo-10-phenyl-anthracene (3.0 g, 9.0 mmol) was dissolved in 60 mL of anhydrous THF in a 250 mL Schlenk flask and cooled to -78 ˚C in an acetone/dry ice bath. To this, 8.43 mL of 1.6 M *n*-butyllithium (13.5 mmol) was added slowly and stirred for 30 minutes. Then 3.12 mL of 2-isopropoxy-4,4,5,5-tetramethyl-1,3,2-dioxaborolane (15.3 mmol) was added and slowly allowed to warm to room temperature. The reaction was stirred overnight and then quenched with brine, the product was extracted into dichloromethane washed again with brine and dried. The crude product was chromatographed on silica gel using 0-10 % ethylacetate in hexane as eluent. Isolated yield = 1.85 g (54 %) as a light yellow solid. . ^{1}H NMR ($CDCl_3$, 300 MHz): δ 8.48 (d, J = 8.7 Hz, 2H), 7.66 (d, J = 8.5 Hz, 2H), 7.59-7.45 (m, 5H), 7.42 (dd, J = 7.8 and 1.7 Hz, 2H), 7.34 (m, 2H), 1.68-1.57 (m, 12H). ^{13}C NMR ($CDCl_3$, 75.46 MHz): δ 139.54, 139.11, 135.36, 131.06, 129.69, 128.36, 128.27, 127.37, 125.38, 124.79, 84.44, 25.20. FDMS

(m/z): 380.1 ($M^{+\bullet}$). Elemental analysis: Calculated for $C_{26}H_{25}BO_2$: C, 82.12; H, 6.63; B, 2.84; O, 8.4; Found: C, 81.99; H, 6.23.

Synthesis of (2,5-di(10-phenylanthracen-9-yl)-1,4-phenylene)di-4'-decylbenzophenone (45)

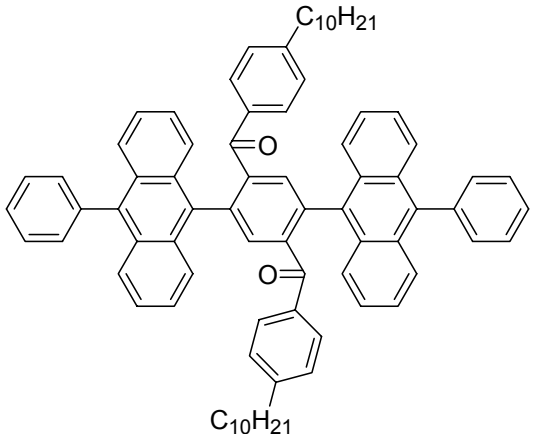

The boronic ester **44** (1.5 g, 3.94 mmol), **41** (1.3 g, 1.79 mmol) was dissolved in THF (20 mL) in a 100 mL Schlenk flask. Aqueous 2 M K_2CO_3 solution (10 mL) was then added and purged with argon for 20 min, then tetrakis(triphenylphosphine)palladium (124 mg, 0.107 mmol) was added and the reaction heated with stirring at 85 ˚C. The reaction was followed by TLC and worked up after 2 days. The cooled mixture was extracted with diethyl ether, washed with brine and then dried over $MgSO_4$. The crude product obtained was purified by chromatography on silica with 0-10 % ethylacetate in hexane as eluent. Isolated yield = 1.5 g (78 %) as a yellow solid. ^{1}H NMR ($CDCl_3$, 300 MHz): δ 8.02 (d, J = 3.7 Hz, 4H), 7.98 (s, 2H), 7.67-7.52 (m, 14H), 7.47-7.38 (m, 12H), 6.85 (d, J = 8.2 Hz, 4H), 2.51-2.40 (m, 4H), 1.30-1.21 (m, 32), 0.88 (t, J = 6.8 Hz, 6H). ^{13}C NMR ($CDCl_3$, 75.46 MHz): δ 196.20, 148.21, 142.91, 138.87, 137.90, 137.77, 134.54, 133.66, 133.21, 131.19, 130.14, 129.64, 129.17, 128.30, 127.66, 127.45, 126.54, 125.62, 124.93, 35.87, 31.86, 31.08, 29.57, 29.46, 29.39, 29.27, 22.65, 14.09. FDMS (m/z): 1071.1 ($M^{+\bullet}$). Elemental analysis: Calculated for $C_{80}H_{78}O_2$: C, 89.68; H, 7.34; O, 2.99; Found: C, 89.87; H, 7.73.

Synthesis of (4-decyl-phenyl)-[4-[(4-decyl-phenyl)-hydroxy-(4-octyl-phenyl)-methyl]-2,5-di-(10-phenyl-anthracen-9-yl)-phenyl]-(4-octyl-phenyl)-methanol (46).

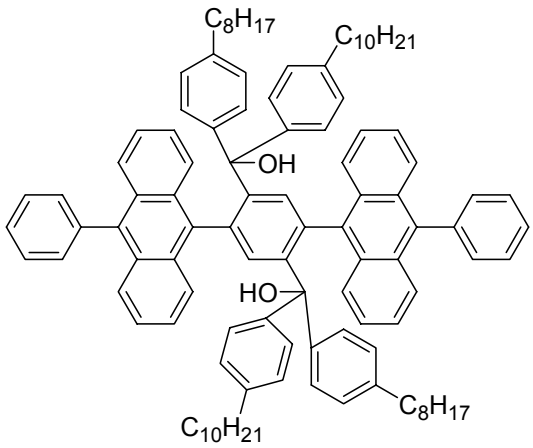

A solution of 4-octylbromobenzene (1.24 mL, 1.38 g, 5.13 mmol) in anhydrous THF (30 mL) in a 250 mL Schlenk flask, was cooled to -78 °C in an acetone/dry ice bath. *n*-Butyllithium in hexane (3.3 mL, 1.6 M, 5.31 mmol) was then added and the mixture was stirred for 20 min. Then a solution of the diketone compound **45** (1.0 g, 0.933 mmol) in anhydrous THF (20 mL) was added dropwise with stirring and the solution was slowly allowed to warm to room temperature. The mixture was stirred overnight and then quenched with 2 M HCl. The crude was extracted into dichloromethane, washed with brine and dried over $MgSO_4$. The crude product obtained was purified by chromatography on silica with 0-10 % ethylacetate in hexane as eluent. Isolated yield = 1.3 g (93 %) as orange solid. ^{1}H NMR ($CDCl_3$, 300 MHz): δ 7.71-7.53 (m, 19H), 7.27-7.17 (m, 10H), 6.98 (dd, J = 21.8 and 8.1Hz, 8H),6.87-6.79 (m, 7H), 2.59-2.40 (m, 8H), 1.52-1.50 (m, 8H), 1.45-1.17 (m, 48H), 0.87 (m, 12H). ^{13}C NMR ($CDCl_3$, 75.46 MHz): δ 145.20, 144.36, 144.02, 143.44, 143.02, 141.78, 141.34, 141.28, 140.83, 139.22, 138.96, 137.48, 137.40, 136.72, 135.85, 135.78, 135.57, 134.86, 133.68, 132.54, 131.30, 129.68, 129.62, 128.35, 127.69, 127.39, 126.99, 126.69, 124.86, 124.82, 83.56, 35.40, 31.89, 31.32, 29.63, 29.55, 29.52, 29.48, 29.44, 29.39, 29.32, 29.27, 29.22, 22.67, 14.10. FDMS (m/z): 1451.2 ($M^{+\bullet}$). Elemental analysis: Calculated for $C_{108}H_{122}O_2$: C, 89.33; H, 8.47; O, 2.20; Found: C, 90.01; H, 8.81.

Synthesis of 9,19-di(4-decylphenyl)-9,19-di(4-octylphenyl)-5,15-diphenyl-9,19-dihydrodinaphtho[3,2,1-*de*:3',2',1'-*op*]pentacene (LMC).

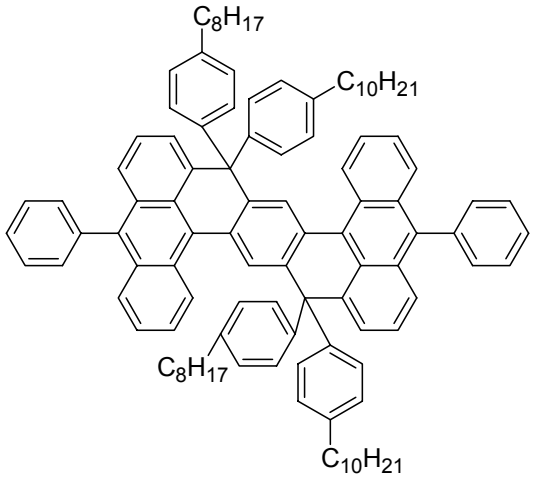

The diol **46** (0.5 g, 0.344 mmol) was dissolved in dichloromethane (15 mL), and boron trifluoride etherate (0.2 mL) was added with stirring at room temperature. The greenish colored solution turned deep brown immediately upon addition and then became dark. The mixture was stirred for 12 h, then extracted into dichloromethane and washed with water. The solvent was removed *in vacuo*, the compound was redissolved in THF (5 mL) and added dropwise to methanol (200 mL). The resulting solid was filtered off and purified by recrystallization from THF in ethanol. Isolated yield = 0.45 g (92 %) as a yellow solid. ^{1}H NMR ($CDCl_3$, 300 MHz): δ 8.06 (d, J = 9.0 Hz, 2H), 7.91 (s, 2H), 7.55 (m, 9H), 7.43 (d, J = 6.5 Hz, 3H), 7.34 (dd, J = 8.7 and 7.0 Hz, 2H), 7.17 (dd, J = 14.7 and 8.0 Hz, 3H), 6.96 (dd, J = 27.3 and 4.5 Hz, 15H), 2.56 (m, 8H), 1.54 (m, 8H), 1.41-1.21 (m, 48H), 0.86 (t, J = 6.7 Hz,12H). ^{13}C NMR ($CDCl_3$, 62.89 MHz): δ 144.35, 142.19, 142.04, 140.78, 139.24, 137.07, 132.71, 131.87, 131.31, 131.25, 130.25, 129.50, 127.53, 127.35, 127.29, 126.99, 126.84, 126.78, 125.46, 124.74, 124.50, 124.42, 60.03, 35.54, 31.87, 31.26, 29.61, 29.57, 29.52, 29.32, 29.23, 22.66, 14.10. FDMS (m/z): 1415.3 ($M^{+\bullet}$). Elemental analysis: Calculated for $C_{108}H_{118}$: C, 91.60; H, 8.40; Found: C, 91.27; H, 8.23.

Synthesis of 9,10-di(4'-decylbenzophenon-2yl)anthracene (47)

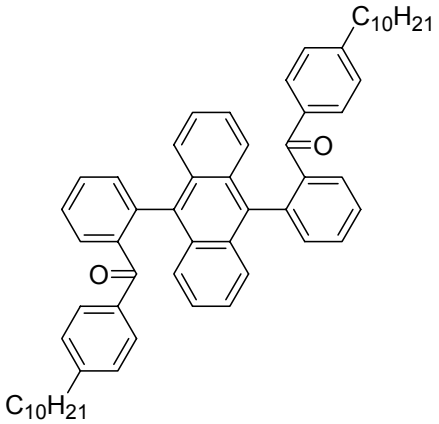

The boronic ester **36** (0.7 g, 1.63 mmol), 2-iodo-4'-decylbenzophenone (1.82 g, 4.07 mmol), and K_2CO_3 (1.1 g, 3.26 mmol) were dissolved in THF (20 mL) and water (10 mL) in a 100 mL Schlenk flask. The solution was purged with argon for 20 min, tetrakis(triphenylphosphine)palladium (230 mg, 0.199 mmol) was added and the reaction followed by TLC and after 16 h was worked up. The cooled mixture was extracted with diethyl ether, washed with brine and then dried over $MgSO_4$. The crude product obtained was purified by chromatography on silica with 0-10 % ethyl acetate in hexane as eluent. Isolated yield = 1.2 g (90 %) as a yellow solid. ^{1}H NMR ($CDCl_3$, 300 MHz): δ 7.55 (ddd, J = 15.0, 8.1, and 5.9 Hz, 6H), 7.40 (m, 4H) ppm 7.31 (dd, J = 7.2 and 1.3 Hz, 2H), 7.20 (d, J = 8.2 Hz, 3H), 7.11 (m, 4H), 7.01 (d, J = 8.2 Hz, 1H), 6.72 (d, J = 8.2 Hz, 3H), 6.61 (d, J = 8.2 Hz, 1H), 2.37-2.23 (m, 4H), 1.48-1.45 (m, 4H), 1.34-1.11 (m, 28H), 0.79 (t, J = 7.6Hz, 6H). ^{13}C NMR ($CDCl_3$, 75.46 MHz): δ 197.54, 147.49, 141.56, 138.05, 135.23, 134.90, 129.65, 129.61, 129.28, 127.72, 126.84, 124.68, 35.81, 35.75, 31.88, 31.18, 31.04, 29.62, 29.57, 29.47, 29.41, 29.32, 29.22, 25.16, 22.66, 14.09. FDMS (m/z): 819.0 ($M^{+\bullet}$). Elemental analysis: Calculated for $C_{60}H_{66}O_2$: C, 87.97; H, 8.12; O, 3.91; Found: C, 88.02; H, 8.32.

Synthesis of (4-decyl-phenyl)-[2-(10-{2-[(4-decyl-phenyl)-hydroxy-(4-octyl-phenyl)-methyl]-phenyl}-anthracen-9-yl)-phenyl]-(4-octyl-phenyl)-methanol (48)

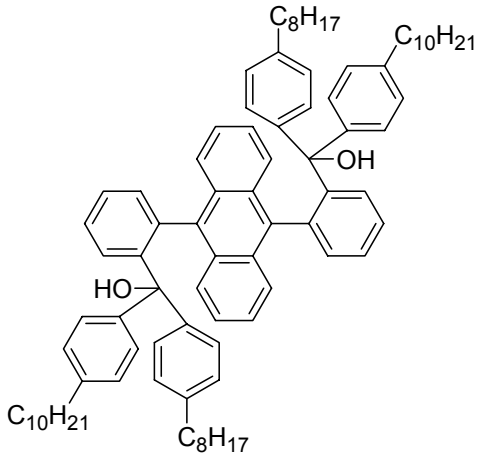

A solution of 4-octylbromobenzene (0.92 ml, 1.02 g, 3.78 mmol) in 20 mL of anhydrous THF (20 mL) in a 250 mL Schlenk flask, was cooled to -78 °C in an acetone/dry ice bath. *n*-Butyllithium in hexane (2.46 mL, 1.6 M, 3.93 mmol) was then added and the mixture was stirred for 20 min. Then a solution of the diketone **47** (597 mg, 0.728 mmol) in anhydrous THF (20 mL) was added dropwise with stirring and the solution was slowly allowed to warm to room temperature. The mixture was stirred overnight and then quenched with brine. The mixture was extracted into diethyl ether, washed with brine and dried over $MgSO_4$. The crude product obtained was purified by chromatography on silica with 0-10 % ethyl acetate in hexane as eluent. Isolated yield = 0.78 g (88 %) as a thick viscous greenish oil. ^{1}H NMR ($CDCl_3$, 300 MHz): δ 7.42 (dd, J = 5.9 and 3.3 Hz, 2H), 7.38 (m, 2H), 7.27-7.19 (m, 12H), 7.00-6.91 (m, 13H), 6.89-6.71 (m, 3H), 2.51-2.43 (m, 8H), 1.58-1.45 (m, 8H), 1.34-1.11 (m, 48H), 0.79 (t, J = 7.1Hz, 12H). ^{13}C NMR ($CDCl_3$, 75.46 MHz): δ 146.61, 144.69, 143.87, 141.30, 140.85, 140.77, 139.57, 137.36, 136.82, 134.38, 129.55, 129.09, 128.87, 127.94, 127.81, 127.73, 127.66, 127.61, 127.22, 126.90, 126.71, 126.26, 125.66, 125.01, 124.23, 83.67, 35.57, 35.43, 31.91, 31.49, 31.25, 29.66, 29.61, 29.59, 29.49, 29.45, 29.33, 29.27, 22.68, 14.10. FDMS (m/z): 1199.8 ($M^{+\bullet}$). Elemental analysis: Calculated for $C_{88}H_{110}O_2$: C, 88.09; H, 9.24; O, 2.67; Found: C, 88.37; H, 9.53.

Synthesis of 8,16-di-(4-decyl-phenyl)-8,16-di-(4-octyl-phenyl)-8,16-dihydro-dibenzo[*a,j*]perylene (SLMC)

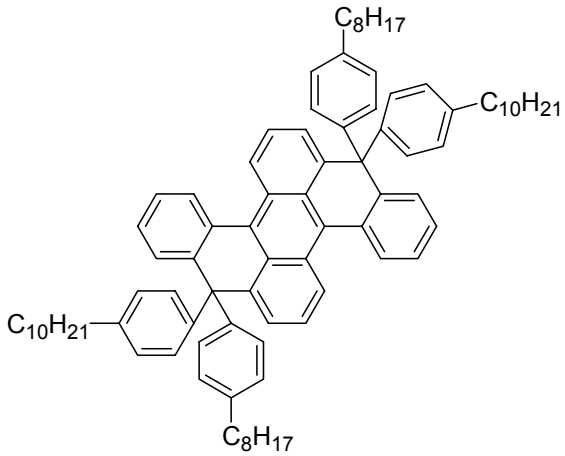

The diol **48** (0.776 g, 0.647 mmol) was dissolved in dichloromethane (15 mL), and boron trifluoride etherate (0.2 mL) was added with stirring at room temperature. The greenish colored solution turned deep brown immediately upon addition and subsequently became a dark solution. The mixture was stirred for 12 h, methanol (50 mL) was added into the solution and the solid filtered. The crude product was washed with methanol and dried. Isolated yield = 0.69 g (92 %) as a thick viscous, reddish oil. ^{1}H NMR ($CDCl_3$, 300 MHz): δ 8.52 (dd, J =6.7 and 3.3 Hz, 2H), 8.06 (d, J = 7.8 Hz, 2H), 7.35 (dt, J = 5.8 and 2.5Hz, 5H), 7.13 (dd, J = 7.8 and 1.3 Hz, 3H), 7.21-7.11 (m, 9H), 6.99-6.75 (m, 9H), 2.57-2.41 (m, 8H), 1.57-1.41 (m, 8H), 1.37-1.21 (m, 48H), 0.87 (t, J = 5.7 Hz, 12H. ^{13}C NMR ($CDCl_3$, 62.89 MHz): δ 144.93, 141.11, 139.82, 134.63, 131.17, 129.72, 129.34, 129.12, 127.74, 127.62, 127.54, 126.52, 126.19, 125.26, 60.17, 35.69, 32.16, 32.13, 31.51, 29.87, 29.76, 29.71, 29.59, 22.94, 14.37. FDMS (m/z): 1162.9 ($M^{+\bullet}$). Elemental analysis: Calculated for $C_{88}H_{106}$: C, 90.82; H, 9.18; Found: C, 90.53; H, 8.99.

General procedure for the synthesis of benzoyl chlorides. A flask equipped with a reflux condenser and a drying tube was charged with benzoic acid and benzene (50 mL). To this mixture was added oxalyl chloride (1.5 equiv) and one drop of N,N-dimethylformamide (catalyst). The reaction mixture was heated at 80 ˚C overnight (bubbling observed), then the reaction was cooled and the solvent was removed *in vacuo*. The crude solid was dissolved in benzene (20 mL) and stirred with calcium hydride for 1 h and filtered. The benzene was removed *in vacuo* to give the benzoyl chloride compound.

General procedure for Ullmann coupling. To the halide compound in anhydrous N,N-dimethylformamide, copper powder (2.3 equiv) was added under argon and heated at 120 ℃ for 12-24 h. The mixture was filtered and extracted into ether, washed with brine and dried over $MgSO_4$. The crude product was then chromatographed on silica gel using

an appropriate eluent.

General Procedure for Yamamoto polycondensation. Bis(cyclooctadiene)nickel (2.4 equiv), cyclooctadiene (2.4 equiv), and 2,2'-bipyridine (2.4 equiv) were dissolved in anhydrous toluene (3.5-5 mL) and anhydrous N,N-dimethylformamide (3.5-5 mL) in a Schlenk flask within a glovebox. The mixture was heated at 60 ℃ with stirring under argon for 20 min to generate the catalyst, and a solution of the monomer in anhydrous toluene (7-10 mL) was added. The reaction was heated at 75 ℃ for 2 days. Then a solution of toluene (2-4 mL) and bromobenzene (0.10 mL) was added and heated at 75 ℃ for an additional 12 h. This was then poured into a mixture of methanol and concentrated HCl (1:1, 300 mL) and stirred for 4 h. The precipitated solid was redissolved in THF (10 mL) and added dropwise to methanol (200 mL). The resulting solid was filtered off and subjected to a Soxhlet extraction for 2 days in acetone. The residue was then redissolved in THF and precipitated again from methanol, filtered, washed with methanol, and dried.

General Procedure for Friedel-Crafts acylation. To the benzoyl chloride in 20 mL of dichloromethane, aluminum chloride (1.5 equiv) and decyl benzene (1.9 equiv) were added, stirred at room temperature for 12-18 h and quenched with aqueous 2 M HCl. The mixture was extracted into dichloromethane and washed with brine. The crude product was then chromatographed on silica gel with an appropriate eluent.

General Procedure the cyclization of dibenzoylbiphenyl units. A solution of boron trichloride in methylene chloride (1.0 M, 2.0 equiv) was introduced to a mixture of the dibenzoylbiphenyl derivative and tricyclohexyltin sulfide (2.2 equiv) in anhydrous toluene at room termperature under argon. After stirring for 10 min at room temperature, the mixture was heated at 110 ℃ overnight. The reaction was then quenched by adding 2 M HCl and extracted with diethyl ether and washed with brine. The crude product was chromatographed on silica gel using hexane as eluent and further purified by two recrystallizations from THF in ethanol and subsequently from dichloromethane in ethanol.

Synthesis of 2',5'-dibromo-undecylphenone (49)

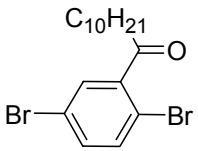

To a solution of *tert*-butyllithium (48.9 ml, 84.0 mmol, 1.7 M in pentane) in anhydrous

ether (30 mL) at -78 ℃ was added 1-iododecane (10 ml, 30 mmol) dropwise. This solution was stirred for 1 h at -78 ℃. The cooling bath was removed and the slurry was transferred via cannula to a slurry of copper(I) cyanide (4.83 g, 54.0 mmol) in anhydrous THF (105 mL) at -78 ℃. The reaction mixture was allowed to stir for 4h, then 2,5-dibromo-benzoyl chloride (7.45 g, 25 mmol) in anhydrous THF (60 mL) was cooled to 0 ℃ and added via cannula to the -78 ℃ solution and the mixture stirred for 1 h at this temperature. The reaction was then quenched by the addition of a 9:1 mixture of saturated ammonium chloride and ammonium hydroxide solution and the mixture was filtered. The aqueous layer was extracted with ether, washed with brine and dried over $MgSO_4$. The crude product was chromatographed on silica gel using 0-5% ethylacetate in hexane as eluent and further purified by recrystallization from hexane. Isolated yield = 7.0 g (70 %) as colorless needlelike crystals. ^{1}H NMR ($CDCl_3$, 300 MHz): δ 7.42 (ddd, *J* = 10.8, 7.0, and 2.7 Hz, 3H), 2.90 (t, *J* = 7.2 Hz, 2H), 1.77-1.61 (m, 2H), 1.55-1.29 (m, 14H), 0.88 (t, *J* = 6.5 Hz, 3H). ^{13}C NMR ($CDCl_3$, 75.46 MHz): δ 202.61, 143.19, 134.56, 133.77, 130.62, 120.98, 116.73, 42.28, 31.44, 29.10, 29.00, 28.92, 28.85, 28.69, 23.50, 22.23, 13.67. FDMS (m/z): 404.2 ($M^{+\bullet}$). Elemental analysis: Calculated for $C_{17}H_{24}Br_2O$: C, 50.52; H, 5.99; Br, 39.54; O, 3.96; Found: C, 50.77; H, 5.53.

Synthesis of 4,4'-dibromo-2,2'-di(undecyloyl)-1,1'-biphenyl (50)

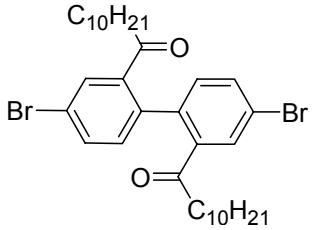

Compound **49** (6.0 g, 14.8 mmol) was used in the Ullmann coupling and purified by chromatography on silica with 0-25 % dichloromethane in hexane as eluent. Isolated yield = 2.1 g (43 %) as a yellow oil. ^{1}H NMR ($CDCl_3$, 300 MHz): δ 7.78 (d, *J* = 2.0 Hz, 2H), 7.59 (d, *J* = 2.0 Hz, 1H), 7.56 (d, *J* = 2.0 Hz, 1H), 6.99 (d, *J* = 8.2 Hz, 2H), 2.69-2.53 (m, 4H), 1.60-1.41 (m, 4H), 1.35-1.15 (m, 28H), 0.89 (m, 6H). ^{13}C NMR ($CDCl_3$, 75.46 MHz): δ 202.27, 139.96, 137.92, 133.38, 131.92, 130.79, 121.57, 41.01, 31.64, 29.30, 29.20, 29.10, 29.05, 28.82, 23.71, 22.42, 13.86. FDMS (m/z): 648.5 ($M^{+\bullet}$). Elemental analysis: Calculated for $C_{34}H_{48}Br_2O_2$: C, 62.97; H, 7.46; Br, 24.64; O, 4.93; Found: C, 63.09; H, 7.95.

Polymer (51)

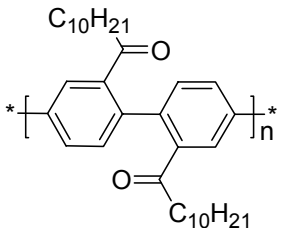

The dibromide **50** (428 mg, 0.66 mmol) was used in the Yamamoto polycondensation. Isolated yield of polymer **51** = 250 mg (78 %). GPC analysis $M_n = 2.32 \times 10^4$ g/mol, $M_w = 4.25 \times 10^4$ g/mol, and D = 1.82 (against PPP standard); $M_n = 3.67 \times 10^4$ g/mol, $M_w = 8.17 \times 10^4$ g/mol, and D = 2.23 (against PS standard). ^{1}H NMR ($CDCl_3$, 300 MHz): δ 8.10-7.72 (br m, 5H), 7.45-7.30 (br m, 1H), 2.80-2.65 (br m, 4H), 1.67-1.50 (br m, 4H), 1.45-1.21 (br m, 28H), 0.97-0.73 (br m, 6H). ^{13}C NMR (THF-d_8, 75.46 MHz): δ 203.92, 141.73, 140.29, 132.53, 129.45, 127.31, 42.36, 32.87, 30.58, 30.53, 30.29, 23.57, 14.47. Elemental analysis: Calculated for $C_{34}H_{48}O_2$: C, 83.55; H, 9.90; O, 6.55; Found: C, 83.99; H, 9.33.

Polymer 2,7-PKP

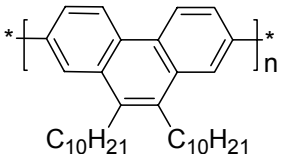

$TiCl_3$ (0.23 g, 1.47 mmol) was added to a Schlenk flask in a glovebox along with 10 mL of anhydrous THF and $LiAlH_4$ (0.75 mL, 1.0 M in THF) and the mixture was then heated at reflux for 1 h. The reaction was cooled to room temperature, a solution of polymer **51** (30 mg, 0.06 mmol) in anhydrous THF (10 mL) was slowly added and heated at reflux for 3 days. This was then poured into a mixture of methanol and 2 M HCl (1:1, 300 mL) and stirred for 4 h. The precipitated solid was redissolved in THF (20 mL) and added dropwise to methanol (200 mL). The resulting solid was filtered off and subjected to a Soxhlet extraction for 1 day in acetone and dried. Isolated yield of polymer **2,7-PKP** = 27 mg (95 %).GPC analysis $M_n = 4.68 \times 10^4$ g/mol, $M_w = 9.78 \times 10^4$ g/mol, and D = 2.09 (against PPP standard); $M_n = 8.11 \times 10^4$ g/mol, $M_w = 2.12 \times 10^5$ g/mol, and D = 2.61 (against PS standard). ^{1}H NMR ($CDCl_3$, 300 MHz): δ 9.10-8.52 (br m, 2H), 8.30-7.50 (br m, 6H), 3.35-3.10 (br m, 4H), 1.77-1.25 (br m, 32H), 0.95-0.87 (br m, 6H). ^{13}C NMR ($CDCl_3$, 75.46 MHz): δ 140.37, 139.95, 133.96, 130.48, 129.96, 127.72, 31.93, 30.81, 30.43, 29.72, 29.57, 29.38, 22.69, 14.12. Elemental analysis: Calculated for $C_{34}H_{48}$: C, 89.41; H, 10.59; Found: C, 89.21; H, 10.72.

Synthesis of 2'-bromo-undecylphenone (52).

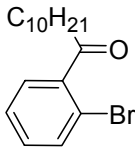

2-bromo-benzoyl chloride (11.9 mL, 91.1 mmol) was used according to the procedure for **1** and purified by chromatography on silica with 0-5 % ethylacetate in hexane as eluent. Isolated yield = 24.7 g (83 %) as a yellow solid. ^{1}H NMR ($CDCl_3$, 300 MHz): δ 7.62 (d, *J* = 7.8 Hz, 1H), 7.38 (d, *J* = 4.8 Hz, 2H), 7.30 (q, *J* = 3.6 Hz, 1H), 2.95 (t, *J* = 7.2 Hz, 2H), 1.75-1.62 (m, 2H), 1.40-1.21 (m, 14H), 0.91 (t, *J* = 5.2 Hz, 3H). ^{13}C NMR ($CDCl_3$, 75.46 MHz): δ 205.03, 141.60, 133.06, 130.75, 127.72, 126.84, 118.05, 42.26, 31.39, 29.21, 29.06, 28.97, 28.81, 28.66, 23.58, 22.18, 13.61. FDMS (m/z): 325.3 ($M^{+\bullet}$). Elemental analysis: Calculated for $C_{17}H_{25}BrO$: C, 62.77; H, 7.75; Br, 24.56; O, 4.92; Found: C, 62.29; H, 7.73.

Synthesis of 2,2'-di(undecyloyl)-1,1'-biphenyl (53)

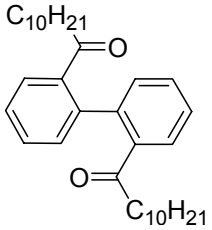

The compound **52** (10.0 g, 30.7 mmol) was used in the Ullmann coupling and purified by chromatography on silica with 0-33 % dichloromethane in hexane as eluent. Isolated yield = 4.2 g (55 %) as a yellow oil. ^{1}H NMR ($CDCl_3$, 300 MHz): δ 7.64 (dd, *J* = 6.1 and 2.9 Hz, 2H), 7.43 (m, 4H), 7.14 (m, 2H), 2.64-2.47 (m, 4H), 1.55-1.41 (m, 4H), 1.30-1.11 (m, 28H), 0.89 (m, 6H). ^{13}C NMR ($CDCl_3$, 75.46 MHz): δ 204.78, 139.81, 139.27, 130.57, 130.27, 127.83, 127.37, 41.46, 31.67, 29.33, 29.23, 29.12, 29.08, 28.91, 23.99, 22.45, 13.88. FDMS (m/z): 490.7 ($M^{+\bullet}$). Elemental analysis: Calculated for $C_{34}H_{50}O2$: C, 83.21; H, 10.27; O, 6.52; Found: C, 83.51; H, 9.99.

Synthesis of 9 3,6-dibromo-9,10-di-decyl-phenanthrene (54)

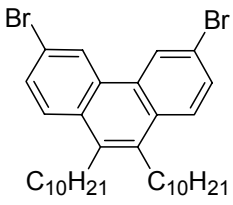

$TiCl_3$ (2.38 g, 15.5 mmol) was added to a Schlenk flask in a glove box along with 10 mL of anhydrous THF and 7.74 mL of $LiAlH_4$ (1.0 M in THF). The mixture was heated at reflux for 1 h and cooled to room temperature. A solution of **53** (3.8 g, 7.74 mmol) in anhydrous THF (10 mL) was slowly added and heated at reflux for 16 h. The reaction was then quenched by adding 2 M HCl, and extracted with dichloromethane. The organic layers were dried over $MgSO_4$, and the solvent was evaporated. The crude product was chromatographed on silica gel using hexane as eluent. Isolated yield = 2.5 g (70 %) as colorless needlelike crystals. ^{1}H NMR ($CDCl_3$, 300 MHz): δ 8.74 (d, *J* = 9.6 Hz, 2H), 8.13 (d, *J* = 9.6 Hz, 2H), 7.61 (m, 4H), 3.15 (t, *J* = 7.8 Hz, 4H), 1.71-1.55 (m, 4H), 1.52-1.31 (m, 28H), 0.95-0.82 (m, 6H). ^{13}C NMR ($CDCl_3$, 75.46 MHz): δ 133.70, 131.14, 129.59, 126.30, 125.10, 124.45, 122.70, 31.72, 20.52, 30.22, 29.51, 29.47, 29.35, 29.17, 22.49, 13.91. FDMS (m/z): 458.7 ($M^{+\bullet}$). Elemental analysis: Calculated for $C_{34}H_{50}$: C, 89.01; H, 10.99; Found: C, 89.37; H, 11.02.

The bromination was performed using a solution of 9,10-di-decyl-phenanthrene (580 mg, 1.26 mmol) and catalytic amounts of iodine in 10 mL CCl_4. To this mixture, bromine (0.3 g, 1.87 mmol) was added dropwise at 0 ˚C. The reaction mixture was slowly allowed to warm to room temperature overnight. Additional bromine (0.05 g, 0.31 mmol) was then added with stirring and the reaction was monitored by FDMS, which showed nearly quantitative formation of the dibromide after 12 h. The reaction was quenched by the addition of aqueous $Na_2S_2O_5$ solution and extracted into dichloromethane, washed with brine and dried over $MgSO_4$. The crude product was chromatographed on silica gel using hexane as eluent and further purified by recrystallization from THF in ethanol. Isolated yield = 420 mg (54 %) as colorless needlelike crystals. ^{1}H NMR ($CDCl_3$, 300 MHz): δ 8.70 (d, *J* = 1.9 Hz, 2H), 7.92 (d, *J* = 8.9 Hz, 2H), 7.70 (dd, *J* = 8.9 and 1.9 Hz, 2H), 3.06 (t, *J* = 8.6 Hz, 4H), 1.70-1.50 (m, 4H), 1.47-1.21 (m, 28H), 0.97-0.85 (m, 6H). ^{13}C NMR ($CDCl_3$, 75.46 MHz): δ 133.77, 129.90, 129.80, 126.12, 125.27, 119.59, 31.48, 30.22, 29.89, 29.21, 29.07, 28.93, 22.26, 13.68. FDMS (m/z): 616.5 ($M^{+\bullet}$). Elemental analysis: Calculated for $C_{34}H_{48}Br_2$: C, 66.23; H, 7.85; Br, 25.92; Found: C, 66.57; H, 7.43.

Polymer 3,6-PKP

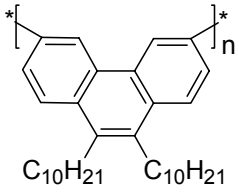

The dibromide **54** (262 mg, 0.425 mmol) was used in the Yamamoto polycondensation. Isolated yield of polymer **3,6-PKP** = 120 mg (62 %). GPC analysis M_n = 3.15 × 10^3

g/mol, M_w = 5.10 × 10^3 g/mol, and D = 1.62 (against PPP standard); M_n = 3.68 × 10^3 g/mol, M_w = 7.21 × 10^3 g/mol, and D = 1.96 (against PS standard). ^{1}H NMR ($CDCl_3$, 300 MHz): δ 9.35-9.00 (br m, 2H), 8.25-7.95 (br m, 4H), 3.29-32.95 (br m, 4H), 1.85-1.10 (br m, 32H), 1.02-0.78 (br m, 6H). Elemental analysis: Calculated for $C_{34}H_{48}$: C, 89.41; H, 10.59; Found: C, 89.25; H, 10.73.

Synthesis of 4-chloro-2-iodo-4'-decylbenzophenone (55)

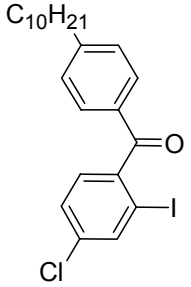

4-Chloro-2-iodo-benzoyl chloride (2.5 g, 8.31 mmol) was used in the Friedel-Crafts acylation and purified by chromatography on silica with 0-5 % ethylacetate in hexane as eluent. Isolated yield = 3.7 g (92 %) as a yellow oil. ^{1}H NMR ($CDCl_3$, 300 MHz): δ 7.99 (d, *J* = 1.9 Hz, 1H), 7.77 (d, *J* = 8.3 Hz, 2H), 7.48 (dd, *J* = 8.2 and 1.9 Hz, 1H), 7.31 (t, *J* = 8.3 Hz, 3H), 2.73 (t, *J* = 7.8 Hz, 2H), 1.77-1.63 (m, 2H), 1.45-1.27 (m, 14H), 0.94 (t, *J* = 6.9 Hz, 3H). ^{13}C NMR ($CDCl_3$, 75.46 MHz): δ 195.33, 149.39, 142.36, 138.54, 135.43, 132.43, 129.99, 128.60, 128.22, 127.46, 92.03, 35.55, 31.30, 30.43, 29.00, 28.95, 28.85, 28.72, 22.09, 13.53. FDMS (m/z): 482.8 ($M^{+\bullet}$). Elemental analysis: Calculated for $C_{23}H_{28}ClIO$: C, 57.21; H, 5.85; Cl, 7.34; I, 26.28; O, 3.31; Found: C, 57.57; H, 5.73.

Synthesis of 5,5'-dichloro-2,2'-di(4-decyl-benzoyl)-1,1'-biphenyl (56)

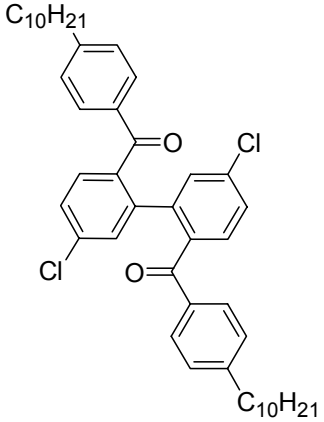

Compound **55** (3.5 g, 7.26 mmol) was used in the Ullmann coupling and purified by chromatography on silica with 0-7 % ethylacetate in hexane as eluent and further purified by two recrystallizations from hexane in ethanol. Isolated yield = 1.7 g (66 %) as a

yellow solid. ^{1}H NMR ($CDCl_3$, 300 MHz): δ 7.51 (d, J = 8.2 Hz, 4H), 7.37 (t, J = 1.2 Hz, 2H), 7.30 (d, J = 1.2 Hz, 4H), 7.31 (d, J = 8.2 Hz, 4H), 2.53 (t, J = 7.9 Hz, 4H), 1.62-1.51 (m, 4H), 1.37-1.21 (m, 28H), 0.88 (t, J = 6.9 Hz, 6H). ^{13}C NMR ($CDCl_3$, 75.46 MHz): δ 195.37, 148.50, 140.92, 136.40, 136.06, 134.26, 131.10, 130.50, 130.21, 127.79, 126.88, 35.79, 31.69, 30.87, 29.41, 29.38, 29.26, 29.12, 22.47, 13.89. FDMS (m/z): 710.8 ($M^{+\bullet}$). Elemental analysis: Calculated for $C_{46}H_{56}Cl_2O_2$: C, 77.61; H, 7.93; Cl, 9.96; O, 4.50; Found: C, 77.28; H, 9.71.

Synthesis of 3,6-dichloro-9,10-di-(4-decyl-phenyl)-phenanthrene (57)

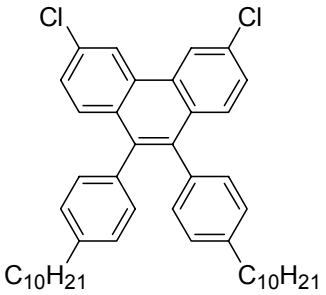

The compound **56** (1.5 g, 2.11 mmol) was used in the cyclization procedure. Isolated yield = 1.2 g (83 %) as colorless needlelike crystals. ^{1}H NMR ($CDCl_3$, 300 MHz): δ 8.64 (d, J = 2.0 Hz, 2H), 7.55 (d, J = 8.8 Hz, 2H), 7.44 (d, J = 8.8 and 2.0 Hz, 2H), 7.01 (q, J = 8.0Hz, 8H), 2.55 (t, J = 7.8 Hz, 4H), 1.77-1.60 (m, 4H), 1.35-1.20 (m, 28H), 0.88 (t, J = 6.8 Hz, 6H). ^{13}C NMR ($CDCl_3$, 75.46 MHz): δ 141.19, 137.21, 135.91, 132.69, 130.80, 130.69, 130.09, 129.65, 127.65, 127.51, 122.07, 33.81, 31.93, 31.11, 29.67, 29.37, 29.16, 28.80, 26.74, 22.69, 14.11. FDMS (m/z): 679.1 ($M^{+\bullet}$). Elemental analysis: Calculated for $C_{46}H_{56}Cl_2$: C, 81.27; H, 8.30; Cl, 10.43; Found: C, 81.65; H, 8.75.

Polymer (58)

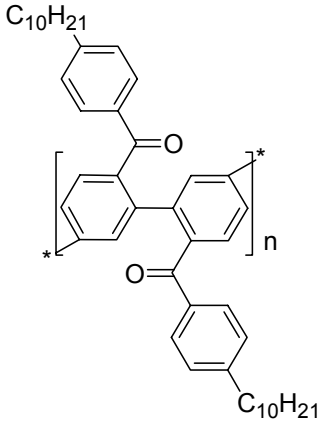

The dichloride **56** (468 mg, 0.66 mmol) was used in the Yamamoto polycondensation.

Isolated yield of polymer **58** = 300 mg (74 %). GPC analysis M_n = 2.14 × 10^3 g/mol, M_w = 4.68 × 10^3 g/mol, and D = 1.25 (against PPP standard); M_n = 2.50 × 10^3 g/mol, M_w = 3.25 × 10^3 g/mol, and D = 1.30 (against PS standard). ^{1}H NMR ($CDCl_3$, 300 MHz): δ 8.30-7.89 (br m, 2H), 7.87-7.35 (br m, 4H), 7.11-6.85 (br m, 8H), 2.65-2.50 (br m, 4H), 1.65-1.30 (br m, 4H), 1.29-1.21 (br m, 28H), 0.91-0.82 (br m, 6H). Elemental analysis: Calculated for $C_{46}H_{56}O_2$: C, 86.20; H, 8.81; O, 4.99; Found: C, 86.29; H, 8.71.

Polymer 3,6-PAP

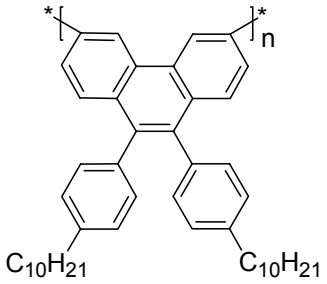

The dichloride monomer **57** (448 mg, 0.66 mmol) was used in the Yamamoto polycondensation. Isolated yield of polymer **3,6-PAP** = 230 mg (57 %). GPC analysis M_n = 3.25 × 10^3 g/mol, M_w = 4.66 × 10^3 g/mol, and D = 1.44 (against PPP standard); M_n = 3.92 × 10^3 g/mol, M_w = 6.29 × 10^3 g/mol, and D = 1.61 (against PS standard). ^{1}H NMR ($CDCl_3$, 300 MHz): δ 9.81-9.11 (br m, 1H), 8.21-7.71 (br m, 4H), 7.21-6.69 (br m, 9H), 2.67-2.51 (br m, 4H), 1.67-1.21 (br m, 32H), 0.95-0.83 (br m, 6H). Elemental analysis: Calculated for $C_{46}H_{56}$: C, 90.73; H, 9.27; Found: C, 90.77; H, 9.73.

Synthesis of MCT

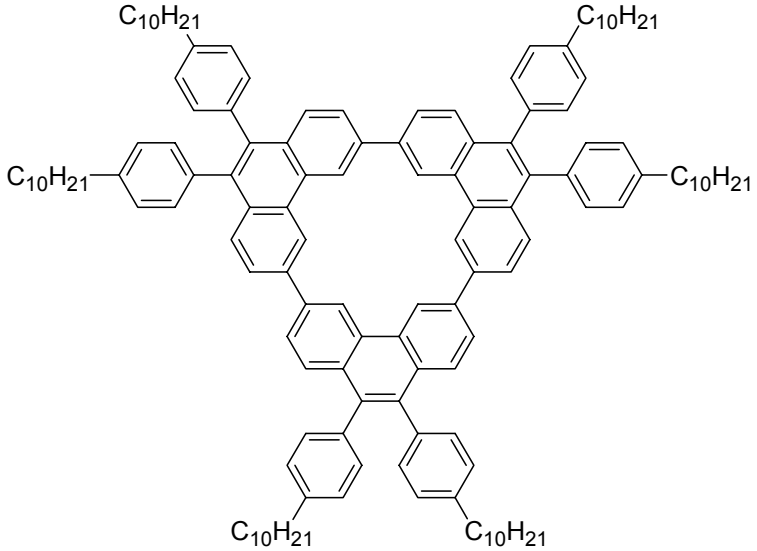

Bis(cyclooctadiene)nickel (430 mg, 1.584 mmol, 2.4 equiv.), cyclooctadiene (192 mL,

1.584 mmol, 2.4 equiv.), and 2,2'-bipyridine (244 mg, 1.584 mmol, 2.4 equiv.) were dissolved in dry toluene (40 mL) and dry *N,N*-dimethylformamide (20 mL) in a Schlenk flask in a glovebox. The mixture was heated at 60 ˚C with stirring under argon for 20 min to generate the catalyst, and then a solution of the 3,6-dichlorophenanthrene (448 mg, 0.66 mmol) in dry toluene (10 mL) was added. The reaction was heated at 75 ˚C for 2 days. The cooled mixture was extracted with dichloromethane, washed with brine and then dried over $MgSO_4$. The crude product was chromatographed on silica using 0-25 % dichloromethane in hexane as eluent. Isolated yield = 50 mg (12 %) as a light yellow solid. ^{1}H NMR ($CDCl_3$, 300 MHz): δ 9.83 (s, 6H), 8.18 (d, *J* = 8.8Hz, 6H), 7.80 (d, *J* = 8.6Hz, 6H), 7.10 (q, *J* = 8.3Hz, 24H), 2.60 (t, *J* = 7.6Hz, 12H), 1.71-1.61 (m, 12H), 1.39-1.25 (m, 84H), 0.90 (t, *J* = 6.7Hz, 18H). ^{13}C NMR ($CDCl_3$, 75.46 MHz): δ 140.51, 136.74, 136.14, 135.07, 131.56, 130.57, 129.96, 127.14, 35.24, 31.54, 30.96, 29.29, 29.16, 28.99, 28.82, 22.30, 13.71. FDMS (m/z): 1825.0 ($M^{+\bullet}$). Elemental analysis: Calculated for $C_{138}H_{168}$: C, 90.73; H, 9.27; Found: C, 90.57; H, 9.53.

Synthesis of 2-iodo-4'-decylbenzophenone (59)

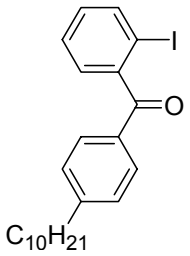

2-Iodo-benzoyl chloride (5.0 g, 18.7 mmol) was used in the Friedel-Crafts acylation and purified by chromatography on silica with 0-10 % ethylacetate in hexane as eluent. Isolated yield = 8.1 g (96 %) as a yellow oil. ^{1}H NMR ($CDCl_3$, 300 MHz): δ 7.92 (dd, *J* = 7.9 and 0.9 Hz, 1H), 7.74 (d, *J* = 8.3 Hz, 2H), 7.43 (dt, *J* = 7.5, 1.1 Hz, 1H), 7.28 (m, 3H), 7.16 (dt, *J* = 7.8 and 1.7 Hz, 1H), 2.68 (t, *J* = 7.7 Hz, 2H), 1.71-1.60 (m, 2H), 1.37-1.27 (m, 14H), 0.89 (t, *J* = 6.7 Hz, 18H). ^{13}C NMR ($CDCl_3$, 75.46 MHz): δ 196.64, 149.53, 144.53, 139.49, 133.16, 130.80, 130.51, 128.60, 128.23, 127.59, 92.15, 36.02, 31.78, 30.91, 29.48, 29.44, 29.34, 29.20, 29.18, 22.57, 14.03. FDMS (m/z): 448.1 ($M^{+\bullet}$). Elemental analysis: Calculated for $C_{23}H_{29}IO$: C, 61.61; H, 6.52; I, 28.30; O, 3.57; Found: C, 61.37; H, 6.73.

Synthesis of 2'-di(4-decyl-benzoyl)-1,1'-biphenyl (60)

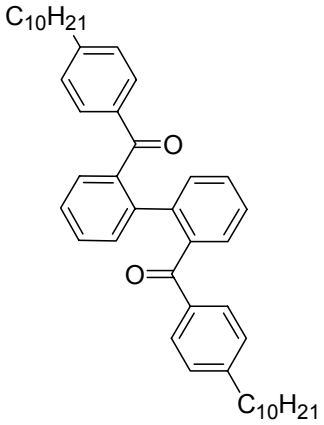

Compound **59** (8.0 g, 17.8 mmol) was used in the Ullmann coupling and purified by chromatography on silica with 0-10 % ethylacetate in hexane as eluent. Isolated yield = 5.2 g (90 %) as a red solid. ^{1}H NMR ($CDCl_3$, 300 MHz): δ 7.63 (d, *J* = 8.2 Hz, 4H), 7.45-7.35 (m, 8H), 7.05 (d, *J* = 8.2 Hz, 4H), 2.55 (t, *J* = 7.7 Hz, 4H), 1.67-1.57 (m, 4H), 1.37-1.27 (m, 28H), 0.89 (t, *J* = 6.7Hz, 6H). ^{13}C NMR ($CDCl_3$, 75.46 MHz): δ 197.01, 148.16, 139.87, 138.31, 134.78, 131.23, 130.34, 129.59, 129.00, 127.76, 126.37, 35.77, 31.68, 30.84, 29.39, 29.36, 29.25, 29.10, 22.46, 13.89. FDMS (m/z): 642.5 ($M^{+\bullet}$). Elemental analysis: Calculated for $C_{46}H_{58}O_2$: C, 85.93; H, 9.09; O, 4.98; Found: C, 85.59; H, 9.51.

Synthesis of 3,6-dibromo-9,10-di-(4-decyl-phenyl)-phenanthrene (61)

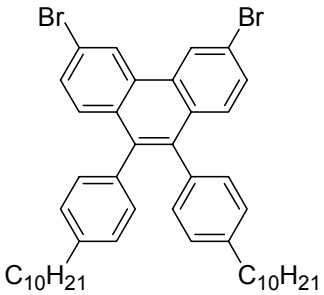

The compound **60** (2.5 g, 3.89 mmol) was used in the cyclization procedure. Isolated yield = 2.2 g (93 %) as colorless needlelike crystals. ^{1}H NMR ($CDCl_3$, 300 MHz): δ 8.80 (d, *J* = 8.1 Hz, 2H), 7.65 (d, *J* = 8.1 Hz, 4H), 7.48 (d, *J* = 8.2 Hz, 2H), 7.02 (s, 8H), 2.56 (t, *J* = 7.8 Hz, 4H), 1.77-1.53 (m, 4H), 1.47-1.27 (m, 28H), 0.89 (t, *J* = 6.9Hz, 6H). ^{13}C NMR ($CDCl_3$, 75.46 MHz): δ 140.54, 137.14, 136.55, 131.86, 130.68, 129.72, 127.70, 127.27, 126.25, 125.98, 122.20, 35.40, 33.62, 31.74, 30.91, 29.48, 29.18, 28.60, 26.54, 22.50, 13.91. FDMS (m/z): 610.5 ($M^{+\bullet}$). Elemental analysis: Calculated for $C_{46}H_{58}$: C, 90.43; H, 9.57; Found: C, 90.58; H, 9.70.

The bromination was performed by the procedure described above (compound **54**). Isolated yield = 500 mg (41 %) as colorless needlelike crystals. ^{1}H NMR ($CDCl_3$, 300

MHz): δ 8.81 (s, 2H), 7.59 (dd, *J* = 8.8 and 1.8 Hz, 2H), 7.48 (d, *J* = 8.8 Hz, 2H), 7.02 (dd, *J* = 17.4 and 8.2 Hz, 8H), 2.55 (t, *J* = 7.9 Hz, 4H), 1.61-1.51 (m, 4H), 1.37-1.21 (m, 28H), 0.93-0.83 (m, 6H). ^{13}C NMR ($CDCl_3$, 75.46 MHz): δ 141.02, 137.23, 135.64, 130.85, 130.46, 130.14, 129.54, 127.46, 125.02, 120.84, 35.37, 31.74, 31.08, 29.47, 29.32, 29.18, 28.97, 22.50, 13.91. FDMS (m/z): 768.2 ($M^{+\bullet}$). Elemental analysis: Calculated for $C_{46}H_{56}Br_2$: C, 71.87; H, 7.34; Br, 20.79; Found: C, 71.77; H, 9.73.

Synthesis of 2,2'-(9,10-di(4-decylphenyl)phenanthrene-3,6-diyl)di(4,4,5,5-tetramethyl-1,3,2-dioxaborolane) (62)

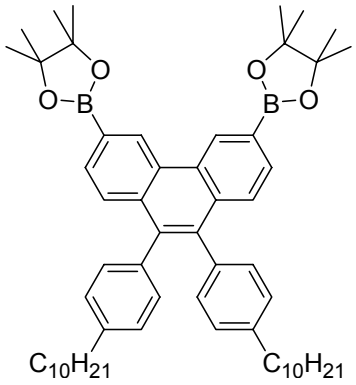

To a 100 mL Schlenk flask, **57** (1.7 g, 2.50 mmol), bis-(pinacolato)diboron (1.89 g, 7.50 mmol), $Pd_2(dba)_3$ (0.2 g, 0.075 mmol), potassium acetate (0.858 g, 8.75 mmol), tricyclohexylphosphine (0.35 g, 1.25 mmol), and 25 mL of anhydrous dioxane were added. The mixture was degassed by gently bubbling argon through for 30 min at room temperature and then heated at 110 ℃ under argon for 2 days. The cooled mixture was extracted with diethyl ether, washed with brine and dried over $MgSO_4$. The crude product was chromatographed on silica gel using hexane as eluent and further purified by recrystallization from THF in ethanol. Isolated yield = 500 mg (23 %) as colorless needlelike crystals. ^{1}H NMR ($CDCl_3$, 300 MHz): δ 9.38 (s, 2H), 7.87 (dd, *J* = 8.2 Hz, 2H), 7.61 (d, *J* = 8.2 Hz, 2H), 7.00 (m, 8H), 2.56 (t, *J* = 7.9 Hz, 4H), 1.60-1.53 (m, 4H), 1.47-1.39 (m, 24H), 1.35-1.25 (m, 28H), 0.93-0.85 (m, 6H). ^{13}C NMR ($CDCl_3$, 75.46 MHz): δ 140.74, 138.50, 136.69, 133.98, 131.88, 130.83, 129.53, 127.45, 126.93, 35.59, 31.94, 31.29, 29.69, 29.54, 29.39, 29.16, 24.92, 22.70, 14.12. FDMS (m/z): 862.6 ($M^{+\bullet}$). Elemental analysis: Calculated for $C_{58}H_{80}B_2O_4$: C, 80.73; H, 9.34; B, 2.51; O, 7.42; Found: C, 80.55; H, 9.59.

Polymer 3,6-LPAP

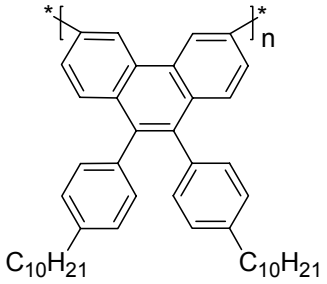

Dibromide **61** (89 mg, 0.12 mmol), monomer **62** (100 mg, 0.12 mmol), Aliquat® 336 (8 mg, 13 mol %), 1.5 mL of 2.0 M Na_2CO_3 and 4.0 mL of toluene were taken together in a Schlenk flask and purged with argon for 15 minutes. To this solution, tetrakis(triphenylphosphine)palladium (5.8 mg g, 9.4 μmol) was added and the reaction mixture was heated at 85 ˚C under vigorous stirring for 24 h. Phenylboronic acid was then added as an endcapper (2.0 mg), heated for 6 h and bromobenzene (5.0 mg) was added and heated again for an additional 6 h. The reaction was poured into a mixture of methanol and 2.0 M HCl (1:1, 300 mL) and filtered. The collected product was redissolved in THF (10 mL) and added dropwise to methanol (200 mL). The resulting solid was filtered off and subjected to a Soxhlet extraction for 24 h in acetone. Isolated yield of polymer **3,6-LPAP** = 110 mg (78 %). GPC analysis $M_n = 5.33 \times 10^3$ g/mol, $M_w = 6.82 \times 10^3$ g/mol, and D = 1.28 (against PPP standard); $M_n = 6.94 \times 10^3$ g/mol, $M_w = 9.58 \times 10^3$ g/mol, and D = 1.38 (against PS standard). ^{1}H NMR ($CDCl_3$, 300 MHz): δ 9.25-9.07 (br m, 1H), 8.01-7.61 (br m, 4H), 7.11-6.39 (br m, 9H), 2.70-2.41 (br m, 4H), 1.77-1.41 (br m, 4H), 1.40-1.01 (br m, 28H), 0.97-0.78 (br m, 6H). Elemental analysis: Calculated for $C_{46}H_{56}$: C, 90.73; H, 9.27; Found: C, 90.50; H, 9.19.

Synthesis of 5-bromo-2-iodo-4'-decylbenzophenone (63)

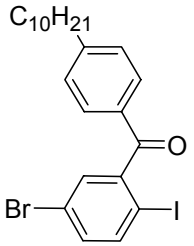

5-Bromo-2-iodo-benzoyl chloride (4.0 g, 11.6 mmol) was used in the Friedel-Crafts acylation and purified by chromatography on silica with 0-10 % ethylacetate in hexane as eluent. Isolated yield = 5.2 g (85 %) as a yellow oil. ^{1}H NMR ($CDCl_3$, 300 MHz): δ 7.73 (dd, J = 10.4 and 8.4 Hz, 3H), 7.40 (d, J = 2.3 Hz, 1H), 7.32-7.28 (m, 3H), 2.66 (t, J = 7.9 Hz, 2H), 1.69-1.58 (m, 2H), 1.37-1.21 (m, 14H), 0.87 (t, J = 6.9 Hz, 3H). ^{13}C NMR ($CDCl_3$, 75.46 MHz): δ 195.53, 150.51, 146.80, 141.32, 134.35, 132.99, 131.44, 130.99,

129.24, 122.75, 90.59, 36.52, 32.24, 31.35, 29.94, 29.90, 29.79, 29.67, 23.03, 14.49. FDMS (m/z): 526.0 ($M^{+\bullet}$). Elemental analysis: Calculated for $C_{23}H_{28}BrIO$: C, 52.39; H, 5.35; Br, 15.15; I, 24.07; O, 3.03; Found: C, 52.77; H, 5.71.

Synthesis of 4,4'-dibromo-2,2'-di(4-decyl-benzoyl)-1,1'-biphenyl (64)

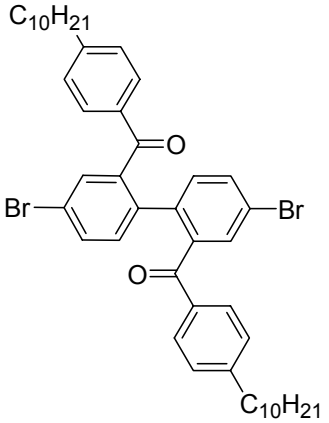

Compound **63** (2.5 g, 4.70 mmol) was used in the Ullmann coupling and purified by chromatography on silica with 0-10 % ethylacetate in hexane as eluent and further purified by recrystallization from hexane in ethanol. Isolated yield = 1.1 g (58 %) as a light yellow solid. ^{1}H NMR ($CDCl_3$, 300 MHz): δ 7.59 (d, J = 8.2 Hz, 4H), 7.49 (m, 4H), 7.18 (d, J = 8.2 Hz, 2H), 7.08 (d, J = 8.2 Hz, 4H), 2.57 (t, J = 7.9 Hz, 4H), 1.62-1.53 (m, 4H), 1.35-1.22 (m, 28H), 0.88 (t, J = 6.9 Hz, 6H). ^{13}C NMR ($CDCl_3$, 75.46 MHz): δ 195.31, 149.20, 140.12, 137.80, 134.13, 130.54, 128.27, 121.16, 36.05, 31.89, 31.05, 29.61, 29.46, 29.32, 22.67, 14.10. FDMS (m/z): 800.2 ($M^{+\bullet}$). Elemental analysis: Calculated for $C_{46}H_{56}Br_2O_2$: C, 69.00; H, 7.05; Br, 19.96; O, 4.00; Found: C, 69.23; H, 7.03.

Synthesis of 2,7-dibromo-9,10-di-(4-decyl-phenyl)-phenanthrene (65)

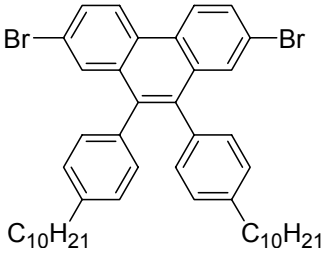

Compound **64** (1.5 g, 1.87 mmol) was used in the cyclization procedure. Isolated yield = 1.1 g (76 %) as colorless needlelike crystals. ^{1}H NMR ($CDCl_3$, 300 MHz): δ 8.58 (d, J = 8.6 Hz, 2H), 7.75 (d, J = 9.5 Hz, 4H), 6.99 (dd, J = 20.8 and 8.1 Hz, 8H), 2.56 (t, J = 7.9 Hz, 4H), 1.72-1.55 (m, 4H), 1.45-1.22 (m, 28H), 0.90 (t, J = 6.5 Hz, 6H). ^{13}C NMR

($CDCl_3$, 75.46 MHz): δ 141.10, 137.56, 135.33, 133.37, 130.44, 128.04, 127.54, 121.05, 33.61, 31.73, 30.91, 29.49, 29.18, 28.59, 26.54, 22.50, 13.91. FDMS (m/z): 768.3 ($M^{+\bullet}$). Elemental analysis: Calculated for $C_{46}H_{56}Br_2$: C, 71.87; H, 7.34; Br, 20.79; Found: C, 71.55; H, 7.70.

Polymer 2,7-PAP

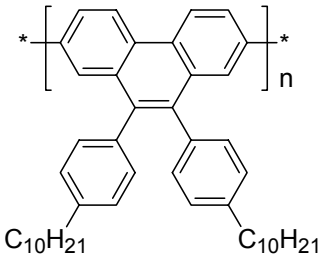

The dichloride **65** (368 mg, 0.60 mmol) was used in the Yamamoto polycondensation. Isolated yield of polymer **2,7-PAP** = 250 mg (68 %). GPC analysis $M_n = 1.13 \times 10^4$ g/mol, $M_w = 5.26 \times 10^4$ g/mol, and D = 4.66 (against PPP standard); $M_n = 1.48 \times 10^4$ g/mol, $M_w = 1.07 \times 10^5$ g/mol, and D = 7.22 (against PS standard). ^{1}H NMR ($CDCl_3$, 300 MHz): δ 8.10-7.57 (br m, 2H), 6.99-6.11 (br m, 12H), 2.65-2.35 (br m, 4H), 1.88-1.21 (br m, 32H), 0.98-0.68 (br m, 6H). Elemental analysis: Calculated for $C_{46}H_{56}$: C, 90.73; H, 9.27; Found: C, 90.62; H, 9.63.

Synthesis of 5-chloro-2-iodo-4'-decylbenzophenone (66)

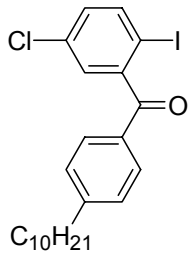

5-Chloro-2-iodo-benzoyl chloride (3.0 g, 10.0 mmol) was used in the Friedel-Crafts acylation and purified by chromatography on silica with 0-10 % ethylacetate in hexane as eluent. Isolated yield = 4.3 g (89 %) as a yellow oil. ^{1}H NMR ($CDCl_3$, 300 MHz): δ 7.81 (d, J = 8.4 Hz, 1H), 7.72 (d, J = 8.3 Hz, 2H), 7.28 (d, J = 7.7 Hz, 3H), 7.15 (dd, J = 8.4 and 2.5 Hz, 1H), 2.66 (t, J = 7.9 Hz, 2H), 1.73-1.61 (m, 2H), 1.45-1.22 (m, 14H), 0.90 (t, J = 6.7 Hz, 3H). ^{13}C NMR ($CDCl_3$, 75.46 MHz): δ 195.24, 150.07, 146.10, 140.67, 134.48, 132.58, 131.01, 130.55, 128.80, 128.23, 36.09, 31.82, 30.92, 29.52, 29.47, 29.37, 29.24, 29.21, 22.61, 14.06. FDMS (m/z): 482.0 ($M^{+\bullet}$). Elemental analysis: Calculated for $C_{23}H_{28}ClIO$: C, 57.21; H, 5.85; Cl, 7.34; I, 26.28; O, 3.31; Found: C, 57.27; H, 5.37.

Synthesis of 2-(4,4,5,5-tetramethyl-[1,3,2]dioxaborolan-2-yl)-4'-decylbenzophenone (67)

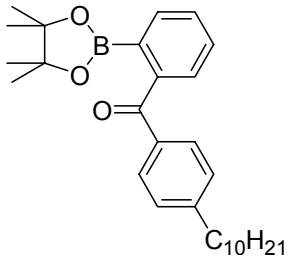

To a 100 mL Schlenk flask, **59** (5.6 g, 12.5 mmol), bis-(pinacolato)diboron (3.78 g, 13.7 mmol), palladium acetate (0.083 g, 0.37 mmol), potassium acetate (3.67 g, 37.5 mmol) and 25 mL of anhydrous N,N-dimethylformamide were added. The mixture was degassed by gently bubbling argon through for 30 min at room temperature. The mixture was then heated at 70 ℃ under argon overnight. The cooled mixture was extracted with diethyl ether, washed with brine and dried over $MgSO_4$. The crude product was chromatographed on silica using 0-10 % ethylacetate in hexane as eluent. Isolated yield = 2.8 g (50 %) as yellow oil. ^{1}H NMR ($CDCl_3$, 300 MHz): δ 7.70 (m, 4H), 7.47 (m, 3H), 7.22 (d, J = 8.2 Hz, 3H), 2.64 (t, J = 7.8 Hz, 2H), 1.69-1.55 (m, 2H), 1.43-1.23 (m, 14H), 1.20-1.55 (m, 12H), 0.87 (t, J = 6.7 Hz, 3H). ^{13}C NMR ($CDCl_3$, 75.46 MHz): δ 197.75, 148.04, 143.92, 135.69, 133.63, 130.12, 129.99, 129.56, 128.65, 128.17, 83.82, 35.91, 31.79, 31.18, 29.50, 29.48, 29.38, 29.22, 29.13, 24.92, 24.44, 22.58, 14.01. FDMS (m/z): 448.3 ($M^{+\bullet}$). Elemental analysis: Calculated for $C_{29}H_{41}BO_3$: C, 77.67; H, 9.22; B, 2.41; O, 10.70; Found: C, 77.72; H, 9.45.

Synthesis of 4-chloro-2,2'-di(4-decyl-benzoyl)-1,1'-biphenyl (68)

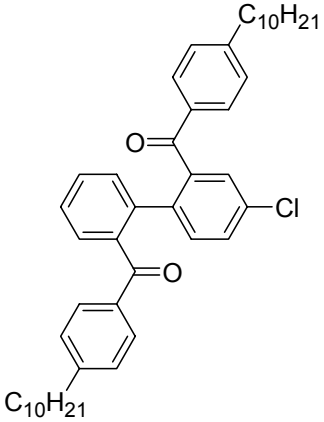

The boronic ester **67** (1.05 g, 2.34 mmol) and **66** (1.13 g, 2.34 mmol) were dissolved in THF (20 mL) in a 100 mL Schlenk flask. To this solution, 2 M K_2CO_3 aqueous solution

(10 mL) was added and the solution purged with argon for 20 min. Tetrakis(triphenylphosphine)palladium (81 mg, 0.07 mmol) was added and the reaction was stirred at 85 ˚C. The reaction was followed by TLC and worked up after 2 days. The cooled mixture was extracted with diethyl ether. The organic layer was washed with brine and dried over $MgSO_4$. The crude product obtained was purified by chromatography on silica with 0-10 % ethylacetate in hexane as eluent. Isolated yield = 1.3 g (82.0 %) as a yellow oil. ^{1}H NMR ($CDCl_3$, 300 MHz): δ 7.71 (d, *J* = 8.3 Hz, 1H), 7.62 (dd, *J* = 8.3 and 4.0 Hz, 3H), 7.40-7.30 (m, 8H), 7.10-7.01 (m, 3H), 2.70-2.55 (m, 4H), 1.63-1.52 (m, 4H), 1.41-1.23 (m, 28H), 0.87 (t, *J* = 6.7 Hz, 6H). ^{13}C NMR ($CDCl_3$, 75.46 MHz): δ 196.91, 195.71, 150.18, 148.86, 148.63, 146.16, 140.73, 140.03, 138.94, 138.42, 134.84, 134.27, 132.82, 130.61, 128.12, 89.31, 25.99, 31.87, 31.07, 30.99, 29.59, 29.44, 29.30, 22.65, 14.08. FDMS (m/z): 676.4 ($M^{+\bullet}$). Elemental analysis: Calculated for $C_{46}H_{57}ClO_2$: C, 81.56; H, 8.48; Cl, 5.23; O, 4.72; Found: C, 81.30; H, 8.73.

Synthesis of 2-chloro-9,10-di-(4-decyl-phenyl)-phenanthrene (69)

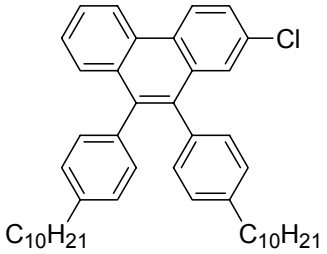

Compound **68** (1.3 g, 1.92 mmol) was used in the cyclization procedure. Isolated yield = 1.1 g (89 %) as colorless needlelike crystals. ^{1}H NMR ($CDCl_3$, 300 MHz): δ 8.71 (m, 2H), 7.60-7.51 (m, 5H), 7.01 (m, 8H), 2.55 (t, *J* = 6.7 Hz, 4H), 1.67-1.55 (m, 4H), 1.41-1.23 (m, 28H), 0.89 (t, *J* = 6.7 Hz, 6H). ^{13}C NMR ($CDCl_3$, 75.46 MHz): δ 140.88, 138.46, 136.33, 136.18, 135.77, 133.10, 132.31, 130.59, 129.30, 128.11, 127.48, 127.33, 35.39, 33.61, 31.73, 30.91, 29.48, 26.54, 22.50, 13.91. FDMS (m/z): 644.4 ($M^{+\bullet}$). Elemental analysis: Calculated for $C_{46}H_{57}Cl$: C, 85.60; H, 8.90; Cl, 5.49; Found: C, 85.71; H, 9.01.

Synthesis of 2-[9,10-di-(4-decyl-phenyl)-phenanthren-2-yl]-4,4,5,5-tetramethyl-[1,3,2]dioxaborolane (70)

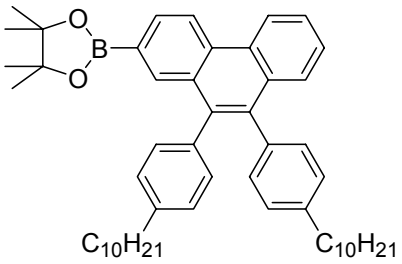

To a 100 mL Schlenk flask, the chloride compound **69** (1.0 g, 1.55 mmol), bis-(pinacolato)diboron (0.51 g, 2.01 mmol), $Pd_2(dba)_3$ (0.042 g, 0.047 mmol), potassium acetate (0.23 g, 2.32 mmol), tricyclohexylphosphine (0.065 g, 0.23 mmol) and 25 mL of anhydrous dioxane were added. The mixture was degassed by gently bubbling argon through for 30 min at room temperature. The mixture was then heated at 110 ˚C under argon for 2 days. The cooled mixture was extracted with diethyl ether, washed with brine and dried over $MgSO_4$. The crude product was chromatographed on silica with 0-5 % ethylacetate in hexane as eluent. Isolated yield = 0.82 g (72 %) as yellow solid. ^{1}H NMR ($CDCl_3$, 300 MHz): δ 8.88 (dd, *J* = 14.3 and 8.4 Hz, 2H), 8.12 (s, 1H), 8.03 (d, *J* = 8.3 Hz, 1H), 7.64 (m, 2H), 7.49 (m, 1H), 7.02 (m, 8H), 2.57 (m, 4H), 1.77-1.55 (m, 4H), 1.40-1.21 (m, 40H), 0.89 (t, *J* = 6.8 Hz, 6H). ^{13}C NMR ($CDCl_3$, 75.46 MHz): δ 140.80, 140.66, 137.98, 137.41, 136.99, 136.68, 135.28, 132.67, 132.11, 131.37, 131.20, 131.08, 129.90, 128.61, 128.42, 127.57, 126.22, 83.61, 44.62, 33.95, 32.07, 31.25, 29.85, 25.14, 22.83, 14.24. FDMS (m/z): 736.5 ($M^{+\bullet}$). Elemental analysis: Calculated for $C_{52}H_{69}BO_2$: C, 84,75; H, 9,44; B, 1,47; O, 4,34; Found: C, 84.70; H, 9.71.

Synthesis of 2,7-MT

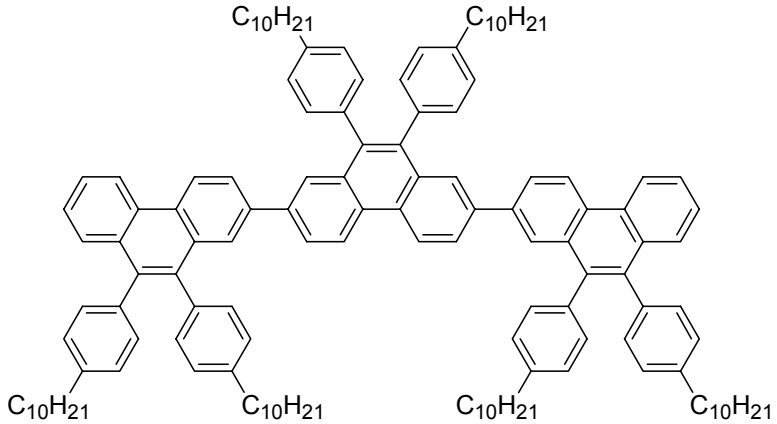

The boronic ester **70** (0.5 g, 0.68 mmol) and **65** (0.24 g, 0.31 mmol) were dissolved in THF (20 mL) in a 100 mL Schlenk flask. To this solution, aqueous 2 M K_2CO_3 solution (10 mL) was added and the solution purged with argon for 20 min. Tetrakis(triphenylphosphine)palladium (21 mg, 18 μmol) was added and the reaction

mixture was stirred at 85 ˚C. The reaction was followed by TLC and after 48 h, the mixture was cooled and extracted with diethyl ether. The organic layer was washed with brine and dried over $MgSO_4$. The crude product obtained was purified by chromatography on silica with 0-25 % dichloromethane in hexane as eluent. Isolated yield = 150 mg (26 %) as a light yellow solid. ^{1}H NMR ($CDCl_3$, 500 MHz): δ 8.78 (m, 6H), 7.84 (m, 8H), 7.63 (d, *J* = 7.8 Hz, 4H), 7.47 (t, *J* = 7.1 Hz, 2H), 7.01 (d, *J* = 11.9 Hz, 24H), 2.69-2.51 (m, 12H), 1.71-1.55 (m, 12H), 1.37-1.21 (m, 84H), 0.95-0.81 (m, 18H). ^{13}C NMR ($CDCl_3$, 125.75 MHz): δ 140.82, 140.66, 139.30, 138.04, 137.87, 137.61, 136.90, 136.64, 132.51, 132.23, 130.98, 129.91, 129.15, 128.99, 127.99, 127.56, 126.54, 126.27, 125.70, 123.05, 122.48, 35.71, 35.66, 31.96, 31.33, 29.73, 29.62, 29.55, 29.38, 29.26, 22.68, 14.05. FDMS (m/z): 1829.1 ($M^{+\bullet}$). Elemental analysis: Calculated for $C_{138}H_{170}$: C, 90.63; H, 9.37; Found: C, 90.57; H, 9.69.

Synthesis of 3-bromo-9,10-di-(4-decyl-phenyl)-phenanthrene (71)

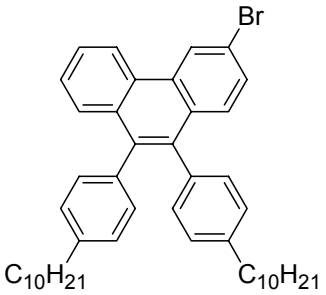

9,10-Di-(4-decyl-phenyl)-phenanthrene (1.0 mg, 1.63 mmol) and catalytic amounts of iodine were dissolved in CCl_4 (10 mL). To this mixture, bromine (0.26 g, 1.63 mmol) was added dropwise at 0 ˚C. The reaction mixture was slowly allowed to warm to room temperature overnight. Additional bromine (0.13 g, 0.82 mmol) was then added with stirring and the reaction monitored by FDMS, which showed nearly quantitative formation of the monobromide after 12 h. This was quenched by addition of aqueous $Na_2S_2O_5$ solution and extracted into dichloromethane, washed with brine and dried. The crude product was chromatographed on silica gel using hexane as eluent and further purified by recrystallization from THF in ethanol. Isolated yield = 250 mg (20 %) as a colorless needlelike crystal. ^{1}H NMR ($CDCl_3$, 300 MHz): δ 8.91 (s, 1H), 8.70 (d, *J* = 8.3 Hz, 1H), 7.65 (dd, *J* = 13.4 and 6.9 Hz, 2H), 7.51 (m, 3H), 7.20-7.00 (m, 8H), 2.65-2.51 (m, 4H), 1.77-1.45 (m, 4H), 1.41-1.25 (m, 28H), 0.89 (t, *J* = 6.7 Hz, 6H). ^{13}C NMR ($CDCl_3$, 75.46 MHz): δ 140.53, 137.136.53, 135.96, 135.79, 131.98, 131.06, 130.38, 128.44, 137.12, 120.30, 35.17, 31.52, 30.88, 29.26, 29.11, 28.96, 28.75, 22.28, 13.69. FDMS (m/z): 689.1 ($M^{+\bullet}$). Elemental analysis: Calculated for $C_{46}H_{57}Br$: C, 80.09; H,

8.33; Br, 11.58; Found: C, 80.32; H, 8.59.

Synthesis of 3,6-MT

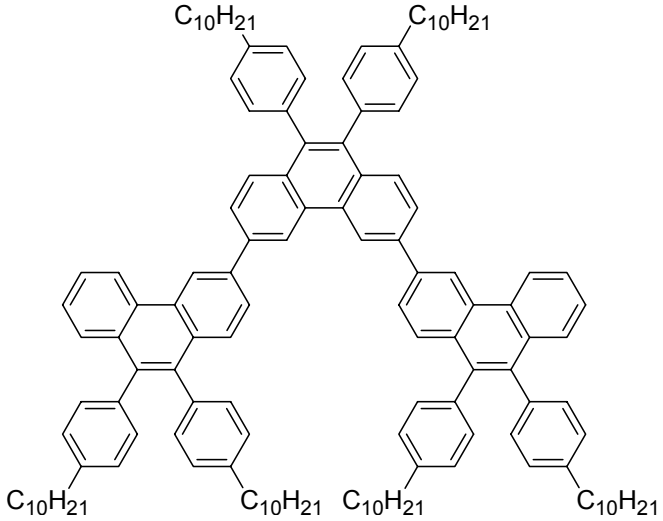

The boronic ester **71** (100 mg, 0.116 mmol) and compound **62** (0.18 g, 0.255 mmol) were dissolved in THF (10 mL) in a 100 mL Schlenk flask. To this solution, aqueous 2 M K_2CO_3 solution (5 mL) was added and the solution was purged with argon for 20 min. Tetrakis(triphenylphosphine)palladium (6.7 mg, 5.80 μmol) was added and the reaction mixture was stirred at 85 ˚C. The reaction was followed by TLC and after 48 h, the mixture was cooled and extracted with diethyl ether. The organic layer was washed with brine and dried over $MgSO_4$. The crude product obtained was purified by chromatography on silica with 0-25 % dichloromethane in hexane as eluent. Isolated yield = 150 mg (71 %) as colorless solid. ^{1}H NMR ($CDCl_3$, 300 MHz): δ 9.28 (s, 2H), 9.18 (s, 2H), 8.94 (d, *J* = 8.3 Hz, 2H), 7.96 (t, *J* = 7.1 Hz, 4H), 7.85-7.71 (m, 4H), 7.66 (t, *J* = 7.8 Hz, 4H), 7.50 (m, 2H), 7.29-7.10 (m, 24H), 2.58 (m, 12H), 1.70-1.52 (m, 12H), 1.42-1.27 (m, 84H), 0.93-0.82 (m, 18H). ^{13}C NMR ($CDCl_3$, 75.46 MHz): δ 140.74, 139.26, 139.04, 137.35, 137.18, 136.98, 136.51, 132.21, 131.48, 131.15, 130.71, 130.25, 130.12, 129.83, 127.41, 126.09, 122.34, 121.22, 23.42, 31.75, 31.14, 29.49, 29.35, 29.26, 29.19, 29.10, 22.51, 13.92. FDMS (m/z): 1828.0 ($M^{+\bullet}$). Elemental analysis: Calculated for $C_{138}H_{170}$: C, 90.63; H, 9.37; Found: C, 90.57; H, 9.83.

Synthesis of *N,N′*-bis(4'-methoxyphenyl)-1,6,7,12-tetra[4-(1,1,3,3-tetramethylbutyl)phenoxy]perylene-3,4,9,10-tetracarboxdiimide (73)

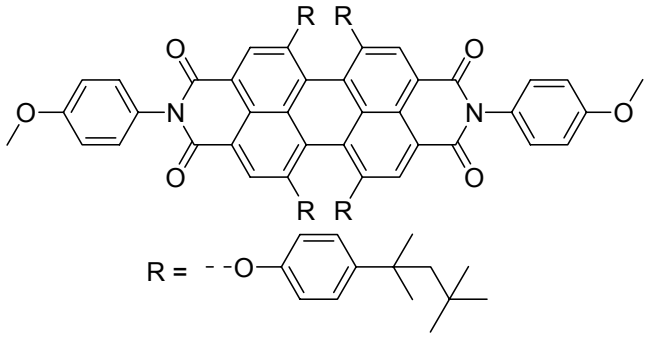

4-Methoxyphenylamine (11.6 g, 10 equiv.) was added to a suspension of finely ground 1,6,7,12-tetrachlorperylene-3,4:9,10-tetracarboxylic acid dianhydride (5 g, 9.43 mmol) in propionic acid (100 ml), and the mixture was refluxed under an argon atmosphere for 12h. The precipitated product was collected by filtration and dried under vacuum at 100 °C to give *N,N'*-bis(4'-methoxy-phenyl)-1,6,7,12-tetrachloroperylene-3,4,9,10-tetracarboxdiimide (**72**) as a red solid (6.28 g, 90 %). Potassium carbonate (4.48 g, 8.0 equiv.) and 4-*tert*-octylphenol (6.68 g, 8.0 equiv.) were added to a suspension of the tetrachlorodiimide **72** (3.0 g, 4.05 mmol) in NMP (150 ml), and the mixture was heated at 120 °C under an argon atmosphere for 5 days. The cooled reaction mixture was added with stirring to a mixture of 10 % aqueous hydrochloric acid (200 ml) and methanol (300 ml) the resulting precipitate was collected by filtration and repeatedly washed with water and methanol. The crude product was chromatographed on silica gel eluted with 0-80 % dichloromethane in hexane. Isolated yield = 1.7 g (30 %) as a red solid. ^{1}H NMR (CD_2Cl_2, 250 MHz): δ 8.11 (s, 4H), 7.33 (d, *J* = 8.7 Hz, 8H), 7.17 (d, *J* = 8.7 Hz, 4H), 7.03 (d, *J* = 8.7 Hz, 4H), 6.91 (*J* = 8.7 Hz, 8H), 3.85 (s, *J* = 8.5 Hz, 6H), 1.72 (m, 8H), 1.35 (m, 24H), 0.73 (m, 36H). ^{13}C NMR (CD_2Cl_2, 75.46 MHz): δ 164.11, 160.19, 156.76, 153.43, 147.29, 133.58, 130.17, 128.64, 128.30, 123.39, 121.01, 120.25, 120.19, 119.98, 115.02, 57.48, 56.05, 38.82, 32.82, 32.14. FDMS (m/z): 1419.7 ($M^{+\bullet}$). Elemental analysis: Calculated for $C_{94}H_{102}N_2O_{10}$: C, 79.52; H, 7.24; N, 1.97; O, 11.27; Found: C, 79.97; H, 7.71; N, 2.10.

Synthesis of *N,N'*-bis(4'-hydroxyphenyl)-1,6,7,12-tetra[4-(1,1,3,3-tetramethylbutyl)phenoxy]perylene-3,4,9,10-tetracarboxdiimide (74)

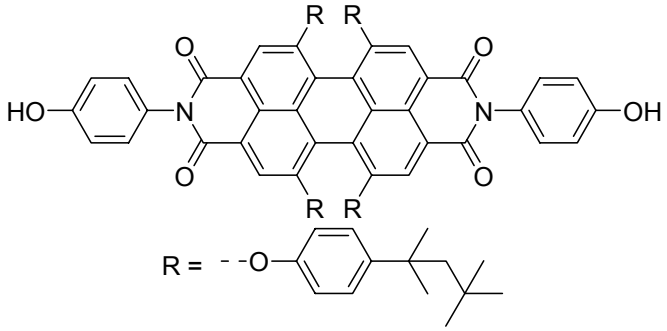

A 100 mL dried flask was charged with compound **73** (0.3 g, 0.21 mmol) and 50 mL of anhydrous methylene chloride. The solution was cooled at -78 °C and 1.2 mL (6.0 equiv.) of boron tribromide (1 M in methylene chloride) was added over 0.5 h. The resulting mixture was stirred under argon at -78 °C for 3 h and additionally at room temperature for 12 h. The mixture was quenched slowly with 20 ml of HCl 10 % (v/v) to destroy the excess of boron tribromide, extracted with dichloromethane and the organic fractions dried over $MgSO_4$. The crude product was chromatographed on silica gel eluted with 0-50 % ethylacetate in hexane. Isolated yield = 0.27 g (95 %) as a red solid. ^{1}H NMR (CD_2Cl_2, 250 MHz): δ 8.10 (s, 4H), 7.31 (d, *J* = 8.7 Hz, 8H), 7.05 (d, *J* = 8.7 Hz, 4H), 6.92 (t, *J* = 8.5 Hz, 12H), 5.21 (s, 2H), 1.72 (m, 8H), 1.53 (m, 24H), 0.73 (m, 36H). ^{13}C NMR ($C_2D_2Cl_4$, 120 °C, 75.46 MHz): δ 162.79, 155.58, 155.08, 152.21, 146.59, 132.45, 129.22, 127.56, 126.94, 122.31, 119.95, 119.33, 119.11, 118.79, 115.54, 56.63, 37.85, 31.61, 31.20, 20.67. FDMS (m/z): 1391.3 ($M^{+\bullet}$). Elemental analysis: Calculated for $C_{92}H_{98}N_2O_{10}$: C, 79.39; H, 7.10; N, 2.01; O, 11.50; Found: C, 79.57; H, 7.53; N, 2.00.

Polymer (P8)

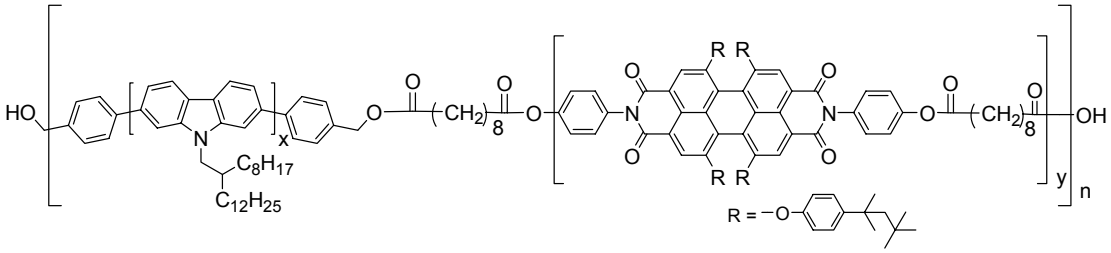

To a 100 mL, three-necked flask quipped with a reflux condenser, a solution of poly(2,7-carbazoles) (PCz) (70 mg, 0.0045 mmol, M_n =15,500 g/mol), the PDI **74** (70 mg, 0.05 mmol), and sebacoyl chloride (0.068 mmol) in 3 mL of toluene was added under an argon atmosphere. After the reaction mixture was allowed to react at 120 °C for 3 days, sebacoyl chloride (0.02 mL) and toluene (3 mL) were added and the mixture was heated at 120 ˚C for an additional 12 h. The mixture was then poured into a mixture of methanol and 2 M hydrochlorid acid (1:1, 300 mL) and stirred for 4 h. The precipitated white solid

was redissolved in THF (10 mL) and added dropwise to methanol (200 mL). The resulting solid was filtered off and subjected to Soxhlet extraction for 2 days using acetone as solvent. The residue was then redissolved in THF and precipitated again from methanol, filtered, washed with methanol, and dried. Isolated yield of polymer **P8** = 120 mg. GPC analysis M_n = 1.26 × 10^4 g/mol, M_w = 3.34 × 10^4 g/mol, and D = 2.66 (against PPP standard); M_n = 1.76 × 10^4 g/mol, M_w = 6.27 × 10^4 g/mol, and D = 3.56 (against PS standard). ^{1}H NMR (CD_2Cl_2, 250 MHz): δ 8.35-8.00 (br m, 10H), 7.89-7.61 (br m, 12H), 7.39-7.11 (br m, 16H), 6.99-6.79 (br m, 8H), 4.55-4.41 (br m, 3H), 2.67-2.45 (br m, 4H), 2.39-2.21 (br m, 4H), 1.91-1.25 (br m, 184H), 1.19-0.71 (br m, 60).

Synthesis of 2,2'-[1-(4-octylphenyl)1-*H*-pyrrole-2,5-diyl]bisbenzoic acid dimethyl ester (78)

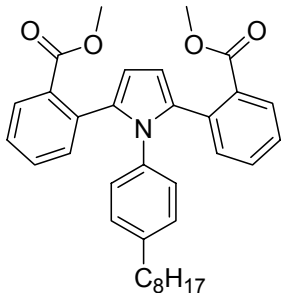

To 2,2'-(1,3-butadiyne-1,4-diyl)bisbenzoic acid dimethyl ester (**77**) (3.0 g, 9.42 mmol) in a 500 mL Schlenk flask, *p*-octylphenylamine (2.13 g, 10.39 mmol) and copper(I) chloride (0.23 g, 2.33 mmol) was added under argon. The reaction was stirred under argon at 170 ˚C for 12 h and then quenched with 2 M hydrochloric acid, the product was then extracted into dichloromethane, washed with brine and dried. The crude product was chromatographed on silica using 0-10 % ethylacetate in hexane as eluent. Isolated yield = 2.0 g (41 %) as a brown oil. ^{1}H NMR (CD_2Cl_2, 300 MHz): δ 7.61 (d, *J* = 6.1 Hz, 2H), 7.40 (dd, *J* = 7.2 and 1.21 Hz, 2H), 7.35-7.28 (m, 4H), 6.84 (d, *J* = 8.3 Hz, 2H), 6.66 (d, *J* = 8.3 Hz, 2H), 6.30 (s, 2H), 3.59-3.57(m, 6H), 2.56-2.38 (m, 2H), 1.56-1.42 (m, 2H), 1.39-1.21 (s, 10H), 0.89 (t, *J* = 6.7 Hz, 3H). ^{13}C NMR (CD_2Cl_2, 75.46 MHz): δ 167.97, 141.38, 135.64, 134.15, 133.97, 132.37, 132.27, 130.94, 129.33, 128.21, 128.00, 127.14, 109.82, 51.93, 35.34, 32.01, 31.34, 29.57, 29.43, 29.09, 22.85, 14.04. FDMS (m/z): 523.9 ($M^{+\bullet}$). Elemental analysis: Calculated for $C_{34}H_{37}NO_4$: C, 77.98; H, 7.12; N, 2.67; O, 12.22; Found: C, 77.59; H, 7.53; N, 2.33.

Synthesis of 2,2'-[1-(4-octylphenyl)1-*H*-pyrrole-2,5-diyl]bisbenzoic acid (79)

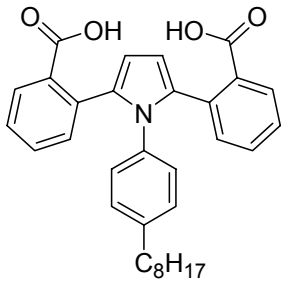

To THF (20 mL), methanol (7 mL) and water (7 mL) in a Schlenk flask, the diester **78** (1.0 g, 1.91 mmol) and potassium hydroxide (3.0 g, 53.5 mmol) was added and heated at 75 ˚C for 15 h under argon. The resulting solution was acidified with excess hydrochloric acid (12 M). The crude product was then extracted into dichloromethane, washed with brine and dried. This was then flash chromatographed on silica using 0-30 % ethanol in ethylacetate as eluent. Isolated yield = 0.8 g (85 %) as a brown solid. ^{1}H NMR (CD_2Cl_2, 300 MHz): δ7.77-7.67 (m, 2H), 7.45-7.30 (m, 5H), 7.21-7.12 (m, 2H), 7.01-6.80 (m, 3H), 6.22 (s, 2H), 2.57-2.39 (m, 2H), 1.51-1.40 (m, 2H), 1.41-1.23 (s, 10H), 0.89 (t, *J* = 7.1 Hz, 3H). ^{13}C NMR (CD_2Cl_2, 75.46 MHz): δ174.62, 141.62, 141.54, 141.31, 135.80, 134.02, 132.37, 128.44, 128.40, 127.47, 109.73, 35.58, 32.27, 31.46, 29.83, 29.67, 29.41, 23.03, 14.27. FDMS (m/z): 495.5 ($M^{+\bullet}$). Elemental analysis: Calculated for $C_{32}H_{33}NO_4$: C, 77.55; H, 6.71; N, 2.83; O, 12.91; Found: C, 77.77; H, 6.85; N, 2.52.

Synthesis of bis-carbonyl bridged 1-(4-Octyl-phenyl)-2,5-diphenyl-1*H*-pyrrole (80)

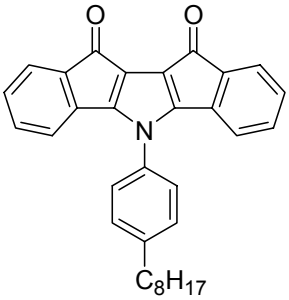

A flask equipped with a reflux condenser and a drying tube was charged with **79** (0.3 g, 0.56 mmol) and benzene (20 mL). To this mixture was added oxalyl chloride (0.14 g, 1.12 mmol) and one drop of N,N-dimethylformamide (catalyst). The reaction mixture was heated at 80 ˚C overnight (bubbling observed), then the reaction was cooled and the solvent was removed *in vacuo*. The crude solid was dissolved in benzene (20 mL) and stirred with calcium hydride for 1 h and filtered. The solvent was removed in *vacuo* to give 5-bromo-2-iodo-benzoyl chloride and used without further purification. To the benzoyl chloride in 20 mL of 1,2-dichloroethane, aluminum chloride (0.18 g, 1.4 mmol) was added, stirred at 75 ˚C for 12 h and then quenched with aqueous 2 M HCl. The

mixture was then extracted into dichloromethane and washed with brine. The crude product obtained was flash chromatographed on silica gel using 0-30 % ethylacetate in hexane as eluent and further purified by recrystallization from dichloromethane in methanol. Isolated yield = 0.03 g (11 %) as brown needlelike crystals. ^{1}H NMR (CD_2Cl_2, 250 MHz): δ 7.57 (d, *J* = 8.4 Hz, 2H), 7.47 (d, *J* = 8.4 Hz, 2H), 7.36-7.22 (m, 2H), 7.16-6.98 (m, 4H), 6.48-6.451 (m, 2H), 2.96-2.51 (m, 2H), 1.85-1.60 (m, 2H), 1.45-1.25 (m, 10H), 0.91-0.83 (t, *J* = 6.9 Hz, 3H). ^{13}C NMR (CD_2Cl_2, 62.89 MHz): δ 184.47, 156.93, 145.92, 137.83, 135.39, 133.39, 132.84, 130.11, 128.58, 125.96, 123.68, 118.83, 117.70, 35.83, 32.03, 31.45, 29.59, 29.49, 29.42, 22.85, 14.05. FDMS (m/z): 459.7 ($M^{+\bullet}$). Elemental analysis: Calculated for $C_{32}H_{29}NO_2$: C, 83.63; H, 6.36; N, 3.05; O, 6.96; Found: C, 83.19; H, 6.95; N, 3.25.